Reservoir characterisation of the deep Upper Jurassic aquifer in the South German Molasse Basin using water chemical data and environmental isotopes

a PhD thesis

by

Florian Heine

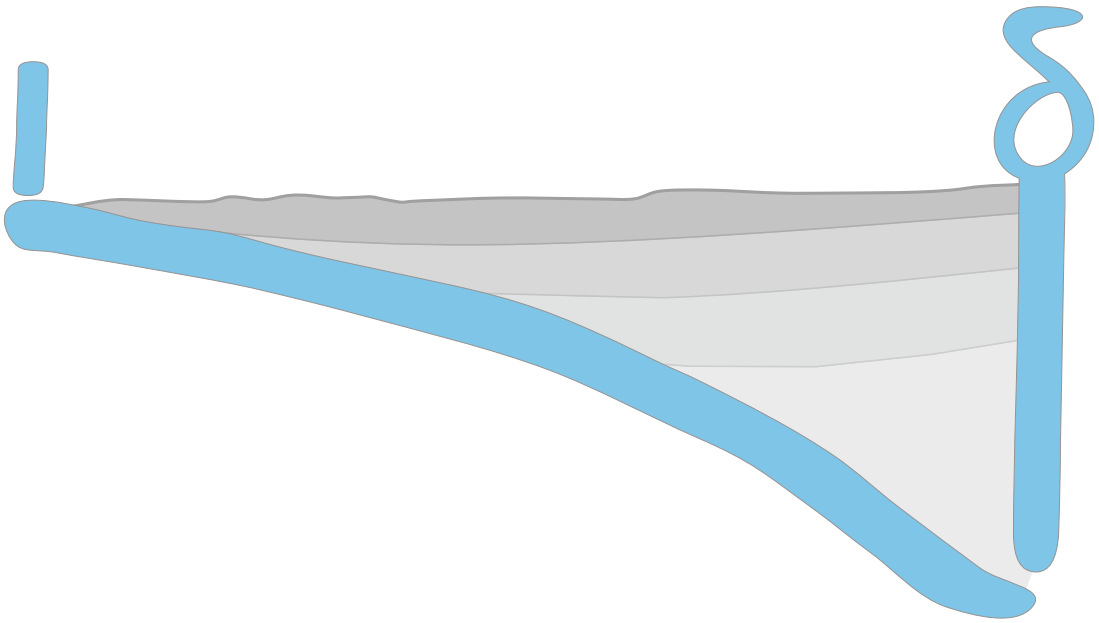

Technische Universität München
TUM School of Engineering and Design

Reservoir characterisation of the deep Upper Jurassic aquifer in the South German Molasse Basin using water chemical data and environmental isotopes

Florian Neil Heine

Vollständiger Abdruck der von der TUM School of Engineering and Design der Technischen Universität München zur Erlangung des akademischen Grades eines

Doktors der Naturwissenschaften (Dr. rer. nat.)

genehmigten Dissertation.

Vorsitzender:

Prof. Dr. rer. nat. Kurosch Thuro

Prüfende der Dissertation:

1. Prof. Dr. rer. nat. Florian Einsiedl
2. Prof. Dr. rer. nat. Martin Elsner
3. Prof. Johannes Barth, PhD.,
   Friedrich-Alexander Universität, Erlangen

Die Dissertation wurde am 05.07.2021 bei der Technischen Universität München eingereicht und durch die TUM School of Engineering and Design am 24.11.2021 angenommen.

If anyone can refute me - show me I'm making a mistake or looking at things from the wrong perspective - I'll gladly change. It's the truth I'm after, and the truth never harmed anyone.
Marcus Aurelius

Summary

The deep Upper Jurassic carbonate aquifer located in the South German Molasse Basin (SGMB) is one of the most important geothermal water resources in Europe. A detailed hydrogeological understanding of this hydrothermally used reservoir is crucial for improved and sustainable groundwater resource management and for future geothermal development.

The hydrogeological characteristics of the Upper Jurassic reservoir in the SGMB, including the delineation of groundwater recharge areas and flow system, have been already of great interest in various studies since the 1950s. Although all authors have determined a more or less consistent flow system for the Upper Jurassic groundwater on the assumption of an integrated supra-regional groundwater flow system in the SGMB, there were some considerable contradictions between the different hydraulic and hydrochemical model concepts. In the course of further exploitation of deep geothermal energy by an increasing number of Upper Jurassic wells and the systematic exploration of various targets (faults, rock matrix), new insights into the Upper Jurassic reservoir have emerged since the beginning of the 2000s. Moreover, the occurrence of different water capacities at the deep wells in the SGMB have necessitated an intensive scientific examination of the Upper Jurassic reservoir. Numerous studies considering the petrological, facial and hydraulic properties of the Upper Jurassic rocks have so far selectively revealed a more complex structure of the reservoir than previously assumed, and that distinct changes in the reservoir properties occur both locally and regionally.

However, a conclusive and comprehensive hydrogeological picture of the entire Upper Jurassic reservoir in the SGMB is still missing. Up to now, large-scale analyses of great and complex aquifer systems in deep sedimentary basins have been successfully performed in hydrogeological studies on the basis of the hydrochemical composition of the deep groundwater. The aim of this thesis is, therefore, to hydrochemically characterise the Upper Jurassic groundwater of numerous wells using water chemical data and environmental isotopes to (i) derive possible relationships between the infiltrating groundwater in the previously assumed recharge areas in the western SGMB and the deep geothermal waters in the central SGMB and to (ii) clarify the existing contradictions in the groundwater flow system of the Upper Jurassic aquifer. To improve the understanding of the groundwater circulation systematic in the Upper Jurassic aquifer, the interactions with overlying Tertiary sediments will also be identified in order to finally obtain a consistent hydrogeological picture of the deep Upper Jurassic reservoir in the SGMB. This is particularly important to reduce the exploration risk when determining future geothermal targets and, thus, to maintain an overall sustainable resource management of the geothermally exploited reservoir.

One challenge in characterising the groundwater circulation is dating groundwater with apparent ages of more than 1,000 years. One of the well established methods for dating old groundwater up to 30,000 years is radiocarbon in dissolved inorganic carbon ($^{14}C_{DIC}$), which can be severely affected in carbonate aquifers by various (bio)chemical and physical processes in the subsurface that can lead to incorrectly calculated $^{14}C_{DIC}$ model ages.

Therefore, in a first part of this work, a promising groundwater dating approach with ^{14}C of dissolved organic carbon ($^{14}C_{DOC}$) is investigated on seven deep Upper Jurassic groundwater wells in the western and northern SGMB to systematically test this dating approach for the first time. As a main issue of $^{14}C_{DOC}$ dating so far has been the complex and time-consuming concentration of datable DOC in groundwater, the pre-concentration of DOC is instead performed in this work by the newly established, easy applicable, time-saving and robust solid phase extraction (SPE) with a styrene-divinylbenzene copolymer sorbent (PPL). The resulting measured $^{14}C_{DOC}$ activities and derived apparent organic radiocarbon ages (ORA) are compared with water chemical data, stable water isotope signatures ($\delta^{18}O$ and δD) and conventional groundwater dating methods using $\delta^{13}C_{DIC}$ and $^{14}C_{DIC}$.

The results show that calculated ORAs at the Upper Jurassic wells with $^{14}C_{DOC}$ are generally lower than the corrected $^{14}C_{DIC}$ ages (IRA), which lead to an overestimation of the apparent groundwater ages. The plausibility of ORA is validated by integrating the calculated apparent groundwater ages with stable water isotope signatures of $\delta^{18}O$ and noble gas infiltration temperatures (NGTs) into atmospheric climate models from literature. This successful integration of climatic information associated with recharge conditions into a temporal sequence over the past support the applicability of the SPE-PPL method for $^{14}C_{DOC}$ dating in the Upper Jurassic groundwater. Furthermore, the inferred groundwater age pattern within the western SGMB can also be integrated into existing concepts of subglacial infiltration and the intermediate groundwater flow system. In addition, a subsequent groundwater flow and drainage to the Danube at the northern margin of the SGMB may be also confirmed, which is important for understanding the flow systematic throughout the Upper Jurassic reservoir.

In a second part, numerous water chemical parameters and well-chosen environmental isotopes of δD, $\delta^{18}O$ and $^{87}Sr/^{86}Sr$ are consistently investigated at all 24 available deep thermal groundwater wells in the central SGMB. These measurements are further coupled with some analyses of noble gases (He, Ne, Ar, Kr, Xe) to assess recharge conditions with calculated NGTs, and noble gas isotopes ($^{3}He/^{4}He$, $^{40}Ar/^{36}Ar$) to determine the temporal evolution of the groundwater by dating with ^{4}He and ^{40}Ar at selected wells. Moreover, in order to elucidate several influencing factors and processes that affect the hydrochemical composition after groundwater recharge and are, thus, responsible for the genesis of the Upper Jurassic groundwater, the data obtained are systematically evaluated for the first time using multivariate statistical methods such as exploratory factor (EFA) and hierarchical cluster analysis (HCA).

The interpretation of HCA has revealed three different water types 1 to 3 with partly different origin, genesis and interaction in the subsurface, which are influenced by different hydrogeological processes. The results show that lowly mineralised groundwater of water types 1 and 2 in the eastern central SGMB was recharged under meteorically cold climatic conditions and that $^{87}Sr/^{86}Sr$ and stable water isotope signatures indicate low water-rock interaction with the Upper Jurassic aquifer rocks. In contrast, highly mineralised groundwater of type 3 occurring in the western central SGMB is characterised by considerable water-rock interaction with terrestrial sediments and show elevated apparent groundwater ages, which may also imply hydraulic contact to the overlying Tertiary sediments.

The geographical occurrence of these water types allows consistent hydrochemical zoning of the Upper Jurassic groundwater in the central SGMB, which together with the $^{14}C_{DOC}$ dating results of groundwater in the western SGMB implies a conclusive hydrogeological picture of the Upper Jurassic aquifer. The groundwater of water types 1 and 2 occurs within a hydraulically active flow system in the eastern central SGMB, which show no hydrochemical-hydraulic interconnection with the western central SGMB. Furthermore, the hydrogeochemical evolution of water types 1 and 2 implies, on the one hand, a delineated flow direction towards the north and, on the other hand, areas of lower permeabilities in the south of the city of Munich, which is also consistent with the distributions of hydraulic matrix permeabilities and porosities as well as thermal groundwater anomalies from literature. Accordingly, the Upper Jurassic groundwater of type 1 and 2 has most likely been recharged subglacially in the south of the SGMB in close proximity to the Bavarian Alps. It is concluded that the subglacial infiltration systematic affirmed in the first part of this work by $^{14}C_{DOC}$ dating in the western SGMB also appears to have occurred in the central SGMB.

In summary, (i) the presence of water type 3 in the western central SGMB and (ii) a hydraulically active groundwater flow system of water type 1 and 2 in the eastern central SGMB with drainage to the north, (iii) a subglacial infiltration in the south of the eastern central SGMB and (iv) a northward groundwater flow direction within the intermediate flow system in the western SGMB, contradict previous concepts of an integrated supra-regional groundwater flow system in the Upper Jurassic reservoir. Based on these results, a groundwater flow direction from the previously assumed recharge areas in the western SGMB to the eastern central SGMB is very unlikely.

This work has shown that groundwater dating with $^{14}C_{DOC}$ and the systematic survey of water chemical data and environmental isotopes of groundwater and their interpretation using multivariate statistical methods lead to a conclusive hydrogeological picture of the Upper Jurassic geothermal reservoir in the SGMB, providing a major contribution for sustainable groundwater resource management and for the future geothermal development.

Zusammenfassung

Die tiefe Geothermie stellt eine der Schlüsseltechnologien für den Übergang zu einer klimafreundlichen Wärme- und Stromversorgung in Deutschland dar. Der tiefe karbonatische Oberjura-Grundwasserleiter im Süddeutschen Molassebecken (SGMB) ist eine der wichtigsten geothermischen Ressourcen in Europa. Dabei ist ein umfassendes hydrogeologisches Verständnis dieses hydrothermal genutzten Reservoirs entscheidend für ein verbessertes und nachhaltiges Grundwassermanagement und für die zukünftige Entwicklung dieser wichtigen, geothermisch genutzten Ressource.

Bereits seit den 1950er Jahren wurden die hydrogeologischen Eigenschaften des Oberjura-Reservoirs im SGMB in verschiedenen hydraulischen und hydrochemischen Studien untersucht. Obwohl alle Autoren mit unterschiedlichen Methoden ein mehr oder weniger konsistentes, gesamtheitlich verbundenes und überregional kommunizierendes Fließsystem für das Oberjura-Grundwasser abgeleitet haben, gibt es zum Teil erhebliche Widersprüche zwischen den hydraulischen und hydrochemischen Modellvorstellungen. Im Zuge der voranschreitenden Nutzung der tiefen Geothermie durch eine zunehmende Anzahl von tiefen Geothermiebohrungen seit Anfang der 2000er Jahre und der gezielten Exploration auf unterschiedliche Strukturen (Störungen, Gesteinsmatrix) konnten neue und wertvolle Erkenntnisse über das Oberjura-Reservoir gewonnen werden. Dabei haben allerdings vor allem die unterschiedlichen Thermalwasserfündigkeiten in den Tiefenbohrungen im SGMB eine weitere intensive wissenschaftliche Auseinandersetzung mit dem Oberjura-Reservoir erforderlich gemacht. Zahlreiche Untersuchungen der petrologischen, faziellen und hydraulischen Eigenschaften der Reservoirgesteine haben gezeigt, dass das Oberjura-Reservoir deutlich komplexer strukturiert ist als bisher angenommen. Es treten lokal und regional deutliche Unterschiede der geologischen und hydraulischen Eigenschaften der Reservoirgesteine sowie der hydrochemischen Beschaffenheit des erschlossenen Grundwassers auf.

Daraus lässt sich schlussfolgern, dass ein gesamtheitliches und konsistentes hydrogeologisches Verständnis des Oberjura-Reservoirs im SGMB bisher noch fehlt. Bei großangelegten hydrogeologischen Untersuchungen großer und komplexer Grundwassersysteme in tiefen Sedimentbecken hat sich die Interpretation der hydrochemischen Zusammensetzung des Tiefengrundwassers als äußerst praktikabel erwiesen. Das Ziel dieser Arbeit ist, das Grundwasser an diversen tiefen Oberjura-Thermalwasserbohrungen mit Hilfe von wasserchemischen Daten und Umweltisotopen hydrochemisch zu charakterisieren, um (i) mögliche Beziehungen zwischen dem infiltrierenden Grundwasser in den bisher angenommenen Neubildungsgebieten im westlichen SGMB und den tiefen Geothermalwässern im zentralen SGMB abzuleiten sowie (ii) die bestehenden Widersprüche im Grundwasserströmungssystem des Oberjura-Grund-

wasserleiters aufzulösen. Um das Verständnis des Grundwasserzirkulationssystems im Oberjura-Grundwasserleiter zu verbessern, werden auch die Wechselwirkungen mit den darüber liegenden tertiären Sedimenten untersucht, um schließlich ein konsistentes hydrogeologisches Verständnis des tiefen Oberjura-Reservoirs im SGMB zu erhalten. Dies ist besonders wichtig, um das Explorationsrisiko bei der Festlegung zukünftiger geothermischer Ziele zu reduzieren und somit zu einem nachhaltigen Ressourcenmanagement des geothermisch genutzten Reservoirs beizutragen.

Eine große Herausforderung bei der Charakterisierung der Grundwasserzirkulation ist die Datierung von Grundwässern mit scheinbaren Altern von mehr als 1.000 Jahren. Die Grundwasserdatierung mit Radiokarbon am gelösten anorganischen Kohlenstoff ($^{14}C_{DIC}$) ist dabei eine sehr etablierte Methode zur Bestimmung scheinbarer Grundwasseralter von bis zu 30.000 Jahren. Allerdings weist die $^{14}C_{DIC}$-Datierung aufgrund von verschiedenen natürlichen (bio)-chemischen und physikalischen Prozessen im Untergrund vor allem in karbonatischen Grundwasserleitern deutliche Einschränkungen auf, was in der Regel zu überschätzenden $^{14}C_{DIC}$-Modellaltern führt.

Im ersten Teil dieser Arbeit wird daher erstmals systematisch ein vielversprechender Ansatz zur Datierung von altem Oberjura-Grundwasser mit ^{14}C am gelösten organischen Kohlenstoff ($^{14}C_{DOC}$) an sieben tiefen Brunnen im westlichen und nördlichen SGMB getestet. Bisher war die komplexe und zeitaufwendige Konzentration des datierbaren organischen Kohlenstoffs im Grundwasser eine der Hauptherausforderungen der $^{14}C_{DOC}$-Datierung. Deswegen wird die Aufkonzentration des DOC in dieser Arbeit stattdessen mit der neu etablierten, einfach anwendbaren, zeitsparenden und robusten Festphasenextraktion (SPE) mit einem Styrol-Divinylbenzol-Copolymer-Sorbent (PPL) durchgeführt. Die im Anschluss ermittelten $^{14}C_{DOC}$-Aktivitäten und berechneten scheinbaren organischen Radiokarbonalter (ORA) werden mit der wasserchemischen Beschaffenheit und den stabilen Wasserisotopensignaturen ($\delta^{18}O$ und δD) sowie den konventionell bestimmten $^{14}C_{DIC}$-Grundwasseraltern verglichen.

Die Ergebnisse zeigen, dass die berechneten ORA am untersuchten Oberjura-Grundwasser mit $^{14}C_{DOC}$ wie erwartet niedriger sind als die korrigierten $^{14}C_{DIC}$-Alter (IRA), die im Allgemeinen zu einer Überschätzung der scheinbaren Grundwasseralter geführt haben. Die Plausibilität der ORA wurde durch die Integration der berechneten scheinbaren Grundwasseralter mit den stabilen Wasserisotopenwerten von $\delta^{18}O$ und Edelgas-Infiltrationstemperaturen (NGTs) in atmosphärische Klimamodelle aus der Literatur überprüft. Diese erfolgreiche Integration der klimatischen Informationen der Grundwasserneubildungsbedingungen in eine zeitliche Abfolge unterstützt die Anwendbarkeit der SPE-PPL-Methode für die $^{14}C_{DOC}$-Datierung im Oberjura-Grundwasser. Darüber hinaus kann das abgeleitete Oberjura-Grundwasseraltersmuster innerhalb des westlichen SGMB auch in bestehende Konzepte der subglazialen Infiltration und des intermediären Grundwasserströmungssystems integriert werden. Zusätzlich

wird auch eine Grundwasserströmung und Entwässerung hin zur Donau als Vorfluter am nördlichen Rand des SGMB bestätigt, was für das Verständnis der gesamtheitlichen Strömungssystematik im Oberjura-Grundwasserreservoir von großer Bedeutung ist.

In einem zweiten Teil dieser Arbeit werden zahlreiche wasserchemische Parameter und ausgewählte Umweltisotope δD, $\delta^{18}O$ und $^{87}Sr/^{86}Sr$ konsistent an tiefen Grundwässern von allen 24 verfügbaren Oberjura-Thermalwasserbohrungen im zentralen SGMB untersucht. Zusätzlich werden an einigen Grundwässern noch Messungen der Edelgaskonzentrationen (He, Ne, Ar, Kr, Xe) und Edelgasisotopen ($^{3}He/^{4}He$, $^{40}Ar/^{36}Ar$) durchgeführt, um die Grundwasserneubildungsbedingungen mit den berechneten NGTs besser zu charakterisieren sowie die zeitliche Entwicklung des Grundwassers durch Datierungen mit ^{4}He und ^{40}Ar zu bestimmen. Um darüber hinaus verschiedene Faktoren und hydrogeologische Prozesse aufzudecken, die einen Einfluss auf die hydrochemische Zusammensetzung und damit auf die Genese des Oberjura-Grundwassers haben, werden die gewonnenen Messwerte erstmals systematisch mit den multivariaten statistischen Methoden der explorativen Faktorenanalyse (EFA) und hierarchischen Clusteranalyse (HCA) ausgewertet.

Anhand der Interpretation der HCA wurden drei verschiedene Wassertypen 1 bis 3 mit zum Teil unterschiedlicher Herkunft und Genese abgeleitet, die durch unterschiedliche hydrogeologische Prozesse beeinflusst worden sind. Die Ergebnisse zeigen, dass gering mineralisierte Grundwässer der Wassertypen 1 und 2 im östlichen zentralen SGMB unter meteorischen kaltklimatischen Bildungsbedingungen infiltiert sind. Die $^{87}Sr/^{86}Sr$-Verhältnisse und Signaturen der stabilen Wasserisotopen deuten zudem überwiegend auf eine geringe Wasser-Gesteins-Interaktion mit der Oberjura-Gesteinsmatrix hin. Im Gegensatz dazu implizieren sowohl die hydrochemische Beschaffenheit als auch die erhöhten scheinbaren Grundwasseralter des hochmineralisierten Grundwassers vom Typ 3 eine nennenswerte Wasser-Gesteins-Interaktion mit terrestrischen Sedimenten. Das Oberjura-Grundwasser vom Typ 3, das ausschließlich im westlichen zentralen SGMB erschlossen wird, besitzt demzufolge eine hydraulische Verbindung zu den darüber liegenden tertiären Sedimenten.

Das räumliche Auftreten dieser Wassertypen erlaubt eine konsistente hydrochemische Zonierung des Oberjura-Grundwassers im zentralen SGMB, die zusammen mit den $^{14}C_{DOC}$-Datierungsergebnissen im westlichen SGMB zu einem schlüssigen hydrogeologischen Verständnis der Grundwasserfließsystematik im Oberjura beiträgt. Das Grundwasser der Wassertypen 1 und 2 wird offenbar innerhalb eines hydraulisch aktiven Fließsystems im östlichen zentralen SGMB erschlossen, das keine hydraulisch-hydrochemische Verbindung zum Grundwasser im westlichen zentralen SGMB aufweist. Darüber hinaus kann anhand der hydrogeochemischen Entwicklung der Wassertypen 1 und 2 sowohl (i) eine allgemeine Grundwasserfließrichtung nach Norden als auch (ii) eine geringere hydraulische Matrixpermeabilität im Oberjura-Grundwasserleiter südlich von München abgeleitet werden. Diese Ergebnisse stehen im Einklang

mit den Verteilungen der hydraulischen Matrixpermeabilitäten und Porositäten der Oberjura-Gesteine sowie der Temperaturanomalie im Wasserburger Trog aus aktuellen Studienergebnissen und Veröffentlichungen. Daraus folgt, dass das Grundwasser von Typ 1 und 2 im östlichen zentralen SGMB demnach wahrscheinlich im Süden des SGMB in unmittelbarer Nähe der bayerischen Alpen subglazial neugebildet worden ist. Es ist deshalb anzunehmen, dass die subglaziale Infiltrationssystematik, die im ersten Teil dieser Arbeit durch $^{14}C_{DOC}$-Datierungen im westlichen SGMB bestätigt werden konnte, wohl auch im zentralen SGMB bei der Grundwasserneubildung vorherrschend war.

Zusammenfassend zeigen die Ergebnisse dieser Arbeit, dass (i) das Vorhandensein des Wassertyps 3 im westlichen zentralen SGMB, (ii) ein hydraulisch aktives Grundwasserfließsystem der Wassertypen 1 und 2 im östlichen zentralen SGMB mit nordwärts gerichteter Fließrichtung, (iii) eine subglaziale Infiltration im Süden des östlichen zentralen SGMB sowie (iv) eine nordwärts gerichtete Grundwasserfließrichtung im intermediären Fließsystem im westlichen SGMB den bisherigen Vorstellungen eines einheitlichen und überregional miteinander kommunizierenden Grundwasserfließsystems im Oberjura-Reservoir widersprechen. Die bisher angenommene Grundwasserströmungsrichtung von den westlichen Infiltrationsgebieten in das östliche und zentrale SGMB kann anhand dieser Ergebnisse nicht bestätigt werden.

Diese Arbeit zeigt, dass die Grundwasserdatierung mit $^{14}C_{DOC}$ und die systematische Erhebung von wasserchemischen Daten und Umweltisotopen des Oberjura-Grundwassers sowie deren Interpretation mit multivariaten statistischen Methoden zu schlüssigen Ergebnissen des geothermischen Oberjura-Reservoirs im SGMB führen und liefert damit einen wichtigen Beitrag für ein nachhaltiges Grundwasserressourcenmanagement und die zukünftige geothermische Erschließung.

Publications

Some text, figures and tables have appeared previously in the following scientific peer-reviewed publications:

Groundwater dating with dissolved organic radiocarbon: A promising approach in carbonate aquifers
Florian Heine & Florian Einsiedl
Applied Geochemistry (2021), Volume 125, 1-13
doi: 10.1016/j.apgeochem.2020.104827

Hydrochemical Zoning and Chemical Evolution of the Deep Upper Jurassic Thermal Groundwater Reservoir Using Water Chemical and Environmental Isotope Data
Florian Heine, Kai Zosseder & Florian Einsiedl
Water (2021), Volume 13(9), 1-35
doi: 10.3390/w13091162

Acknowledgements

This thesis is the product of an idea of some people, their effort to turn the idea into a project, the given time to carry out this project and the environment that was created to finally reach the goal.

First of all, I would like to thank my supervisors Prof. Florian Einsiedl and Dr. Kai Zosseder for providing me with a PhD position in an interesting environment at the Chair of Hydrogeology. I appreciate very much that I had the opportunity to work in my preferred research areas and to be a part of the scientific geothermal group. Furthermore, I would like to thank my mentor Dr. Stephan Weise for advising me and taking over the mentorship. I would like to thank everyone for the supervision I have received over the past few years and the freedom I have had in my work, as well as for the opportunities to meet interesting people and, above all, to grow with the tasks I have been given.

I would also like to thank Dr. Jochen Schneider very much, who accompanied and supported me and my research during the sampling campaign with advice, equipment, manpower and always an open ear, and also gave me the appropriate platform for presenting my work. Furthermore, I would like to thank Mr. Michael Heidinger, who became an important contact person towards the end of my PhD and with whom I discussed many complex interrelationships of various isotope methods. Without all your support, this work would not have become what it is today.

Furthermore, I would like to thank all those responsible for funding and executing the various research projects in which I was allowed to work, to name IsoMol, IsoChem, GAB, GeoMare and Dolomitkluft. In this context, I would especially like to thank Dr. Thomas Fritzer and Dr. Timo Spörlein as direct contacts at the LfU. Without the doors that were opened by these projects, I would not have been able to carry out my work. I would also like to thank all the operators of the geothermal and balneological plants and spas where I was allowed to take samples, as well as the numerous contact persons and helping hands on site.

The entire PhD team of the Chair of Hydrogeology, to whom I would also like to express my warmest thanks, also played a major role in the completion of this work. Thanks to Alejandra, Anne, Daniel, Fabian, Felix, Florian, Lisa, Manuel, Markus and Theis for the good and collegial cooperation, the great lunch breaks, the shared hobbies and the few amazing conferences and PhD events. With you guys, it was possible to get through some of the difficult phases that occur in every PhD. I can truly say that we have become not only colleagues but also good friends. Special thanks to Susanne Thiemann for her untiring efforts in the lab measuring my samples, Dr. Bernhard Köhl for shared sampling experiences and Dr. Elena Mraz for proofreading this thesis and all her help during the last years.

I would also like to thank all the people who accompanied me on my way in my studies and showed me the way into the wonderful world of hydrogeology. I was lucky enough to be guided by many idols, the list of which would be endless here. Above all, I would like to thank Prof. Traugott Scheytt and Dr. Dirk Radny, as well as Kazem Bazrafshan and the entire Eschenbräu Group.

Last but not least, I would like to thank my whole family and especially my love Karin for the unfailing support over the past years. You have always been an anchor, kept up or taken the pressure off me and I am very fortunate that I can always count on you. I am happy to announce that we can improve the work-life balance back into a life-work balance.

Contents

Summary v

Zusammenfassung ix

Publications xiii

Acknowledgements xv

Contents xvii

List of Figures xxi

List of Tables xxv

Acronyms xxvii

Glossary xxix

1 Introduction 1
- 1.1 The role of geothermal heat as a renewable energy in Germany 1
- 1.2 The Upper Jurassic aquifer in the South German Molasse Basin 4
- 1.3 Structure of the thesis 5

2 State of the Art 7
- 2.1 Deep groundwater in sedimentary basins 7
- 2.2 Reservoir characterisation based on hydrogeochemical groundwater evolution . 9
- 2.3 The concept of the apparent groundwater age 11
- 2.4 Hydrochemical tools for tracing hydrogeological processes 13
  - 2.4.1 Water chemistry 13
  - 2.4.2 Stable water isotopes 14
  - 2.4.3 Strontium isotopes 15
- 2.5 Groundwater dating 16
  - 2.5.1 Dating with radioactive isotopes 17
    - 2.5.1.1 Processes affecting the $^{14}C_{DIC}$ dating 18
    - 2.5.1.2 Advantages of $^{14}C_{DOC}$ dating 21
    - 2.5.1.3 Preparation methods of dissolved organic carbon 22

2.5.2 Dating with radiogenic isotopes . . . 26
2.5.2.1 Helium . . . 27
2.5.2.2 Argon . . . 28
2.6 The study area in the South German Molasse Basin . . . 29
2.6.1 Geological description . . . 29
2.6.2 Upper Jurassic groundwater flow system: a historical review . . . 35
2.6.2.1 The first phase of deep groundwater studies . . . 36
2.6.2.2 Second phase: further development of the hydrogeological system . . . 39
2.6.2.3 The third phase to expand the concepts for the hydrogeological model . . . 44
2.6.2.4 Short summary . . . 50

3 Motivation, aims and objectives 53

4 Methods 57
4.1 Sampling und sample preparation . . . 57
4.1.1 Water chemical parameters . . . 58
4.1.2 Stable water isotopes . . . 59
4.1.3 Strontium isotopes . . . 59
4.1.4 Noble gases, $^{3}He/^{4}He$ and $^{40}Ar/^{36}Ar$ . . . 59
4.1.5 Inorganic radiocarbon ($^{14}C_{DIC}$) and $\delta^{13}C_{DIC}$ . . . 60
4.1.6 Organic radiocarbon ($^{14}C_{DOC}$) . . . 60
4.1.6.1 Sampling and extraction method . . . 60
4.1.6.2 $^{14}C_{DOC}$ measurements . . . 63
4.2 Calculation of radiocarbon ages . . . 63
4.3 Calculation of noble gas infiltration temperatures (NGTs) . . . 64
4.4 Determination of apparent groundwater ages with radiogenic noble gas isotopes 66
4.5 Multivariate statistical techniques . . . 68
4.5.1 Exploratory factor analysis EFA . . . 69
4.5.2 Hierarchical cluster analysis HCA . . . 71

5 Results and discussion 73
5.1 Groundwater dating with dissolved organic radiocarbon . . . 73
5.1.1 Hydrochemical composition and stable water isotopes of groundwater . . 73
5.1.2 Comparison of $^{14}C_{DIC}$ and $^{14}C_{DOC}$ activities . . . 75
5.1.3 Differences of dating results with the radiocarbon species of DIC and DOC 80
5.1.4 Cross check of the dating results with existing temperature models . . . 81

5.1.5 Synopsis of the dating results in the hydrogeological context 83
5.1.6 Extraction efficiencies and limitations of SPE-PPL 84
5.1.6.1 Extraction efficiencies 84
5.1.6.2 Discussion of possible limitations of the proposed extraction method 85
5.1.7 Short conclusion 86
5.2 Hydrochemical zoning and chemical evolution of the deep Upper Jurassic thermal groundwater in the central SGMB 88
5.2.1 Results of multivariate statistical analyses HCA and EFA 88
5.2.1.1 Classification of different water types of the Upper Jurassic reservoir in the SGMB based on HCA 88
5.2.1.2 Identification of factors and hydrogeological processes affecting the hydrochemical water composition 90
5.2.2 Chemical analyses of grouped water types 94
5.2.3 Assessing recharge conditions and water-rock interaction 101
5.2.3.1 Noble gas infiltration temperatures NGTs and stable water isotopes 101
5.2.3.2 Tracing water-rock interaction with $^{87}Sr/^{86}Sr$ signatures 104
5.2.3.3 Mixing processes and origin of salinity using $\delta^{18}O$ and Cl^- . . . 106
5.2.4 Calculation of apparent water ages by radiogenic noble gas isotopes . . . 108
5.2.5 Regional linking of water type classification and hydrogeochemical genesis of the Upper Jurassic reservoir 111
5.2.6 Subglacial groundwater recharge - a plausibility assessment 114
5.2.6.1 Specific signatures of stable water isotopes 115
5.2.6.2 Subglacial recharge systematic and recharge area 115
5.2.7 Short conclusion 117

6 Synoptic discussion and conclusions 119
6.1 Implications of groundwater dating with $^{14}C_{DOC}$ 119
6.2 Deduction of the groundwater circulation system in the central SGMB 120
6.2.1 Groundwater recharge and flow system 120
6.2.2 Increased water-rock interaction - an indicator for low matrix permeabilities 122
6.2.3 Outlook and future research 123

Bibliography 125

Appendices 157
A.1 Results of data measurements for Sec. 5.2 160

A.2 Correlation matrix for Sec. 5.2 163
A.3 Results of Monte Carlo simulation for deriving NGT 164
A.4 Supplementary figures 166

List of Figures

1.1 Contribution of renewable energies to the total energy market in Germany. . . . 2
1.2 Geothermal resources in Germany. . . . 3

2.1 Main aspects of the hydrogeochemical evolution of groundwater. . . . 10
2.2 Piston-flow model for determining the apparent groundwater age. . . . 11
2.3 Different flow models for the calculation of the apparent groundwater age. . . . 12
2.4 Relationship between stable water isotope signatures of meteoric groundwater caused by exchange processes in the water cycle and specific water-rock interaction (Clark, 2015). . . . 15
2.5 Distribution of the strontium isotope ratio in Phanerozoic seawater. . . . 16
2.6 Approximate dating range for isotopes and other tracer applications. . . . 17
2.7 Cycle and associated fractionation of inorganic radiocarbon ^{14}C. . . . 19
2.8 Comparison of correction models with the relationship of $^{14}C_{DIC}$ and $\delta^{13}C_{DIC}$. . . 20
2.9 Processes to consider for groundwater dating with $^{14}C_{DIC}$ and $^{14}C_{DOC}$. . . . 21
2.10 Differentiation of the operational species of dissolved organic carbon (DOC). . . . 23
2.11 Comparison of the main DOC extraction methods 24
2.12 Overview of the South German Molasse Basin (SGMB). . . . 30
2.13 Chronostratigraphical chart. . . . 31
2.14 Simplified geological cross section through the western South German Molasse Basin (SGMB). . . . 32
2.15 Distribution of the depositional environment, permeable domains and transition zone facies for the Upper Jurassic during the Oxfordian (Mraz, 2019). . . . 33
2.16 Regionalised matrix permeability in the greater area of the city of Munich. . . . 34
2.17 Temperature distribution of the SGMB based on data from GeotIS (Agemar et al., 2014a). . . . 35
2.18 Comparison of hydrogeological groundwater concepts for the Upper Jurassic aquifer in the South German Molasse Basin (SGMB). . . . 36
2.19 Hydraulic groundwater potentials for the Upper Jurassic aquifer in the South German Molasse Basin (SGMB) (modified from Lemcke (1976)). . . . 38
2.20 Hydraulic groundwater potentials for the Upper Jurassic aquifer in the South German Molasse Basin (SGMB) and southern Upper Jurassic outcrops (Andres and Wirth, 1981; Andres and Frisch, 1981). . . . 39
2.21 Hydraulic groundwater potentials for the Upper Jurassic aquifer in the South German Molasse Basin (SGMB) after Lemcke (1987). . . . 40

2.22 Hydraulic groundwater potentials for the thermal water in the Upper Jurassic aquifer of the South German Molasse Basin (SGMB) after Frisch and Huber (2000). 43
2.23 Hydraulic groundwater potentials for the Upper Jurassic aquifer in the South German Molasse Basin (SGMB) based on data from geothermal wells in the central SGMB after Wagner et al. (2009) and Savvatis et al. (2015). 45
2.24 Distribution of water chemical types and hydrochemical provinces in the Bavarian SGMB with hydrochemical evolution paths after Birner et al. (2011). 46
2.25 Overview of apparent ^{81}Kr model ages and delineated recharge areas via cross-formational flow after Heidinger et al. (2019). 48
2.26 Chloride distribution within the Upper Jurassic aquifer in the South German Molasse Basin (SGMB) after Stober et al. (2014). 49

4.1 Overview of sampling points in the South German Molasse Basin (SGMB). 58
4.2 Sample preparation and extraction procedure for DOC of groundwater samples according to a modified scheme after Dittmar et al. (2008) and Li et al. (2016). . . 61
4.3 Loading of the SPE-PPL cartridge. 62
4.4 Visualisation of the principles of multivariate statistical methods exploratory factor analysis and hierarchical cluster analysis. 69

5.1 Piper plot of the water samples. 74
5.2 Plot of stable water isotope signatures. 75
5.3 Measured radiocarbon activities of organic and inorganic carbon. 77
5.4 Linear mixing of the two Endmembers OF and BW. 79
5.5 Plot of the calculated radiocarbon ages with DIC (IRA) and DOC (ORA). 80
5.6 Plot of the temperature sensitive stable water isotope δ^{18}O and calculated organic radiocarbon ages (ORA). 82
5.7 Synopsis of the dating results. 83
5.8 Optimal cluster numbers. 89
5.9 Dendrogram plots of hierarchical cluster analysis (HCA). 90
5.10 Scree plots of **(a)** parallel analysis and **(b)** empirical Kaiser criterion with cumulative variance of the eigenvalues. 91
5.11 Factor loadings (>0.4) for the exploratory factor analysis (EFA). 93
5.12 Piper plot and characterisation of the hydrochemical facies after Furtak and Langguth (1967) for thermal water samples. 94
5.13 Distribution plots of water chemical parameters. 100
5.14 Plot of stable water isotope signatures for samples of water types 1 to 3 with global (GMWL) and local (LMWL) meteoric water lines. 103

5.15 $^{87}Sr/^{86}Sr$ ratios of the thermal water in dependency of (**a**) the Sr^{2+} concentration and (**b**) the stable water isotope $\delta^{18}O$. 105
5.16 Cl^- concentrations and $\delta^{18}O$ values of the thermal waters. 107
5.17 Results of noble gas isotope measurements. 109
5.18 Areal distribution of the water types and hydrochemical zoning of the Upper Jurassic aquifer with Stiff diagrams. 112

A.1 Output of PANGA (Jung and Aeschbach, 2018) for Monte Carlo simulation results (5000 runs) for the fitting parameter A (excess air) using the CE-model (Aeschbach-Hertig et al., 2000). 164
A.2 Output of PANGA (Jung and Aeschbach, 2018) for Monte Carlo simulation results (5000 runs) for the fitting parameters F (fractionation factor) and T (noble gas equilibrium temperature) using the CE-model (Aeschbach-Hertig et al., 2000). 165
A.3 Cross section along an ice flow line showing hydraulic conditions during a glacial cycle after Lemieux et al. (2008) and Grundl et al. (2013) 166
A.4 Tectonic map of the Subalpine Molasse of Upper Bavaria between Rosenheim and Salzburg with extent of glaciers during the last ice ages. 166

List of Tables

5.1 Physico-chemical composition of the groundwater samples. 76
5.2 Isotopic data and calculated inorganic (IRA) and organic (ORA) radiocarbon ages. 76
5.3 Linear mixing of isotope data with the two end members OF and BW for the mixing of two water bodies around the well GR. 79
5.4 Efficiencies of extracted PPL fraction based on the DOC concentration, extraction volume, theoretical extracted carbon ($C_{max,extr.}$) and factual extracted carbon ($C_{extr.}$). 85
5.5 Factor loadings (>0.4) of the three-factor solution with the multi likelihood method and oblique (oblimin) rotation with communalities (h^2) and uniqueness (u^2) for each parameter, factor loadings and explained variance for each factor, as well as results of statistical tests. 92
5.6 Minimum (min), maximum (max) and mean values (mean) and standard deviation (SD) of the hydrochemical parameters for all water samples (summary) and for water type 1 to 3. 95
5.7 Noble gas infiltration temperatures (NGTs) with PANGA (Jung and Aeschbach, 2018) using the CE-model (Aeschbach-Hertig et al., 2000) with Ne, Kr and Xe. . . 101
5.8 Determination of crustal fluxes $J_{^4He}$ and $J_{^{40}Ar}$ with apparent ^{81}Kr groundwater ages. 110

A.1 Physico-chemical composition of the groundwater samples. Key:$^+$ results from duplicate measurements. 160
A.2 Isotope measurements and noble gas concentration results. Key:$^+$ results from duplicate measurements of stable water isotopes. 161
A.3 Results of noble gas concentrations. 162
A.4 Ranked correlation matrix with Spearman's ρ coefficient. 163

Acronyms

λ	Decay rate of a radionuclide, in 1/s
$\lambda_{1/2}$	Half-life of a radionuclide, in years
CHP	Combined power and heating plants
DIC	dissolved inorganic carbon
DOC	dissolved organic carbon
EFA	Exploratory factor analysis
EGS	Enhanced-Geothermal-Systems
GeotIS	The Geothermal Information System for Germany, www.geotis.de
HCA	Hierarchical cluster analysis
LIAG	Leibniz-Institut für Angewandte Geophysik
LNH	Landshut-Neuoetting High
MSF	Munich & Markt-Schwaben Fault (MSF) represents an important major fault system in the greater area of the city of Munich
mTVD	Metres true vertical depth
NGT	Noble gas infiltration temperature, in °C
OMM	Upper Marine Molasse
OSM	Upper Freshwater Molasse
PPL	Styrene divinylbenzene polymer sorbent
ppm	parts per million, e.g. mg/kg or simplified mg/l

SGMB	South German Molasse Basin
SPE	Solid phase extraction
SPE-PPL	Solid phase extraction with styrene divinylbenzene polymer sorbents
TDS	Total dissolved solids, in mg/l or ppm
UBA	Umweltbundesamt
UMM	Lower Marine Molasse
UNFCCC	United Nations Framework Convention on Climate Change
USM	Lower Freshwater Molasse

Glossary

Age mass	The age mass is the product of the water mass and its age, and age mass is assumed to be conserved during mixing (Goode, 1996). It is defined as the "total water mass" $\times$ "the average residence time" (total mass divided by rate of recharge) $\times$ "the age mass production rate" (Phillips and Castro, 2014)
Apparent groundwater age	The average age over the water molecules or accumulated age masses in a sample, calculated using a geochemical age dating technique, how long each molecule has resided in the subsurface (Bethke and Johnson, 2008)
Brine	or "fossil brine". The term is generally used for highly saline groundwater with TDS >100,000 ppm (Davis, 1964; Carpenter, 1978)
Connate water	From Latin "con" and "natus" - born with. Describes unaltered (meteoric) fresh- or seawater that is syn-sedimentary trapped in the pore matrix of the rocks (Lane, 1908)
Formation water	Groundwater that is pore water present in the reservoir rock in sedimentary basins prior to the disturbance of the reservoir rock by e.g. drilling (Case, 1955)
Fossil water	Groundwater that has been out of contact with the atmosphere for at least an appreciable part of a geologic period and is synonymously to connate water and its evolutes (White, 1957)
Juvenile water	From Latin: "juvenis" - young water. Juvenile water originates from a young magmatic cycle deep in the earth's crust and has never been participated in the hydrological circle (Lane, 1908; Müller, 1999)

Mean residence time	The residence time is the time since the aliquots of water in a sample were recharged. A water sample comprises numerous aliquots of water with a distribution of residence times, which is expressed as the mean residence time (Cartwright et al., 2017, 2020)
Meteoric water line	Represents a line in the plot of stable water isotopes (δD and δ^{18}O) of precipitated fresh rain, snow or meltwater (Craig, 1961). Subtypes can be the global meteoric water line (GMWL) [dD = 8 $\times$ δ^{18}O +10]. or local meteoric water lines (LMWL) (Stumpp et al., 2014)
Meteoric water	From Greek: "meteoron" -celestial phenomenon. Meteoric water derived from rain, snow, streams, and other bodies of surface water that has entered the subsurface and percolates throug the rocks (Lane, 1908; Kharaka and Hanor, 2014)
Oilfield waters	Commonly defined as water resources which are accompanying oil or gas in hydrocarbon-rich fields, which may have been formed syngenetically to petroleum production, accompanied by fossil water or influenced by younger meteoric water (Chebotarev, 1955b; White, 1957; Collins, 1975). They generally fall in the category of formation water (Amajor and Gbadebo, 1992; Whittemore, 1995)
Salinity	Criteria for the differentiation of groundwater. The salinity is the mass of dissolved salts in the groundwater which are not subject to hydrolysis, e.g. NaCl, $CaCl_2$. Commonly in mg/l or ppm

Chapter 1

Introduction

When the water starts boiling it is foolish to turn off the heat.

Nelson Mandela

The 197 countries of the United Nations Framework Convention on Climate Change (UNFCCC) have reached a climate agreement on the 21st Conference of the Parties in 2015 in Paris to reduce the increase of the global mean temperature to preferably 1.5 °C (and maximum 2 °C) compared to the pre-industrial levels and to achieve greenhouse gas neutrality in 2050 (UNFCCC, 2015). In order to attain these ambitious goals, the German government has therefore formulated the climate targets (Klaus et al., 2010) and has adopted the Climate Protection Program 2030, which promotes the expansion of renewable energies and 100 % renewable electricity supply by 2050 (BRD, 2019).

1.1 The role of geothermal heat as a renewable energy in Germany

Geothermal energy is a key technology in the context of the heat and power transition to a climate-friendly supply with growing importance worldwide (Bertani, 2016; Weber et al., 2019). The "apparently endless" and carbon-free energy source can be used for electrical power generation and for (district) heating purposes. The advantages of geothermal energy are the independence of seasonal and daily fluctuations, decentralised generation and baseload capability (Agemar et al., 2014b; Bauer et al., 2014; Eyerer et al., 2020). In Germany, a fundamental distinction is made between the use of the shallow geothermal energy down to a depth of approximately 400 m and the deep geothermal energy with depths higher than 1,000 m (Bauer et al., 2014; Fritzer et al., 2019).

The contribution of renewable energies to the total energy budget was around 17.4 % in 2019 in Germany (Fig. 1.1). About 54 % of the final energy consumption is required for district and space heating, hot water, and process heat but renewable energies covered only 14.5 % of the heat consumption in 2019 (UBA, 2020; Weber et al., 2019). Up to now, the geothermal electric power generation plays with $<$0.1 % of the total renewable electricity budget only a minor role in Germany (UBA, 2020). In contrast, the contribution of geothermal heat to the renewable energies budget is slightly higher with 3 % and the development of district heating plants is growing continuously (UBA, 2020; Weber et al., 2019). For example, the district heating vision of the "Stadwerke München (SWM)" for the city of Munich in Southern Bavaria includes the

development of 400 MW_{th} provided by the optimised placement of around 40 deep geothermal wells as a major contributor by 2040 (Rioseco et al., 2018; Weber et al., 2019). The vision is in line with the "Masterplan Geothermie" of the Bavarian state government to cover 25 % of the required heat by geothermal energy in the long term (GAB, 2020).

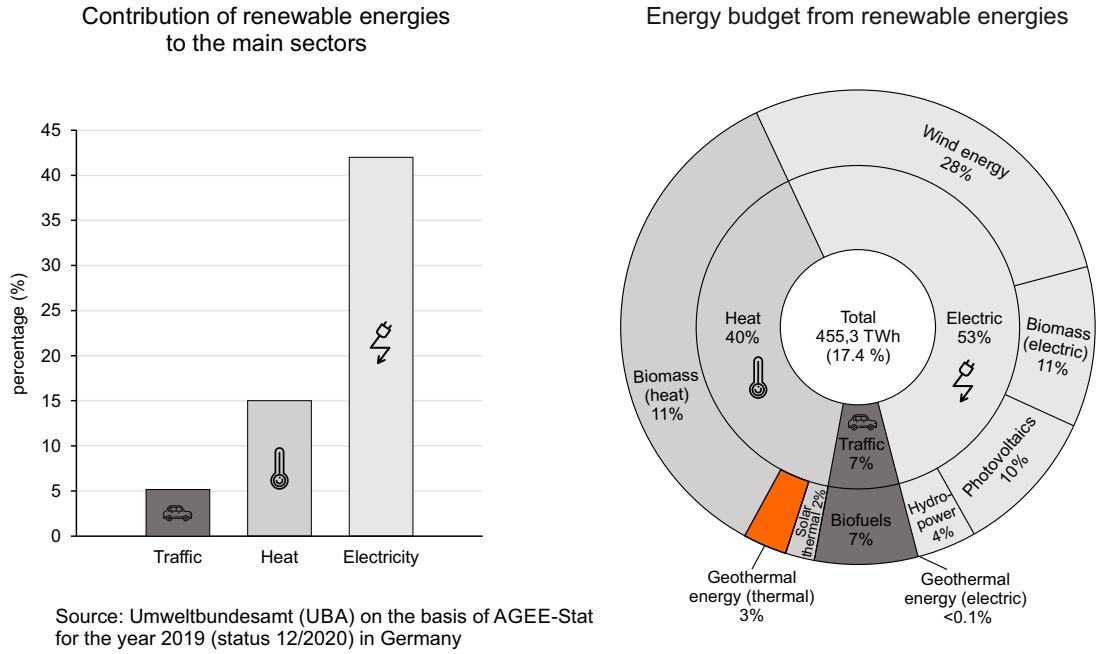

Figure 1.1: Contribution of renewable energies to the total energy market in Germany and contribution of each sector in 2019. Data from UBA (2020).

Geothermal heat that is stored beneath the subsurface can be exploited for deep geothermal applications in hydrothermal or petrothermal systems (Bauer et al., 2014). The suitability of geological formations for exploitation by hydrothermal or petrothermal systems is mainly determined by thermal (temperature) and hydraulic (effective matrix porosity, permeability and aquifer thickness) properties. The main difference between these both concepts is the water availability in the subsurface (Agemar et al., 2014b).

In hydrothermal systems, the hot groundwater hosted in the aquifer is used directly by pumping it to the surface, deheating, and injecting it back underground via an injection well. Aquifers, including faults and fault zones, are classified by the groundwater temperature into hot (>100 °C), warm (between 60 and 100 °C) and thermal (at least 20 °C) hydrothermal systems (Agemar et al., 2014b). For electric power generation, fluid temperatures must be at least >100 °C, whereas the inlet temperature for district heating can be considerably lower (>60 °C) (Bauer et al., 2014; Stober et al., 2014; TUM, 2020). The water supply of the aquifer for successful deep geothermal energy exploitation is depending on the aquifer type with reservoir temper-

atures of >60 °C) and, depending on the inlet temperature, pumping rates of approximately >35 l/s (Bauer et al., 2014; Agemar et al., 2014b).

In petrothermal systems, the heat is stored in rocks with low porosities (<10 %) and permeabilities (<1 mD) and is exploited without any need of water-bearing rock formations by using the application of Enhanced-Geothermal-Systems (EGS) (Agemar et al., 2014b; Moeck, 2014). To increase the permeability with EGS, an artificial fluid is pumped through an injection well into a hot (commonly >150 °C), low permeable and brittle reservoir rock where induced fractures systems and fault are used as a natural heat exchanger (Bauer et al., 2014).

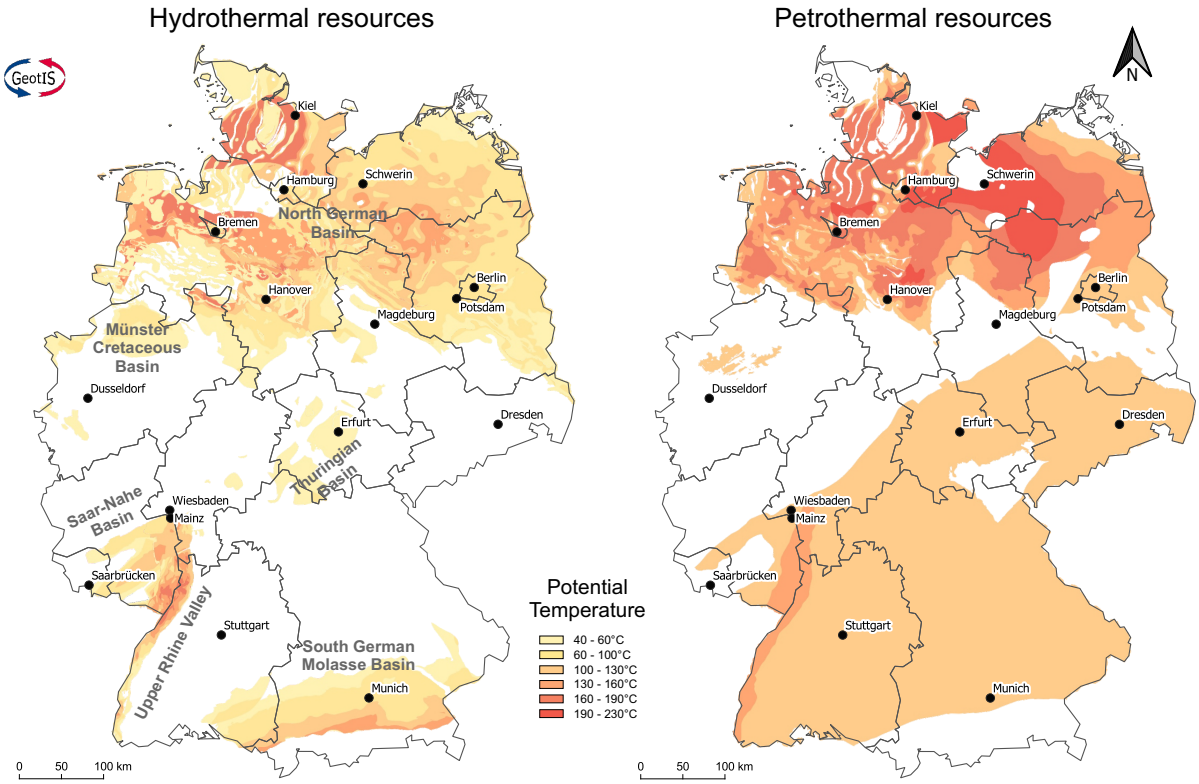

Figure 1.2: Geothermal resources in Germany with potential areas for hydrothermal and petrothermal systems. Data from GeotIS (LIAG) (Agemar et al., 2014a).

In Germany, the (theoretical) geothermal potential of hydrothermal systems is only around 10 to 15 % compared to petrothermal systems, but it is the main source for geothermal energy (Paschen et al., 2003; Bauer et al., 2014). Geothermal heat is produced directly with hydrothermal systems in more than 180 larger installations, but around 85 % of the total geothermal capacity is produced by only 29 district heating and combined power and heating plants (CHP) (Weber et al., 2019). The main hydrothermal resources with the highest energy potential are predominantly concentrated in three regions: the North German Basin, the Upper Rhine Valley and the South German Molasse Basin (Fig. 1.2). These regions are characterised by different

aquifers types, rock materials and, thus, have different potentials in terms of thermal and hydraulic properties (Agemar et al., 2014a; Stober et al., 2014). Additionally, the water chemical composition and characteristics of the geothermally used fluids from these regions are very different, which is of central importance in terms of scalings, corrosion and thermal performance of the systems (Stober et al., 2014; Bozau et al., 2015). Despite the very large potential of petrothermal systems, they do not currently play a major role in Germany. However, they are considered to have the greatest development potential in the future (Jain et al., 2015; GAB, 2020).

1.2 The Upper Jurassic aquifer in the South German Molasse Basin

The deep Upper Jurassic carbonate aquifer in the South German Molasse Basin (SGMB) is one of the most important low to intermediate enthalpy hydrothermal water resources in Europe (Goldscheider et al., 2010; Stober, 2014). Its enormous potential in depths of >2000 m of true vertical depth below surface (mTVD) is estimated as approximately 400 MW_{el} and 1800 MW_{th} (Dussel et al., 2016). The aquifer is also extensively used for drinking water and industrial purposes in the shallower parts at the northern and western margins and, therefore, represents an altogether important water reservoir for southern Germany.

The history of the deep geothermal exploitation of this reservoir reaches back to 1983 with a fatefully failed hydrocarbon well in Erding, which is today successfully used for district heating and famous for the world's largest thermal spa (Agemar et al., 2014a). In the further course of exploration, the first geothermal wells in Unterschleißheim for district heating and Unterhaching for electrical power generation have been developed in the years 2003 and 2006, which represent a starting point for the deep geothermal exploitation in the central SGMB (Wolfgramm et al., 2007; Schellschmidt et al., 2010). Today, more than 22 hydrothermal doublets and triplets are installed in the Upper Jurassic thermal reservoir with depths up to 5,000 mTVD and several new deep geothermal wells and power plants are currently planned or already being implemented (Agemar et al., 2014a; GAB, 2020).

The thermal groundwater of shallower wells (<2,000 mTVD) from the Upper Jurassic aquifer is used for balneological purposes since 1947, with the former hydrocarbon well Füssing 1 in the so-called "Bäderdreieck" in the Braunauer Trog at the eastern margin of the SGMB, and since 1977 in the southwestern SGMB (Nathan, 1949; Bertleff et al., 1987b). In contrast to the geothermal power plants where the deheated water is reinjected to the reservoir (closed system), the thermal water of balneological applications is generally only extracted (open system), which implies the conciseness of sustainable resource management (Frisch and Huber, 2000; Bertleff et al., 1987b).

Regional and local heterogeneities in the hydrochemical, petrophysical and hydraulic properties of the Upper Jurassic hydrothermal reservoir cause varying productivities of the geothermal wells (Konrad et al., 2021; Bohnsack et al., 2020; Konrad et al., 2019; Stober et al., 2014; Birner, 2013). Up to now, four deep geothermal wells were technically or economically unsuccessful with very low water availabilities (occasionally <5 l/s) in the south of the central and western SGMB (Amro et al., 2013; Mraz et al., 2018; TUM, 2020). As temperature stability plays a major role in the constant management of the reservoir in addition to sufficient water availability, a regulated water balance of the geothermal resource is a key condition. Therefore, an improved understanding with regard to a sustainable use of this complex geothermal reservoir is of considerable practical concern.

1.3 Structure of the thesis

This thesis is structured into six chapters. Chapter 1 introduces the role of the geothermal energy in Germany as a renewable energy and the excellent geological conditions of the South German Molasse Basin for geothermal exploitation.

Chapter 2 contains a brief review of the state of the art of deep groundwater in sedimentary basins (Sec. 2.1), reservoir characterisation based on the hydrogeochemical groundwater evolution (Sec. 2.2), the concept of apparent groundwater age (Sec. 2.3), hydrochemical tools for groundwater characterisation (Sec. 2.4), groundwater dating methods (Sec. 2.5) and an elaborated reflection of the geological and hydrogeological situation of the study area in the SGMB (Sec. 2.6).

The motivation, aims and objectives are presented in Chapter 3 that are based on the findings of the state-of-the-art in Chapter 2, on which the significance of revising the hydrogeological concepts for the deep thermal aquifer of the SGMB is identified.

Chapter 4 describes the methods used to address the research questions. In the first part in Sec. 4.1, the sampling points of the (thermal) groundwater wells and geothermal boreholes as well as the sampling procedure is shown. The novel preparation and extraction method of organic radiocarbon is also presented in detail in Sec. 4.1.6. The following sections Sec. 4.2 to 4.4 describe the calculations of radiocarbon ages, noble gas infiltration temperatures (NGTs) and apparent groundwater ages using noble gas isotopes. The Chapter 4 ends with a brief overview of the statistical methods used (Sec. 4.5).

The results and discussion are illustrated in Chapter 5, which is divided in two sections. Sec. 5.1 contains the results of Heine and Einsiedl (2021) showing the promising approach to dissolved organic radiocarbon dating in carbonate aquifers using the example of a local study area within the SGMB. In Sec. 5.2, the results of the hydrochemical zoning and hydrogeochem-

ical evolution of the deep Upper Jurassic geothermal groundwater in the central SGMB using water chemistry data and environmental isotopes are presented according to Heine et al. (2021).

Chapter 6 synthesises the main findings of this work and discusses their implications in a broader scientific context and existing hydrogeological models known from literature. The thesis is then concluded with a short outlook on future research objectives.

Chapter 2

State of the Art

> While Internet searching and .pdf versions of more recent published material make "keeping up" easier, there is a body of important early work that is often ignored by young researchers. As a result, we stand at the beginning of the 21st century in danger of memory loss of our young sciences.
>
> *Jeffrey J. McDonnell*

2.1 Deep groundwater in sedimentary basins

The study of deep groundwater has long been underrepresented in the hydrogeological sciences and is becoming increasingly important due to new fields of application such as geothermal exploitation or the storage of thermal energy and CO_2 (Hebig et al., 2012; Bozau et al., 2015; Ueckert and Baumann, 2019). Historically, several terms and underlying concepts have been used and discussed in literature to describe deep groundwater in sedimentary basins. An elaborated review can be found in Hebig et al. (2012) and Kharaka and Hanor (2014). Briefly, deep aquifers are seen as dynamic systems, which are influenced by both surface processes from the meteoric cycle and subsurface processes (Hebig et al., 2012; Bozau et al., 2015). Therefore, groundwater can be defined by its several specific characteristics such as depth, genesis, apparent groundwater age, and hydrochemical composition (Einsele et al., 1983; Glynn and Plummer, 2005; Hebig et al., 2012). The concepts for the differentiation of groundwater are based on the origin of the initial H_2O as well as the origin and concentration of various dissolved constituents, which may be different from that of the initial H_2O (Kharaka and Hanor, 2014).

However, the term "deep groundwater" comprises various types of groundwater, which some have been used synonymously in the past: oilfield water (or brine), fossil water (or brine), basinal water (or brine), (extreme) formation water, and connate water (Lane, 1908; Chebotarev, 1955a; White, 1957; Collins, 1975; Kharaka and Thordsen, 1992; Whittemore, 1995; Kharaka and Hanor, 2014; Phillips and Castro, 2014). The relevant terms and concepts are briefly described in the following.

The first fundamental differentiation between groundwater is the classification of its origin. "Meteoric water" has entered the subsurface from rain or surface waters whereas "juvenile

water" originates from a young magmatic cycle deep in the earth's crust and has never been participated in the hydrological circle (Lane, 1908; Müller, 1999; Kharaka and Hanor, 2014). To specify the last contact of the meteoric water with the atmosphere, the time of origin can be further qualitatively defined (Kharaka and Hanor, 2014). This definition of meteoric waters would include seawater, lake water and rainwater. In contrast, in groundwater studies based on stable water isotopes, the term meteoric is commonly used for natural freshwaters precipitated from rain, snow or meltwaters that are plotting on the meteoric water line, which are regularly isotopically unaltered (Craig, 1961; Dansgaard, 1964). Although seawater and surface waters that show evaporation processes, e.g. in lakes, are by definition meteoric waters, they would not fall under the category of meteoric waters by stable water isotopes. In this thesis, the term meteoric water is used for groundwater explicitly associated with meteoric precipitation due to the specific stable water isotope signatures.

"Connate water" is (meteoric) fresh- or seawater that is syn-sedimentary (syngenetic) trapped in the pore matrix of the rocks, stagnant and unaltered (Lane, 1908; Chebotarev, 1955a). The original connate water may have been geochemically, physically and isotopically altered by various processes and, therefore, would no longer be connate. Relevant processes are rock compaction and mineral diagenesis, as well as the expulsion of water from the sediments and subsequent migration into more permeable rock formations (Chebotarev, 1955a; White et al., 1963; Collins, 1975; Kharaka and Hanor, 2014). Due to the unworkable restriction of connate waters and the difficult differentiation from their altered evolutes, White (1957) proposed using "fossil water". This term summarises the water that has not been in contact with the atmosphere for at least an appreciable part of a geological period. However, this time-depending definition is not clearly defined and, therefore, not to be understood uniformly. For example, the term fossil groundwater is often used for paleo-groundwater that was recharged by precipitation prior to Holocene age more than approximately 12,000 years ago (Clark and Fritz, 1997; Jasechko et al., 2017; Ferguson et al., 2020). In this context, the definition of the term "fossil" is problematic and misleading, so that in this thesis it is used for groundwater that no longer shows a meteoric origin based on the stable water isotopes. In order to categorise the hydrochemical character of these fossil waters, the term "extreme" could also be used, although this is not clearly defined by any parameter and is, therefore, not used in this thesis.

A common terminology for categorising the apparent age of (meteoric) groundwater is to use the more meaningful terms "modern" (<40-50 years), "submodern" (50 to 1,000 years), "old" (1,000 to 50,000 years) and "very old" (>50,000 years) (Clark, 2015), which leads away from the problem of the term "fossil".

The level of mineralisation can also give an indication of the type of water. Groundwater can be classified according to its level of mineralisation (expressed by the total dissolved solids (TDS)) as freshwater (TDS 0-1,000 ppm), brackish water (TDS 1,000-10,000 ppm), saline water

(TDS 10,000-100,000 ppm) or brine (TDS $>$ 100,000 ppm) (Davis, 1964). Although this type of categorisation is not necessarily related to the apparent age or origin of the groundwater in sedimentary basins, it can serve as a rough guide to the origin of the water, since recently infiltrated meteoric waters (except in areas with rock salt deposits) usually do not have a high mineralisation, whereas considerably older deep (fossil) waters are usually more highly mineralised.

Case (1955) proposed the use of the term "formation water" for groundwater that is pore water present in the reservoir rock prior to the disturbance of the reservoir rock by e.g. drilling, which can be used synonymously for any water irrespective of hydrogeochemical genesis, mineralisation or age (Kharaka and Hanor, 2014). On this basis, formation water in sedimentary basins is traced back to its host formation in the subsurface and can additionally be specified by the terms meteoric or fossil, which seems to be most appropriate for the terminology of deep groundwater.

However, besides the presented concepts for the terminology of (deep) groundwater in sedimentary basins by origin, mineralisation or age, "oilfield waters" are commonly defined as water resources which are accompanying oil or gas in hydrocarbon-rich fields (White, 1957; Collins, 1975). They generally fall in the category of formation water but the genetic definition is not very sharp (Amajor and Gbadebo, 1992; Whittemore, 1995). Oilfield waters may have been formed syngenetically to petroleum production or methanogenesis, e.g. condensed water vapor produced with natural gas, or are accompanied by fossil water or younger meteoric water and show, therefore, diverse and varied geochemical composition (Chebotarev, 1955b; White, 1957; Kharaka and Hanor, 2014).

2.2 Reservoir characterisation based on hydrogeochemical groundwater evolution

Groundwater has the ability to fundamentally interact with the ambient environment and is influenced by the spatial distribution of its flow (Tóth, 1999). The nature of groundwater in deep reservoirs may act as general geologic agent for various hydrogeological processes and is, therefore, an important factor for reservoir characterisation in deep sedimentary basins.

Three main types of interaction between groundwater and its environment can be identified: (bio-)geochemical, physical and kinetic interaction. The (bio)chemical composition of groundwater can be influenced by processes of dissolution, hydration, hydrolysis, oxidation-reduction, attack by acids, chemical precipitation, base exchange, sulphate reduction, concentration, ultrafiltration or methanogenesis (Tóth, 1999; Phillips and Castro, 2014; Cartwright et al., 2017). Knowing these processes and separating the different components is the key for understanding the hydrogeochemical evolution of deep groundwater in sedimentary basins

(Glynn and Plummer, 2005). The time scales of these occurring hydrogeological processes at the basin scale also remain of fundamental interest.

The hydrogeochemical evolution of groundwater after recharge depends generally on the aquifer properties, water-rock interaction and chemical/biogeochemical processes as well as mixing processes and the mean residence time (Fig. 2.1).

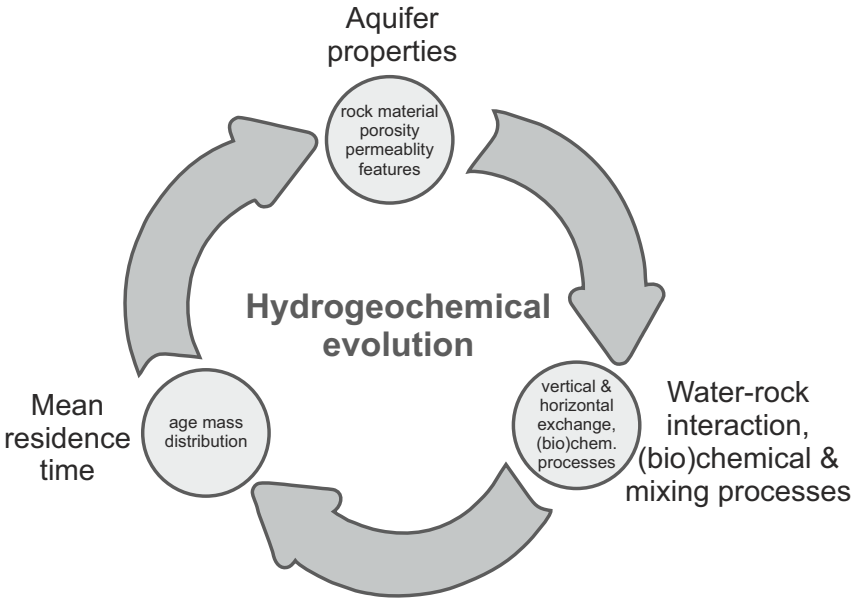

Figure 2.1: Main aspects of the hydrogeochemical evolution of groundwater and the relationship between aquifer properties, water-rock interaction & mixing processes, and mean residence time.

The aquifer properties such as rock material (e.g. carbonate, silicate), porosity, including tortuosity, permeability and (structural) features such as faults or karstic phenomena define the aquifer type with characteristic groundwater flow systematics (advective-dispersive-diffusive) and flow path geometry. These characteristics are crucial for the possibility and intensity of water-rock interaction, occurring chemical and biogeochemical processes as well as mixing processes with other fluids in the reservoir. They have also an impact on the mean residence time, which is the time since the water molecules in a sample were recharged considering the age distribution by advection, hydrodynamic dispersion, and molecular diffusion (Bethke and Johnson, 2002; Cartwright et al., 2020)

Fossil formation water in sedimentary basins undergoes a profound diagenetic evolution. The main hydrogeochemical processes that affect the hydrochemical composition of very old groundwater are (i) seawater evaporation, (ii) salt dissolution (e.g. halite), (iii) feldspar transformation, (iv) dolomitisation, (v) interaction with organic matter in sediments with generation, transport, accumulation, and production of petroleum (hydrocarbons), (vi) chemical interaction with low-permeable rocks (e.g. ion-exchange processes) and (vii) transport of thermal

energy in geothermal and geopressured–geothermal systems (White et al., 1963; Chaudhuri, 1978; Carpenter, 1978; Kharaka and Thordsen, 1992; Kharaka and Hanor, 2014; Bozau et al., 2015). In deep sedimentary basins, the fossil formation water can be dynamic and mobile and the hydrochemical composition may also be influenced by organic-inorganic interaction, migration processes of hydrocarbons and their oilfield waters from other formations as well as mixing processes with meteoric freshwater or other (highly saline) formation or connate water and diffusion processes (Clayton et al., 1966; Kharaka and Thordsen, 1992; Bottomley et al., 1994; Whittemore, 1995; Stichler, 1997; Greene et al., 2008; Kharaka and Hanor, 2014).

2.3 The concept of the apparent groundwater age

In most hydrogeological studies for quantitative analysis of groundwater systems, knowledge of the "apparent groundwater age" or "mean residence time" is invaluable (Goode, 1996; Phillips and Castro, 2014; Cartwright et al., 2017). The concept of "groundwater age" has been intensively and partly controversial discussed in literature, e.g. in Bethke and Johnson (2008). The most intuitive definition of the apparent groundwater age is the average time elapsed that a water molecule was isolated from the atmosphere after recharge and is, therefore, closely related to the rate it migrates (Davis and Bentley, 1982; Bethke and Johnson, 2002, 2008). This simplified concept assumes an one-dimensional, advective and non-dispersive flow, known as the piston-flow model (Fig. 2.2).

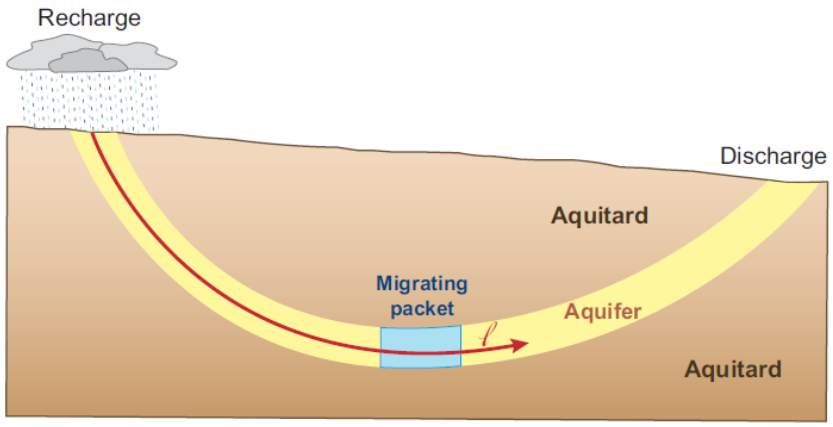

Figure 2.2: Piston-flow model for determining the apparent groundwater age (Bethke and Johnson, 2008).

According to this concept, an isolated packet of water migrates along flow path l within an aquifer, from recharge to discharge point or well, without exchanging water molecules with neighbouring aquitards or adjacent packets (Bethke and Johnson, 2008). This isolated water packet that contains many water molecules and represents a "groundwater age mass", which

is defined as the product of water density, volume and its residence time. (Goode, 1996; Bethke and Johnson, 2002). The flow velocity of this migrating packet is then the reciprocal of the age gradient along a flow distance l and could be determined by Darcy's law (Bethke and Johnson, 2008). Strictly defined, this calculated piston-flow model age is likely to be approximated only a few metres below the water table or in large confined aquifer systems with relatively small recharge areas (Cartwright et al., 2017).

However, groundwater consists of many water molecules and, therefore, different groundwater masses with different residence times. These groundwater age masses generally follow different flow paths in three dimensions, depending on the flow scale, spatial distribution, as well as characteristics of the aquifer and its surrounding aquitards. Moreover, processes of dispersion, diffusion and other hydrodynamic processes, such as sorption or mixing, lead to a distribution of groundwater age masses that is better described by the term "apparent groundwater age" or "mean residence time" (McGuire and McDonnell, 2006; Phillips and Castro, 2014; Clark, 2015; Cartwright et al., 2017). For this reason, the mean residence time and groundwater age distribution is calculated using complex lumped-parameter models (LPM) that consider different transit time distribution functions such as the piston-flow model (PFM), exponential mixing model (EMM), exponential piston-flow model (EPM) and/or dispersion model (DM) (Fig. 2.3) (Małoszewski and Zuber, 1982; Małoszewski, 2000; Jurgens et al., 2012).

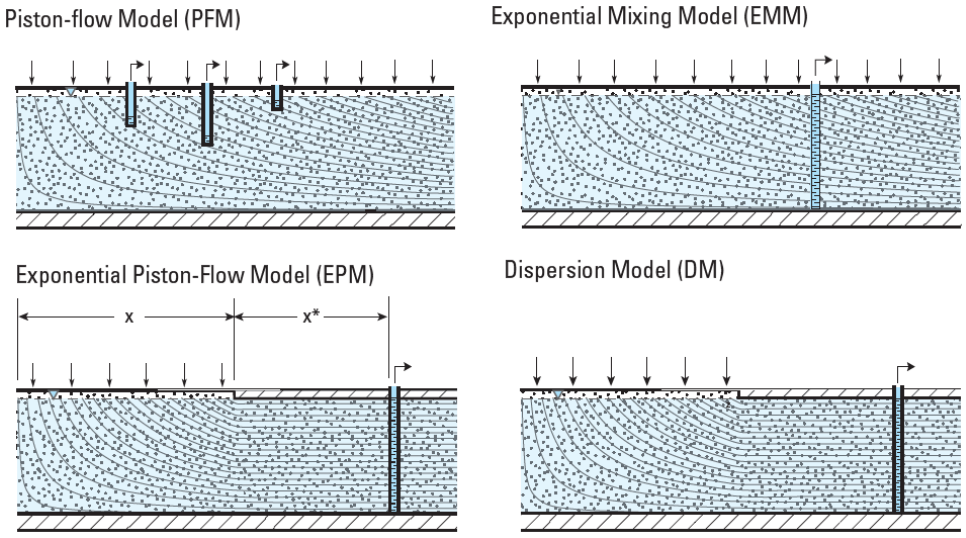

Figure 2.3: Different flow models for the calculation of the apparent groundwater age (after Jurgens et al. (2012)).

2.4 Hydrochemical tools for tracing hydrogeological processes

The water chemical composition and especially environmental isotope signatures in groundwater convey useful information on the hydrogeochemical evolution of the groundwater system, water-rock interaction, groundwater recharge conditions as well as apparent water ages (Glynn and Plummer, 2005; Zhu et al., 2007; Bouchaou et al., 2008; Varsányi et al., 2011; Ettayfi et al., 2012; Mayer et al., 2014; Batlle-Aguilar et al., 2017; Jasechko, 2019). This information can be used for various issues such as the determination of recharge areas, groundwater flow rates, mixing processes of younger and older groundwater and overall for the calibration of groundwater flow models, which are essential in the context of sustainable groundwater resource management (Glynn and Plummer, 2005; Carreira et al., 2008; Cartwright et al., 2020).

At present, several hydrochemical parameter are available for the characterisation of thermal waters (Kharaka and Hanor, 2014). Common parameter for delineating and differentiating the origin of the dissolved constituents are the (conservative) water chemical components, trace elements as well as distinct environmental isotopes such as stable water isotopes and strontium isotopes (Dasch, 1969; Collins, 1975; Kharaka and Thordsen, 1992; Davis et al., 1998; Capo et al., 1998; Probst et al., 2000; Gemici and Tarcan, 2002; Glynn and Plummer, 2005; Dotsika et al., 2006; Millot et al., 2011; Varsányi et al., 2011; Ettayfi et al., 2012; Sahib et al., 2016; Santoni et al., 2016; Bouchaou et al., 2017).

2.4.1 Water chemistry

The assessment of water chemistry is, among others, the most intuitive and important method to get a first impression of possible occurring hydrogeochemical processes in groundwater. The concept of "hydrochemical facies" based on the major ion concentration of groundwater gives a valuable diagnostic insight into the water chemical composition (Back, 1960, 1966; Furtak and Langguth, 1967; Hebig et al., 2012). Hydrochemical facies in trilinear diagrams, such as the Piper plot, reflects the response of water chemical processes occurring in the subsurface and may suggest the dominant water chemical influences in the subsurface (Back, 1966). Based on the hydrochemical facies, processes of mineral dissolution, ion-exchange or mixing, such as (re)refreshment or salinisation, can be delineated (Fetter, 2001).

Moreover, the concentration of selected ions can be used for retracing occurring processes in the subsurface. The conservative ions chloride and bromide are fairly closely coupled and often provide most conclusive identification of the origin of the groundwater salinity (Kharaka and Thordsen, 1992; Bottomley et al., 1994; Whittemore, 1995). The contents of sulphate, bicarbonate and organic acids may result from (bio-)chemical reactions of organic matter and can be linked to these processes (Kharaka and Hanor, 2014). Boron can be considered an element of marine origin and, together with bromide, is always associated with waters accompanying

petroleum, which may therefore provide information of the degree of water-rock interaction or influences of oilfield water (Collins, 1975; Davis et al., 1998; Kharaka and Hanor, 2014).

2.4.2 Stable water isotopes

The stable isotopes of hydrogen and oxygen in H_2O are very useful tools for determining the origin and evolution of groundwater (Kharaka and Hanor, 2014). Hydrogen and oxygen isotope ratios are expressed in the δ-notation (Eq. 2.1) with respect to the standard VSMOW (Vienna-Standard Mean Ocean Water):

$$\delta(‰_{\mathrm{VSMOW}}) = \frac{R_{\mathrm{sample}} - R_{\mathrm{standard}}}{R_{\mathrm{standard}}} \times 1{,}000 \tag{2.1}$$

where R stands for $^{2}H/^{1}H$ and $^{18}O/^{16}O$ ratios of the sample and standard, respectively.

The stable water isotopic composition of precipitation is mainly controlled by the two factors of temperature and the proportion of residual water vapour during precipitation. Several fractionation effects, including the continental, altitude, latitude and amount effect, are driven by these factors (Clark, 2015). Due to these specific fractionation processes, the stable water isotopes in meteoric groundwater are capable of storing information regarding the climate conditions during recharge (Clayton et al., 1966; Bottomley et al., 1994; Clark, 2015).

The global meteoric water line GMWL ($\delta D = 8 \times \delta^{18}O + 10$ ‰) after Craig (1961) expresses the global relationship of δD and $\delta^{18}O$ in precipitation and can be used to determine a meteoric origin as well as the fractionation effects during precipitation. In the pre-alpine Molasse basin, the local meteoric water lines (LMWL) of Garmisch-Partenkirchen ($\delta D = 8.12 \times \delta^{18}O + 8.5$ ‰) and Constance ($\delta D = 8.02 \times \delta^{18}O + 7.1$ ‰) after Stumpp et al. (2014) may be representative for the precipitation in the study area.

With the help of the stable water isotopes δD and $\delta^{18}O$, information can be deduced concerning the origin of the water (meteoric, juvenile), evaporation effects, its interaction with e.g. carbon dioxide (CO_2), methane (CH_4) or hydrogen sulphide (H_2S) as well as (geo)thermally induced interaction with rocks or rock-forming minerals (Fig. 2.4) (Clayton et al., 1966; Bottomley et al., 1994; Clark, 2015). Moreover, since the stable water isotopes can provide information on the climatic recharge conditions, it may be possible to draw conclusions about a warm climatic recharge or a cold climatic recharge, neglecting possible altitude effects. Thus, qualitative age statements can be made about the groundwater, whether it was recharged during the Holocene or Pleistocene age.

The groundwater in several sedimentary basins was found to be predominantly of meteoric origin by the stable water isotope signature (Clayton et al., 1966). But the isotopic composition of groundwater in sedimentary basins can also be modified by isotopic exchange between groundwater and other fluids such as hydrocarbons or associated gases, evaporation and con-

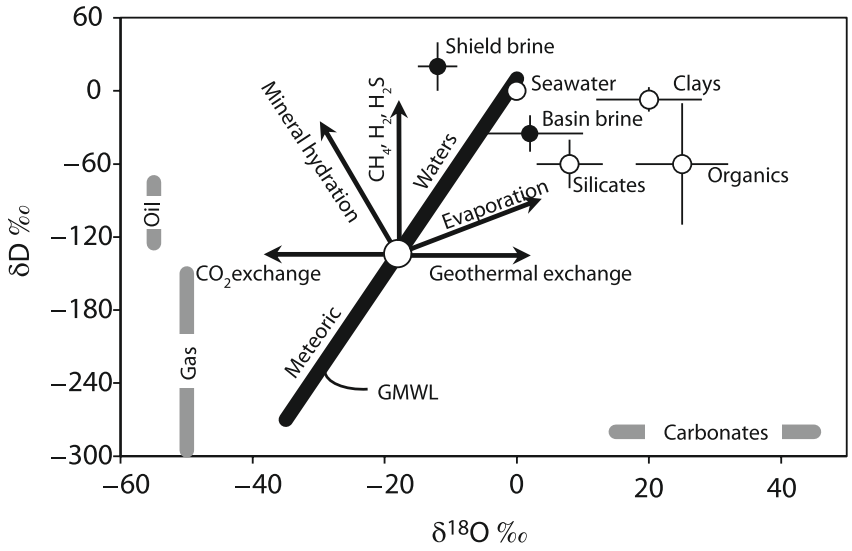

Figure 2.4: Relationship between stable water isotope signatures of meteoric groundwater caused by exchange processes in the water cycle and specific water-rock interaction (Clark, 2015).

densation, dissolved species, and fractionation caused by the membrane properties of rocks (Kharaka and Hanor, 2014). Especially enriched $\delta^{18}O$ values are typical due to geothermally driven oxygen exchange with carbonate rocks in thermal waters (Clayton et al., 1966). The low $\epsilon^{18}O_{CaCO_3-H_2O}$ enrichment factor at temperatures between 50 and 100 °C creates a disequilibrium between meteoric waters and carbonate minerals in the reservoir rock. This can cause that $\delta^{18}O$ signatures slowly shift to more positive values of the rock or mineral signature. A small enrichment of δD, on the other hand, can occur partly through exchange with or dehydration of gypsum and clay minerals in evaporated seawater and through exchange with CH_4 and H_2S (Clark and Fritz, 1997).

2.4.3 Strontium isotopes

Strontium (Sr^{2+}) occurs mainly in carbonate rocks when it substitutes calcium (Ca^{2+}), or in feldspars in place of potassium (K^+) (Faure and Powell, 1972). In carbonates, it is incorporated into the mineral by both calcite and dolomite in place of calcium and released by dissolution processes. The dissolution ratio of Sr^{2+} between calcite and dolomite is 2:1 (Jacobson and Usdowski, 1976). The isotopes of the trace elements Sr^{2+} and Rb^+ are stable except for the radioactive ^{87}Rb, which forms the radiogenic strontium ^{87}Sr through β-decay ($\lambda_{1/2} = 4.8 \times 10^{10}$ years). Radiogenic ^{87}Sr is therefore enriched in rubidium bearing minerals such as mica and K-feldspars (Veizer et al., 1999; Elderfield, 1986; Burke et al., 1982).

Various authors (e.g. Veizer and Compston (1974); Burke et al. (1982); Veizer (1989); Smalley et al. (1994); McArthur et al. (2012)) have analysed the $^{87}Sr/^{86}Sr$ signatures of marine carbonates and fossils (brachiopods) to evaluate the typical seawater curve for the Phanerozoic (Fig. 2.5). Weathering and, thus, the influence of terrestrial rubidium-rich rocks (e.g. granites, mudstones) as well as rubidium-poor oceanic crustal basalts (MORB) control the $^{87}Sr/^{86}Sr$ signature in the Phanerozoic seawater (Elderfield, 1986). Typical $^{87}Sr/^{86}Sr$ ratios for Upper Jurassic carbonates with low rubidium concentrations range between 0.7068 and 0.7079 (Koepnick et al., 1990; Veizer et al., 1999) and $^{87}Sr/^{86}Sr$ ratios are elevated (>0.71) for terrestrial rocks with higher rubidium contents such as shales and granites (Dasch, 1969; Elderfield, 1986; Probst et al., 2000).

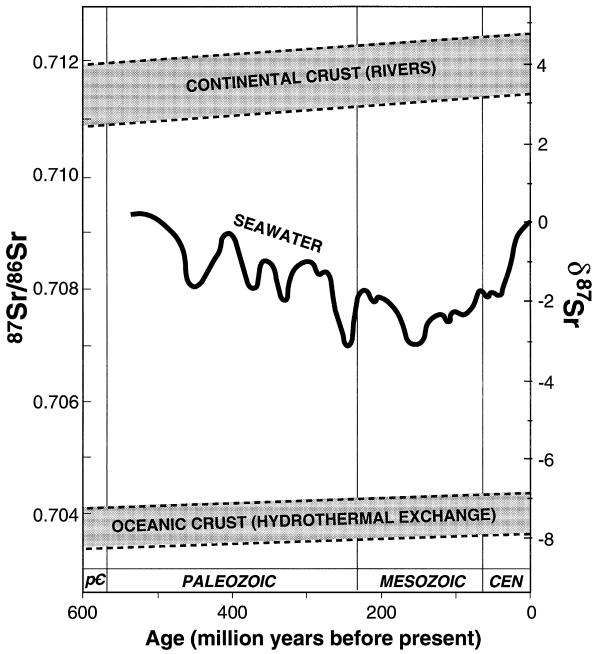

Figure 2.5: Distribution of the strontium isotope ratio in Phanerozoic seawater and its influencing factors (in Capo et al. (1998) after Burke et al. (1982)).

The $^{87}Sr/^{86}Sr$ ratio of groundwater depends on the chemical evolution during infiltration through the unsaturated zone, the aquifer lithology, the rocks alteration level and intensity of water-rock interaction (Capo et al., 1998; Probst et al., 2000). The primordial ratio of $^{87}Sr/^{86}Sr$ is 0.699 (Elderfield, 1986). Infiltrating (ground)water receives the $^{87}Sr/^{86}Sr$ ratio in the soil zone where the ratio once in solution is not fractionated. The initial soil zone isotope signature is preserved unless mineral dissolution of the aquifer host rocks occurs (Baublys et al., 2019). At temperatures below 400 °C, the $^{87}Sr/^{86}Sr$ ratio is neither temperature-dependent nor does fractionation occur during crystallisation (Matter et al., 1987) and is not subject to biogeochemical processes (Pu et al., 2012). Therefore, the $^{87}Sr/^{86}Sr$ ratio of groundwater is a very practical tool for determining solute sources, water-rock-interaction, geochemical processes and mixing processes in groundwater (Dasch, 1969; Capo et al., 1998; Probst et al., 2000; Shand et al., 2009; Ettayfi et al., 2012; Sahib et al., 2016; Santoni et al., 2016; Baublys et al., 2019).

2.5 Groundwater dating

Groundwater dating is often based on the concentration of radioactive or radiogenic isotopes or isotopes or molecules that mark an anthropic event, such as nuclear weapons testing (Fig. 2.6)

(Bethke and Johnson, 2008). Three basic classes of age tracers can be distinguished: (i) radioactive tracers, (ii) accumulation tracers, and (iii) event tracers (Cook and Herczeg, 2000; Phillips and Castro, 2014). A distinction is made between environmental isotopes and artificial tracers, the latter not being the subject of this work.

Dating of groundwater itself may only be possible with the isotopes of water: δD, $\delta^{18}O$ and Tritium (^{3}H). These parameters would be very well suited for dating if they were not severely limited in their resolution and time scale (Fig. 2.6). Therefore, it is common to date the dissolved water constituents and combine several methods when determining the apparent groundwater age. Thus, the apparent groundwater age is determined by the decay rate of radioactive isotopes, for e.g. ^{39}Ar, ^{36}Cl, ^{81}Kr, ^{85}Kr, ^{14}C or ^{36}Cl; the accumulation rate of radiogenic isotopes, for e.g. ^{4}He or ^{40}Ar; or a combination of decay and accumulation with daughter-parent isotopes, for e.g. Tritium to tritigenic Helium-3 (^{3}H-$^{3}He_{trit}$) (Cook and Herczeg, 2000; Bethke and Johnson, 2008; Phillips and Castro, 2014). It is only possible to apply the lumped-parameter models (LPM) and thus obtain a distribution of the groundwater age masses (mean residence time) if different isotope tracers are linked together. Otherwise, the dating is carried out with the simplified piston-flow models (PFM).

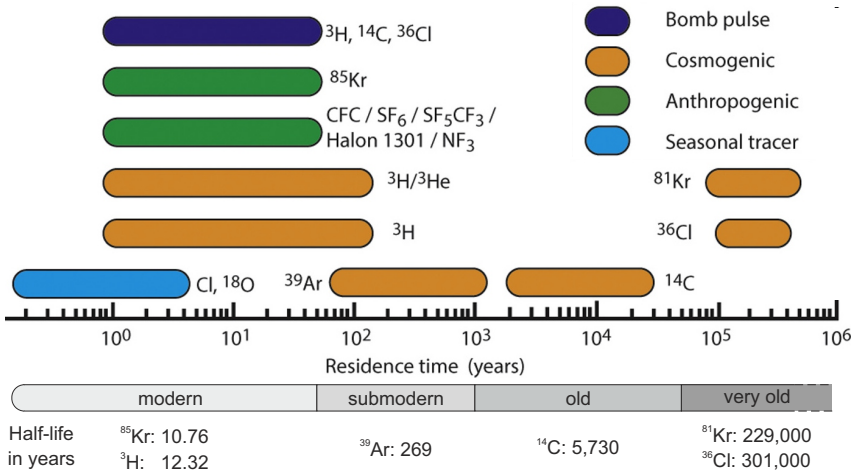

Figure 2.6: Approximate dating range for isotopes and other tracer applications after Cartwright et al. (2017) with groundwater age ranges (Clark, 2015) and half-lifes of typical environmental radionuclides (Phillips and Castro, 2014).

2.5.1 Dating with radioactive isotopes

Several dissolved radionuclides with different specific decay rates λ are used in groundwater research for calculating the apparent groundwater age. It is assumed that a radionuclide with a certain initial concentration is introduced into the groundwater during recharge and decreases only by the radioactive decay with time in a closed system. The time elapsed t_r is then deter-

mined based on the piston-flow model using the decay equation Eq. 2.2 (Bethke and Johnson, 2008; Phillips and Castro, 2014):

$$t_r(yr) = -\frac{1}{\lambda} \times \ln\left(\frac{C_{meas}}{C_0}\right) \tag{2.2}$$

with the specific decay rate λ, the measured (C_{meas}) and initial (C_0) concentrations of the radionuclide.

Whereas ^{85}Kr, ^{3}H and ^{39}Ar are commonly used for dating modern and submodern groundwater, only radiocarbon with a half-life $\lambda_{1/2}$ of around 5,730 years allows dating old paleogroundwater with residence times between approximately 1,000 and 40,000 years (Fig. 2.6) (Taylor et al., 1992; Geyh, 2000). ^{81}Kr and ^{36}Cl with considerably higher half-lifes are suitable for dating very old groundwater in sedimentary basins (Phillips and Castro, 2014).

In deep sedimentary basins, groundwater dating with radiocarbon is a widespread applied method (Cartwright et al., 2020). But dating with radiocarbon of dissolved inorganic carbon (DIC) is often problematic in determining realistic apparent groundwater ages (Taylor et al., 1992; Tullborg and Gustafsson, 1999; Geyh, 2000; Gallagher et al., 2000; Han et al., 2012; Hershey et al., 2016; Cartwright et al., 2020). However, dating of natural groundwater with radiocarbon in dissolved organic carbon (DOC) represents a very promising alternative (O'brien and Stout, 1978; Murphy, 1987; Murphy et al., 1989b,a; Wassenaar et al., 1990, 1991; Purdy et al., 1992; Geyer et al., 1993; Artinger et al., 2000; Ivanovich et al., 1996; Burr et al., 2001; Hershey et al., 2016; Lang et al., 2016).

2.5.1.1 Processes affecting the $^{14}C_{DIC}$ dating

The $^{14}C_{DIC}$ activity that is introduced into the groundwater during recharge can be affected by various chemical, biological or physical processes in the carbon cycle (Figs. 2.7 & 2.9) such as the dissolution or precipitation of carbonates (Vogel and Ehhalt, 1963), isotope exchange processes, bacterial (BSR) or thermochemical (TSR) sulphate reduction (Clark et al., 1996), methanogenesis (Barker et al., 1979; Aravena and Wassenaar, 1993; Aravena et al., 1995; Han and Plummer, 2013) or hydrodynamic diffusion and mixing processes (Gallagher et al., 2000; Geyh, 2000; Bethke and Johnson, 2002; Cartwright et al., 2020). Therefore, $^{14}C_{DIC}$ dating particularly in carbonate aquifers requires models that consider for these chemical, biological and physical interaction processes (Gallagher et al., 2000), which have also a considerable effect on the $\delta^{13}C_{DIC}$ chemistry (Fig. 2.7). $\delta^{13}C$ (of DIC and DOC) expresses the ratio of stable carbon isotopes $^{13}C/^{12}C$ with respect to the standard VPDB (Vienna-Pee-Dee-Belemnite) in the δ-notation (Eq. 2.3):

$$\delta^{13}C(‰_{VPDB}) = \frac{R_{sample} - R_{standard}}{R_{standard}} \times 1{,}000 \tag{2.3}$$

where R stands for $^{13}C/^{12}C$ ratio of the sample and standard, respectively.

One of the main problems of radiocarbon dating in DIC is the dilution of the inital $^{14}C_{DIC}$ activity by "dead" inorganic carbon from the aquifer rock, which is free of $^{14}C_{DIC}$. The atmospheric CO_2, and thus also the dissolved carbon in the precipitation, has values of -6.5 ‰ for $\delta^{13}C$ and >100 pmC for ^{14}C (Fig. 2.7). In the soil zone, where the groundwater mainly receives its initial DIC, the $\delta^{13}C_{DIC}$ value of the gaseous CO_2 is about -23 ‰ and around 100 pmC for $^{14}C_{DIC}$, which are mainly controlled by the $\delta^{13}C$ and ^{14}C values of the vegetation. The DIC of water infiltrating into the aquifer then has a $\delta^{13}C_{DIC}$ value around -15 ‰ and a $^{14}C_{DIC}$ activity of around 100 pmC. In contrast, marine carbonates, such as those of the Upper Jurassic, have $\delta^{13}C_{DIC}$ values of around 0 ‰ and are free of $^{14}C_{DIC}$. Due to dissolution of inorganic carbon from the carbonate aquifer rock into groundwater, the DIC undergoes in closed systems a geochemical evolution, which is then visible in the $\delta^{13}C_{DIC}$ signature <-15 ‰. Therefore, $\delta^{13}C_{DIC}$ is often used to take the aquifer carbonate dilution processes into account (Clark and Fritz, 1997).

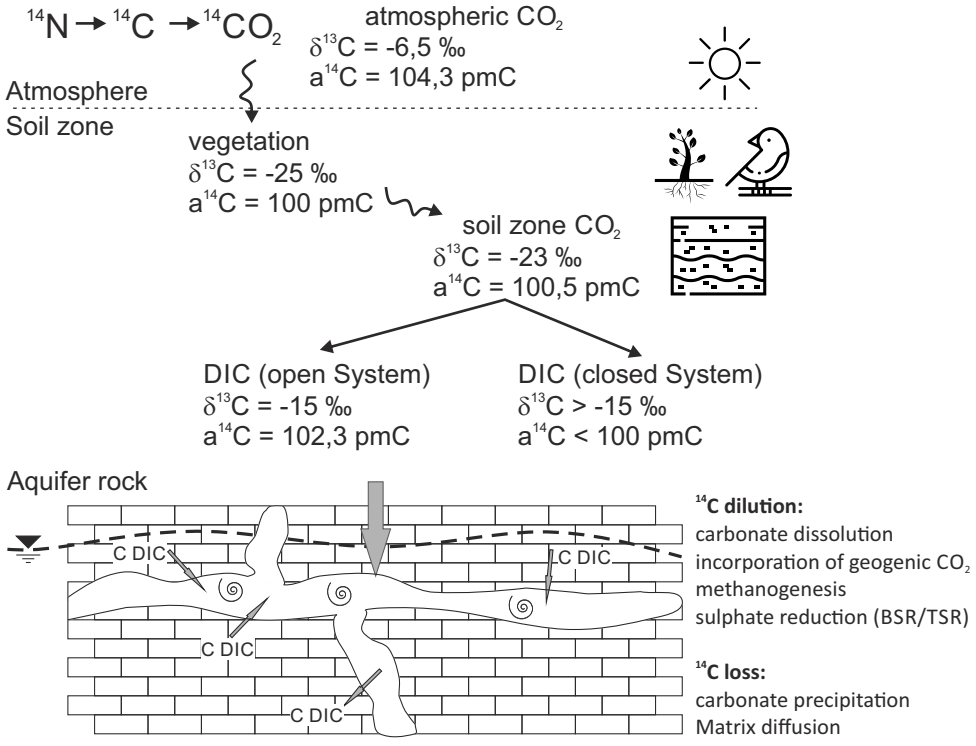

Figure 2.7: Cycle and associated fractionation of inorganic radiocarbon ^{14}C, its activity ($a^{14}C$) and $\delta^{13}C$into CO_2 during photosynthesis, root respiration and hydro-bio-geochemical processes in groundwater (after Clark and Fritz (1997)).

Accordingly, geochemical correction models with increasing complexity have been proposed to correct the measured initial radiocarbon activity $^{14}C_{0,DIC}$ and the DIC budget in groundwa-

ter (Vogel and Ehhalt, 1963; Pearson and White, 1967; Tamers, 1975; Mook, 1976; Wigley, 1976; Evans et al., 1979; Fontes and Garnier, 1979; Eichinger, 1983; Aravena et al., 1995; Gallagher et al., 2000; Han and Plummer, 2013, 2016). In these models, the initial radiocarbon concentration $^{14}C_{0,DIC}$ is corrected with a correction factor in Eq. 2.2, which reduces the $^{14}C_{0,DIC}$ value and, thus, the possible dating range. This correction factor can be determined by various models such as statistical correction model (STAT model), alkalinity correction model (ALK model), chemical mass balance correction model (CMB model), $\delta^{13}C_{DIC}$ mixture model, dolomite dissolution model or matrix exchange models (Clark and Fritz, 1997; Han and Plummer, 2016). Especially of the single-sample-based-models for the estimation of $^{14}C_{0,DIC}$, the more sophisticated models after Pearson (Pearson and White, 1967), Mook (Mook, 1976) and Fontes & Garnier (FGM) (Fontes and Garnier, 1979) with the revised FGM (Han and Plummer, 2013), which all consider matrix-exchange processes that cause a linear relationship between $^{14}C_0$ and $\delta^{13}C$ from carbonates are recommended (Han and Plummer, 2016). The differences between selected models are shown in Fig. 2.8 with the relationship of $^{14}C_{DIC}$ and $\delta^{13}C_{DIC}$ (Han and Plummer, 2013).

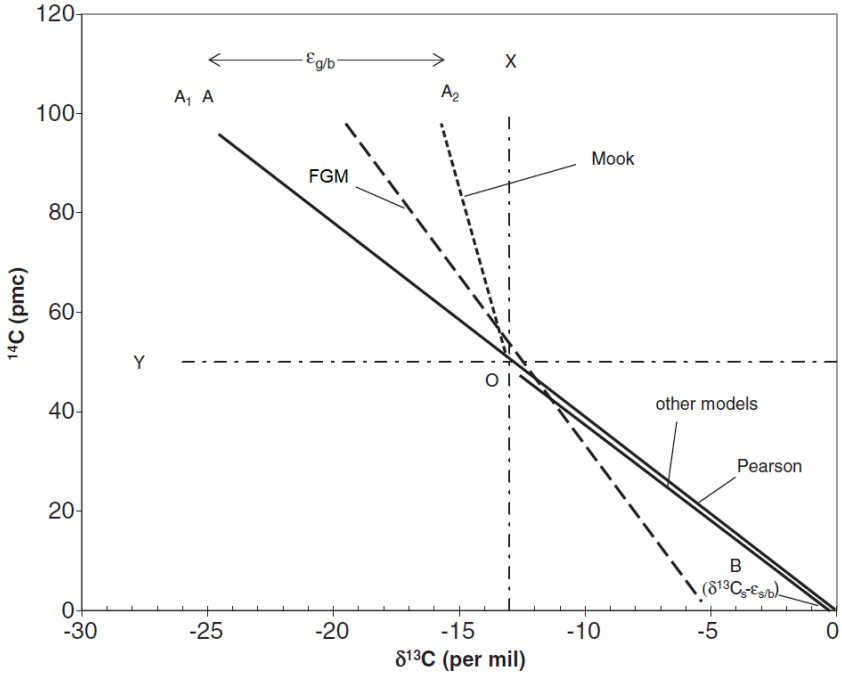

Figure 2.8: Comparison of correction models with the relationship of $^{14}C_{DIC}$ and $\delta^{13}C_{DIC}$. Points: A (gaseous soil CO_2), A1 (dissolved CO_2 in water) & A2 (HCO_3^-). Line O–B: simulated models of Wigley (1976), Evans et al. (1979), Eichinger (1983), and revised Fontes & Garnier model (FGM) (Han and Plummer, 2013); line from origin to A & A1: Pearson's model (Pearson and White, 1967); line from origin to A2: Mook's model (Mook, 1972). X and Y represent 0.5 $\delta^{13}C_{a0}$ and 0.5 $^{14}C_{a0}$ (modified from Han and Plummer (2013)).

However, although these correction methods consider various influences of physical, biological and chemical interaction in closed systems, they may not be possible to estimate a meaningful apparent groundwater age in many cases with $^{14}C_{DIC}$, especially in carbonate aquifers (Cartwright et al., 2020).

2.5.1.2 Advantages of $^{14}C_{DOC}$ dating

A considerable fraction of the DOC, the fulvic acids (FA), are expected to be of high physicochemical stability in deep groundwater in terms of microbial degradation and geochemical transformation processes (Artinger et al., 2000; Einsiedl et al., 2007; Hershey et al., 2016). They are supposed to be very suitable for dating old groundwater as shown in various studies (Murphy, 1987; Murphy et al., 1989b,a; Wassenaar et al., 1991; Bauer et al., 1992; Aravena and Wassenaar, 1993; Geyer et al., 1993; Geyer, 1994; Artinger et al., 1996; Aravena et al., 1995; Ivanovich et al., 1996; Buckau et al., 2000; Artinger et al., 2000; Burr et al., 2001; Hershey et al., 2016; Cartwright et al., 2017; Thomas et al., 2021).

Uncertainties of the radiocarbon dating method with DOC in groundwater may be only the unknown initial radiocarbon content $C_{0,DOC}$, probable dissolution effects of sedimentary organic carbon (SOC) in presence of, e.g. kerogen or lignite, redox reactions or $^{14}C_{DOC}$ sorption and diffusion processes (Fig. 2.9) (Murphy et al., 1989b,a; Ivanovich et al., 1996; Artinger et al., 2000; Thomas et al., 2021). The SOC in carbonate aquifers appears typically in the form of alkanes or HA, which is released by lignites, rather than compounds of FA (Frye and Thomas, 1993; Ivanovich et al., 1996). However, various studies have shown, that the apparent groundwater ages derived with $^{14}C_{DOC}$ of FA with high-molecular weight (HMW) are often younger and more realistic compared to $^{14}C_{DIC}$ ages (Murphy et al., 1989b; Wassenaar et al., 1991; Wassenaar and Aravena, 1992; Purdy et al., 1992; Geyer, 1994; Cartwright et al., 2017).

Processes to consider for ^{14}C dating	$^{14}C_{DIC}$	$^{14}C_{DOC}$
Mineral/gas dissolution	✓	✗
Mineral/gas precipitation	✓	✗
Cation ion exchange	✓	✗
Carbon isotopic exchange with aquifer material	✓	✗
Dissolution of organic matter	✗	✓
Redox reactions	✓	✓
^{14}C sorption on aquifer materials	✓	✓
^{14}C matrix diffusion	✓	✓

Advantages/Disadvantages	$^{14}C_{DIC}$	$^{14}C_{DOC}$
Correction of raw data	✓	✗
Many geochemical correction methods	✓	✗
Large volumes needed	✗	✓
Longer processing times	✗	✓
Unknown initial $^{14}C_0$	✓	✓

Figure 2.9: Processes to consider for groundwater dating with $^{14}C_{DIC}$ and $^{14}C_{DOC}$ after Thomas et al. (2021) as well as advantages of both dating methods after Wassenaar and Aravena (1992). Symbols: tick – process/advantage occur; cross – process/advantage does not occur.

Although $^{14}C_{DOC}$ dating has been successfully applied in a number of environmental settings, it has not found general applicability in hydrological studies so far (Burr et al., 2001). Up to now, one of the biggest disadvantages of groundwater dating with $^{14}C_{DOC}$ has been the

time-consuming and labour intensive extraction and isolation of the desirable humic substance as natural groundwater contains on average only 0.7 mg/l DOC (Thurman, 1985). Although accelerator mass spectrometry (AMS) measurements require only small sample sizes for radiocarbon dating (around 0.5 mg), often large volumes of groundwater samples have to be concentrated to extract an sufficient amount of the desired and datable fraction of DOC. In addition, the generally low levels of DOC in groundwater imply that any sample pretreatment procedure may be susceptible to carbon contamination (Thurman and Malcolm, 1981; Burr et al., 2001). Therefore, the main advantage is the applicability of a simple and efficient extraction method for datable organic matter from natural groundwater with low DOC contents.

2.5.1.3 Preparation methods of dissolved organic carbon

Preparation methods for the pre-concentration and isolation of dissolved organic radiocarbon ($^{14}C_{DOC}$), which are both summarised by the term extraction (Minor et al., 2014), depend on the operational definition of the organic carbon in groundwater (Thurman and Malcolm, 1981). DOC is defined as the organic carbon dissolved in water, the size of which is less than 0.45 µm (Thurman, 1985). Its definition comprises a heterogeneous pool of substances or classes and, therefore, DOC is a collective term for macro molecules with sizes ranging from one to ten thousands Daltons (unified atomic mass units, u) and different spectroscopic, chemical and physical properties (Aiken et al., 1985; Malcolm, 1990; Geyer, 1994). The DOC species can be operationally defined by their specific ad- and desorption properties on macroporous resins in dependency of the pH value and classified into compound classes (Fig. 2.10). The classification is based on the adsorption behaviour and retention capacity of the organic substances on the XAD-8 nonionic resin, which mainly depends on the water solubility of the substance. Thus, the first distinction of DOC is between hydrophobic and hydrophilic acids, the latter neither adsorbing to the resin XAD-8 nor precipitating with hydrochloric acid (HCl) (Thurman and Malcolm, 1981).

The hydrophobic humic substances comprise 50 to 75 % of the DOC and are the major class of organic compounds in natural waters (Thurman, 1985). They consist of fulvic acids (FA) and humic acids (HA). These substances are more or less similar in their elemental composition, functional groups and spectroscopic behaviour. Contrary to the smaller and lighter FAs, the larger and heavier HAs precipitate at a pH of 1-2, while the FAs remain in solution. The FAs are therefore defined as macro molecules that adsorb on the XAD-8 nonionic resin at a pH of 2 and eluate at pH 13 (Thurman and Malcolm, 1981). Based on this definition, the HA and FA are high-molecular-weight humic substances (HMW) and the remaining humic substances such as simple organic molecules, aromatic compounds or substituted alcohols are considered of low-molecular-weight (LMW) (Fig. 2.10) (Thurman and Malcolm, 1981; Thurman, 1985; Malcolm, 1990).

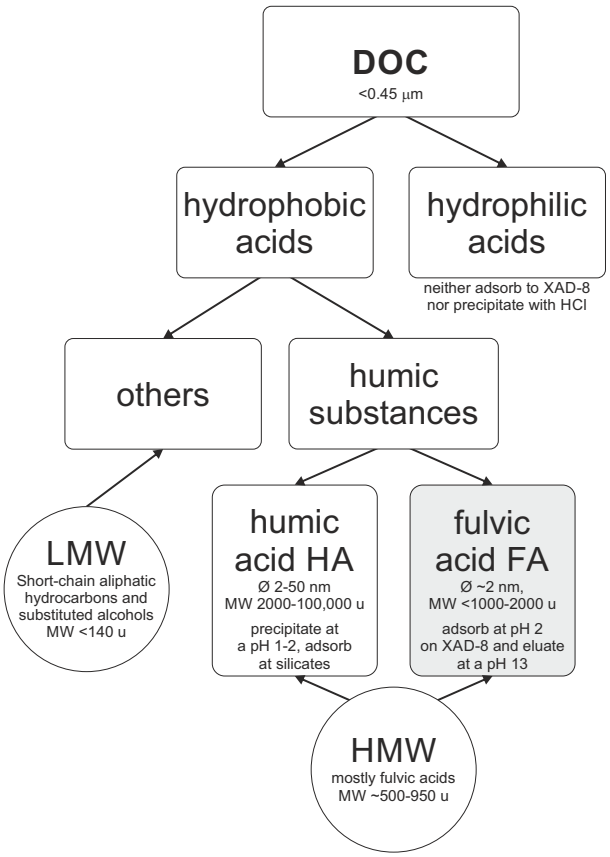

Figure 2.10: Differentiation of the operational species of dissolved organic carbon (DOC) (after Aiken et al. (1985); Thurman (1985); Murphy et al. (1989b); Geyer (1994)). XAD-8 is a nonionic resin, MW the molecular weight, HMW and LMW are humic substances of high- or low-molecular-weight, respectively.

The different extraction methods (pre-concentration and/or isolation) of organic substances dissolved in water are elaborately described in Geyer (1994), Swenson (2014) and Minor et al. (2014). Briefly, several methods have been applied for the extraction of DOC such as (i) reverse osmosis coupled with electrodialysis (RO/ED), (ii) ultrafiltration, (iii) solid phase extraction (SPE) or (iv) direct (evaporation) or freeze drying (lyophilisation) and oxidation (Fig. 2.11) (Minor et al., 2014; Swenson, 2014). These methods differ in the concentration of organic compounds, recovery rate, the purity, chemical and fraction size of isolated carbon as well as equipment and operational costs (Green et al., 2014).

While during direct or freeze drying of water, organic substances and almost all other inorganic substances such as salts were concentrated only, the methods RO/ED, ultrafiltration and SPE both concentrate and isolate the desired organic substances. The co-concentration of salts, especially in higher saline waters, may be problematic for commonly applied nuclear magnetic

resonance (NMR), mass spectrometry (MS), or elemental analysis and salts needs, therefore, be removed prior to analysis (Minor et al., 2014).

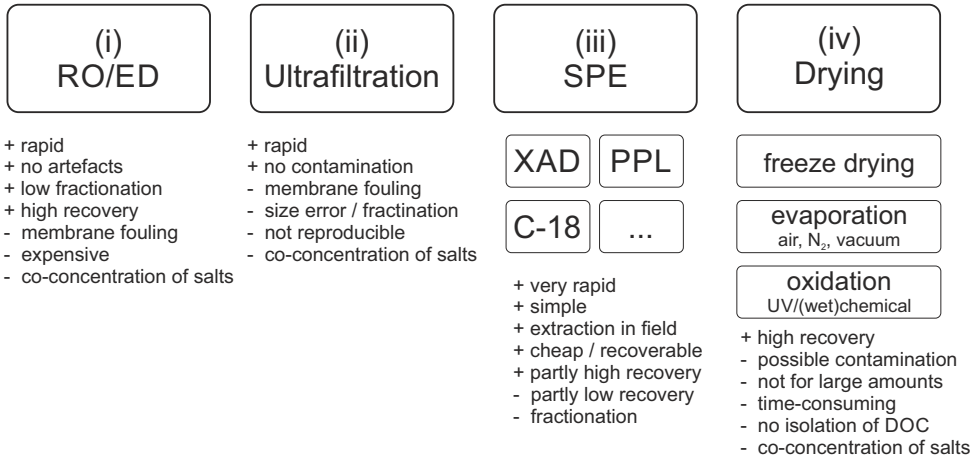

Figure 2.11: Comparison of the main DOC extraction methods (i) reverse osmosis coupled with electrodialysis (RO/ED), (ii) ultrafiltration, (iii) solid phase extraction (SPE) or (iv) direct or freeze drying (lyophilization) with evaluation of pros (+) and contras (-) of the applied method (Geyer, 1994; Burr et al., 2001; Minor et al., 2014; Swenson, 2014; Thomas et al., 2021).

Due to the very long concentration time of freeze drying (around 1 l in 5 days) and possible contamination by oil-backstreaming of the pump, freeze drying is generally inappropriate for pre-concentration of organic substances from natural waters with low DOC contents (Burr et al., 2001). Other drying methods based on evaporation are partly faster and less vulnerable to contamination of the used pump. However, evaporation in air may induce contamination by atmospheric carbon, while evaporation by nitrogen avoids the contamination by atmospheric carbon, but this concentration method is also very slow (around 1 l in 5 days). Another appropriate evaporation method is the vacuum drying, where the sample has no contact to air, but this method is also not suitable for samples where large amounts of natural water needs to be evaporated (Burr et al., 2001; Minor et al., 2014). Overall, these drying methods are not capable to isolate desirable organic substances and show problems with highly saline water samples, as the salts co-concentrate, precipitate and may incorporate $^{14}C_{DOC}$ during the drying process. However, direct or freeze drying is often combined with one of the other methods after isolation of DOC species and desalinisation of the sample.

Beaupré et al. (2007) have developed a modified, low blank, ultraviolet oxidation and vacuum line system to convert marine dissolved organic carbon into CO_2 for concentration, which is only suitable for sample sizes of 1 l (Bauer et al., 1992; Griffin et al., 2010; Druffel et al., 2016). In a somewhat similar approach, Hershey et al. (2016) and Thomas et al. (2021) have adapted this method with chemical removing of inorganic substances and subsequently conversion of the remaining DOC to CO_2 by oxidation with potassium permanganate. This method also re-

quires a vacuum line system and is also moderately time consuming as the evaporation vessels are suitable for sample sizes of 1 l, which may also be inappropriate for large amounts of natural groundwater. An other elaborated oxidation method with low blanks and short preparation time (1 day for 12 ml sample volumes) is using wet chemical oxidation (WCO) (Lang et al., 2012, 2013, 2016). However, all these drying methods are suitable for small sample volumes of groundwater and concentration needs to be conducted in a well equipped laboratory.

The methods RO/ED and ultrafiltration retain organic substances by a similar physical mechanism as the water sample is forced through a membrane of different permeabilities. Thus, the remaining solution (retentate) has an elevated DOC concentration. Theoretically, RO membranes retain all sizes of organic matter as well as inorganic salts while ultrafiltration retains only the HMW fraction (>1,000 u) of the DOC. Desalination of the sample is performed by electrodialysis (ED) coupled with RO and by diafiltration in ultrafiltration. The elution of DOC using RO/ED is rinsed from the membrane by pH 12 NaOH whereas the DOC extract of ultrafiltration is chemically not manipulated by pH changes (Minor et al., 2014).

Although the RO/ED method provides very high recoveries compared to other DOC extraction methods and the DOC extracts are more representative of the DOC found in the original (marine) water samples, the disadvantages of this method are the comparatively very high costs and the extremely time-consuming procedure (Minor et al., 2014; Swenson, 2014).

Ultrafiltration has been widely used for DOC extraction, but considerable differences have been found in the extraction and recovery of organic compounds with different ultrafiltration systems and operating conditions. In addition, smaller organic compounds cannot be isolated with ultrafiltration due to the atomic size cut-off of 1,000 u. However, ultrafiltration does not require chemical manipulations such as pH changes that may alter or degrade the extracted dissolved organic substances. DOC recoveries for open ocean samples ranged from 20 to 40 %, and 50 to 70 % and were higher for coastal and freshwater samples (Minor et al., 2014; Benner et al., 1992; Guo and Santschi, 1996; Simjouw et al., 2005; Kruger et al., 2011).

Compared to both other extraction methods RO/ED and ultrafiltration, SPE is the most widely used extraction method of organic substances as it is considered to be easier, quicker and cheaper. The mechanism of SPE for retaining organic carbon is very different compared to RO/ED and ultrafiltration. In SPE, organic substances within a water sample are adsorbed onto a stationary phase and then eluted in a small volume of a solvent of suitable polarity. However, this method subjects the water sample to extreme pH changes and it may be time consuming if samples are used in multiple columns of different resins. This may also increases the possibility of chemical changes to the native DOC and can lead to both contamination and incomplete recoveries (Minor et al., 2014).

The classic extraction approach of using XAD resins, such as XAD-8 for the classification of organic compounds, was very common in the past, but some of the XAD resin types are

no longer manufactured. Therefore, novel non-polar stationary phases based upon styrene divinylbenzene (e.g. XC resins or Bond Elut PPL) or hydrocarbons bonded to a silica matrix (e.g. C-18) are mainly used nowadays with different preferential adsorption behaviours (Minor et al., 2014). SPE shows recoveries between 5 and 89 % depending on the used resin, which tends to achieve higher recoveries in freshwater and coastal samples than in open ocean samples (Mills and Quinn, 1981; Thurman, 1985; Hedges, 1992; Lara and Thomas, 1994; Kim et al., 2003; Simjouw et al., 2005; Coppola et al., 2015; Dittmar et al., 2008; Dalzell et al., 2009; Kruger et al., 2011; Green et al., 2014; Li et al., 2016).

It was shown recently that SPE of organic substances using PPL resins is a very reliable and sufficient method for extracting the DOC stemming from natural water with very low DOC contents (Dittmar et al., 2008; Swenson et al., 2014; Swenson, 2014; Coppola et al., 2015; Li et al., 2016). The SPE-PPL method is particularly capable of extracting hydrophobic and highly to non-polar organic substances such as FA and the extracted DOC shows a comparable composition to the intrinsic dissolved organic matter of the water (Green et al., 2014; Swenson et al., 2014; Swenson, 2014; Li et al., 2016). Moreover, the SPE with PPL revealed the robust and highest recoveries compared to all other SPE resins (Minor et al., 2014; Swenson et al., 2014; Swenson, 2014).

2.5.2 Dating with radiogenic isotopes

Hypothetically, the exact age distribution in closed systems could be determined by the accumulation of an ideal isotope into groundwater in a closed system with a uniform and constant rate per unit volume without any chemical reactions or diffusive exchange (Bethke and Johnson, 2002). Noble gases are, among other elements, nearly chemically inert and relatively rare, which apparently makes them an ideal isotope (Ozima and Podosek, 2002). Only physical processes may affect and fractionate their proportions in groundwater. They originate in groundwater from three main sources: the atmosphere; the mantle, from magmatic activity or diffusive ascending flux; and produced by radioactive decay processes in the crust (Ballentine and Burnard, 2002). The concentrations of dissolved noble gases in groundwater are mainly controlled by the atmospheric input and convey information on physical properties of the water during air-equilibration at the air/water interface during recharge (Andrews and Lee, 1979; Andrews et al., 1985; Aeschbach-Hertig et al., 2000; Kipfer et al., 2002).

Helium and argon contents in basin aquifers consist of natural atmospheric background and terrigenous excess components. Both components are easily identifiable by their specific noble gas isotope ratios. The isotopes of ^{4}He and ^{40}Ar are produced by decay of naturally occurring radionuclides of U, Th and K with very long half-lifes and constant production rates of the daughter product (Bethke and Johnson, 2008). The linear accumulation of stable radiogenic noble gas isotopes, ^{4}He and ^{40}Ar, provide under the assumption of closed systems a suitable

dating tool to estimate apparent residence times of submodern to old groundwater in deep sedimentary basin aquifers (Andrews et al., 1985, 1987; Stichler et al., 1987; Weise and Moser, 1987; Torgersen et al., 1989; Castro et al., 1998b,a; Greene et al., 2008; Torgersen and Stute, 2013; Gerber et al., 2017).

The apparent groundwater age with in-situ accumulating radiogenic noble gas isotopes is defined as the time t_{ex} required to accumulate the excess contribution C_{ex} of the radiogenic isotope, which is calculated using Eq. 2.4 (Stute et al., 1992; Torgersen and Clarke, 1985; Lippmann et al., 2003):

$$t_{ex}(yr) = \frac{C_{ex}}{A_{is} + \frac{J_c}{\phi \times z \times \rho_w}} \tag{2.4}$$

with the excess contribution C_{ex}, in-situ accumulation rate A_{is} and crustal flux J_c of the radiogenic isotope as well as the rock porosity ϕ, aquifer thickness z and water density ρ_w.

The challenge in dating with the accumulation rates of radiogenic noble gas isotopes is the often unknown and elusive crustal flux J_c and the diffusion of the noble gases into the surrounding aquifers or aquitards/aquicludes, which depends on the specific diffusion rates of the individual noble gases (Stute et al., 1992). The diffusive crustal fluxes may vary basin wide (Tolstikhin et al., 1996) and can be estimated by either differences of noble gas concentrations in a vertical or horizontal aquifer profile (Stute et al., 1992; Castro et al., 1998b; Osenbrück et al., 1998) or with the exactly known groundwater age derived from other dating methods (Torgersen and Clarke, 1985; Torgersen et al., 1989). The effect of diffusion on the noble gas concentrations in groundwater is relatively low in advective systems and increases in aquifers with low hydraulic conductivities (Castro et al., 1998b; Boving and Grathwohl, 2001).

2.5.2.1 Helium

Helium dissolved in groundwater is composed of several components from different sources that determine the measured helium isotope ratio $^3He/^4He$ (R_{meas}) of a sample (Eq. 2.5): an atmospheric component (He_{atm}) from air equilibrium during infiltration (He_{eq}) or air bubbles (He_a) and non-atmospheric components ($He_{non\text{-}atm}$) such as the terrigenous excess helium fraction (He_{ex}) from radiogenic in situ production in the rocks (He_{is}) and in the deep crust (He_c), as well as a mantle component (He_m), and a tritiogenic component (^3He_t) (Torgersen, 1980; Kipfer et al., 2002; Kulongoski and Hilton, 2012). The excess ^3He is formed by the radioactive decay of tritium (^3H) in the water, which is negligible in groundwater within deep sedimentary basins, and lithium (^6Li) in the crust.

$$
\begin{aligned}
R_{meas} &= \frac{^3He_{meas}}{^4He_{meas}} = \frac{^3He_{atm} + ^3He_{non\text{-}atm}}{^4He_{atm} + ^4He_{non\text{-}atm}} \\
&= \frac{^3He_{eq} + ^3He_a + ^3He_{is} + ^3He_c + ^3He_m + ^3He_t}{^4He_{eq} + ^4He_a + ^4He_{is} + ^4He_c + ^4He_m}
\end{aligned}
\tag{2.5}
$$

with the measured (meas), atmospheric (atm) and non-atmospheric, terrigenic excess (non-atm) helium ratios, which can be further subdivided into the components that are caused by equilibrium with air (eq), (excess)air-bubbles (a), the in-situ production (is), crustal flux (c) and mantle flux (m) or tritiogenic production (t).

In general, the non-atmospheric, terrigenous excess helium fraction, $^4He_{ex}$, is composed of the in-situ produced $^4He_{is}$ by the radioactive α-decay of uranium (^{235}U [7 ^4He atoms], ^{238}U [8 ^4He atoms]) and thorium (^{232}Th [6 ^4He atoms]) in the aquifer rocks, and the external sources of the (deep) crustal ^4He_c or mantle fluxes ^4He_m (Tolstikhin et al., 1996; Kulongoski et al., 2003; Phillips and Castro, 2014).

These terrigenous as well as atmospheric sources in groundwater can be separated with the $^3He/^4He$ ratios (R) and the Ne content of the sample (Weiss, 1971; Osenbrück et al., 1998; Kulongoski et al., 2003). The atmospheric $^3He/^4He$ ratio is R_a 1.38×10^{-6} and is stored in air-saturated water depending on salinity and temperature with R_{ASW} 1.36×10^{-6} (Clarke et al., 1976). $^3He/^4He$ ratios of crustal origin (R_c) typically range between 0.01 R_a and 0.1 R_a (Ballentine and Burnard, 2002; Kulongoski and Hilton, 2012; Phillips and Castro, 2014)) and mantle-derived helium has typical values of R_m between 5 and 10 R_a (Graham, 2002)). Using the measured radiogenic helium component and the calculated component based on the rock composition, the mean residence time of the water can be calculated, as the exchange of ^4He from rocks to fluid is assumed to be fast (Kulongoski and Hilton, 2012).

2.5.2.2 Argon

The radiogenic ^{40}Ar production in the crust is dominated by the decay of ^{40}K, and is, therefore, directly proportional to the K concentration in the subsurface (Ballentine and Burnard, 2002). The decay constant of ^{40}K is λ_K 5.463×10^{-10} per year. ^{36}Ar production in the crust is usually neglected as it is small compared to the ambient background of atmosphere-derived ^{36}Ar that is dissolved in groundwater (Ballentine and Burnard, 2002).

However, the measured $^{40}Ar/^{36}Ar$ ratio (R_{meas}) can be used to evaluate terrigenous $^{40}Ar_{ex}$ component (Eq. 2.6), which is composed of the radiogenic and in-situ produced contribution from ^{40}K decay ($^{40}Ar_{is}$) and the crustal flux ($^{40}Ar_c$) (Lippmann et al., 2003). The atmospheric $^{40}Ar/^{36}Ar$ ratio (R_a) ranges between 295.5 (Ozima and Podosek, 2002) and 298.5 (Lee et al.,

2006). Higher $^{40}Ar/^{36}Ar$ ratios point to a radiogenic $^{40}Ar_{ex}$ input and accordingly long residence times (Tolstikhin et al., 1996; Aeschbach-Hertig and Solomon, 2013).

$$R_{meas} = \frac{^{40}Ar_{meas}}{^{36}Ar_{meas}} = R_a + \frac{^{40}Ar_{ex}}{^{36}Ar_{meas}} = R_a + \frac{^{40}Ar_{is} + ^{40}Ar_c}{^{36}Ar_{meas}} \tag{2.6}$$

with the measured (meas) and atmospheric (a) $^{40}Ar/^{36}Ar$ ratios, R_{meas} and R_a, the measured components, $^{36}Ar_{meas}$ and $^{40}Ar_{meas}$, the radiogenic excess from in-situ production $^{40}Ar_{is}$ and the crustal $^{40}Ar_c$.

2.6 The study area in the South German Molasse Basin

The study area extends over the federal states of Bavaria and Baden-Wuerttemberg in southern Germany and is located in the South German Molasse Basin (SGMB). The SGMB is part of a Cenozoic foreland basin at the northern front of the Alps. It extends from eastern parts of France (F), Switzerland (CH), Germany to Austria (AU) with a length up to 1,000 km (Fig. 2.12).

The SGMB is a "foreland basin play type" with the "Upper Jurassic aquifer" as a play (Moeck et al., 2020). The primary geologic controls on this play, containing mainly limestones, are deposition or faulting, compaction, and diagenesis, and, thus, episodes of basin subsidence and burial history that have a strong influence on reservoir productivity (Mraz et al., 2019; Moeck et al., 2020).

2.6.1 Geological description

The SGMB was formed in consequence of the Euro-Adriatic continental collision during the Alpine orogeny and is limited in the north and west by the outcropping Upper Jurassic carbonate formations of the Franconian Alb and Swabian Alb, in the south by the Alpine orogeny (Alps) and in the east by the crystalline basement rocks of the Bohemian Massif. The Upper Jurassic rocks are inclined to the south due to the Alpine orogenesis to a depth of 6 km at the fringe of the Alps (Fig. 2.12) (Lemcke, 1988).

The post-Palaeozoic sedimentation have occurred in three epidiagenetic cycles: the first phase in the time between the Triassic Bunter Sandstone and Mesozoic Upper Jurassic, with the transgression of the post-Permian land surface and the "Vindelician Land" between the northern and southern sea; the second phase starting in the Mesozoic Cretaceous until the Neogene (Miocene), which comprises the evolution of the Molasse Basin; and the process of the Alpine orogeny as the third phase. The sedimentary structure of the SGMB begins with deposits of the Upper Carboniferous and Permian, which were deposited in several troughs into the Paleozoic crystalline basement. During the Mesozoic, the Tethys successively transgressed from the west and north over the indenting Vindelician Land between the Bohemian Massif and the Black

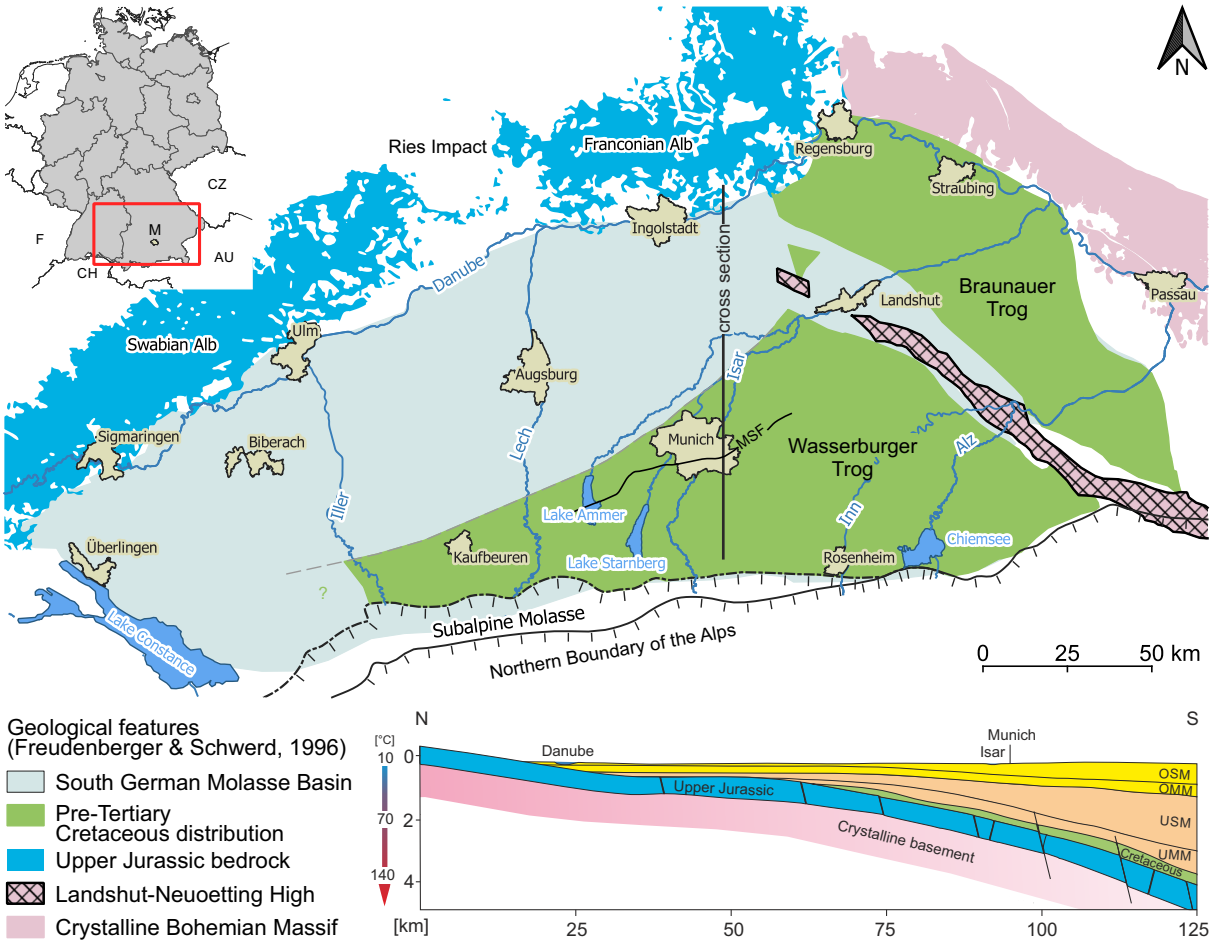

Figure 2.12: Overview of the South German Molasse Basin (SGMB) with important geological features after Freudenberger and Schwerd (1996) and a geological cross-section through the central SGMB (modified from Lemcke (1988)).

Forest until the deposited marine sediments have covered the old mainland completely. This sedimentation processes began in the Alpine Foreland with the deposition of the terrestrial Bunter Sandstone on the western side of Lake Constance and have ended after an almost complete subsidence of the Vindelician Land with the reaching of the marine Upper Jurassic into Upper Austria. The marine environment receded from the foreland to the south and southwest in the direction of the Tethys ocean at the end of the Upper Jurassic. During this subsidence of the marine environment, a northwest-southeast-striking crystalline threshold region, the so-called "Landshut-Neuoetting High" (LNH) evolved, which divides the troughs of the central Molasse Basin, the so-called "Wasserburger Trog" in the west from the "Braunauer Trog" in the north-east. Further on, the marine Cretaceous was deposited and deeper erosion and karstification began from south to north due to a gradual inclination of the Upper Jurassic sediments towards the south. The Upper Cretaceous sea regression was followed by several cycles of

marine transgressions and regressions, which created large river and drainage systems in the sediments in the Molasse Basin area. During the Pleistocene, the Quaternary deposits were dominated by glaciers with great extensions and thicknesses over 1,000 m in the south of the SGMB (Fig. 2.12). (Udluft, 1975; Lemcke, 1981; Villinger, 1988; Lemcke, 1988)

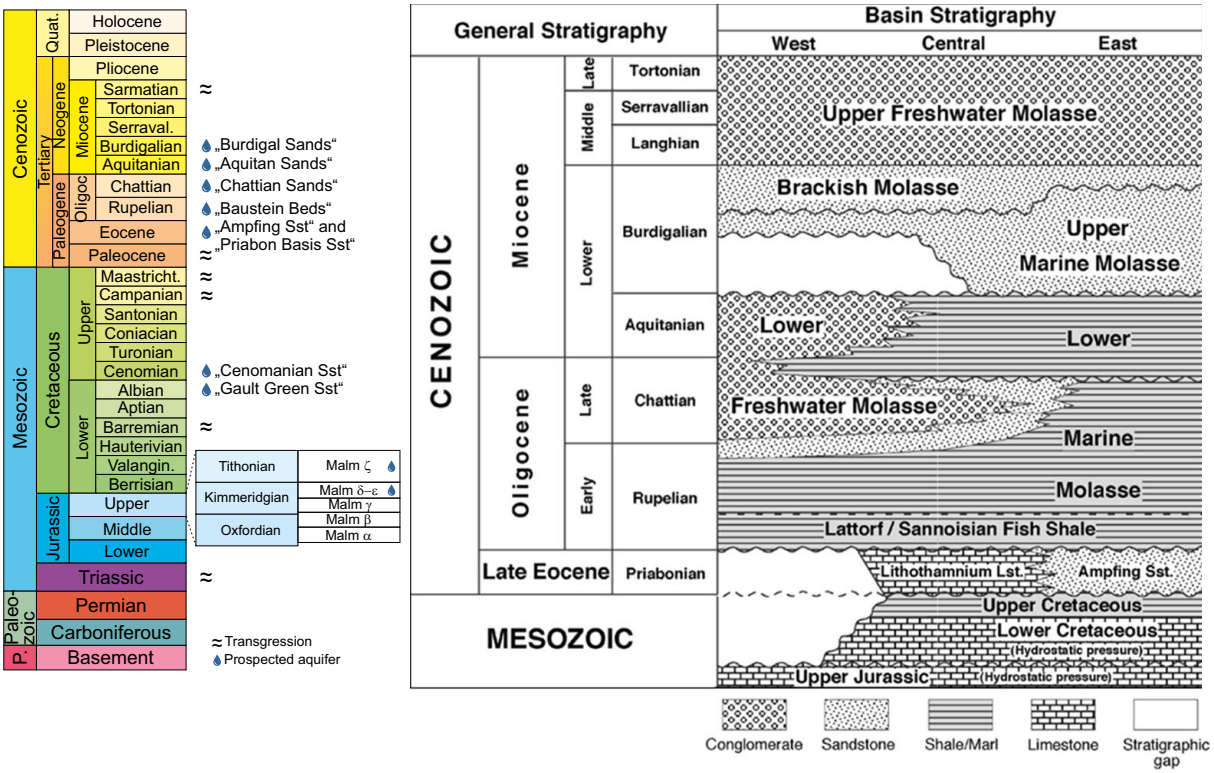

Figure 2.13: Chronostratigraphical chart (modified from Cohen et al. (2013) and Kuhlemann and Kempf (2002)) with important prospected aquifers of the SGMB after Hänel et al. (1984) and Fritzer et al. (2019) and stratigraphic framework of the Alpine Foreland Basin (modified from Drews et al. (2020)).

The foreland Molasse Basin sediments consist of alternating Cenozoic sequences, the so-called Tertiary Molasse sediments (Figs. 2.12 & 2.13). These Molasse strata is composed of fluviatile (OSM: Upper Freshwater Molasse and USM: Lower Freshwater Molasse) and shallow marine (OMM: Upper Marine Molasse and UMM: Lower Marine Molasse) sediments, such as sand-, clay- and limestones, from the Paleogene and Neogene which cover the south- and eastward dipping Mesozoic sedimentary rocks (Freudenberger and Schwerd, 1996; Véron, 2005; Ortner et al., 2015).

Some of the Tertiary Molasse sediments show good hydraulic conductivities and are groundwater bearing. Relevant aquifers in the SGMB, with different hydraulic characteristics, are the “Burdigal Sands” (OMM), “Aquitan Sands” (USM), “Chattian Sands”, “Baustein Beds”, “Ampfing Standstones” and “Priabon Basis Sandstones” (all UMM) (Hänel et al., 1984; Fritzer

et al., 2019). In addition, the so-called Graupensand valley containing partly highly permeable sandy and gravelly sediments from the Miocene Grimmelfingen and Kirchberger Formation extends more or less parallel south to the river Danube from south-west to north-east and overlay the Upper Jurassic aquifer next to the city of Ingolstadt (Reichenbacher et al., 1998; Buchner et al., 2003). In contrast, some Tertiary low permeable beds (shales) in the southern and eastern part of the SGMB are considerably overpressured (Drews et al., 2020, 2018).

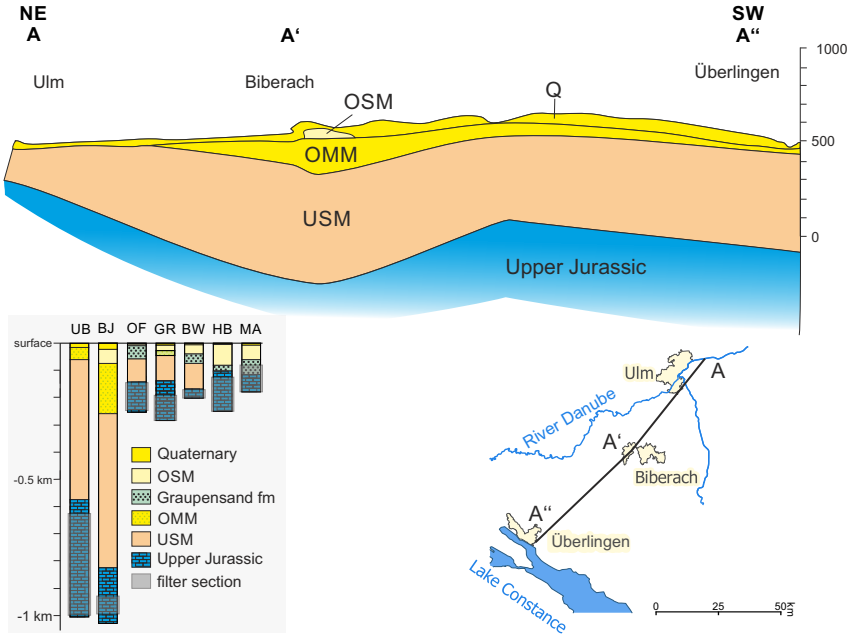

Figure 2.14: Simplified geological cross section through the western South German Molasse Basin (SGMB) based on Bertleff (1986) and Bertleff and Watzel (2002) as well as lithological borehole profiles from the investigated wells including the position of the well screens (for locations, see Fig. 4.1).

Although the Cretaceous has been completely eroded in some parts of the SGMB, it is still preserved there due to the formation of sedimentation troughs (Wasserburger and Braunauer Trog). In these areas, the Upper Jurassic sediments forming the aquifer are covered by Mesozoic sediments of the Purbeck and Cretaceous (Lemcke and Tunn, 1956; Udluft, 1975; Bachmann et al., 1987; Freudenberger and Schwerd, 1996) (Fig. 2.12). Relevant aquifers of the Cretaceous strata are the “Cenomanian Sandstone” and the “Gault (Green) Sandstone” (Hänel et al., 1984; Fritzer et al., 2019). In the remaining regions where the Cretaceous sediments are not present, especially towards the west of the SGMB, the Tertiary Molasse sequences overstep and cover the Upper Jurassic directly (Lemcke, 1981). In the western SGMB, the Upper Jurassic carbonates are mostly covered by the lowermost Molasse sediments of USM, which consist of clayey marls and clays (OF, GR, BW) or partly by freshwater carbonates (BJ, UB) with overall low hydraulic

permeabilities (Fig. 2.14) (Bertleff, 1986; Bertleff et al., 1993; Frisch and Huber, 2000; Geyer and Gwinner, 2011; Stober, 2013).

The Upper Jurassic carbonates forming the aquifer is composed of mainly dolomitised and highly permeable carbonate rocks of the Kimmeridgian stage (Malm $\delta - \epsilon$) with karstic features and the partly karstified rocks that belong to the Tithonian stage (Malm ζ) (Fig. 2.13) (Villinger, 1988; Mraz et al., 2019). The Upper Jurassic rocks were rather deposited in the Franconian, Swabian or Transition zone facies in the study area (Fig. 2.15). The Swabian and Franconian facies can be subdivided into the hydraulic permeable massive facies or reef facies and the lower permeable bedded facies (Meyer and Schmidt-Kaler, 1989; Mraz et al., 2019). The Swabian Marl Basin separates the massive facies of the Swabian facies in the west from the Franconian facies in the wast of the SGMB. The reef facies and Swabian Marl Basin intersect with the very lowly permeable transition zone facies (formerly and commonly known as the "Helvetian facies") in the south of the SGMB (Lemcke, 1988; Mraz et al., 2019). The Danube flows along the western and northern margin of the SGMB and is partly deeply cut into the Upper Jurassic karst where it then represents the preliminary drainage for the Upper Jurassic groundwater. In some places, however, it is also separated from the Upper Jurassic aquifer by clayey sediments of the Upper Freshwater Molasse (OSM), where no hydraulic interaction takes place (Lemcke, 1976).

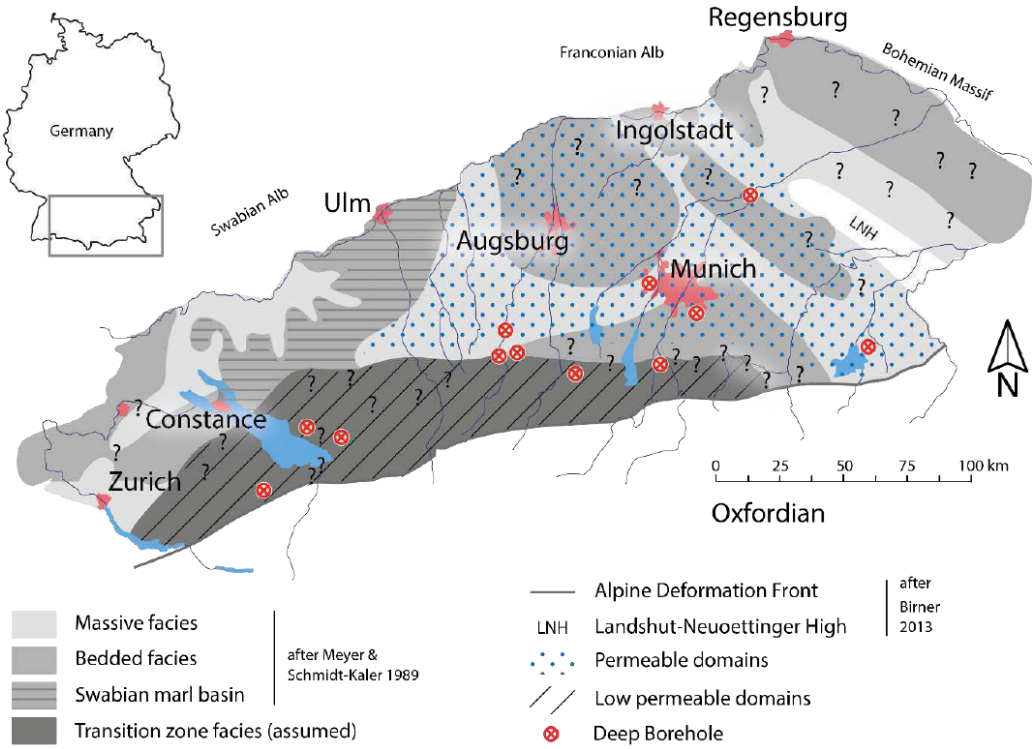

Figure 2.15: Distribution of the depositional environment, permeable domains and transition zone facies for the Upper Jurassic during the Oxfordian (Mraz, 2019).

In addition, fault systems are also present in the foreland basin, especially normal faults in the Upper Jurassic strata Normal faults that are orientated parallel to the Alps (Konrad et al., 2019; Drews et al., 2019). In the Munich area, the main normal fault systems, the Munich & Markt-Schwaben Fault (MSF) (Fig. 2.12) represents a main target for the geothermal exploration.

The thickness of the Upper Jurassic aquifer is around 400 to 600 m and the rocks are composed of limestones and dolostones with a wide range of matrix porosities (<1 up to 20 %) and hydraulic matrix permeabilities (1×10^{-16} to 1×10^{-9} m^2 (0.01 to 1013 mD)) (Birner et al., 2012; Böhm et al., 2013; Mraz et al., 2018; Konrad et al., 2019; Bohnsack et al., 2020; Konrad et al., 2021). A general overview of permeable and low permeable areas for the western and central SGMB is shown in Fig. 2.15. In the greater area of the city of Munich, the matrix permeabilities of the Upper Jurassic aquifer decrease from north to the south and south-west from 1×10^{-12} to 1×10^{-16} (Fig. 2.16, Konrad et al. (2021)), which could be related to the extension of low permeable transition zone facies in that area (Mraz, 2019) or to the stress induced reduction of pore space during burial (Bohnsack et al., 2021).

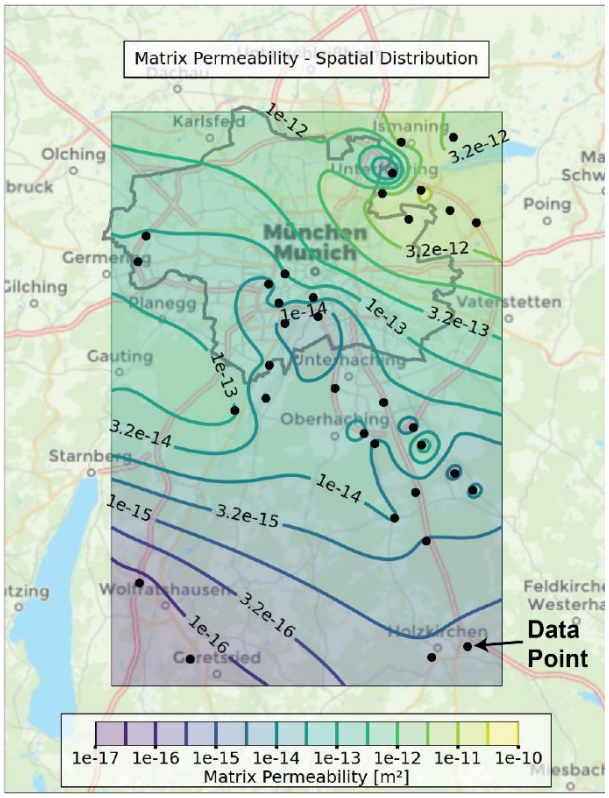

Figure 2.16: Regionalised matrix permeability in the greater area of the city of Munich after Konrad et al. (2021).

The geothermal gradient of this deep aquifer is regularly around 3.3°K, but can locally be increased up to 12.5°K (Wrobel et al., 2002). Thus, the reservoir temperatures can reach >155 °C in the south of the SGMB. In addition, a negative temperature anomaly was described for the Wasserburger Trog, indicating a low geothermal gradient in the east of the central basin in the Wasserburger Trog east of the city of Munich (Fig. 2.17) (Agemar et al., 2014a).

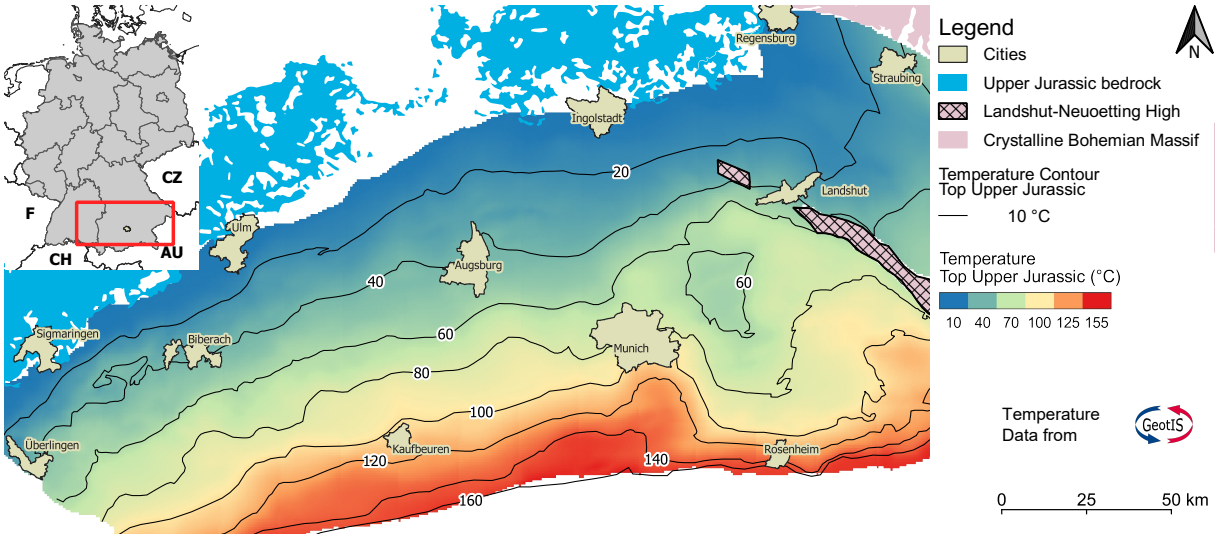

Figure 2.17: Temperature distribution of the SGMB based on data from GeotIS (Agemar et al., 2014a).

The SGMB also comprises further oil and gas reservoirs (Hahn-Weihnheimer et al., 1979). Especially, the Mesozoic sediments of the Middle and Upper Triassic Muschelkalk and Keuper are considered to be the mother rocks for the hydrocarbons. Prominent source rocks of the hydrocarbons are the carbonates and sandstones of the Eocene (UMM), Oligocene (UMM and USM) and Miocene (OMM) (Stichler, 1997). In the west of the SGMB, hydrocarbons occur predominantly as Triassic-Lias oils in the early Chattian Baustein Beds or as clast oil from the bituminous Helvetic Upper Jurassic. In the eastern SGMB, hydrocarbons occur predominantly in the deep Tertiary base Sandstones (Priabon) south-east of Munich. However, the Upper Jurassic sediments also contain crude oil and are, thus, considered to be both, source and reservoir rock (Hahn-Weihnheimer et al., 1979).

2.6.2 Upper Jurassic groundwater flow system: a historical review

The systematic exploration of hydrocarbons in the SGMB started in the year 1948 and was continuously accompanied by scientific investigations of the oilfield groundwater that have also occurred in the hydrocarbon wells (Udluft, 1975; Lemcke, 1976). The progressive geothermal exploration of the Upper Jurassic aquifer in the last years has steadily provided new data and interpretations of recharge areas and infiltration conditions, groundwater flow direction

as well as possible exchange processes between the overlying and underlying formations and sediments with the Upper Jurassic groundwater in the SGMB. In the last decades, different hypotheses about the groundwater flow regime and reservoir understanding have been proposed, which essentially resulted in different and in some areas contradicting hydrogeological model concepts, e.g. in the Wasserburger Trog (Fig. 2.18). The various hydrogeological models that are shown in Fig. 2.18 are explained in detail in the following sections in terms of their history of development, the methods used and relevant statements regarding the derived groundwater flow direction.

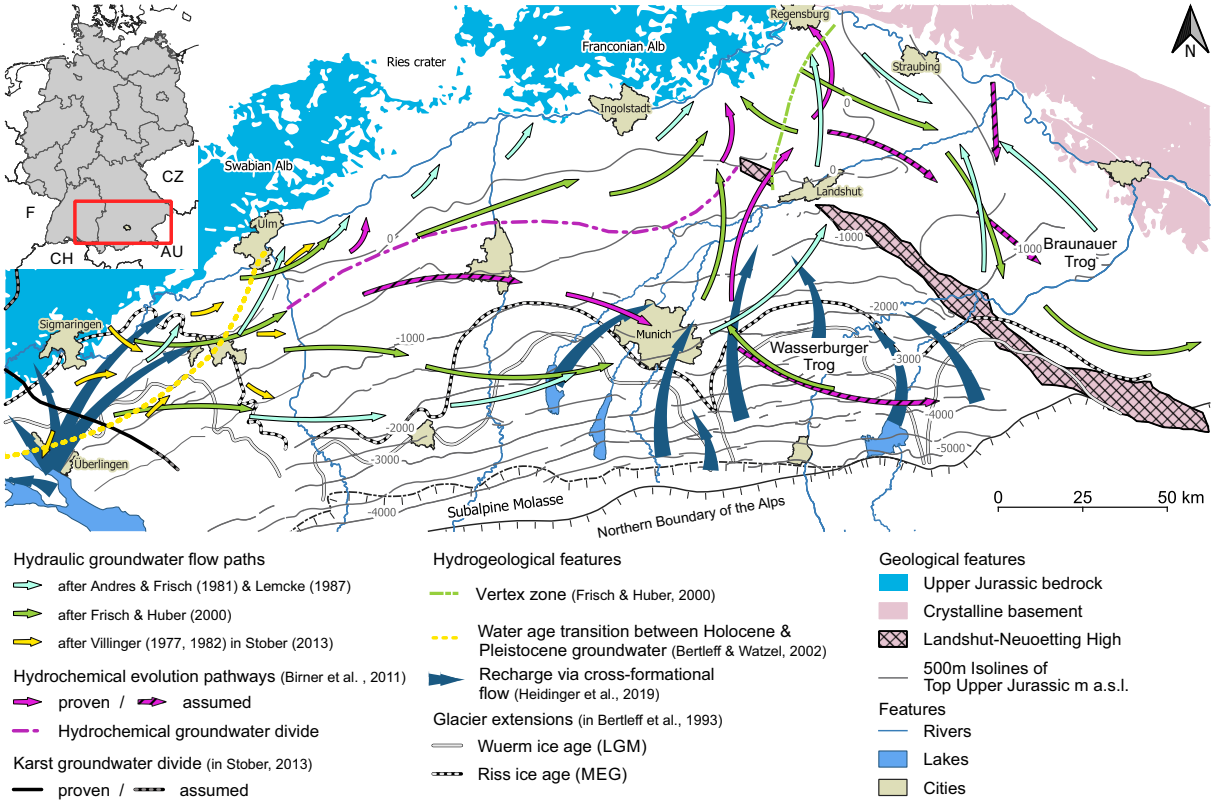

Figure 2.18: Comparison of hydrogeological groundwater concepts for the Upper Jurassic aquifer in the South German Molasse Basin (SGMB) with hydraulic flow paths and hydrochemical evolution pathways (Andres and Wirth, 1981; Lemcke, 1987; Bertleff et al., 1993; Frisch and Huber, 2000; Stober, 2013; Birner, 2013; Heidinger et al., 2019).

2.6.2.1 The first phase of deep groundwater studies

One of the first authors to study the systematics of Upper Jurassic groundwater and the overlying Tertiary horizons on a large-scale was Kurt Lemcke (e.g. Lemcke and Tunn (1956); Lemcke (1976, 1987)). Based on a few water chemical analyses from different formations in the SGMB obtained during hydrocarbon exploitation, the water chemical composition of the Upper Juras-

sic groundwater was surprisingly found to be regularly lowly saline (fresh water) in contrast to most overlying highly saline Tertiary formation waters (Nathan, 1949; Cramer, 1953; Aldinger et al., 1955; Lemcke and Tunn, 1956). Therefore, it was tried to systematically develop a regional distribution concept of fresh and saline water using resistance and potential measurements in vertical profiles of hydrocarbon wells (Lemcke and Tunn, 1956). In the Upper Jurassic sediments and the overlying Cretaceous or Tertiary formations that are in direct hydraulic contact with each other, mainly freshwater was observed. In contrast, in Tertiary sandstones (USM and UMM) where Cretaceous sediments with low hydraulic conductivity overlie the Upper Jurassic aquifer, the water was regularly highly saline. Above these formations with highly saline waters, the water chemical composition in the uppermost Tertiary formations (OSM and OMM) was again found to be dominated by fresh water. The resulting sharp vertical fresh-saline water boundaries detected along the borehole sections suggested that the salinity in the pore water was distributed independently of the syngenetic formation water when the sediments were deposited. It was also detectable that the upper fresh-saline water boundary were shifted stratigraphically upwards from west to east (Lemcke and Tunn, 1956). Consequently, the regional distribution of this fresh-saline water boundary and Upper Jurassic karst water levels led to a wider picture of the hydraulic interaction of the Upper Jurassic and Tertiary aquifers. Moreover, the surface water and groundwater of the entire SGMB was found to discharge on the surface mainly to the river Danube or, in the southwestern SGMB, partly to the river Rhine. The Upper Jurassic groundwater table is either open in the areas close to the outcrops of the Franconian and Swabian Alb and discharging river Danube or confined to the deeper parts of the basin. The river Danube's lowest surface water level with the most hydraulic impact on the Upper Jurassic groundwater drainage were found to be located between the cities of Sigmaringen and Ulm, and especially around Regensburg (Lemcke and Tunn, 1956).

In the further course of exploration, Lemcke (1976) refined the large-scale hydraulic model of the deep groundwater in the SGMB and developed a first comprehensive hydraulic model of the groundwater potentials based on new findings from the progressive hydrocarbon exploration (Fig. 2.19). This model was supported by local near-surface studies of the Upper Jurassic aquifer at the Franconian Alb and south to the river Danube (e.g. Andres and Claus (1964); Apel (1971); Traub (1971)). The hydraulic potential studies were based on the important and required assumption of a coherent pressure level in the karst aquifer of the Upper Jurassic (Lemcke, 1976; Villinger, 1977; Andres and Wirth, 1981). It is worth noting that this hydraulic model of groundwater potentials for the Upper Jurassic aquifer was mainly based on data from hydrocarbon wells tapping the overlying Chattian and Rupelian "Baustein Beds" and Cretaceous "Gault Sandstones". Although these strata are predominantly hydraulically separated from the Upper Jurassic aquifer, it was assumed that the potentials were similar due to, among other things, the hydrochemical similarity of the waters (Udluft, 1975; Andres and Wirth, 1981).

Especially in deeper areas, only few direct measured data from the Upper Jurassic aquifer was available at that time. Moreover, the groundwater potential isolines were derived from static water levels or closing pressures of the wells, which may have additionally led to improper results, as no necessary temperature correction could be carried out at many wells (Lemcke, 1976; Villinger, 1977; Andres and Wirth, 1981).

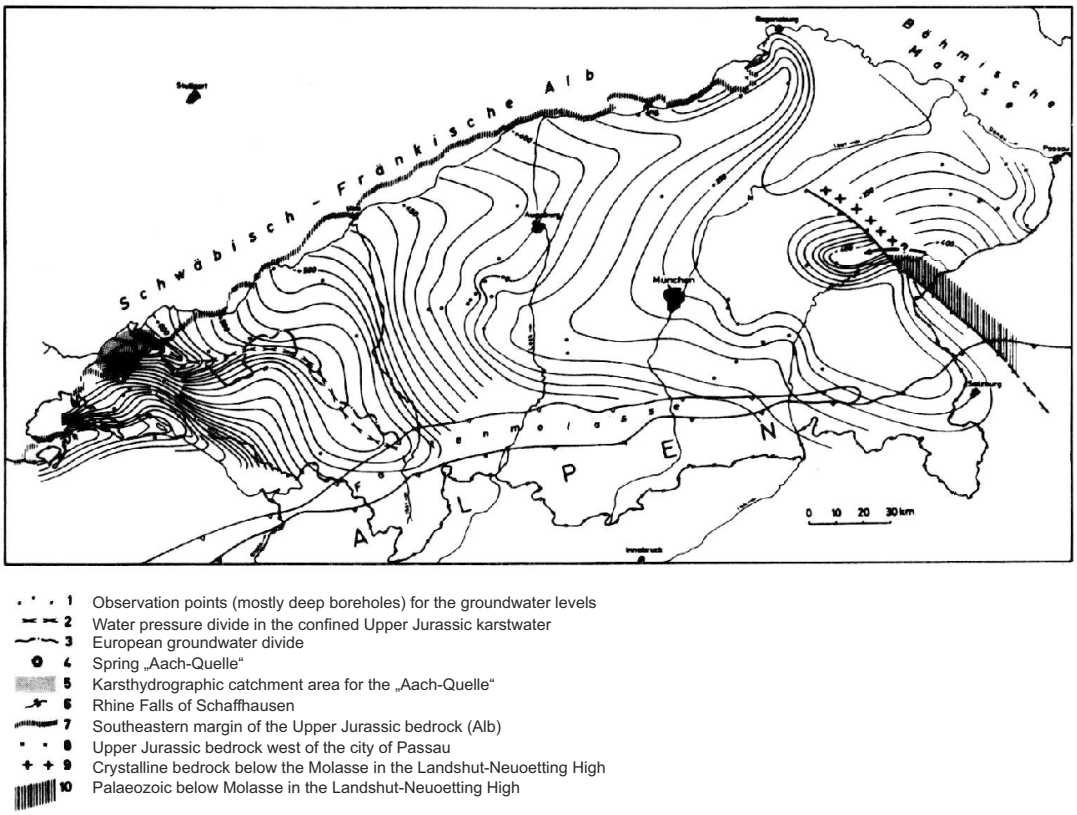

Figure 2.19: Hydraulic groundwater potentials for the Upper Jurassic aquifer in the South German Molasse Basin (SGMB) (modified from Lemcke (1976)).

However, due to the discovery of the crystalline barrier in the eastern area of the SGMB, the Landshut-Neuoetting High (LNH), the basin was further subdivided into different subareas. Specifically, the subareas were formed with the use of geological borders (e.g. LNH) or oriented along national borders (e.g. Bavarian and Upper Austrian border). For example, the thermal water of the central SGMB in the Wasserburger Trog was divided from the thermal water in the eastern SGMB within the Braunauer Trog by the hydraulic barriers LNH and the so-called "Zentrale Schwellenzone" adjoining in the south (Udluft, 1975). The subarea Braunauer Trog is thus framed by the crystalline structures LNH and the Bohemian Massif and forms, therefore, together with the Upper Austrian Molasse Basin in the south a relatively independent hydrogeological system.

2.6.2.2 Second phase: further development of the hydrogeological system

Based on this first groundwater model, several authors developed the hydrogeological system understanding from the 1970s to the 1990s using different hydrological, hydraulic, water chemical and environmental isotopic methods to clarify various hydrogeological problems in the subareas of the SGMB. The most prominent authors are namely Peter Udluft (Udluft, 1975), Eckhard Villinger (Villinger, 1977, 1986, 1988), Gerhard Andres (Andres and Wirth, 1981), Bruno Bertleff (Bertleff, 1986; Bertleff et al., 1987b,a, 1993), Willibald Stichler (Stichler et al., 1987; Stichler, 1997), and Stephan Weise (Weise and Moser, 1987).

Andres and Wirth (1981) compiled the previous work of Lemcke and Tunn (1956), Andres and Claus (1964), Udluft (1975), Lemcke (1976) and Villinger (1977), which resulted in an overall hydraulic groundwater potential plan for the Upper Jurassic aquifer of the entire SGMB and of adjacent Upper Jurassic outcrops at the southern Franconian and Swabian Albs (Figs. 2.20 & 2.18). They not only used measured hydraulic potentials as Lemcke (1976) did, which, as already mentioned above, could be subject to error, but also considered information from hydrochemical analyses.

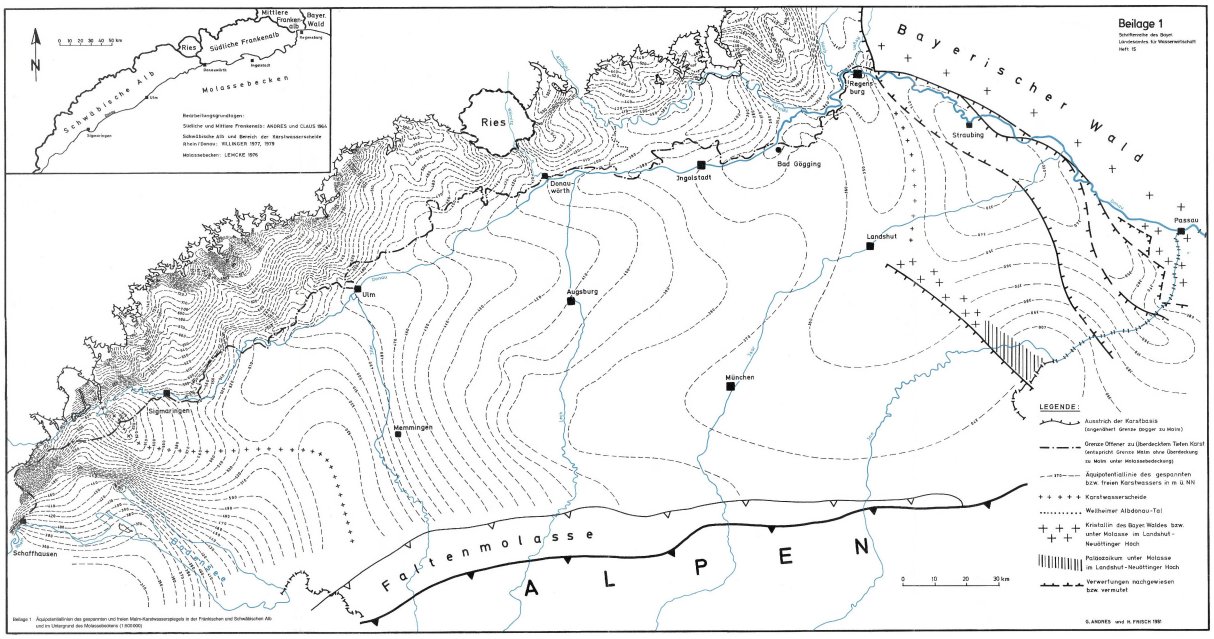

Figure 2.20: Hydraulic groundwater potentials for the Upper Jurassic aquifer in the South German Molasse Basin (SGMB) and southern Upper Jurassic outcrops (Andres and Wirth, 1981; Andres and Frisch, 1981). Translation of important features: Äquipotentiallinie - hydraulic potential lines; Karstwasserscheide - groundwater divide

As a result, a general SW-NE tending flow direction of the Upper Jurassic groundwater parallel to the river Danube was further promoted (Fig. 2.18). Above all, they have emphasised the river Danube's substantial drainage effect for the southward-flowing waters of the Franco-

nian Alb and pointed out a backwater of the waters flowing towards the river Danube from the north and south (Apel, 1971; Udluft, 1975). Between the Rhenish and Danubian discharge systems, a groundwater divide was postulated north of the lake Constance. The main discharge of the deep Upper Jurassic groundwater was found around the city of Regensburg in the east of the SGMB due to the karst water pressure depression. Contrary to the general flow direction of the western and central SGMB, the groundwater potentials east of the LNH indicated in the Braunauer Trog a flow from south to north, which was explained by the hydraulic barrier of the Landshut-Neuoetting High (Lemcke and Tunn, 1956; Udluft, 1975; Lemcke, 1976).

A further extended and slightly revised version of the model from Lemcke (1976) and Andres and Wirth (1981) was performed by Lemcke (1987) based on newly integrated data from hydrocarbon wells (Fig. 2.21). However, this hydraulic groundwater potential plan for the Upper Jurassic aquifer is almost similar to the plan of Andres and Wirth (1981) and does not result in a substantially different flow system for the deep Upper Jurassic groundwater (Fig. 2.18).

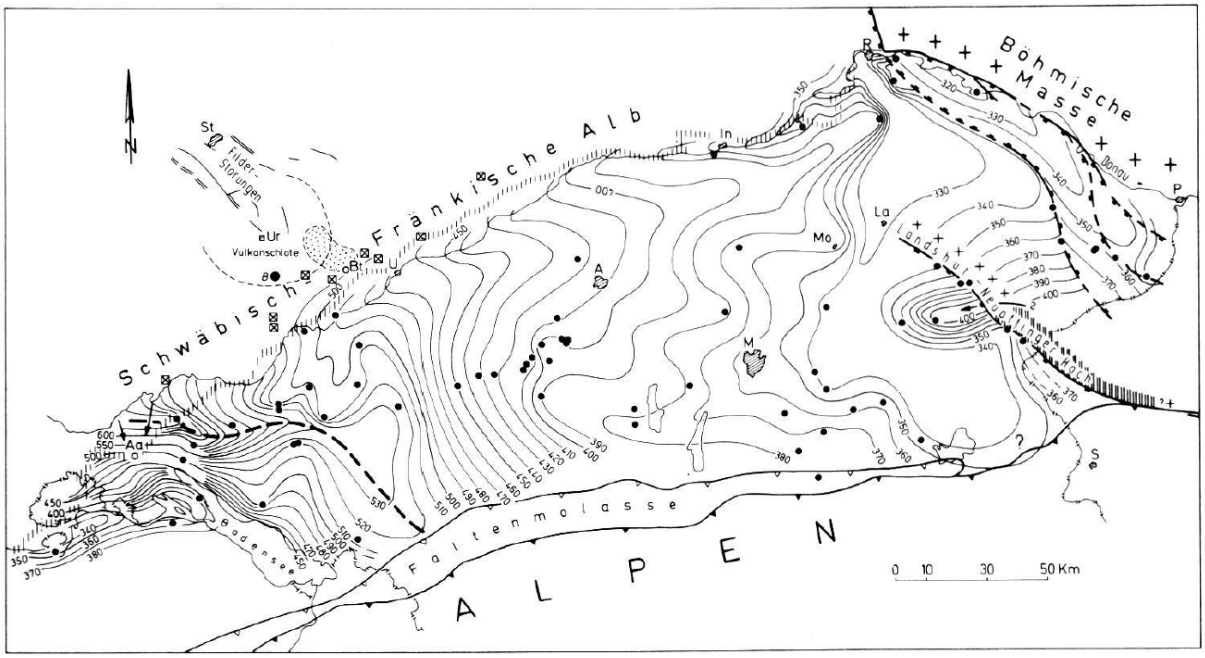

Figure 2.21: Hydraulic groundwater potentials for the Upper Jurassic aquifer in the South German Molasse Basin (SGMB) after (Lemcke, 1987). Points: Observation points (mostly deep boreholes); strong rifted line north of Lake Constance: presumed pressure water divide in the stressed Upper Jurassic karst water; short vertical hatching: southeastern edge of the Alb's overlying Upper Jurassic; crosses or vertical thick/thin hatching: crystalline or Palaeozoic of the Landshut-Neuoetting High (LNH); squares with horizontal cross: important karst springs and caves on the SE edge of the Swabian Alb; arrows: karst water drainage to the Aach spring and (possibly) via the LNH to the Wasserburger Trog.

In the course of exploring geothermal energy and assessing its potential, a hydrogeothermal pilot study (Hänel et al., 1984) and a comprehensive research project (Werner, 1987; Frisch and

Werner, 1991a,b) were conducted. Due to these comprehensive and multifaceted studies, the existing groundwater model was partially extended, revised or homogenised with models of surrounding areas, e.g. the Swiss part (e.g. Balderer (1990)) or the Upper Austrian part (e.g. Goldbrunner (1987, 1999); Andrews et al. (1985, 1987)) of the Molasse basin.

Besides the determination of the groundwater flow systematic, one of the most crucial questions for many authors continued to be the location of the recharge areas and the infiltration mechanisms for the deep Upper Jurassic groundwater and its water balance. The most prominent recharge area was postulated at the Upper Jurassic outcrops of the Swabian Alb in the western SGMB. Lemcke and Tunn (1956) and Villinger (1977) hypothesized the main recharge area for the deeper Upper Jurassic karst in the greater area of the city of Sigmaringen, which has been elaborately confirmed in detail by Bertleff (1986); Bertleff et al. (1993); Bertleff and Watzel (2002). Their considerations led to the conclusion that pressure differences between the free karst water table of the Upper Jurassic and the Tertiary groundwater caused a downward pore fluid migration in areas with negative hydraulic potentials. Thus, a considerable amount of groundwater have recharged via the Tertiary Molasse sediments according to the assumed leaky aquifer principle, which was also supported by various studies (e.g. Udluft (1975); Andres and Wirth (1981); Hänel et al. (1984); Stichler et al. (1987); Prestel (1988); Weise et al. (1991)).

For the western SGMB, a sophisticated infiltration and groundwater flow model with three different major currents in the flow system was developed (Bertleff, 1986; Bertleff et al., 1987a, 1993): (i) a locally occurring, shallow, dynamic and fast circulation system in the northern part with recently recharged karst groundwater; (ii) an intermediate flow system in the deeper southern part of the western SGMB with a discharge into the river Danube around the city of Ulm, which is in line with the developed flow path of Villinger (1977) in Fig. 2.18; and (iii) a regional circulation system towards the discharge area around the city of Regensburg according to Andres and Wirth (1981) and Lemcke (1987).

The Upper Jurassic groundwater in the (i) local circulation system is restricted to the valley of the partly draining river Danube. In the local and shallow circulation system, a still occurring recent recharge of Ca-(Mg)-HCO_3 type water with detectable (inorganic) radiocarbon and tritium contents was found to take place at the Alb plateaus (Weise et al., 1991; Bertleff et al., 1993; Stober, 2014).

While the groundwater recharge and discharge areas as well as the principles of interaction with the Tertiary sediments had been intensively studied and well understood for the local circulation system, the recharge systematics of the deeper and thermal water in this area still is still unclear. Recent recharge of younger groundwater in the deeper parts through the covering sediments was assumed to be very small (Bertleff and Watzel, 2002). The water age transition in Fig. 2.18 represents the boundary between the local and the intermediate/regional

groundwater flow systems, with groundwater of Holocene origin to the north and Pleistocene thermal water in the south (Bertleff and Watzel, 2002). In the (ii) intermediate and (iii) regional circulation systems, the groundwater showed ion-exchange character (Na-HCO_3 and Na-HCO_3-Cl) and had been recharged under considerably colder climate conditions than today (Bertleff et al., 1993). In this model concept, the Pleistocene groundwater is supposed to flow northwards, where it possibly mixes with younger water that has been recently recharged in the Alb plateaus, and/or drains into the river Danube (Weise et al., 1991; Fischer et al., 1992; Bertleff and Watzel, 2002). In contrast, the chloride concentration of the thermal groundwater was found to increase in southeastern direction from 10 up to 15,000 mg/l (Fig. 2.26), which indicates a distinct influence of highly saline formation water caused by the occurring very low permeabilities and low water exchange with the hydraulically active flow system in this area (Stober, 2014; Mraz et al., 2019).

To explain this complex infiltration system, Bertleff et al. (1993) proposed a novel hydrodynamic system, where the recharge was via cross-formational flow. This concept is based on the principle of the subglacial groundwater recharge in overdeepened glacial basins into the Tertiary Molasse sediments. The main recharge was postulated during the ice ages in areas with no permafrost and a permeable hydraulic connection through the mostly lowly permeable Tertiary covers. The so-called Schussen area (not displayed in Fig. 2.18), south of the city of Überlingen at the Lake Constance was assumed to be geological suitable for the infiltration according this recharge model. However, the model had been continuously refined mainly by works of Ingrid Stober (Stober and Jodocy, 2011; Stober, 2013, 2014; Stober et al., 2014) and was recently supported by groundwater dating of the thermal water from Heidinger et al. (2019) (see Fig. 2.25) for this area as well as by Waber et al. (2014) in the adjoining Swiss Molasse basin.

Taking all this work into account, a very prominent hydrogeological and numerical groundwater flow model with a focus on the Braunauer Trog in the eastern part has been developed for the SGMB by Huber et al. (1998), Huber (1999) and Frisch and Huber (2000) (Fig. 2.22). This hydrogeological model was mainly adapted from Andres and Wirth (1981) and Lemcke (1987). Huber (1999) and Frisch and Huber (2000) tried to determine the groundwater recharge and water balance for the balneological wells in the Braunauer Trog and adjoining Upper Austrian Molasse Basin. These observations were based on interpolation of the hydraulic potentials in the west and north-east, data from hydrocarbon wells, and only few wells that were tapping the Upper Jurassic aquifer in the central SGMB at this time.

To integrate their model into the existing regional flow system of Andres and Wirth (1981) and Lemcke (1987), they interpreted an arched shaped vertex zone between the cities of Landshut and Regensburg. In consequence, the channel-shaped drainage zone in the direction of the city of Regensburg was assumed narrower and a thermal rise zone due to a pressure

depression south of Regensburg became considerably more important. The hydrogeological model resulted in a SW-NE regional flow direction for the Upper Jurassic groundwater with the main discharge into the river Danube at the greater areas of the cities of Ulm and Regensburg (Fig. 2.22). A new aspect, however, was the determined groundwater flow direction from south to north in the subarea of the Wasserburger Trog and from north to south in the eastern subarea Braunauer Trog, which contradicts previous concepts in the eastern SGMB (Fig. 2.18) (Frisch and Huber, 2000).

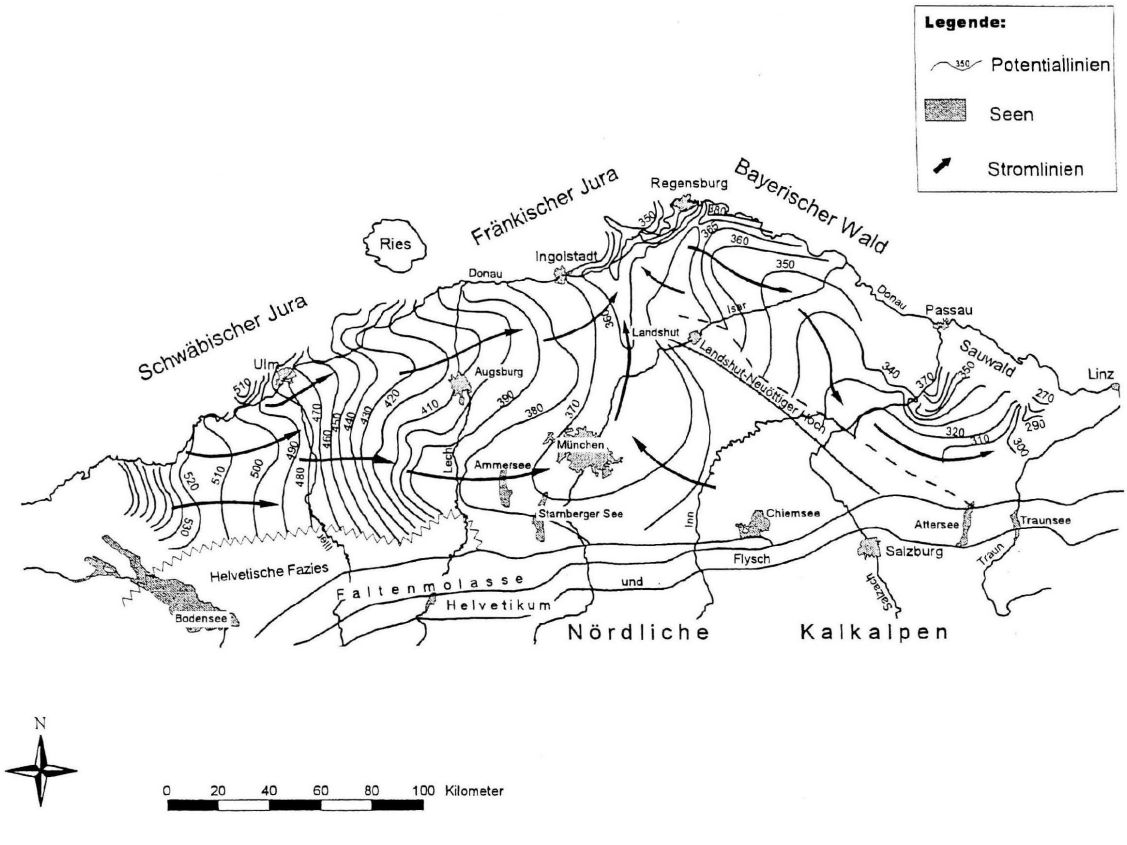

Figure 2.22: Hydraulic groundwater potentials for the thermal water in the Upper Jurassic aquifer of the South German Molasse Basin (SGMB) after Frisch and Huber (2000). Translation of important features: Potentiallinien - hydraulic potential lines; Seen - lakes; Stromlinien - groundwater stream lines.

The Upper Jurassic groundwater in the Braunauer Trog was found to be dominated by ion-exchange processes resulting in mostly Na-HCO_3-Cl water (Prestel, 1988). The relatively high mineralisation compared to waters occurring in local near-surface indicated a marginal inflow from deep circulation crystalline waters from the Bohemian Massif (Frisch and Huber, 2000). Additionally, a considerable high groundwater recharge was postulated through the so-called "Schierlinger Kreidehoch" south-west of the city of Regensburg (not displayed in Fig. 2.18).

This recently recharged groundwater was then assumed to flow southwards into the Braunauer Trog and further into the Upper Austrian Molasse basin. In the central SGMB, it was assumed by Frisch and Huber (2000), that the groundwater recharge had occurred through marginal inflows from the western area of the Swabian Alb (regional groundwater flow system) as well as through leakage across the overlying strata of the Tertiary.

Contrary to all existing hydrogeological models, only Udluft (1975) introduced a different hypothesis regarding a further infiltration area for the deep Upper Jurassic groundwater of the central SGMB based on hydrochemical data of groundwater stemming from the Upper Jurassic and overlying strata. The recharge was assumed to take place in the south of the SGMB via deep fault zone structures and a potential recharge area was proposed south of the Northern Limestone Alps ("Nördliche Kalkalpen"). However, this model had been consistently disregarded by other authors in the past due to the absence of geological-tectonic evidence and the difficulty of conceptualising an infiltration system through several thousand metres of Molasse sediments or across large fault structures in the Alps (Andres and Wirth, 1981; Villinger, 1988; Frisch and Huber, 2000).

2.6.2.3 The third phase to expand the concepts for the hydrogeological model

Due to the ongoing geothermal exploration in the greater area of Munich and in the Wasserburger Trog since the early 2000s, several new insights into the characterisation of the flow system in the central SGMB have been gained in a third phase. Each newly drilled deep borehole was investigated both hydraulically and hydrochemically and attempts were made to incorporate the data into the existing hydrogeological models. The most prominent studies concerning the hydraulic characterisation of the Upper Jurassic aquifer and the hydrochemical composition and evolution of its groundwater were conducted by Johannes Birner (Birner et al., 2011, 2012; Birner, 2013). In addition, the hydrogeological characteristics of the Upper Jurassic aquifer in the central SGMB were also investigated within the framework of joint research projects, taking into account hydraulic, hydrochemical, geological, thermal and other hydrogeological aspects (Schneider et al., 2009; Schneider and Thomas, 2012; Schulz and Thomas, 2012; Mayrhofer et al., 2014). This work was prompted by new hydraulic groundwater potential measurements on geothermal wells in the greater area of Munich that were summarised by Wagner et al. (2009) and the resulting inconsistencies with the previous models (Figs. 2.18 & 2.23).

Birner et al. (2011) used mainly hydrochemical data and hydraulic transmissivities to determine the groundwater evolution and flow system, as Savvatis et al. (2015) had found that the methodology for determining groundwater potentials in the past was based on a fundamental erroneous assumption in the calculation. To calculate groundwater potentials with groundwaters of different temperature and mineralisation, which has a considerable influence on density,

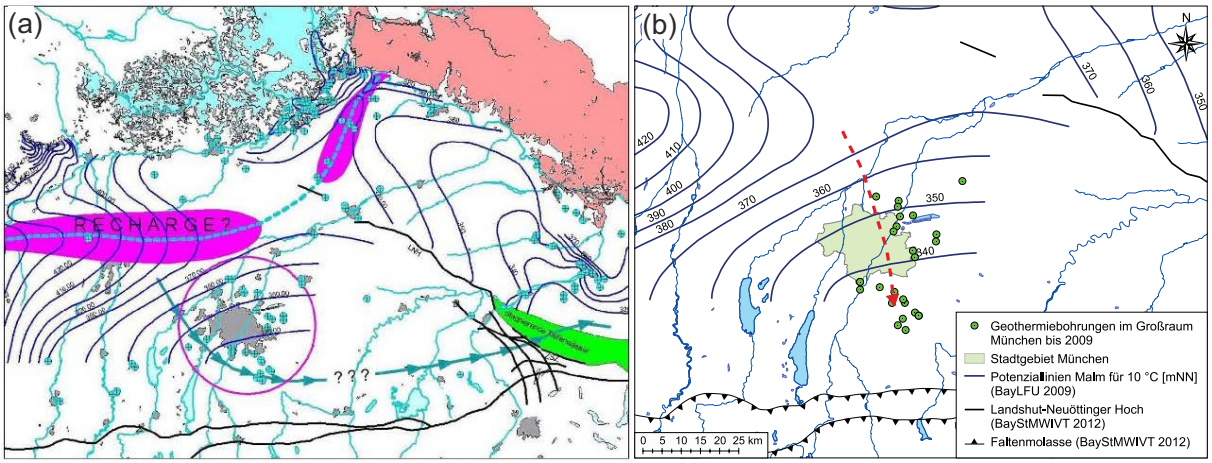

Figure 2.23: Hydraulic groundwater potentials for the Upper Jurassic aquifer in the South German Molasse Basin (SGMB) based on data from geothermal wells in the central SGMB. (**a**) with delineated recharge areas (purple colour) and zones of stagnant deep groundwater (green colour) after Wagner et al. (2009), (**b**) delineated groundwater flow direction (red ticked line with arrow) from Savvatis et al. (2015). Translation of important features: Potenziallinien Malm für 10 °C - groundwater potential lines for the Upper Jurassic (Malm) at 10 °C.

the tapped thermal waters were standardised to a model water with constant temperature and mineralisation (Villinger, 1977; Huber et al., 1998; Frisch and Huber, 2000; Wagner et al., 2009). It turned out that the assumption to calculate groundwater potentials with a model water of the same equal density implied an error that automatically oriented the flow direction towards a water with higher temperature (Savvatis et al., 2015). This resulted in the groundwater flow direction of thermal waters at geothermal boreholes in the central SGMB pointing towards the south (Fig. 2.23), which would result in an unrealistic underflow of the Alps (Savvatis et al., 2015).

Based on a large data set of water chemical data from the newly drilled geothermal wells in the central SGMB, including literature data (e.g. Prestel (1988); Weise et al. (1991)), Birner et al. (2011) divided the groundwater of the Bavarian Molasse Basin by their different water chemical characteristics into five hydrochemical provinces (Fig. 2.24). Although the investigated groundwater samples used were subjected to a quality investigation based primarily on the ion balance, it cannot be traced to what extent the analyses were still influenced by external influences from the drilling work, that may have had a significant impact on the quality of the sample (Hebig et al., 2012; Mayrhofer et al., 2014; Heine et al., 2018, 2019). However, the characteristics of the groundwater within the five hydrochemical provinces according to Birner et al. (2011) and the resulting similarities and differences to other hydrogeological models, including the newest ^{81}Kr groundwater dating results by Heidinger et al. (2019), are briefly described below:

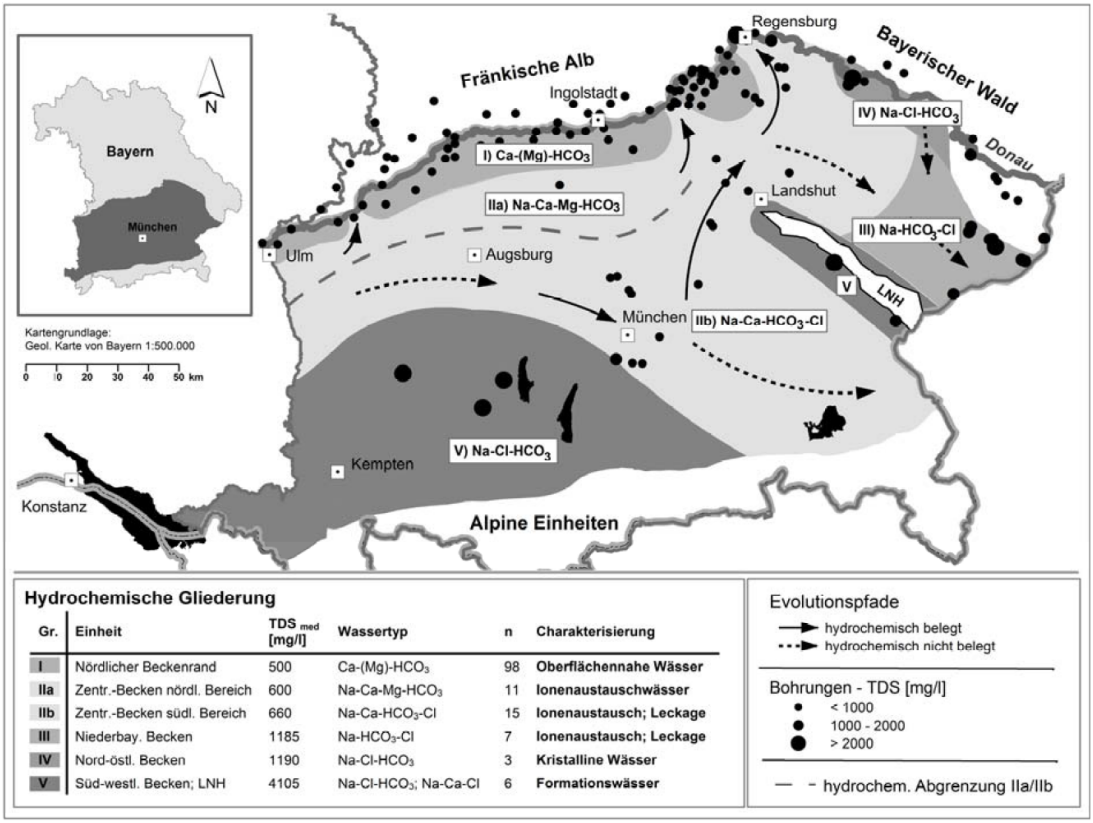

Figure 2.24: Distribution of water chemical types and hydrochemical provinces in the Bavarian SGMB with hydrochemical evolution paths after Birner et al. (2011). Translation of important features: Hydrochemische Gliederung - hydrochemical province; Einheit - unit; Wassertyp - water type; Evolutionspfade - evolutional pathways; hydrochemisch belegt/nicht belegt - hydrochemically proven/assumed.

I) Recently recharged and lowly mineralised groundwater of Ca-[Mg]-HCO_3 were found to occur in the shallow aquifer in zone I at the northern boundary of the SGMB in proximity to the river Danube. Their recharge areas were assumed to be in the nearby Upper Jurassic outcrops of the Swabian and Franconian Alb, which corresponds to the findings of Villinger (1977) and Bertleff et al. (1993).

II) In the central SGMB, two hydrochemical provinces were distinguished along a groundwater divide according to Frisch and Huber (2000) with Na-Ca-Mg-HCO_3 waters (IIa) north and Na-Ca-HCO_3-Cl waters south (IIb) of it. Groundwater in both zones showed cold climatic recharge conditions based on stable water isotopes and partly noble gas infiltration temperatures (NGTs) (Weise et al., 1991; Weise and Stichler, 1997; Bertleff and Watzel, 2002). As groundwater of similar hydrochemical characteristics have also been found in the western SGMB, the hydrochemical province of the central basin was interpolated to this area.

The groundwater of the northern central basin (IIa) was assumed to flow eastwards with discharge into the river Danube at few regional limited areas (Andres and Wirth, 1981; Prestel, 1988; Weise et al., 1991; Birner et al., 2011). Furthermore, the discharge area of water from the southern central basin (IIb) was hydrochemically identified only in the northern area of the SGMB around the city of Regensburg, where the groundwater chemistry indicated mixing processes of water from the central basin water with recently recharged zone I groundwater (Birner et al., 2011; Weise and Stichler, 1997; Weise et al., 1991). Birner et al. (2011) followed the interpretation of leakage of ion-exchange water from the overlying Tertiary sediments into the Upper Jurassic aquifer (Lemcke and Tunn, 1956; Lemcke, 1976; Villinger, 1977; Andres and Wirth, 1981). They assumed that south of the west-east trending Tertiary fresh-saline boundary, which was described by Lemcke (1976), small amounts (1 %) of highly mineralised deep formation water might have been infiltrated from lowly permeable Tertiary sediments (e.g. Baustein beds) into the Upper Jurassic aquifer. This influence of highly saline formation water might therefore have caused the higher chloride contents in the groundwater within the southern central basin (IIb) (Birner et al., 2011; Schneider and Thomas, 2012).

The groundwater occurring in Provinces IIa/b was assumed to have been recharged thousands to tens of thousands of years ago due to the comparable recharge conditions and water chemical similarities to the thermal waters in the western SGMB (Schneider and Thomas, 2012). The delineated hydrochemical evolution paths of the groundwater in the southern central basin (IIb) suggested an inflow from the western SGMB towards Munich, with a discharge to the north-east (area of Regensburg) and an assumed more extensive flow direction south-east towards the Alps. It is worth noting that the flow towards the Alps in the south-east of the Wasserburger Trog was only suspected and hydrochemically not proven, as there was not a single deep well tapping the Upper Jurassic aquifer in the area at that time (Fig. 2.24).

However, recently derived apparent ^{81}Kr-groundwater ages from Heidinger et al. (2019) between 60,000 years in the south of the SGMB and 135,000 years north of the city of Munich also clearly contradict the hypothesis of a southwards flow direction (Figs. 2.18 & 2.25). In this study, it was assumed that the groundwater recharge in the Upper Jurassic of the central SGMB has been occurred subglacially in the south of the SGMB. Thus, the groundwater has entered the Upper Jurassic aquifer via cross-formational flow through the covering Tertiary beds along preferential flow paths according to the infiltration model in the western SGMB (Bertleff et al., 1993; Bertleff and Watzel, 2002; Waber et al., 2014). The previous hypothesis of a large and connected regional flow system with uniform groundwater recharge areas in the west for the Upper Jurassic aquifer, which has been the basis for previous hydraulic considerations, was considered to be widely refuted in this study (Heidinger et al., 2019).

III) The Na-HCO_3-Cl groundwater in the Braunauer Trog and adjoining Upper Austria Molasse basin was found to be chemically altered due to ion-exchange processes and more matu-

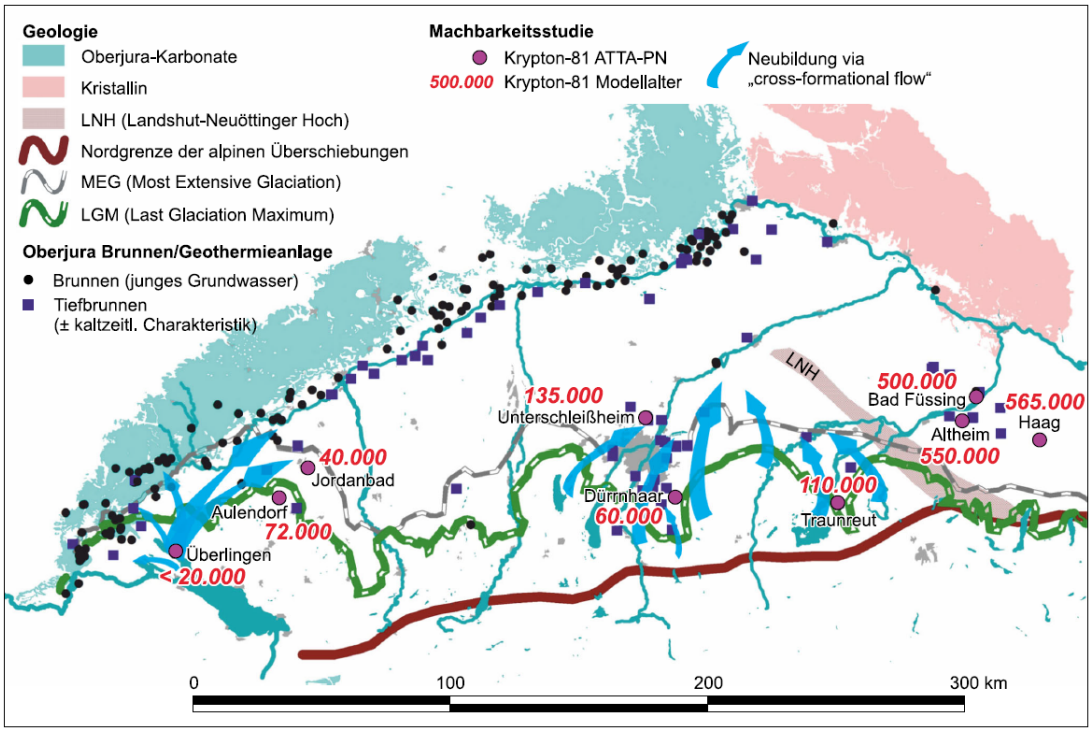

Figure 2.25: Overview of apparent ^{81}Kr model ages and delineated recharge areas via cross-formational flow after Heidinger et al. (2019). Translation of important features: Brunnen (junges Grundwasser) - wells with young groundwater; Tiefbrunnen (kaltzeitl. Charakteristik) - deep wells (cold cimate recharge characteristics); Neubildung - recharge.

rated than the groundwater in the central SGMB (Birner et al., 2011; Goldbrunner, 1999). These ion-exchange waters were considered as the end point of the hydrogeochemical evolution in the Upper Jurassic aquifer. They were assumed to be in contact with the overlying Tertiary sediments and influenced by infiltrating oilfield waters (Prestel, 1988). Their apparent groundwater ages were assumed to be higher than in the central SGMB and the groundwater circulation system showed very low hydraulic dynamics. The hydrochemical evolution by Birner et al. (2011) indicate a path from north to south, but was only assumed and not proven by the water chemical nature of these groundwaters. Consequently, locally occurring recent recharge of young groundwater was supposed to only play a minor role (Fig. 2.18 & 2.24).

Dating results of groundwater with ^{81}Kr at some wells in the Braunauer Trog and adjoining Upper Austrian Molasse Basin have resulted in very high apparent groundwater ages between 550,000 and 565,000 years (Heidinger et al., 2019), which is in accordance to mean residence times based on ^{4}He accumulation from Andrews et al. (1985) between 536,000 and 646,000 years at one well in the Braunauer Trog. In conclusion, these results may indicate a hydrogeological system of low hydraulic dynamic with only minor influences of recently recharged groundwater.

IV) North-east of the Braunauer Trog in the hydrochemical province IV, Birner et al. (2011) have concluded a locally occurring influence of deep circulating and at fault zones ascending crystalline groundwater in the Upper Jurassic aquifer. The Na-Cl-HCO_3 water showed clear characteristic hydrochemical influences from crystalline waters as well as mixing processes with younger recently recharged groundwater (Weise et al., 1991; Frisch and Huber, 2000). These waters were assumed to discharge southwards into the Braunauer Trog (Fig. 2.18 & 2.24).

V) In the southwestern SGMB between the western SGMB and the city of Munich, and in proximity of the Landshut-Neuoetting High, the occurring Upper Jurassic groundwater was found to be considerably higher mineralised than in other hydrochemical provinces and showed a domination of the ion sodium and chloride. The data set of Birner et al. (2011) was expanded with groundwater analyses from the SGMB in Baden-Wuerttemberg (Stober et al., 2014). They presented a chloride distribution (Fig. 2.26) within the Upper Jurassic aquifer, which revealed a consistent picture for the western and central SGMB. The highly saline hydrochemical province V from Birner et al. (2011) seems to extend south-west to the Lake Constance and the lower mineralised zones I, IIa and IIb continue parallel south of the river Danube to the west.

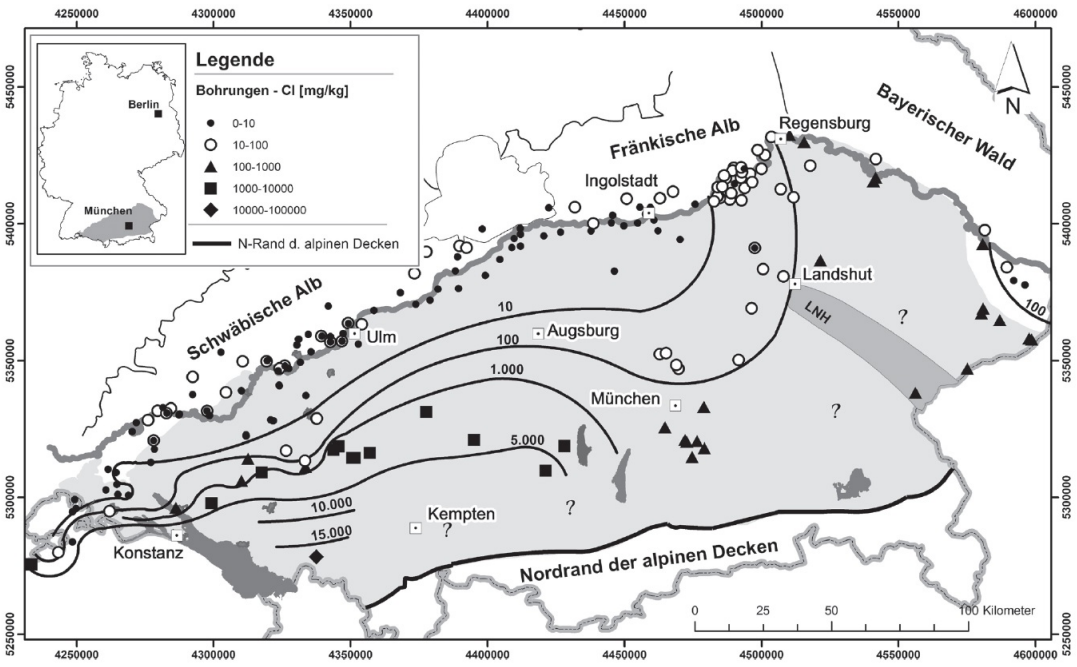

Figure 2.26: Chloride distribution within the Upper Jurassic aquifer in the South German Molasse Basin (SGMB) after Stober et al. (2014).

The highly mineralised groundwater in the southwestern SGMB was found in areas of low hydraulic permeabilities and especially in the transition to the lowly permeable transition zone facies ("Helvetian facies"). Birner et al. (2011) concluded due to the comparability to Tertiary

formation and oilfield waters (Stichler et al., 1987; Stichler, 1997) that the highly saline Upper Jurassic groundwater was typical for formation water in sedimentary basins. Although the occurrence of this hydrochemical province was based on only three Upper Jurassic wells, the hydrochemical province was extrapolated in a large area, among others also according to Stober et al. (2014) (Fig. 2.26).

It was assumed that the groundwater in the southwestern SGMB was not involved in the groundwater balance of the Upper Jurassic aquifer, or only to a very small extent (Birner et al., 2011). However, this finding contradicted all previous assumptions about the consistent and coherent regional flow system in the Upper Jurassic aquifer in Fig. 2.18 postulated until recently by Frisch and Huber (2000) and Wagner et al. (2009).

2.6.2.4 Short summary

The regional groundwater flow system of the Upper Jurassic aquifer (Fig. 2.18), which is based on the interpretation of hydraulic groundwater potentials, was found to have a substantial effect on the hydrogeochemical composition of the Upper Jurassic groundwater (Lemcke, 1987; Bertleff et al., 1993; Frisch and Huber, 2000; Stober, 2013).

The river Danube was considered to have a drainage effect on the southward-flowing waters of the Franconian Alb and, thus, to create a backwater of the waters flowing towards the Danube from the north and south, making it impossible to supply the central SGMB with groundwater from the northern Upper Jurassic outcrops (Apel, 1971; Udluft, 1975). The Upper Jurassic groundwater in the Wasserburger Trog was divided from the water in the Braunauer Trog in consequence of the hydraulic barriers Landshut-Neuoetting High (LNH) and Zentrale Schwellenzone (Udluft, 1975). As the subarea Braunauer Trog is framed by two crystalline structures, it was assumed to form an independent hydrogeological system that is not in hydraulic contact with the central SGMB.

The thermal water composition in the Upper Jurassic aquifer was found to change from recently recharged lowly mineralised Ca-[Mg]-HCO_3 waters at the northern and western margins of the SGMB to higher mineralised ion-exchange waters of Na-HCO_3-Cl, Na-Cl-HCO_3 and Na-Cl type with sodium as the dominant cation in the southern, eastern and central SGMB (Prestel, 1988; Weise et al., 1991; Birner et al., 2011; Stober et al., 2014).

The different groundwater flow models based on hydraulic potential analyses (Lemcke and Tunn, 1956; Lemcke, 1976; Villinger, 1977; Andres and Wirth, 1981; Lemcke, 1987; Frisch and Huber, 2000; Wagner et al., 2009; Savvatis et al., 2015) and hydrochemical analyses (Udluft, 1975; Stichler et al., 1987; Prestel, 1988; Bertleff et al., 1993; Stichler, 1997; Weise et al., 1991; Bertleff and Watzel, 2002; Birner et al., 2011; Stober et al., 2014; Mayrhofer et al., 2014; Heidinger et al., 2019) revealed a contradicting hydrogeological picture of the Upper Jurassic aquifer in the SGMB.

- It was assumed that the recharge areas of the Upper Jurassic groundwater were located at the north-western boundary of the SGMB in the Swabian Alb. The general flow regime was determined by hydraulic potential analysis to be along the river Danube with a flow direction to the east and in direction to the central SGMB (Lemcke, 1976; Andres and Wirth, 1981; Frisch and Huber, 2000; Birner et al., 2011). Observed higher mineralised ion-exchange waters at the north-eastern margin showed some evidence of groundwater flow from the central basin to the north-east of the SGMB (Prestel, 1988; Weise et al., 1991);
- The fossil Upper Jurassic formation water was washed out of the aquifer. The lowly mineralised groundwater in the central SGMB was believed to be a mixture of meteoric water and higher mineralised formation or oilfield waters, presumably seeping from the overlying Tertiary sediments (leaky aquifer), which were responsible for the higher and dominating amounts of sodium and chloride (Lemcke and Tunn, 1956; Udluft, 1975; Lemcke, 1976; Stichler et al., 1987; Balderer, 1990; Prestel, 1988; Stichler, 1997; Birner et al., 2011; Stober, 2014; Mayrhofer et al., 2014). Subsequently, on the basis of the assumed geochemical evolution of the Upper Jurassic groundwater in the central SGMB, it was assumed that the groundwater flows from west to south-east towards the Alps (Birner et al., 2011);
- The concept of subglacial recharge in the south-west of the SGMB (lake Constance region) and ion-exchange of paleo-groundwater during cross-formational flow with an assumed northwards flow direction to the draining river Danube by Bertleff et al. (1993) was recently supported by ^{81}Kr groundwater dating results by (Heidinger et al., 2019). Based on these results, recharge areas for the Upper Jurassic groundwater in the central SGMB were also postulated to be at the northern fringe of the Alps (Heidinger et al., 2019), or previously in the south of the Northern Calcareous Alps (Udluft, 1975).

Chapter 3

Motivation, aims and objectives

One never notices what has been done;
one can only see what remains to be done.

Marie Curie

The findings of the state of the art review in Chapter 2 implicate the motivation of this work. As the hydrochemical and hydraulic properties of the Upper Jurassic aquifer system in the SGMB have been already of great interest in various studies since the 1950s, a conclusive overall hydrogeological picture of the Upper Jurassic reservoir in the SGMB is still missing (Sec. 2.6.2)

The research focus of these studies was mainly to determine the recharge systematic and areas as well to understand the groundwater flow system of the Upper Jurassic aquifer for enhanced and sustainable resource management. Investigations considering the influences of (fractured) fault zones, matrix porosities and permeabilities of the surrounding host rocks, karst features and different inflow zones on the productivity of the thermal water supplies have so far continuously resulted in a better understanding of the hydraulic situation of the Upper Jurassic aquifer. Since the Upper Jurassic aquifer is partly very heterogeneous in geological and hydrogeological structure with small-scale changes in diagenesis and facies and, therefore, in the effective porosity and permeability of the host rocks (see Sec. 2.6.1), extrapolation from the information obtained at only few boreholes may be subject to great uncertainty. Moreover, only a few Upper Jurassic boreholes and thus direct investigations over large spatial distances were available to the authors in previous hydrogeological studies, especially in deeper areas of the central and southern SGMB, which was a major limitation for the validity of their investigations (see sec. 2.6.2). In addition, it was found that the correction method of the measured hydraulic potentials for the comparison was flawed due to the temperature and density differences of the thermal water caused by the different depths of the Upper Jurassic wells. A further limitation in the determination of the hydraulic potentials may also have been present due to permanent management, which also made it difficult to determine the delineated flow direction of the thermal aquifer.

A large-scale analysis of the hydrogeological characteristics of great aquifer system in the deep Upper Jurassic reservoir in the SGMB can only be conducted on the basis of the hydrochemical composition of the deep groundwater and, above all, of the information that is obtained from several environmental isotopes. Therefore, the aim of this thesis is to provide a comprehensive and consistent hydrochemical and hydrogeological picture of the deep Upper

Jurassic reservoir in the SGMB using water chemical data and environmental isotopes, and to characterise the different hydrogeochemical processes and factors influencing the deep groundwater. Moreover, due to the increasing problems of corrosion and scalings in geothermal facilities caused by the chemical composition of the fluids, as well as the occurrence of occasionally high amounts of oil and gas phases at some geothermal wells of the SGMB (Köhl et al., 2020b,a; Wanner et al., 2017; Mayrhofer et al., 2014), understanding the water chemical characteristics and their regional differences is of great importance for sustainable and economic operation.

One main challenge in the characterisation of deep groundwater is the issue of dating old groundwater. But groundwater dating for determining the apparent groundwater age is especially in deep sedimentary basins one of the hydrochemical key methods for delineating the groundwater flow direction and recharge areas. In contrast to the dating of younger groundwater, only few methods (^{14}C, ^{36}Cl, ^{81}Kr, ^{4}He and ^{40}Ar) are suitable for dating old groundwater, with almost exclusively ^{14}C being applicable for the dating range of groundwater between 1,000 and 30,000 years (see Sec. 2.5, Fig. 2.6). Radiocarbon dating in dissolved inorganic carbon ($^{14}C_{DIC}$) is a very well established method, which, however, can be severely affected in carbonate aquifers by various (bio)chemical or physical processes in the subsurface (see Sec. 2.5.1.1). In contrast, dating of natural groundwater with radiocarbon in dissolved organic carbon ($^{14}C_{DOC}$) represents a very promising alternative (see Sec. 2.5.1.2). A significant fraction of the DOC is expected to be of high physico-chemical stability in deep groundwater, which is supposed to be very suitable for dating old groundwater (Murphy et al., 1989a; Bauer et al., 1992; Geyer et al., 1993). Nevertheless, up to now, one of the biggest disadvantages of groundwater dating with $^{14}C_{DOC}$ have been the time-consuming extraction and isolation methods of the desirable humic substance in natural groundwater with very low DOC contents (<1 mg/l) (Burr et al., 2001). The great effort and high complexity of the commonly used extraction methods as well as the high demands on the technical requirements for concentration, e.g. in RO/ED or ultrafiltration (see Sec. 2.5.1.3), have led to the fact that groundwater dating with $^{14}C_{DOC}$ has not achieved widespread use. Therefore, the first objective of this thesis is to firstly and systematically test the applicability of $^{14}C_{DOC}$ groundwater dating using the novel and innovative SPE-PPL method on the example of the deep Upper Jurassic groundwater with very low DOC contents in the western and northern parts of the SGMB. The SPE-PPL of dissolved organic matter is a very reliable and sufficient method for extracting the DOC stemming from seawater and natural water with low contents of DOC (Dittmar et al., 2008; Swenson et al., 2014; Swenson, 2014; Coppola et al., 2015; Li et al., 2016). It is assessed whether the determined $^{14}C_{DOC}$ activities of the extracted SPE-PPL-DOC and derived apparent groundwater ages in the Upper Jurassic carbonate aquifer lead to plausible results and whether this promising dating method is suitable. The validation of the method is based on the comparison with the corrected $^{14}C_{DIC}$ ages as well as with the stable water isotope signatures of the investigated groundwater sam-

ples, which allow an assessment of Holocene or Pleistocene recharge conditions derived from the atmospheric temperature record of the last 30,000 years. The dating results will then be integrated into existing groundwater flow models in the western SGMB to gain a better understanding of the general infiltration and flow systematics for the entire Upper Jurassic reservoir.

In order to obtain a comprehensive hydrogeological picture of the deep upper Jurassic aquifer in the central SGMB, various water chemical and environmental isotopic methods can be applied in the deep groundwater. Combining this information, interaction of the deep Upper Jurassic groundwater with other formations can be identified and groundwater flow directions as well as possible groundwater recharge areas may be delineated. In particular, the use of multivariate statistical techniques are very advantageous in hydrogeological studies for the interpretation of large hydrochemical multi-parameter data sets. The hierarchical cluster (HCA) and exploratory factor analyses (EFA) are well established methods to identify different water types and unravel hydrogeological processes based on the hydrochemical groundwater composition.

Therefore, the second objective of this thesis is to hydrochemically characterise the occurring Upper Jurassic groundwater in the central SGMB and to conduct a hydrochemical zoning of this extensively geothermally exploited deep reservoir. For this purpose, water chemical data and environmental isotopes (δD, δ^{18}O, ^{87}Sr/^{86}Sr) are assessed at every geothermal well in the deeper parts of the central SGMB. For the first time, multivariate EFA and HCA of the obtained hydrochemical data are used to identify and characterise hydrogeological processes influencing the hydrochemical composition of the deep Upper Jurassic groundwater and to classify the occurring thermal water into discriminable water types. In addition, noble gas isotopes (^{3}He/^{4}He, ^{40}Ar/^{36}Ar) and noble gas concentrations (Ne, He, Ar, Kr, Xe) are determined on selected deep Upper Jurassic groundwater samples. As already mentioned in Sec. 2.5.2, there is a crucial limitation in dating with radiogenic noble gas isotopes due to the unknown terrigenous noble gas fluxes. Therefore, for the very first time, the noble gas fluxes of ^{4}He and ^{40}Ar in the Upper Jurassic aquifer of the central SGMB are calculated with recently derived apparent ^{81}Kr ages (Heidinger et al., 2019) to allow qualitative estimates of apparent groundwater ages for different water types. Moreover, noble gas infiltration temperatures (NGTs) are calculated to improve the characterisation of recharge conditions based on the stable water isotope signatures and apparent groundwater ages. The results of the apparent groundwater ages derived with noble gas isotopes and calculated NGTs at selected deep thermal wells are used to further support the classification of water types based on HCA and the identification of hydrogeochemical processes delineated by EFA. Finally, the findings are discussed and evaluated in the context of existing groundwater flow models for the deep Upper Jurassic aquifer in the SGMB from literature and the feasibility of a new recharge area and subglacial infiltration model for the deep Upper Jurassic groundwater is outlined.

Chapter 4

Methods

Knowing is not enough, we must apply.
Willing is not enough, we must do.

Johann Wolfgang von Goethe

4.1 Sampling und sample preparation

Sampling was conducted between December 2017 and June 2020 in the western and central SGMB. Water samples were collected for chemical analyses, stable water isotopes, $\delta^{13}C_{DIC}$ and radiocarbon dating at seven groundwater wells in the western and northern SGMB (UB, BJ, OF, GR, BW, HB and MA), which are used for balneological and water consumption purposes (Fig. 4.1). The wells tap the deep groundwater of the Upper Jurassic aquifer either at around 100 metres total vertical depth (mTVD) or considerably deeper at depths between 600 and 800 mTVD. Most of the sampled wells are screened in the Upper Jurassic aquifer (Fig. 2.14). Only well MA is tapping water from the Upper Jurassic aquifer and the overlying sandstone aquifer from the so-called Graupensand formation (Reichenbacher et al., 1998; Buchner et al., 2003).

At 22 deep geothermal production wells and two deep groundwater research wells in the central SGMB, water samples (1-24) were taken for chemical analyses, stable water isotopes, strontium isotopes, noble gases as well as noble gas isotopes of helium and argon. The geothermal wells are screened in the confined Upper Jurassic aquifer in depths between 1800 and 5000 mTVD.

All samples from geothermal, balneological and water consumption wells were obtained during the continuous operation of the wells and physico-chemical parameters were measured directly in the outflow. Water samples of the two groundwater research wells with depths of 537 and 796 mTVD were taken after the water volume of the wells had been replaced at least twice and physico-chemical parameters (pH value, specific electrical conductivity (EC) and redox potential (Eh_{25})) were stabilised (Dehnert et al., 1996). During this study, no gas separation was performed prior to sampling.

The thermal water at the geothermal wells was sampled in systems with operating pressures up to 18 bar and temperatures between 60 and 150 °C. Because of these physical circumstances,

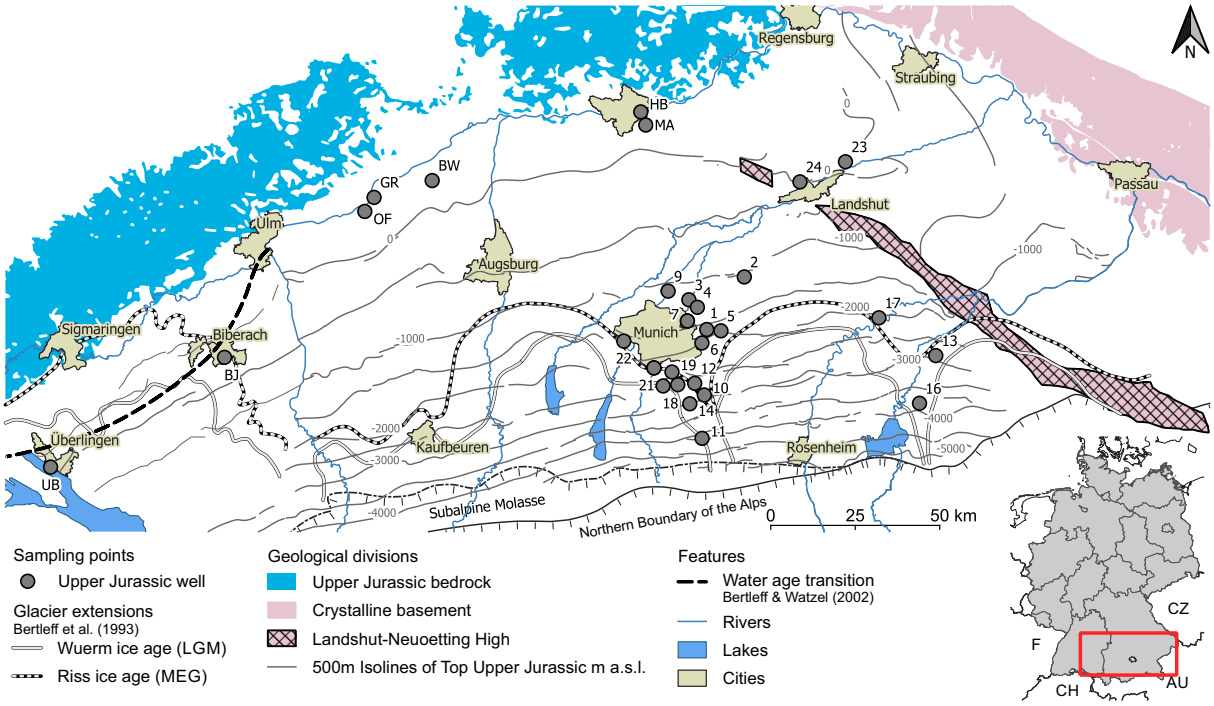

Figure 4.1: Overview of sampling points in the South German Molasse Basin (SGMB).

the samples were cooled below 60 °C with a mobile heat-exchanger using high-temperature and high-pressure steel-teflon tubes and stainless steel fittings.

4.1.1 Water chemical parameters

The physico-chemical parameters pH, EC, Eh_{25} and temperature (T) were determined with a set of WTW Multi 3430 sensors in the field. The carbonate species HCO_3^- and H_2CO_3 were determined by volumetric titration with 0.1 M HCl and NaOH on site, with an approximate analytical error of $\pm$ 0.1 mmol/l (6.1 mg/l for HCO_3^- and 4.4 mg/l for H_2CO_3).

Water samples for major ions and trace elements were field-filtered with a 0.22 µm filter, stored in 50 ml HDPE vials and sub-samples for cations (HNO_3 (65 %), cooled (4 °C)) and anions (frozen) were stabilised prior to analysis.

The major ions were analysed with an ion chromatograph Dionex ICS1100 (Thermo Fisher Scientific) with an analytical uncertainty of less than $\pm$5 %. The quality of hydrochemical analyses is expressed as the charge balance error (CBE) which should be <5 % (Appelo and Postma, 2004).

The trace element bromide was analysed using an ion chromatograph Dionex IC25 and lithium, rubidium and strontium using a flame atomic absorption spectrometry AAS 3300 (Perkin Elmer) at the Institute of Water Chemistry (IWC, Technical University of Munich). De-

tection limits were 0.1 mg/l for bromide and 0.01 mg/l for lithium, rubidium and strontium with an analytical precision $<\pm 5$ %. Samples for boron analyses were filled to the brim in 500 ml HDPE bottles and analysed after filtration (0.45 µm) using a spectrofluorometer Double Beam UV-190 (Shimadzu) with a detection limit of <0.25 mg/l.

The DOC samples were filtered through a 0.45 µm filter into brown glass vials, acidified to pH 2 with a few drops of HCl (10 %), and cooled (4 °C) prior to measurements. The DOC concentrations were determined with a catalytic high-temperature combustion method using Multi N/C 3100 (Analytik Jena). The analytical error is regularly $<\pm 10$ %, but below the detection limit of 0.5 mg/l it can rises up to approx. ± 60 %.

4.1.2 Stable water isotopes

The samples for stable water isotopes were filtered in the field using a 0.22 µm filter into 15 ml or 50 ml HDPE vials and cooled (4 °C) prior to analysis in the laboratory. To determine the signature of stable water isotopes, hydrogen ($^{2}H/^{1}H$) and oxygen ($^{18}O/^{16}O$) isotope ratios were measured with a liquid water isotope analyser IWA-45EP (Los Gatos Research). The analytical precision is ± 0.1 ‰ for $\delta^{18}O$ and ± 1 ‰ for δD.

4.1.3 Strontium isotopes

The samples for strontium isotopes were filled in 15 ml LDPE or 50 ml HDPE bottles and $^{87}Sr/^{86}Sr$ isotope ratios were measured by thermal ionization mass spectrometry (TIMS) VG Sector 54 (Micromass) in the laboratory of IsoAnalysis UG (Berlin). The TIMS raw data were evaluated using the international conventional method (Rosner, 2010). Mass fractionation was corrected using a $^{86}Sr/^{88}Sr$ ratio of 0.1194 and the $^{87}Sr/^{86}Sr$ data were normalised to a $^{87}Sr/^{86}Sr$ ratio of 0.71025 for NIST SRM 987. The accuracy and reproducibility were controlled with the analysis of the seawater standard IAPSO and the 2SD in-run-precision was $<1.5 \times 10^{-5}$.

4.1.4 Noble gases, $^{3}He/^{4}He$ and $^{40}Ar/^{36}Ar$

Samples for noble gas measurements were collected into copper tubes fixed on aluminium racks (Sültenfuß et al., 2009; Aeschbach-Hertig and Solomon, 2013), which were connected with the sampling tubes via special ferrule fittings from Swagelok and closed vacuum-tight with stainless steel clamps.

For 12 samples, analyses of Ne, ^{4}He and $^{3}He/^{4}He$ ratios were conducted at the noble gas laboratory of the Institute of Environmental Physics, University of Bremen, with a high resolution mass spectrometer MAP215-50 (Mass Analyser Products (MAP)) (Sültenfuß et al., 2009).

The analytical precision was better than ±1 % for Ne and ^{4}He, and better than ±0.5 % for ^{3}He/^{4}He.

The measurements of noble gas concentrations as well as isotopic ratios of ^{3}He/^{4}He and ^{40}Ar/^{36}Ar were performed for six samples with a mass spectrometer MM5400 (GV Instruments) at the Institute of Environmental Physics, Heidelberg University. The analytical precision of He and Ne (^{20}Ne) concentrations were ±1.1 % and ±0.5 %, respectively and for ^{3}He and thus ^{3}He/^{4}He ratios between ±3 % and ±5 %. For noble gas concentrations, the precision was better than ±1 % for He and Ar and between ±1 % and ±2 % for Ne, Kr, and Xe. The argon isotope ratio was calculated directly in the mass spectrometer by alternately determining the signals of ^{40}Ar and ^{36}Ar in certain time periods and by using the absolute concentrations of the two isotopes to form the isotope ratio. The values given in Tables 5.6 and A.2 are the mean values of both methods.

Depending on the analysing institute, the copper tubes contained 5 g, 20 g (University of Heidelberg) or 40 g (University of Bremen) of the sample.

4.1.5 Inorganic radiocarbon ($^{14}C_{DIC}$) and $\delta^{13}C_{DIC}$

In this study, radiocarbon analysis of dissolved inorganic carbon was performed on three samples stemming from wells BW, HB and MA. For each sample, two thoroughly cleaned (with ultrapure water and 10 % HCl) 1 l HDPE bottles were filled to the brim with groundwater and sent immediately to the GADAM Centre of the Silesian University of Technology (Gliwice, Poland). The analysis with an accelerator mass spectrometer (AMS) follows the protocol of Piotrowska (2013) with an accuracy of less than ±0.1 pmC, and the results are reported in relation to the standard of the NBS oxalic acid and normalised in percent modern radiocarbon (pmC) (Stuiver and Polach, 1977; Donahue et al., 1990).

For determining the interaction of the DIC budget with the aquifer for each sample and for corrections of the initial carbon content, the inorganic $\delta^{13}C_{DIC}$ value was measured at samples BW, HB, MA and OF. Therefore, the water was filled into 0.5 l glass bottles with pre-added NaOH from the bottom to the top to stabilise the inorganic carbon at pH >11. The samples were stored cooled and measured at the laboratory of Hydroisotop GmbH with an isotope-ratio mass spectrometry (IRMS) with an accuracy of ± 0.3 ‰.

4.1.6 Organic radiocarbon ($^{14}C_{DOC}$)

4.1.6.1 Sampling and extraction method

The bottles, tubes or fittings for sampling and extraction were thoroughly cleaned with ultrapure water and 10 % HCl for several days prior to the sampling campaign. Groundwater sam-

ples for $^{14}C_{DOC}$ measurements were filled in opaque HDPE jerrycans (20 l) and stored cooled (4 °C) after acidification to pH 2 with ±25 ml ultrapure HCl (36 %) until extraction (Fig. 4.2). The groundwater samples of wells MA and HB were prepared in duplicates in order to determine the reproducibility of the extraction and dating method. After sampling, the SPE-DOM of groundwater was subsequently extracted over a period of up to 30 days. Only for one sub sample of HB (HB_2), the extraction was performed after three months.

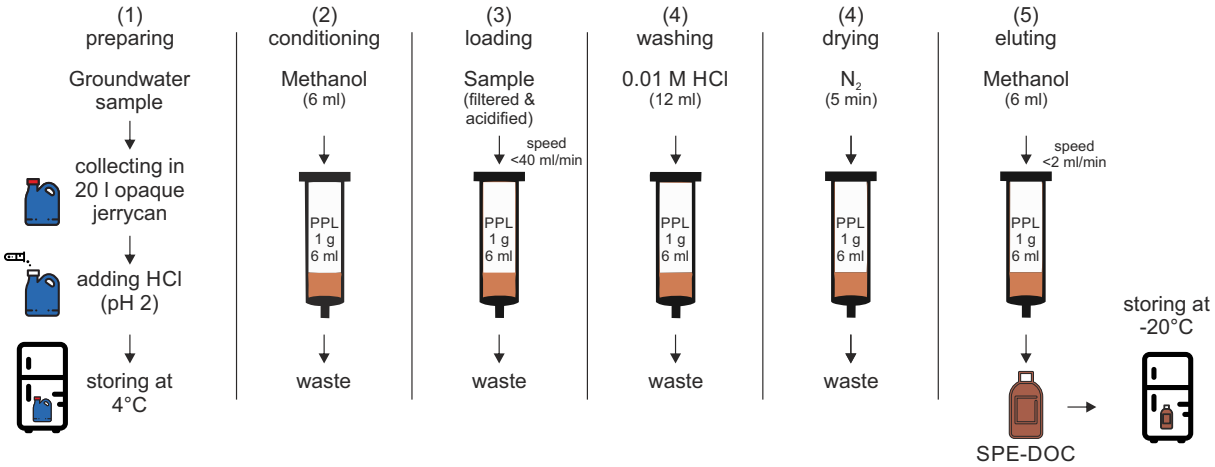

Figure 4.2: Sample preparation and extraction procedure for DOC of groundwater samples according to a modified scheme after Dittmar et al. (2008) and Li et al. (2016).

The extraction of the organic carbon was carried out using Bond Elut PPL cartridges from Agilent (1 g, 6 ml) according to a modified scheme of Dittmar et al. (2008) and Li et al. (2016) that is displayed in Fig. 4.2. The Teflon tubing used was connected to the pump and cartridges via Luer-Lok fittings and adapters, and everything was additionally sealed with Teflon tape.

Briefly, the acidified water was filtered through a precombusted (150 °C for min. 10 h) glass microfibre filter (Whatman GF/F, 25 mm) in the laboratory with a vacuum pump or peristaltic pump (only sample UB). The set up using a peristaltic pump allowed simultaneous loading of the cartridges and DOC extraction depending on the pump specifics of up to four samples (Fig. 4.3).

The cartridges were activated with one cartridge volume (6 ml) of ultrapure methanol (HPLC grade >99.9 %) and loaded with a maximum speed of 40 ml/min. The flow rate with the set-up was regularly between 20 to 40 ml/min. The extraction volume for each cartridge varied between 4 l and 12 l for SPE depending on the DOC content of the groundwater samples while the extraction time per sample ranged between two and five hours. After the loading process, the cartridge was rinsed with 12 ml of ultrapure 0.01 M HCl and dried for 5 min with nitrogen (N_2). The absorbed SPE-DOM was eluted with one cartridge volume (6 ml) of ultrapure methanol with a speed of <2 ml/min into brown glass vials and stored frozen (-20 °C) until

sending off to the Leibniz Laboratory for Radiometric Dating and Stable Isotope Research at the Christian-Albrechts-University of Kiel for AMS measurements.

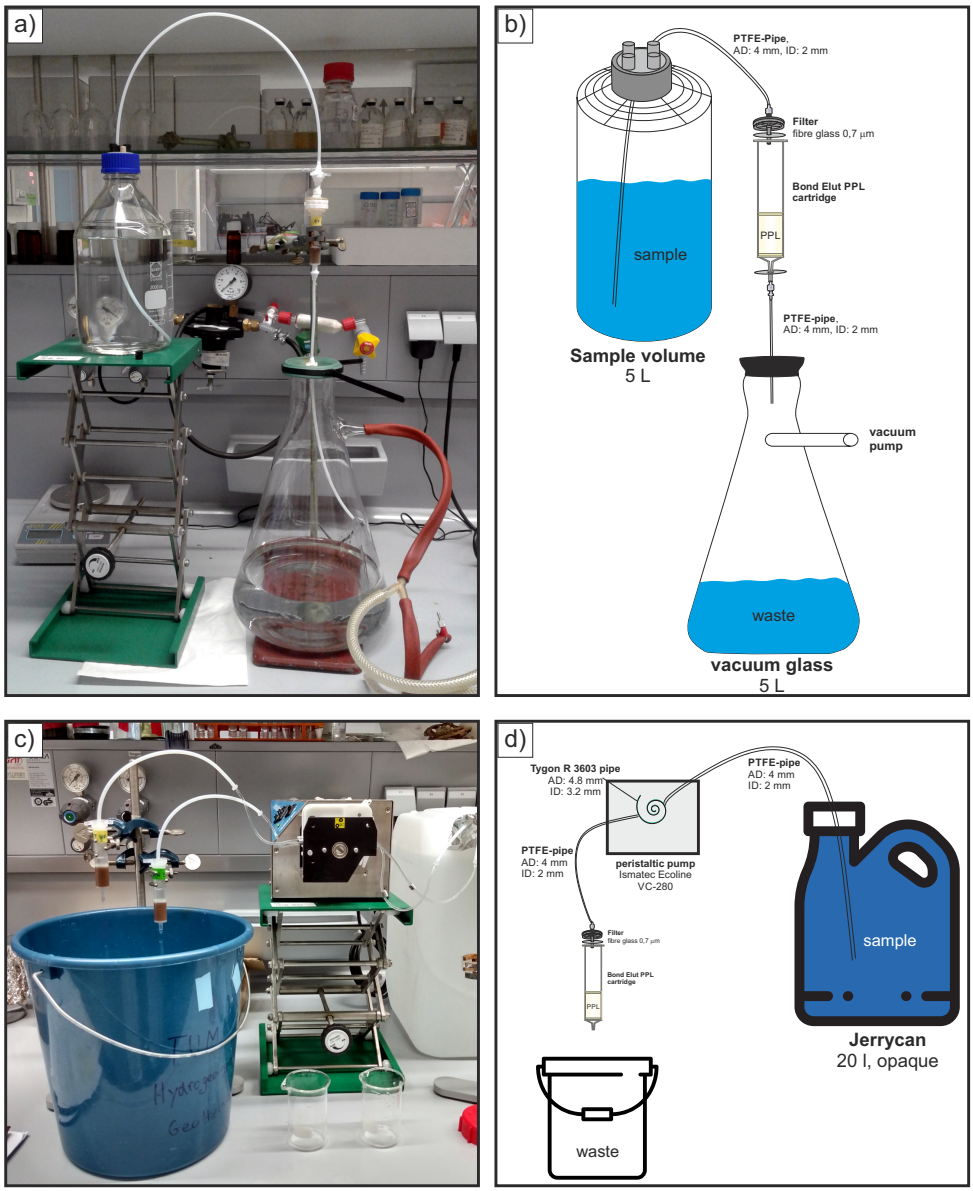

Figure 4.3: Loading of the SPE-PPL cartridge (Step 3 in Fig. 4.2) with sample using a vacuum pump (a,b) and a peristaltic pump (c,d).

To evaluate the efficiency of the SPE-PPL extraction method, the carbon recovery is calculated using Eq. 4.1:

$$\text{Efficiency } (\%) = \frac{C_{extr.}}{C_{max,extr.}} \times 100 = \frac{C_{extr.}}{[DOC] \times V} \times 100 \tag{4.1}$$

where $C_{extr.}$ is the actual extracted carbon, $C_{max,extr.}$ the calculated maximum extracted carbon (both in mg), V the sample volume (in l) for extraction and [DOC] the DOC concentration (in mg/l) of the sample.

4.1.6.2 $^{14}C_{DOC}$ measurements

Following the protocol of the Leibniz Laboratory, the samples were filled in a precombusted quartz ampule where the methanol was evaporated in a vacuum. The remaining carbon was combusted (900 °C) with CuO and silver wool to CO_2 and subsequently reduced to graphite at 600 °C with added H_2 and iron powder. The measurement was performed with an AMS HVE 3MV Tandetron 4130 (Grootes et al., 2004).

4.2 Calculation of radiocarbon ages

The radiocarbon age, which is simplified based on piston-flow model, is calculated according to Eq. 2.2 with equation Eq. 4.2:

$$\text{Radiocarbon age (yr)} = -8267 \times \ln\left(\frac{^{14}C_t}{^{14}C_0}\right) \tag{4.2}$$

where $^{14}C_t$ is the measured and $^{14}C_0$ the initial radiocarbon activity of DIC or DIC entering the groundwater system.

To obtain corrected $^{14}C_{DIC}$ groundwater ages, geochemical correction models are required that take into account chemical, biological and physical processes affecting both $\delta^{13}C_{DIC}$ and $^{14}C_{DIC}$. In this study, $^{14}C_{0,DIC}$ is determined with the revised Fontes & Garnier's model (rev. FGM) using Eq. 4.3 after Han and Plummer (2013):

$$\begin{aligned} ^{14}C_{0,DIC}\ (\text{pmC}) = &\left(\frac{C_a}{C_T} \times ^{14}C_{a0} + \frac{C_b}{C_T} \times ^{14}C_{b0}\right) + (^{14}C_s - ^{14}C_{b0} - 0.2 \times \epsilon_{s/b}) \\ &\times \left(\frac{\delta^{13}C - \frac{C_a}{C_T} \times \delta^{13}C_{a0} - \frac{C_b}{C_T} \times \delta^{13}C_{b0}}{\delta^{13}C_s - \delta^{13}C_{b0} - \epsilon_{s/b}}\right) \end{aligned} \tag{4.3}$$

using the estimated parameters for the initial carbon isotopic composition of the gaseous (g) and aqueous (a) soil CO_2, $^{14}C_g$ and $^{14}C_{a0} = 100$ pmC, $\delta^{13}C_g$ = -23 ‰, for the solid (s) carbonate minerals $^{14}C_s = 0$ pmC as well as the calculated mean of measured $\delta^{13}C_{s_{UJ}} = 2.4$ ‰ (1.1 to 3.3 ‰ for Upper Jurassic carbonates (Liedmann and Koch, 1990; Wersin et al., 2013; Nowak et al., 2019)). The parameter $\epsilon_{s/b}$ is the fractionation factor of the carbonate minerals with respect to HCO_3^- in a closed system, $^{14}C_{b0}$ and $\delta^{13}C_{b0}$ are related to the initial carbon isotopic

composition of HCO_3^- at the start of the isotopic exchange, C_a and C_b are the total concentrations of $CO_{2,aq}$ and HCO_3^-, respectively, and C_T is the sum of both C_a and C_b.

No geochemical correction model is needed for groundwater dating with organic radiocarbon when influences of sedimentary organic carbon (SOC) are considered to be very small and negligible (Burr et al., 2001; Hershey et al., 2016). For the study area it can be assumed that the Upper Jurassic carbonate aquifer contains no or only very small amounts of SOC (Fischer et al., 1992; Geyer et al., 1993). Consequently, SOC may have no considerable influence on groundwater dating with $^{14}C_{DOC}$, but nevertheless, the resulting apparent piston-flow "ages" needs to be considered as maximum $^{14}C_{DOC}$ ages (Coppola et al., 2015; Hershey et al., 2016).

In addition, there are uncertainties to determine the initial $^{14}C_{0,DOC}$ content (Hershey et al., 2016) and a few $^{14}C_{0,DOC}$ values were estimated for the Upper Jurassic aquifer ranging from 85 $\pm$ 10 pmC (Geyer et al., 1993) up to 120 pmC (Einsiedl et al., 2007). The latter stems from soil derived FA activities of an epikarst system at the top of the vadose zone. Hershey et al. (2016) reported $^{14}C_{0,DOC}$ values of $\geq$ 100 pmC for modern groundwater of an aquifer in southern Nevada sampled at upgradient locations with detectable tritium contents. In this study, a $^{14}C_{0,DOC}$ value of 85 pmC seems to be applicable for deriving reasonable organic radiocarbon ages (ORAs).

Consequently, in this study the inorganic radiocarbon ages (IRAs) were calculated with $^{14}C_{0,DIC}$ using the rev. FGM correction model, while a $^{14}C_{0,DOC}$ value of 85 pmC were applied as initial radiocarbon activity for the ORAs.

4.3 Calculation of noble gas infiltration temperatures (NGTs)

The concentration of dissolved noble gases in groundwater are mainly controlled by two components: the equilibrium component from atmospheric input, which convey information on physical properties of the water during air-equilibration at the air/water interface during recharge, and the so-called "excess air", which is an additional component caused by air entrapment (Andrews and Lee, 1979; Andrews et al., 1985; Aeschbach-Hertig et al., 2000; Kipfer et al., 2002). The interaction of groundwater with gas phases can lead to a loss of dissolved gases, which is usually referred to as degassing (Aeschbach-Hertig et al., 2008; Aeschbach-Hertig and Solomon, 2013; Jung and Aeschbach, 2018). The equilibrium component can be used for calculating the noble gas infiltration temperatures (NGTs) during groundwater recharge (Stute and Schlosser, 1993; Wilson and McNeill, 1997; Aeschbach-Hertig et al., 2000).

Considering the effects of excess air and degassing, which is necessary for the calculation of NGTs, different models can be applied that are elaborately described in Aeschbach-Hertig and Solomon (2013) and Jung and Aeschbach (2018). All models are based on Henry's law, which relates the concentrations in the two phases gas and water in equilibrium, and the phys-

ical characteristics of the noble gases during recharge such as temperature (T), salinity (S) and pressure (P) (Aeschbach-Hertig et al., 2008). Among all models for determining the equilibrium component in groundwater, the closed system model (CE-model) after Aeschbach-Hertig et al. (2000) has proven to be the best, as it includes simpler models as limiting cases, also describes degassing and provides realistic estimates of physically considerable parameters such as the excess air (Jung et al., 2013).

The CE-model is described by the following equations in Eq. 4.4 (Aeschbach-Hertig et al., 2000):

$$C_i(T, S, P, A, F)\ (ccSTP/g_{water}) = C_i^*(T, S, P) + \frac{(1-F) \times A \times z_i}{1 + F \times z_i / C_i} \tag{4.4}$$

with C_i^* as the moist-air solubility equilibrium concentrations as functions of (recharge) temperature T, salinity S, and pressure P for i = Ne, Kr & Xe, z_i as the volume fractions of the noble gases in dry air, A as the initial amount of entrapped air and F as the fractionation parameter.

The dimensionless fractionation factor F has a physical meaning and is the ratio of the entrapped gas volumes in the final and initial state, ν, and the ratio of the dry gas pressure in the trapped gas to that in the free atmosphere q (Aeschbach-Hertig et al., 2000). F ranges usually between 0 and 1 and becomes 1 when no excess air is trapped and is equal to 0 when pure excess air is present. In cases of degassing, F exhibits values larger than 1 (Jung and Aeschbach, 2018). The parameter A describes the initial amount of entrapped air per unit mass of water and is formulated by Eq. 4.5:

$$A\ (ccSTP/g_{water}) = \frac{A^*}{\rho_e} \times \frac{P \times e}{P_0} \times \frac{T_0}{T} \tag{4.5}$$

with A^* as the (dimensionless) ratio of entrapped air per unit mass of water in molar concentration, T_0 and P_0 as standard conditions (STP) for temperature and pressure, T and P as temperature and pressure governing atmospheric equilibrium, the saturation vapor pressure e and the water density ρ_w.

Typical values for A using the CE-model are below 0.05 to 0.1 ccSTP/g and values above 0.2 to 0.3 ccSTP/g are seen not to be realistic for natural groundwater as they imply more than 20 % pore space was initially occupied with entrapped air (Aeschbach-Hertig et al., 2000; Jung et al., 2013). However, high values for A may imply non-uniform degassing of the noble gases (Jung et al., 2013).

The NGTs were calculated using the program PANGA (Program for the Analysis of Noble GAs data) (Jung and Aeschbach, 2018) and the closed system equilibration (CE) model (Aeschbach-Hertig et al., 2000) with the concentrations of Ne, Kr and Xe due to radiogenic contribution of He and Ar in the samples (Tab. 5.7). The used salinities S varied according to their TDS (Tab. A.1) and atmospheric pressure P was set to 0.948 atm (infiltration at approximately

530 m above sea level). According to Jung and Aeschbach (2018), the initial values for the modelling were 0.01 ccSTP/g for the excess air A and 0.5 for the fractionation factor F. The initial temperature T was 1 °C as stable water isotope signatures indicated cold climatic recharge conditions during Pleistocene (see Sec. 5.2.3.1). An initial modelling and inspection of the derived parameters F, A and T with the CE-model showed that the errors in particular were high and the parameters A and F did not yield physically realistic values. Therefore, the parameters were fitted in two modelling steps with an adjusted starting value of 0.9 for the fractionation factor F. Firstly, the fractions of entrapped excess-air A were determined with Monte Carlo simulations (5000 simulation runs). The results were evaluated (Appendix A.3) and subsequently a second modelling was carried out in which A was now also specified as an input parameter. In the second modelling the fractionation parameters F and NGT were determined with a weighted least squares fitting approach and Monte Carlo simulation (5000 simulation runs) (Jung and Aeschbach, 2018). The graphical results of the second Monte Carlo simulation are presented in the Appendix A.3. The results of both simulation steps are summarised in Tab. 5.7 in Sec. 5.2.3.1.

4.4 Determination of apparent groundwater ages with radiogenic noble gas isotopes

Helium and argon contents in basin aquifers consist of natural atmospheric background and terrigenous excess components. Both components are easily identifiable and the exchange of ^{4}He from rocks to fluid can be assumed to be fast (Kulongoski and Hilton, 2012). Hypothetically, best estimates of the mean residence time could be determined by the accumulation of noble gas isotopes into groundwater with a uniform and constant rate per unit volume without any chemical reactions or diffusive exchange (Bethke and Johnson, 2002).

In general, the non-atmospheric, terrigenous excess helium fraction, $^4He_{ex}$, in a sedimentary basin is composed of the in-situ produced $^4He_{is}$ by the radioactive α-decay of uranium and thorium in the aquifer rocks, and the external sources of the (deep) crustal ^4He_c or mantle fluxes ^4He_m (Tolstikhin et al., 1996; Kulongoski et al., 2003). These terrigenous as well as atmospheric sources in groundwater, such as air-equilibrated helium ($^4He_{eq}$) and dissolved air-bubbles (^4He_a), can be separated with the $^3He/^4He$ ratios and the Ne content (Kulongoski et al., 2003). The atmospheric $^3He/^4He$ ratio is R_a 1.38×10^{-6} and is stored in air-saturated water (ASW) depending on salinity and temperature with R_{ASW} 1.36×10^{-6} (Clarke et al., 1976). $^3He/^4He$ ratios of crustal origin (R_c) typically range between 0.01 R_a and 0.1 R_a (Ballentine and Burnard, 2002; Kulongoski and Hilton, 2012; Phillips and Castro, 2014) and mantle-derived helium has typical values of R_m between 5 and 10 R_a (Graham, 2002).

The $^{40}Ar/^{36}Ar$ ratios can be used to evaluate terrigenous $^{40}Ar_{ex}$ component, which is composed of the radiogenic and in-situ produced contribution from ^{40}K decay, $^{40}Ar_{is}$, and the crustal fluxes ($^{40}Ar_c$) (Lippmann et al., 2003). The atmospheric $^{40}Ar/^{36}Ar$ ratio R_a ranges between 295.5 (Ozima and Podosek, 2002) and 298.5 (Lee et al., 2006). Higher ratios point to a radiogenic $^{40}Ar_{ex}$ input and accordingly long residence times (Tolstikhin et al., 1996).

The radiogenic excess helium $^4He_{ex}$ and argon $^{40}Ar_{ex}$ contributions can be used for groundwater dating (Andrews et al., 1985, 1987; Weise and Moser, 1987; Stichler et al., 1987; Osenbrück et al., 1998; Lippmann et al., 2003; Torgersen and Stute, 2013). The amount of excess $^4He_{ex}$ accumulated in groundwater can be expressed as the non-atmospheric contribution $^4He_{non\text{-}atm}$, which is calculated using the simplified Eq. 4.6 under the assumptions that the proportion of the terrigenous component is considerably higher than the atmospheric ^4He component and that the difference between both the equilibrium and excess air ^4He components is also very small (Petersen et al., 2018):

$$^4He_{ex}\ (ccSTP/g_{water}) \approx\ ^4He_{non\text{-}atm} =\ ^4He_{meas} - \frac{Ne_{meas}}{Ne_{eq}} \times\ ^4He_{eq} \tag{4.6}$$

with the measured $^4He_{meas}$ and Ne_{meas} concentrations and the equilibrium concentrations of helium $^4He_{eq} = 4.90 \times 10^{-8}$ ccSTP/g and neon $Ne_{eq} = 2.25 \times 10^{-7}$ ccSTP/g under infiltration conditions at 0 °C (Weiss, 1971; Clarke et al., 1976).

The excess $^{40}Ar_{ex}$ component is calculated using Eq. 4.7 (Petersen et al., 2018):

$$^{40}Ar_{ex}\ (ccSTP/g_{water}) =\ ^{40}Ar_{meas} \times \frac{R_{meas} - R_a}{R_{meas}} \tag{4.7}$$

with the measured argon concentration $^{40}Ar_{meas}$ as well as the measured and atmospheric $^{40}Ar/^{36}Ar$ ratios R_{meas} and R_a, respectively.

The in situ production rates P_i (i = ^4He and ^{40}Ar) of the aquifer rocks are proportional with the content of the radiogenic elements uranium ([U] in ppm) and thorium ([Th] in ppm) for ^4He (Eq. 4.8) and potassium ([K] in weight %) for ^{40}Ar (Eq. 4.9) in the host rock. Accordingly, the accumulation rates $A_{i,is}$ of in situ produced $^4He_{is}$ and $^{40}Ar_{is}$ can be calculated using Eq. 4.10: (Lippmann et al., 2003):

$$P_{^4He}\ (ccSTP/g_{rock}/yr) = 1.19 \times 10^{-13} \times [U] + 2.88 \times 10^{-14} \times [Th] \tag{4.8}$$

$$P_{^{40}Ar}\ (ccSTP/g_{rock}/yr) = 3.887 \times 10^{-14} \times [K] \tag{4.9}$$

$$A_{i,is}\ (ccSTP/g_{water}/yr) = \lambda_i \times \frac{1-\phi}{\phi} \times \frac{\rho_{rock}}{\rho_w} \times P_i \tag{4.10}$$

with the production rates P_i, the helium release factor λ_i, the effective porosity ϕ of the rock, as well as the rock and water densities ρ_{rock} and ρ_w.

The time t_{ex} required to produce the excess contribution $C_{i,ex}$ of $^4He_{ex}$ and $^{40}Ar_{ex}$ depends on the in situ accumulation rate $A_{i,is}$ and the advective accumulation of crustal flux J_i within the aquifer with a thickness z (in cm) and is calculated using Eq. 4.11 according to Eq. 2.4 (Stute et al., 1992; Torgersen and Clarke, 1985; Lippmann et al., 2003):

$$t_{ex}\ (yr) = \frac{C_{i,ex}}{A_{i,is} + \frac{J_i}{\phi \times z \times \rho_w}} \tag{4.11}$$

For the calculation of the in situ production rates P_i, the accumulation rates $A_{i,is}$ and the accumulation of crustal fluxes J_i using Eq. 4.11, mean values of the Upper Jurassic rock porosity ϕ = 0.1 and rock density ρ_{rock} = 2.57 g/cm^3 (Bohnsack et al., 2020); uranium (U = 1.0 ppm), thorium (Th = 0.5 ppm) and potassium (K = 0.06 weight %) content (Thuro et al., 2019); an aquifer thickness of approx. 400 m; and assumed values for the water density ρ_w = 1 g/cm^3 and release factors $\lambda_{He} = \lambda_{Ar}$ of 1 were used.

4.5 Multivariate statistical techniques

Multivariate statistical techniques are very useful for data reduction and interpretation of large multi-constituent data sets (Matiatos et al., 2014; Menció et al., 2012; Belkhiri et al., 2010; Cloutier et al., 2008; Panda et al., 2006) and have been used to identify distinct water types and unravel hydrogeological processes based on hydrochemical water composition. In hydrogeological studies with large data sets, two multivariate statistical techniques, exploratory factor analysis (EFA) and hierarchical cluster analysis (HCA), are well established and are explained below with their application in this work (Fig. 4.4).

All hydrochemical parameters (m = 17) of the n = 24 samples (Tables A.1 & A.2), with the exception of noble gas data, which were not obtained for each well, were considered for HCA and EFA. The pH values have not been used for the multivariate statistical analyses because they were not representative due to an affection by degassing of CO_2 and H_2S during sampling. In addition, to reduce the complexity and to increase the variance of the data set, the stable water isotope signatures of δD and $\delta^{18}O$, representing mainly infiltration conditions, evaporation and water-rock interaction processes, were combined to the SWI-dist parameter, which depicts the orthogonal distance from the GMWL. Thus, the data set was reduced to m = 17 parameters for the statistical analyses.

The HCA and EFA were performed and displayed in this thesis with the statistical program R (R Core Team, 2020) using the integrated *stats* package and the packages *psych* (Revelle, 2019), *semTools* (Jorgensen et al., 2020) and *ggplot2* (Wickham, 2008).

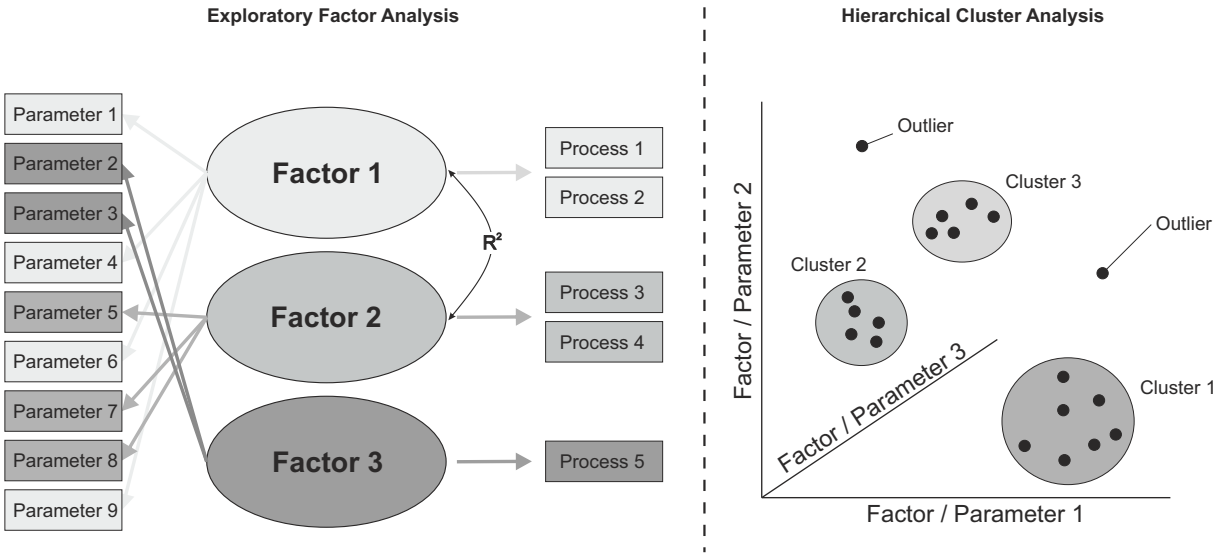

Figure 4.4: Visualisation of the principles of multivariate statistical methods exploratory factor analysis and hierarchical cluster analysis.

4.5.1 Exploratory factor analysis EFA

Exploratory factor analysis (EFA) provides the basis to uncover the underlying structure of a data set consisting of a large number of inter-related variables and to reduce its dimensionality and complexity. By transforming the data with linear combinations to a new set of variables, the dimension of the data set is reduced to a number of significant factors that are responsible for most of the variation in the data set. In the process, several parameters build up a common factor, which is indicated by the common shared variance of a set of variables and represents a process or construct (Schumacker, 2016; Tabachnik and Fidell, 2013). In some cases, the different factors, and thus the processes explained by them, may correlate with each other, the dependence of which is expressed by the regression coefficient (R^2) (Fig. 4.4).

Each factor has a specific factor loading that describes the weighting of the factor. In addition, each factor explains the data set with a specific variance. In contrast to a principal component analysis (PCA), EFA attempts to explain the data set with as many statistically significant factors as possible. In a PCA, one necessarily specifies a number of principal components that are explained by the individual parameters. It is therefore possible that the cumulative variance of the statistically significant factors is less than 1 in EFA and that the extracted factors do not explain the entire data set (Backhaus et al., 2016).

The necessary steps of the EFA are listed as followed (Backhaus et al., 2016; Schumacker, 2016; Tabachnik and Fidell, 2013):

- Initial survey of m parameters at n observations (n >m).
- Standardisation of the parameter matrix.
- Calculation of correlation matrix R. Selection of the method (Pearson, Spearman or Kendall) according to normality test.
- Fulfilment of the basic requirements: sample size adequacy, factorability of R, normality and linearity of variables, no multicollinearity (singularity), no nonpositive definite matrix and reliability with necessary tests (Kaiser-Meyer-Olkin (KMO) test, Cronbach's α test, Bartlett's test of sphericity, calculation of matrix determinant).
- Communality estimation and Factor extraction.
- Determination of factor numbers ((cumulative) Kaiser criterion, parallel analysis, Scree test).
- Factor rotation with type of rotation (varimax, oblique).
- Interpretation.

Prior to EFA, basic requirements were concerned for the same data set used for HCA of m = 17 parameters of n = 24 water samples (Schumacker, 2016). The Shapiro-Wilk test of normality showed a non-Gaussian distribution of the z-standardised data set (p-values <0.05 for every parameter except of F^- and $^{87}Sr/^{86}Sr$ ratio with p-values of 0.17 and 0.11, Tab. 5.5). Therefore, the ranked correlation matrix was calculated with Spearman's ρ coefficient (Backhaus et al., 2016) (Tab. A.4 in Appendix A.2).

The suitability of the data set was tested prior to analysis (Tab. 5.5) with the Kaiser-Meyer-Olkin (KMO) test on the condition of a measure of sampling adequacy (MSA value) >0.5 (Schumacker, 2016). The KMO test was statistically significant and showed a "middling" factor adequacy with an overall MSA value of 0.7. Bartlett's test of sphericity with χ^2 of 371 indicated with a p-value of 1×10^{-23} <0.05 overall statistically significant correlations within the correlation matrix. Cronbach's α of 0.9 suggested a high internal consistency and reliability of the data set. The determinant of the correlation matrix was positive (1.7×10^{-10}) indicating no non-positive definite matrix. Hence, the basic requirements for proceeding with EFA were achieved.

It is essential to determine the correct number of factors and, therefore, parallel analysis (Horn, 1965), Kaiser criterion (eigenvalues >1) (Kaiser, 1960), empirical Kaiser criterion (Braeken and van Assen, 2017) and Scree test (Cattell, 1966) were applied (Zwick and Velicer, 1982; Costello and Osborne, 2005).

4.5.2 Hierarchical cluster analysis HCA

Clustering is an important tool for unbiased identification of patterns in a data set. Hierarchical cluster analysis (HCA) allows individual observations (objects) to be grouped into an indefinite number of clusters that aggregate together based on similarities (Fig. 4.4) (Kassambara, 2017; Panda et al., 2006).

The HCA can be carried out either with all parameters in the entire data set or also with the extracted factor value matrix determined using EFA. It should be noted, however, that the extracted factors do not a priori explain the entire data set, but only up to the cumulative variance. Therefore, in some cases it is reasonable not to use the factor value matrix for grouping water samples, but to use all parameters. The result of hierarchical clustering is a tree-based representation of the objects, which is also known as dendrogram (Kassambara, 2017).

The procedure of HCA is listed as followed (Kassambara, 2017; Backhaus et al., 2016):

- Preparing the data and cleaning the data set.
- Computing (dis)similarity information between every parameter with distance measures (e.g. Euclidean distance).
- Using linkage function (e.g. single linkage method, Ward method) to group objects into hierarchical cluster tree, based on the distance measure.
- Detect outliers (with highest distances) and remove from data set. Then start again with the cleaned data set.
- Determining where to cut the hierarchical tree into significant clusters (e.g. Elbow method, Silhouette method, Gap statistic).

HCA was conducted with the z-standardised data set of m = 17 parameters of n = 24 water samples. The single linkage method (nearest-neighbour method) with Euclidean distance connects two points in a multi dimensional space with the closest distance (Backhaus et al., 2016; Schumacker, 2016; DiStefano et al., 2009), where the number of water samples (n) define the dimension. It can be used to detect outliers with the greatest distances to each other in the data set. In order to reduce the internal heterogeneity within the data set, the outliers were separated from the data set. Subsequently, the Ward's linkage method using the minimum variance criterion and squared Euclidean distances was applied to find the most distinctive cluster with the lowest variance within the cluster (Ward, 1963). In order to determine the optimal number of significant cluster, the "Elbow method", "Silhouette method" and "Gap statistic" were applied using the packages *factoextra* (Kassambara, 2017) as well as *NbClust* (Charrad et al., 2014) to compute 30 methods at once (Kassambara, 2017).

Chapter 5

Results and discussion

The waters are like the subsoil through which they flow.

Pliny the Elder

5.1 Groundwater dating with dissolved organic radiocarbon

5.1.1 Hydrochemical composition and stable water isotopes of groundwater

The hydrochemical parameters and stable water isotope data for all sampled wells are shown in Tab. 5.1 and 5.2. According to Appelo and Postma (2004), the calculated CBEs <5 % for each sample indicate an acceptable quality of the analyses.

The groundwater in the study area was lowly mineralised and the specific EC varied between 456 to 777 µS/cm. The pH values ranged from 7.3 to 7.8 indicating an alkaline nature while the redox potential (Eh_{25}) varied between 186 and 414 mV at wells MA, OF, BW, UB and GR. Only at well BJ was a negative redox potential of -190 mV found, which documents strongly reduced redox conditions. The nitrate content at all sampled wells was, as expected for deep carbonate aquifers, below the detection limit of 0.8 mg/l.

The groundwater at the four wells BW, GR, HB and MA was of Ca-Mg-HCO_3 type (field A) as displayed in the piper plot in Fig. 5.1. In contrast, the groundwater sample of well OF was identified as Ca-Na-Mg-HCO_3 type (field D). The sample of well BJ was of Na-(Ca)-HCO_3 type, whereas the water sample of UB was of Na-HCO_3-(Cl) type (both field F). The groundwater at the wells OF, BJ and UB (fields D and F in Fig. 5.1) also showed some indications of ion-exchange processes between Ca^{2+} and Na^{+}. These processes may have occurred in the USM with high cation-exchange capacities which also indicate cross-formational flow (Bertleff et al., 1993; Bertleff and Watzel, 2002; Heidinger et al., 2019).

The sodium content of the calcium dominated waters had a maximum of 13.1 mg/l (at well GR), whereas the ion-exchange dominated waters showed an increasing sodium concentration of up to 181 mg/l (UB). Only samples of wells UB and BJ had relevant amounts of chloride (54.0 mg/l and 26.1 mg/l) which might be caused by a slight influence of saline formation waters (see Fig. 2.26) that may stem from the low permeable transition zone facies (Mraz et al., 2019).

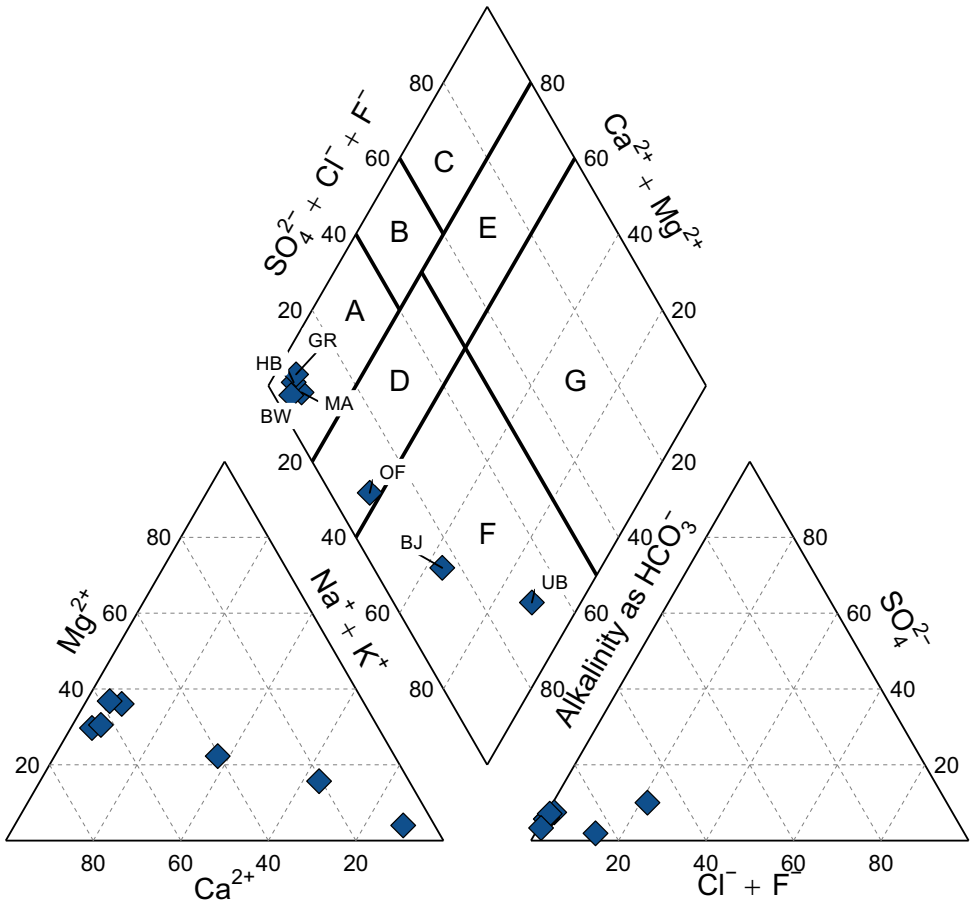

Figure 5.1: Piper plot of the water samples with water type classification after the system of hydrochemical facies from Furtak and Langguth (1967).

The stable water isotopes signatures of the groundwater scatter in Fig. 5.2 between the global (GMWL) and local (LMWL) meteoric water lines for that region (city of Constance) after Stumpp et al. (2014) and indicate a meteoric origin. A recent recharge in this pre-alpine region (Constance) showed a mean value of around -9.6 ‰ for $\delta^{18}O$ and -69.9 ‰ for δD (Stumpp et al., 2014). Paleo-groundwater with Pleistocene origin in the proximity of this study area was characterised by $\delta^{18}O$ and δD values of <-10.6 ‰ and <-73.8 ‰ whereas stable water isotope signatures of Holocene recharged groundwater are more isotopically enriched (van Geldern et al., 2014).

Therefore, the isotopic composition of the groundwaters at wells BW, HB and MA with $\delta^{18}O$ values ranged from -10.0 ‰ to -9.8 ‰ and δD values between -73.4 ‰ and -70.9 ‰ might be indicative for groundwater recharge during warm climate conditions in the Holocene. At wells OF and BJ, the $\delta^{18}O$ signatures ranged from -12.5 ‰ to -12.3 ‰ and the δD values varied between -89.4 ‰ and -88.4 ‰ and therefore may have infiltrated under Pleistocene cold climatic conditions which indicates mean transit times higher than approx. 12,000 years (late

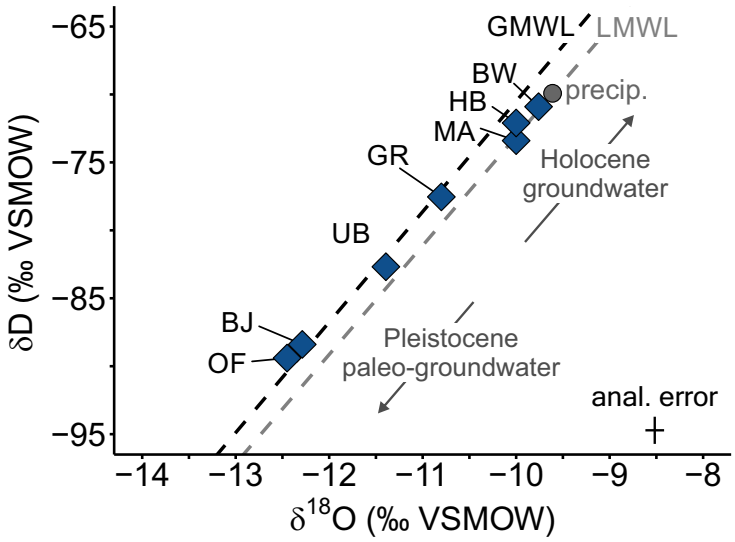

Figure 5.2: Plot of stable water isotope signatures scattering between the Global (GMWL) and Local Meteoric Water Line (LMWL for that region (Constance) after Stumpp et al. (2014)). Recent precipitation (precip.) from the city of Constance (Stumpp et al., 2014). Infiltration age characterisation for groundwater in that region after van Geldern et al. (2014)

Pleistocene age) (van Geldern et al., 2014; Bertleff et al., 1993; Fischer et al., 1992). According to van Geldern et al. (2014), the samples of wells UB and GR with values of -11.4 ‰ and -10.8 ‰ for $\delta^{18}O$ and isotope signatures of -82.7 ‰ and -77.5 ‰ for δD may indicate a slightly cold climatic to intermediate climatic groundwater infiltration conditions during the warming period between late Pleistocene and Holocene.

However, on the basis of the stable water isotope results, it cannot be excluded that also mixing between Holocene and Pleistocene groundwater along a flow path leads to the observed isotopic shift in $\delta^{18}O$ and δD of the groundwater at wells UB and GR.

5.1.2 Comparison of $^{14}C_{DIC}$ and $^{14}C_{DOC}$ activities

The measured radiocarbon activities of $^{14}C_{DIC}$ and $^{14}C_{DOC}$ as well as $\delta^{13}C_{DIC}$ data of the seven sampled wells are noted in Tab. 5.2. The inorganic $^{14}C_{DIC}$ activities ranged from 1.4 pmC (at well OF) to 21.3 pmC (at well HB). For well UB, Heidinger et al. (2019) reported a $^{14}C_{DIC}$ value of $<$2 pmC. The $^{14}C_{DOC}$ values varied between 5.7 pmC (well OF) and 51.1 pmC (well BW). Duplicate measurements of groundwater samples at wells MA and HB showed mean values and standard deviations of 34.3 $\pm$ 0.4 pmC for well MA and 35.1 $\pm$ 0.8 pmC for well HB. The very low standard deviations indicate a very good reproducibility of the proposed extraction and dating method.

The measured radiocarbon species in Fig. 5.3 shows that the $^{14}C_{DIC}$ activities in groundwater were generally lower compared to the $^{14}C_{DOC}$ values obtained from the same water samples.

Table 5.1: Physico-chemical composition of the groundwater samples.

Sample ID	T (°C)	pH (-)	Eh_{25} (mV)	EC (µS/cm)	Ca^{2+}	Mg^{2+}	Na^{+}	K^{+}	HCO_3^-	Cl^-	SO_4^{2-}	F^-
					(mg/l)							
BJ	45.0	7.3	-190	476	22.0	10.1	75.3	4.7	275	26.1	4.9	<0.6
BW	14.9	7.3	376	501	68.5	20.1	7.54	0.9	311	1.2	8.5	<0.6
GR	20.7	7.3	186	456	68.8	18.9	5.01	1.4	285	1.3	17.2	<0.6
HB	14.7	7.5		663	88.8	34.3	8.86	0.9	464	1.6	22.2	<0.6
MA	12.6	7.4	414	634	79.2	31.2	13.1	1.4	387	1.7	19.6	<0.6
OF	17.1	7.6	386	450	39.8	13.3	40.0	3.5	250	1.6	15.7	0.5
UB	28.9	7.8	271	777	12.9	4.37	181	4.4	346	54.0	39.8	5.1

Sample ID	CBE (%)	Water type
BJ	-0.4	Na-(Ca)-HCO_3
BW	1.1	Ca-Mg-HCO_3
GR	1.9	Ca-Mg-HCO_3
HB	-2.8	Ca-Mg-HCO_3
MA	2.4	Ca-Mg-HCO_3
OF	4.5	Ca-Na-Mg-HCO_3
UB	4.0	Na-HCO_3-(Cl)

CBE is the calculated charge balance error after Appelo and Postma (2004)

Table 5.2: Isotopic data and calculated inorganic (IRA) and organic (ORA) radiocarbon ages.

Sample ID	$\delta^{18}O$ (‰VSMOW)	δD	$^{14}C_{DOC}$ (pmC)	$\delta^{13}C_{DIC}$ (‰VPDB)	$^{14}C_{DIC}$ (pmC)	$^{14}C_{0,DIC}$	$ORA_{C_{0,85}}$ (yr)	IRA
BJ	-12.3	-88.4	9.6 ± 0.1	-4.2[a,b]	1.4[a,b]	25.5	18,073	23,996
BW	-9.8	-70.9	51.1 ± 0.2	-11.0	11.0	51.2	4,200	12,623
GR	-10.8	-77.5	39.6 ± 0.2	-10.7[a,b,c]	8.1[a,b,c]	51.3	6,325	14,978
HB+	-10.0	-72.1	35.1 ± 0.1	-11.9	21.3	56.3	7,320	8,057
MA+	-10.0	-73.4	34.3 ± 0.2	-12.2	18.2	55.5	7,495	9,206
OF	-12.5	-89.4	5.7 ± 0.1	-10.3	1.9[a,c]	47.5	22,397	26,901
UB	-11.4	-82.7	14.2 ± 0.3	-3.0[d]	<2[d]		14,816	>30,000

$^{14}C_{0,DIC}$ calculated with revised Fontes-Garnier Model after Han and Plummer (2013).

literature data from: a: Bertleff (1986); b: Weise et al. (1991); c: Fischer et al. (1992); d: Heidinger et al. (2019).

If several annotations are mentioned, the cited values represent mean values.

+: $^{14}C_{DOC}$ values and calculated organic radiocarbon ages (ORA) are mean values of duplicate measurements.

However, the differences in DIC and DOC activities of the same water samples were not constant and may indicate other processes as the natural decay reaction of radiocarbon. In addition to physical diffusion processes, inorganic chemical reactions and biogenic processes such as the dissolution of inorganic $CaCO_3$ from the aquifer rock, precipitation of carbonate minerals, bac-

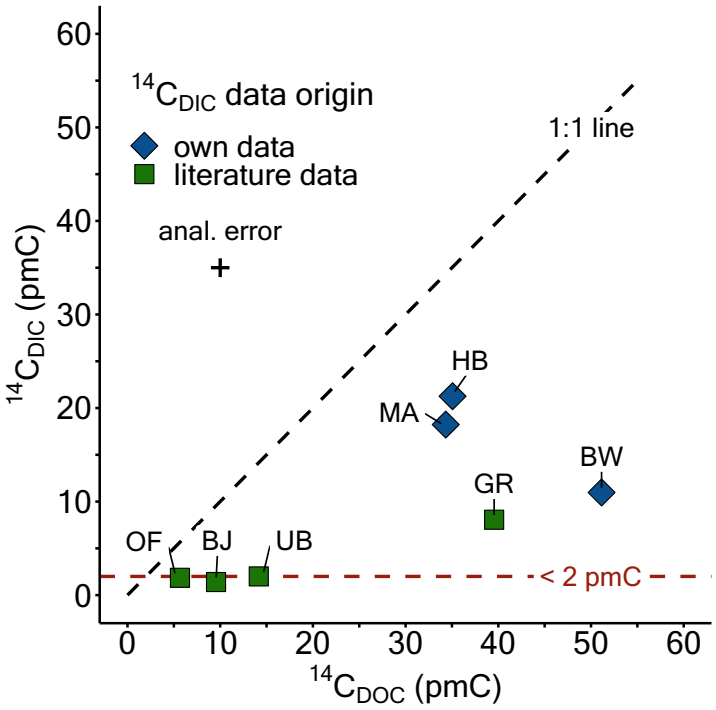

Figure 5.3: Measured radiocarbon activities of organic and inorganic carbon. Key: blue diamonds - $^{14}C_{DIC}$ data from this study; green squares - $^{14}C_{DIC}$ data from literature studies (Bertleff, 1986; Weise et al., 1991; Fischer et al., 1992; Heidinger et al., 2019). The <2 pmC line reflects the commonly used limit of determination for radiocarbon measurements.

terial sulphate reduction (BSR) or methanogenesis, can contribute to the observed differences in ^{14}C activities (Murphy et al., 1989a; Purdy et al., 1992; Hershey et al., 2016; Cartwright et al., 2020).

In detail, the observed differences of the $^{14}C_{DIC}$ and $^{14}C_{DOC}$ activities in the groundwater samples of wells MA and HB with $^{14}C_{DIC}$ values of 18.2 pmC for MA and 21.3 pmC for HB as well as $^{14}C_{DOC}$ values of 34.3 pmC for well MA and 35.1 pmC for well HB were comparatively small to all other groundwater samples. In addition, the $\delta^{13}C_{DIC}$ values of -12.2 ‰ (well MA) and -11.9 ‰ (well HB) represent typical values of groundwater in a closed carbonate aquifer system and suggest only little or no effect of microbial oxidation or reduction processes and water/rock interaction on the DIC pool (Cartwright et al., 2020).

In contrast, the $^{14}C_{DIC}$ activities of the samples at wells OF, BJ and UB were just below the limit of determination of 2 pmC while $^{14}C_{DOC}$ values were significantly above the detection limit of this method with measured values of 5.7 pmC, 9.6 pmC and 14.2 pmC, respectively. The less negative $\delta^{13}C_{DIC}$ values between -4.2 ‰ and -3.0 ‰ at wells BJ and UB compared to wells MA and HB might indicate dilution and/or matrix-exchange processes leading to lower $^{14}C_{DIC}$ activities than $^{14}C_{DOC}$ activities. Moreover, Fischer et al. (1992) and Einsiedl et al. (2007)

have shown using stable δ^{34}S-SO_4 values of dissolved sulphate and δ^{34}S-FA values of FA that BSR has occurred in the groundwater of well OF. Fischer et al. (1992) also presented additional field data that may indicate reduced redox conditions in the aquifer. In contrast, our own field measurements of 386 mV may indicate aerobic conditions. However, we cannot exclude that our field measurements may fall short because the redox sensor was damaged or that there have been mixing processes between an old reduced groundwater component stemming from the Upper Jurassic aquifer and a younger aerobic water component over the last couple of years. Nevertheless, it can be assumed that the DIC pool of the groundwater at the well OF, as discussed above, and well BJ with a low sulphate content of 4.9 mg/l and a reducing redox potential of -190 mV (Tab. 5.1) may have been strongly influenced by BSR, which may have led to lower $^{14}C_{DIC}$ activities.

At well BW, the difference between the organic ($^{14}C_{DOC}$ 51.1 pmC) and inorganic ($^{14}C_{DIC}$ 11.0 pmC) radiocarbon activities was remarkably high with 40.1 pmC. This was also observed by Fischer et al. (1992) and Geyer et al. (1993) in a former groundwater study which may confirm the results of this study. It was suggested by these authors using $\delta^{13}C_{DIC}$ that an exchange with the freshwater carbonates from the overlying USM strata (Fig. 2.14) affects the $^{14}C_{DIC}$ pool of the groundwater of the Upper Jurassic aquifer (Fischer et al., 1992; Geyer et al., 1993).

The great difference between $^{14}C_{DOC}$ (39.6 pmC) and $^{14}C_{DIC}$ (8.1 pmC) of around 31.5 pmC in the groundwater at well GR may also be explained by the interaction of groundwater between the Upper Jurassic aquifer and the freshwater carbonates from the USM which affects the inorganic carbon species. But compared to BW, the stable water isotope signatures of groundwater at well GR indicated considerably colder recharge conditions (Fig. 5.2). Therefore, it can be assumed that another hydrogeological process has led to the different isotopic groundwater composition of well GR. The well GR is located in close proximity to the wells BW and OF which are all only screened in the Upper Jurassic aquifer (Fig. 2.12 & 2.14) and covered by USM sediments with low hydraulic conductivities. The groundwater at well BW showed the highest $^{14}C_{DOC}$ activity compared to the other wells and a δ^{18}O value of -9.8 ‰, while the groundwater at well OF showed the lowest level of $^{14}C_{DOC}$ activities and a δ^{18}O value of -12.5 ‰ (Tab. 5.2). Therefore, mixing processes between these two groundwater bodies with different ^{14}C activities and stable water isotope signatures may be supposedly the reason for the isotopic composition of the groundwater at well GR (see Sec. 5.1.1).

To attest the hypothesis according to which mixing processes could explain the data at well GR, a simplified linear mixing calculation with the stable water isotopes and radiocarbon species as proxies was performed with the characteristics of OF and BW as the two end members.

The deviation of measured and calculated signatures of stable water isotopes in Tab. 5.3 of MIX I (35 % OF and 65 % BW) and MIX II (30 % OF and 70 % BW) with -10.7 ‰ and -10.6 ‰

Table 5.3: Linear mixing of isotope data with the two end members OF and BW for the mixing of two water bodies around the well GR. The values in brackets express the difference between the calculated and measured values at well GR.

Sample ID	Description	$\delta^{18}O$	δD	$^{14}C_{DOC}$	$^{14}C_{DIC}$
		(‰ VSMOW)		(pmC)	
MIX I	OF/BW: 35/65 %	-10.7 (+0.1)	-77.4 (+0.1)	35.2 (-4.4)	7.8 (-0.3)
MIX II	OF/BW: 30/70 %	-10.6 (+0.2)	-76.5 (+1.0)	37.5 (-2.1)	8.2 (+0.1)

for $\delta^{18}O$ as well as -77.4 ‰ and -76.5 ‰ for δD was more or less within the analytical error of the measured values at well GR ($\delta^{18}O$ -10.8 ‰ and δD -77.5 ‰, Tab. 5.2) and showed a very good fit for the mixing calculation (Fig. 5.4a).

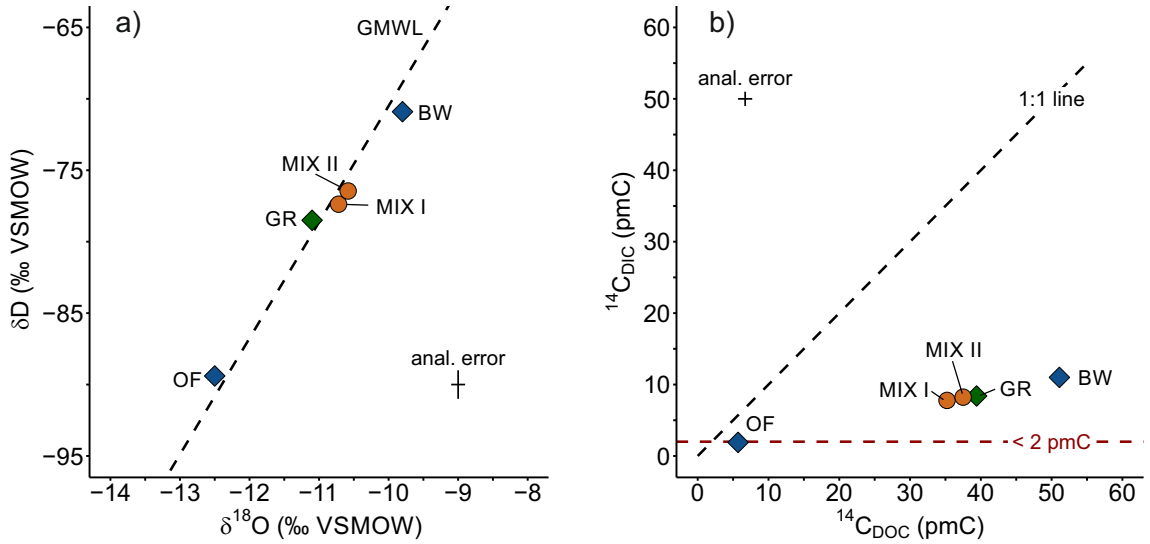

Figure 5.4: Linear mixing of the two Endmembers OF and BW with various ratios. MIX I: 35 % OF and 65 % BW; MIX II: 30 % OF and 70 % BW. (**a**) shows stable water isotopes and (**b**) the radiocarbon species.

The calculated radiocarbon contents of the mixing members resulted also in a good fit compared to the measured values at well GR (Fig. 5.4b) with 35.2 pmC (MIX I) and 37.5 pmC (MIX II) for $^{14}C_{DOC}$ and 7.8 pmC (MIX I) and 8.2 pmC (MIX II) for $^{14}C_{DIC}$. The deviations from the measured $^{14}C_{DIC}$ activity at well GR ($^{14}C_{DIC}$ 8.1 pmC) to the calculated activities of MIX I & II was very low and showed a difference of approx. 0.2 pmC (2.5 %). For the $^{14}C_{DOC}$ activity, the deviation from the measured value at well GR ($^{14}C_{DOC}$ 39.6 pmC) to the calculated activities of the mixing members were 2.1 pmc (around 5 %) (MIX II) and 4.4 pmC (approx. 11 %) (MIX I). Therefore, the groundwater at GR is highly likely formed by a mixture of two water sources

with a contribution of 30 to 35 % of Pleistocene origin and 65 to 70 % of younger Holocene origin.

5.1.3 Differences of dating results with the radiocarbon species of DIC and DOC

The results of calculated inorganic radiocarbon ages (IRA) with the revised FGM after Han and Plummer (2013) and organic radiocarbon ages (ORA) are noted in Tab. 5.2 and displayed in Fig. 5.5.

The IRA of groundwater sample UB could not be calculated because of the indistinct $^{14}C_{DIC}$ < 2 pmC and were estimated to be >30,000 years (Heidinger et al., 2019). Some of the sampled groundwater wells showed significant differences between IRA and ORA, which supports the results of former studies (Fischer et al., 1992; Geyer et al., 1993). The greatest differences between IRAs and ORAs were found at well UB (>15,184 years), well GR (8,653 years) and well BW (8,423 years). At well GR the great difference between the calculated water ages might be due to the mixing of two different water sources (see Sec. 5.1.2).

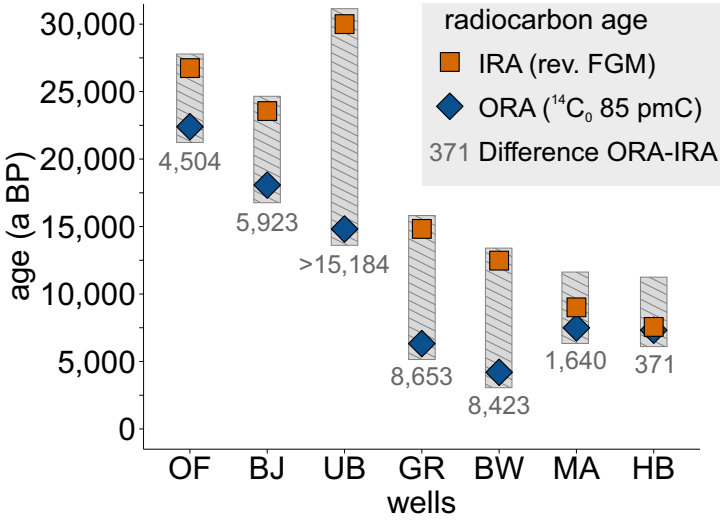

Figure 5.5: Plot of the calculated radiocarbon ages with DIC (IRA) and DOC (ORA) based on varying values for the initial concentration $^{14}C_0$ (DIC: $^{14}C_{0,DIC}$ with rev. FGM; DOC: $^{14}C_{0,DOC}$ 85 pmC (Tab. 5.2)).

For the groundwaters at well BW and UB, the numerous sources and sinks for inorganic carbon in the saturated and unsaturated zone could not be adequately described by the geochemical correction with the revised FGM model after Han and Plummer (2013) because of the diverse complexity (Murphy et al., 1989a; Purdy et al., 1992; Hershey et al., 2016; Cartwright et al., 2020).

The IRA of the wells BJ (IRA 23,996 years, ORA 18,073 years) and OF (IRA 26,901 years, ORA 22,397 years) seemed to be adequate to the ORA, but they were, despite the geochemical correction, still overestimating them with a difference about 4,504 to 5,923 years.

In contrast, the radiocarbon ages calculated with the piston-flow model at wells MA and HB were almost identical (IRA 8,057 and 9,206 years, ORAs between 7,320 and 7,495 years). The redox potential of groundwater at well MA indicates aerobic conditions (Eh_{25} 414 mV), which suggests that there is no effect of reducing processes such as BSR on the DIC. Therefore, it seems plausible that IRA's match the calculated ORA's for the groundwater at wells MA and HB.

The well MA is partially screened in the hydraulic active Graupensand sediments which also overlay the Upper Jurassic at well HB (Fig. 2.14). Since the groundwater at HB shows a similar radiocarbon systematic as well as similar hydrochemical and isotopic characteristics compared to the groundwater of well MA, it is likely that the Upper Jurassic aquifer is hydraulically in contact with the overlying Graupensand sediments in this area.

5.1.4 Cross check of the dating results with existing temperature models

The stable water isotope signatures of all groundwater samples indicate a meteoric origin and the groundwater also shows considerable variations in isotopic compositions, reflecting an infiltration under warm and cold climatic conditions (Fig. 5.2). Therefore, it is hypothesised that the signatures of the stable water isotopes for the groundwater of each well correlate with the atmospheric temperature distribution for the Holocene and late Pleistocene age. To test this hypothesis, the stable water isotope signatures of $\delta^{18}O$ and the calculated water ages (IRAs and ORAs) of all groundwater samples are compared with the temperature record of the northern hemisphere in Fig. 5.6 which was reconstructed using data from the EPICA Dome C core (0 to >30,000 years (Masson-Delmotte, 2007)), foraminifera (0 to 23,000 years (Dokken et al., 2015)) and alkenone (0 to 12,000 years (Leduc et al., 2010)).

All of the temperature models show varying temperatures around 0 ± 2 °C during the Holocene age. In the transition period between Holocene and Pleistocene, the temperature decreases dependent on the reconstruction model more or less rapidly to around -7 °C (foraminifera) or less than -7.5 °C (EPICA) compared to recent temperatures. The differences between the absolute temperature anomalies among each other may be due to the different methodologies applied and, as well, to the studies being performed in different areas.

However, it can be concluded that the temperature-dependent stable water isotopes of $\delta^{18}O$ of each groundwater sample were very well suited to the used temperature reconstruction models (Fig. 5.6). Except for well GR where mixing processes control the ^{14}C activities and the isotopic composition of the groundwater (see Sec. 5.1.3), the calculated ORAs also showed an excellent fit to the temperature distribution curves. The $\delta^{18}O$ values of the groundwater of

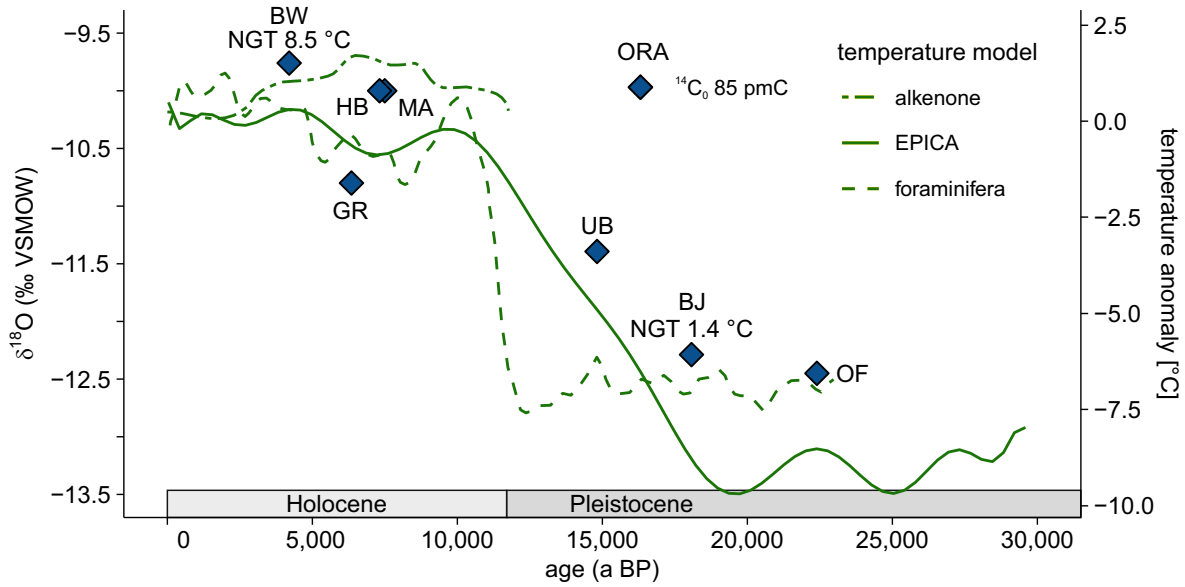

Figure 5.6: Plot of the temperature sensitive stable water isotope $\delta^{18}O$ and calculated organic radiocarbon ages (ORA) with a $^{14}C_{0,DOC}$ of 85 pmC. The green lines display the temperature anomaly for the last tens of thousands of years for different reconstruction models in relation to the present temperature based on the EPICA Dome C ice core (Masson-Delmotte, 2007) (solid), foraminifera (Dokken et al., 2015) (dashed) and alkenones (Leduc et al., 2010) (dashdotted). The noble gas infiltration temperatures (NGTs) are from Weise et al. (1991).

wells BW, HB, MA and even GR indicated postglacial origin (<12,000 years) which was also confirmed by the calculated ORAs compared to the three temperature models proposed by Masson-Delmotte (2007), Leduc et al. (2010) and Dokken et al. (2015).

In contrast, the $\delta^{18}O$ from the groundwater samples from wells BJ and OF implied clearly Pleistocene cold climatic infiltration conditions and their ORAs also matched the temperature trend from the distribution curves from Masson-Delmotte (2007) (EPICA) and Dokken et al. (2015) (foraminifera). As deduced from the stable water isotopes, the ORA at well UB confirmed that the groundwater infiltrated during the transition warming period which began at the end of the Pleistocene age.

Moreover, the results are also affirmed by the noble gas infiltration temperatures (NGTs) from Weise et al. (1991). The authors found NGTs of 8.5 °C for BW and 1.4 °C for well BJ, which may also lead to the conclusion that the ORA, especially for well BW, may represent the more realistic apparent radiocarbon age than the IRA. In addition, the difference between the two NGTs may indicate that in this area the absolute temperature spread between Holocene and Pleistocene can be better represented by the foraminifera temperature model by Dokken et al. (2015) compared to the temperature models proposed by Masson-Delmotte (2007).

5.1.5 Synopsis of the dating results in the hydrogeological context

Fig. 5.7 displays the ORA, calculated with an initial $^{14}C_{0,DOC}$ activity of 85 pmC, together with the hydrochemical characteristics expressed as stiff diagrams.

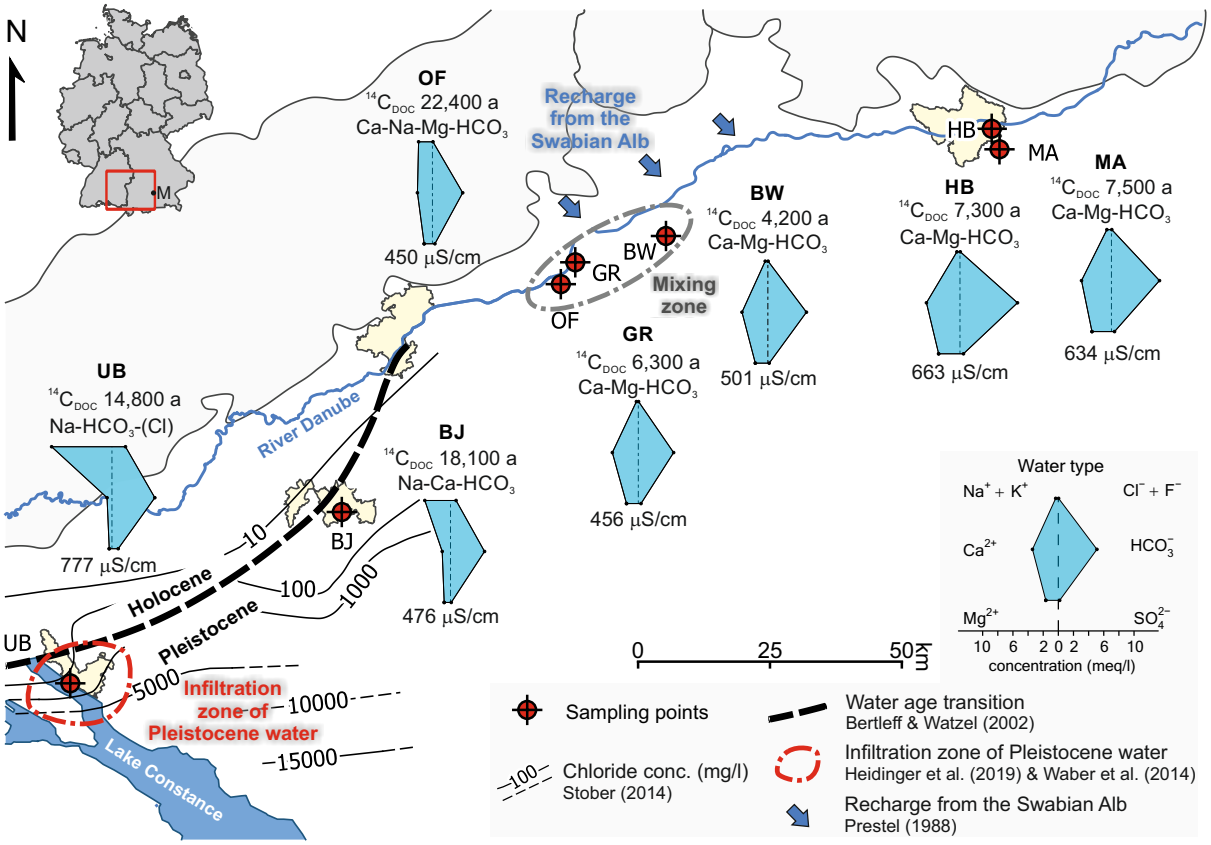

Figure 5.7: Synopsis of the dating results in comparison with the hydrochemical characteristics expressed as stiff diagrams including chloride concentrations from Stober (2014), water age transition after Bertleff and Watzel (2002), infiltration zone of Pleistocene groundwater after Heidinger et al. (2019) and Waber et al. (2014) and recharge areas of the Upper Jurassic aquifer from the Swabian Alb after Prestel (1988).

The ORAs of >12,000 years and their correlation with the stable water isotopes at wells UB (14,800 years) and BJ (18,100 years) fit very well to the understanding of the existing regional hydrogeological model of the complex, karstic carbonate Upper Jurassic aquifer. The ORA distribution at wells UB and BJ, which are south of the proposed Holocene/Pleistocene water age transition, is in accordance with subglacial infiltration during the Pleistocene and cross-formational flow in the infiltration zone at the Lake Constance (Bertleff et al., 1993; Bertleff and Watzel, 2002; Waber et al., 2014; Heidinger et al., 2019). It is likely that the formation water of the Upper Jurassic aquifer with higher contents of chloride, which occur in the south-west

of the transition, was repeatedly flushed by infiltrating waters with low salinities in the more permeable facies of the aquifer, at least during Pleistocene.

The highest ORA were observed next to the river Danube at well OF (22,400 years). In contrast, the occurring groundwater at well BW with an ORA of around 4,200 years and stable water isotope signatures indicating Holocene recharge seems to have its origin supposable in the Swabian Alb. The groundwater at well GR between the two wells BW and OF with water of Pleistocene origin is most probably a mixture of these two water bodies. This leads to the assumption that the Pleistocene waters from the Lake Constance area and the younger waters with a Holocene origin from the Swabian Alb are mixing there in a locally occurring mixing zone which is hydraulically controlled by the draining influence of the river Danube (Weise et al., 1991; Fischer et al., 1992) (Fig. 5.7).

The very comparable IRA and ORA distribution as well as hydrochemical composition of groundwater at wells HB and MA may indicate that the Upper Jurassic aquifer is hydraulically in contact with the overlying Graupensand sediments in this region.

5.1.6 Extraction efficiencies and limitations of SPE-PPL

5.1.6.1 Extraction efficiencies

It was possible to extract and process sufficient graphite-reduced carbon for all samples for radiocarbon measurements with a low sample volume (<12 l). It is worth mentioning that most of the measured DOC concentrations and calculated extraction efficiencies can only be used as a rough estimation due to the high uncertainties of the measured DOC concentrations close to the detection limit of 0.5 mg/l (Tab. 5.4).

Nevertheless, the extraction efficiencies of the SPE-PPL method ranged from 17 % for groundwater DOC at well BW to 111 % for DOC at well OF with a mean of 68 % and median of 70 % for all analysed samples (Tab. 5.4). Higher extraction efficiencies are in good accordance with observed recoveries from other freshwater studies (Li et al., 2016). Differences between $C_{extr.}$ and $C_{max,extr.}$ could either be explained by the uncertain carbon content of the extracted water sample with high standard deviations (very low DOC contents mostly below the detection limit of 0.5 mg/l) or by contents of non-retained organic substances in the SPE-DOM elution such as hydrophilics.

The lowest extraction efficiencies were determined from groundwater samples at wells BW and UB with 17 $\pm$ 2 % and 18 $\pm$ 18 % respectively (Tab. 5.4). The good correlation between the ORA and the stable water isotope signature with the temperature record in Fig. 5.6 for the groundwater from wells BW and UB may indicate that the proposed SPE-PPL is despite the low recoveries very applicable for groundwater dating. At the sample of well UB with a DOC content of 0.41 $\pm$ 0.25 mg/l, the high standard deviation indicates that the uncertain

determination of the DOC below the detection limit could be responsible for the low recovery. For the groundwater at well BW, Geyer (1994) had determined a proportion of less than 40 % for the FA fraction with no considerable proportion of HA less than 1 % and more than 60 % residual DOC such as hydrophilics of the total DOC in this groundwater. Consequentially, that could explain the low extraction efficiency for sample BW since the high amount of residual DOM was most probably not retained by the SPE-PPL. Assuming that only 40 % of the DOC is extractable with SPE-PPL, which would be 0.25 mg/l, the extraction efficiency would increase to approx. 44 %, which is also in good accordance to comparable freshwater studies (Li et al., 2016).

Table 5.4: Efficiencies of extracted PPL fraction based on the DOC concentration, extraction volume, theoretical extracted carbon ($C_{max,extr.}$) and factual extracted carbon ($C_{extr.}$). The efficiency of this method was calculated by comparison of $C_{max,extr.}$ to $C_{extr.}$. The organic carbon is combusted to CO_2 (C_{CO_2}) and reduced to graphite (C_g) for radiocarbon measurements.

Sample ID	DOC (mg/l)	extract. vol. V (l)	$C_{max,extr.}$	$C_{extr.}$ (mg)	C_{CO_2} / C_g	efficiency (%)
BJ	0.14 ± 0.01	10	1.4	0.8	0.8 / 0.8	57 ± 4
BW	0.63 ± 0.06	10	6.3	1.1	1.1 / 1.1	17 ± 2
GR	0.07 ± 0.05	10	0.7	0.6	0.6 / 0.6	85 ± 35
HB_1	0.20 ± 0.12	10	2.0	1.8	0.9 / 0.9	90 ± 30
HB_2	0.20 ± 0.12	10	2.0	1.4	0.8 / 0.8	70 ± 30
MA_1	0.13 ± 0.02	10	1.3	1.2	1.2 / 0.9	96 ± 15
MA_2	0.13 ± 0.02	8.5	1.1	0.7	0.7 / 0.7	66 ± 10
OF	0.11 ± 0.02	22[a]	2.3	2.6	2.6 / 1.0	111 ± 21
UB	0.41 ± 0.25	4	1.6	0.3	0.3 / 0.3	18 ± 18

a: The amount of carbon was extracted with two cartridges loaded with 10 and 12 l and then combined to one sample.

5.1.6.2 Discussion of possible limitations of the proposed extraction method

The limitations of the groundwater dating method with radiocarbon which is extracted with SPE-PPL might be the influence of "dead organic carbon" originating from SOC or the selective concentration and fractionation of DOM during pre-concentration.

The SOC in carbonate aquifers appears typically in the form of alkanes or HA, which is released by lignites, rather than compounds of FA (Frye and Thomas, 1993; Ivanovich et al., 1996). Coppola et al. (2015) showed that the SPE-PPL fraction eluted with methanol, retained mostly polar to semi-polar DOM. Therefore, it can be assumed that covalent (non-polar) alkanes, if present, are not dominantly retained by SPE-PPL and represent no or negligible proportions of the SPE-DOM. Geyer et al. (1993) have shown that the proportion of HA for water from well BW was very small (below 1 %), which therefore indicates that the influence of SOC di-

lution in form of HA is also negligible small. However, the presence of SOC in form of FA in the aquifer would influence the calculated ORA which needs to be considered as maximum apparent water ages.

Another limitation of the proposed extraction method is the selective concentration of DOM during the extraction. Studies of Dittmar et al. (2008), Green et al. (2014), Coppola et al. (2015) and Broek et al. (2017) have shown that the elemental and isotopic structure of PPL SPE-DOM is very representative for the total DOM despite recoveries around 40 to 60 % for SPE-PPL with no noteworthy fractionation of old refractory DOM such as FA. The comparison of the SPE-DOM and total DOM from ocean water (with ultrafiltration and reverse osmosis/electrodialysis) indicated tendencies of C enrichment or N depletion during extraction with SPE-PPL (Green et al., 2014; Broek et al., 2017). Geyer (1994) showed that contents of nitrogen are very low in FA in groundwaters from different aquifers, which also indicates that FA may not be fractionated during extraction with SPE-PPL.

However, comparisons of the elemental structure and natural abundances of radiocarbon for deep ocean water with minor influences of younger and semi-labile components indicated no difference between SPE-DOM and the total DOM (Broek et al., 2017). In contrast, Coppola et al. (2015) showed that natural abundances of radiocarbon of selectively extracted polar to non-polar SPE-PPL fractions were different. The SPE-PPL method used in this study lead to equal or slightly lower radiocarbon abundances. Considering this fact, the ORA ages needs also to be considered as maximum ages.

It can be concluded, that the calculated piston-flow ages at the SPE-DOM represent the maximum possible organic radiocarbon ages caused by the presence of SOC and the possibility of fractionation during the SPE-PPL. For deriving mean residence times from the ORA, the aquifer characteristics must be well known and the possible influence of SOC needs to be considered.

5.1.7 Short conclusion

Organic and inorganic radiocarbon ages, stable water isotope signatures and water chemistry data of the Upper Jurassic aquifer in the South German Molasse Basin provided the basis for a better understanding of the deep groundwater reservoir with respect to water age dating, flow direction and probable recharge areas.

It was demonstrated that the estimation of radiocarbon ages with $^{14}C_{DOC}$ fits very well to $\delta^{18}O$ signatures, the temperature trend of the Holocene and late Pleistocene of the northern hemisphere after Dokken et al. (2015) and NGTs from Weise et al. (1991). In addition, it can be concluded that the geochemical correction for the inorganic radiocarbon age determination is inadequately for the deep Upper Jurassic carbonate aquifer as shown for several other aquifers (Murphy et al., 1989b; Wassenaar et al., 1991; Purdy et al., 1992; Geyer, 1994; Cartwright et al., 2017).

The findings presented in this study not only reflect the promising applicability of the proposed $^{14}C_{DOC}$ dating method in carbonate aquifers with low DOC contents, but also reveal the need for a consistent isotopic database from which information can be generated for a future groundwater resource management in the South German Molasse Basin.

5.2 Hydrochemical zoning and chemical evolution of the deep Upper Jurassic thermal groundwater in the central SGMB

The results of all hydrochemical and noble gas analyses are presented in Tabs. A.1–A.3 in Appendix A.1 and summarised in Tab. 5.6. All thermal waters were dominated by a mixture of sour gas (H_2S) and aromatics such as hydrocarbons and some also had a separate oil phase. During sampling, degassing and separate phases of water and gas were observed at a few wells, particularly of samples 20 to 22.

The pH values of all samples varied between 6.3 and 7.5 indicating slightly acidic to alkaline conditions. The water chemical composition of the thermal waters differed between Na-Ca-HCO_3-Cl, Na-HCO_3-Cl, Na-Cl-HCO_3 and Na-Cl-type after Furtak and Langguth (1967) (Fig. 5.12). The mineralisation ranged from relatively low to highly mineralised groundwater with EC between 587 and 7702 µS/cm and showed a broad range of values for almost every parameter within the data set (Tab. 5.6). Therefore, the groundwater samples were clustered into distinctive groups that were deduced by the HCA.

5.2.1 Results of multivariate statistical analyses HCA and EFA

5.2.1.1 Classification of different water types of the Upper Jurassic reservoir in the SGMB based on HCA

The groundwater of the 24 sampled geothermal wells was clustered with the HCA to identify different groundwater types in the central SGMB (Schumacker, 2016; DiStefano et al., 2009). The dendrograms in Fig. 5.9 are the main results of the HCA. Based on the HCA of a first step (Fig. 5.9a), three samples (20 to 22) were identified with the greatest single linkage Euclidean distance to the other samples in the data set. Although these three samples also differ among themselves, they may form a distinctive group due to their clear differentiation from the other samples. Therefore, they were separated from the data set.

The determination of the optimal number of significant clusters in the remaining data set shows inconsistent results depending on the method used (Elbow method, Silhouette method and gap statistics). The optimal number of clusters in these well-established methods ranges from two to four. In addition, the summary of the cumulative analysis of 30 statistical methods suggests an optimal cluster number of 3 (n = 10 methods), but also indicates the number of statistically significant clusters as two (n = 6) or four (n = 6) (Fig. 5.8).

However, in step 2 (Fig. 5.9b), the remaining samples were clustered using Ward's method and squared Euclidean distances. The interpretation of the dendrogram led to four different significant clusters, which is in accordance to the determined number of clusters using the "Elbow-method". Thus, two main clusters could be clearly separated with a relatively high

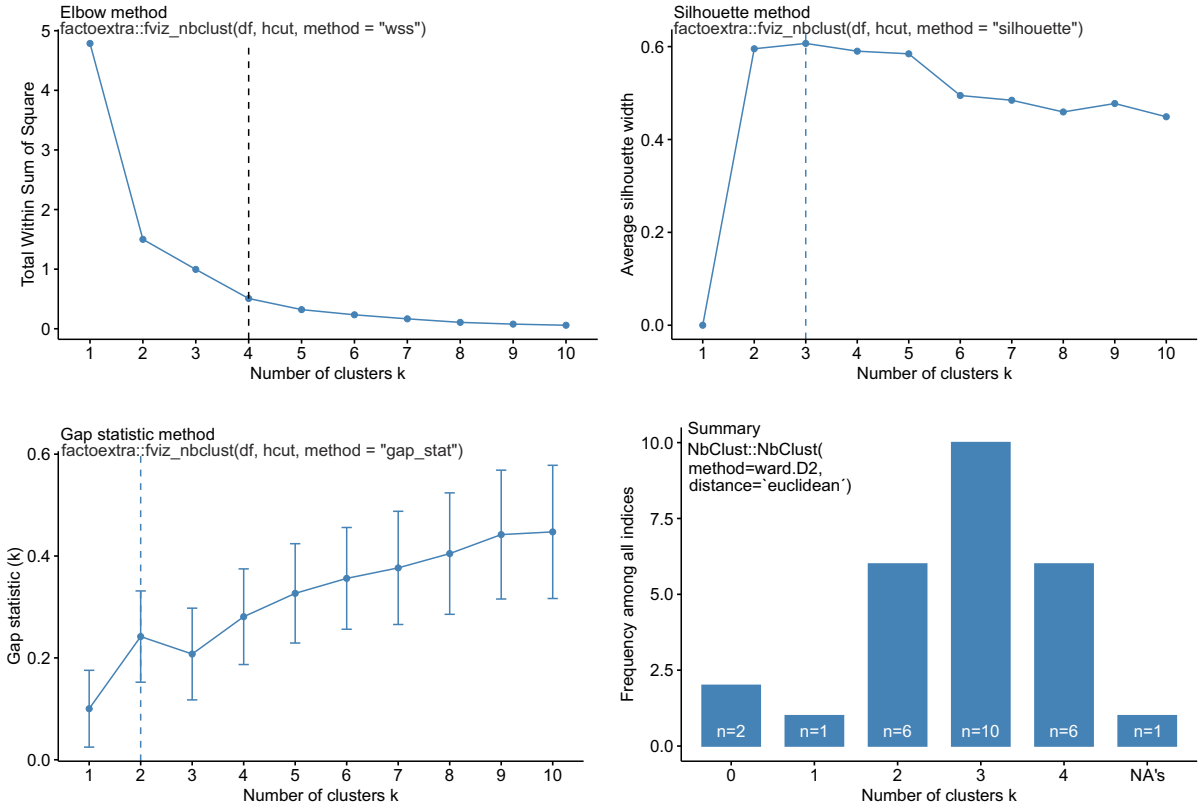

Figure 5.8: Optimal cluster numbers applied with the "Elbow method", "Silhouette method" and "Gap statistic" using the package *factoextra* (Kassambara, 2017) and computing 30 methods using *NbClust* (Charrad et al., 2014).

distance measure, which was also indicated by the Gap statistic: C1 and C2. In these clusters, further significant sub-clusters could also be distinguished, which resulted in four clusters C1-1, C1-2, C2-1 and C2-2. The interpretation of two main clusters and four subclusters is in good accordance to the range of optimal cluster numbers between two and four (Fig. 5.8).

Subsequently, the water types were classified based on the results of HCA and the interpretation of the hydrochemical composition. Cluster C1 was defined as water type 1 with the subdivision of subtypes 1a (C1-1) and 1b (C1-2) and cluster C2 as water type 2 with the subdivision of subtypes 2a (C2-1) and 2b (C2-2). The outliers were summarised as water type 3 (Fig. 5.9).

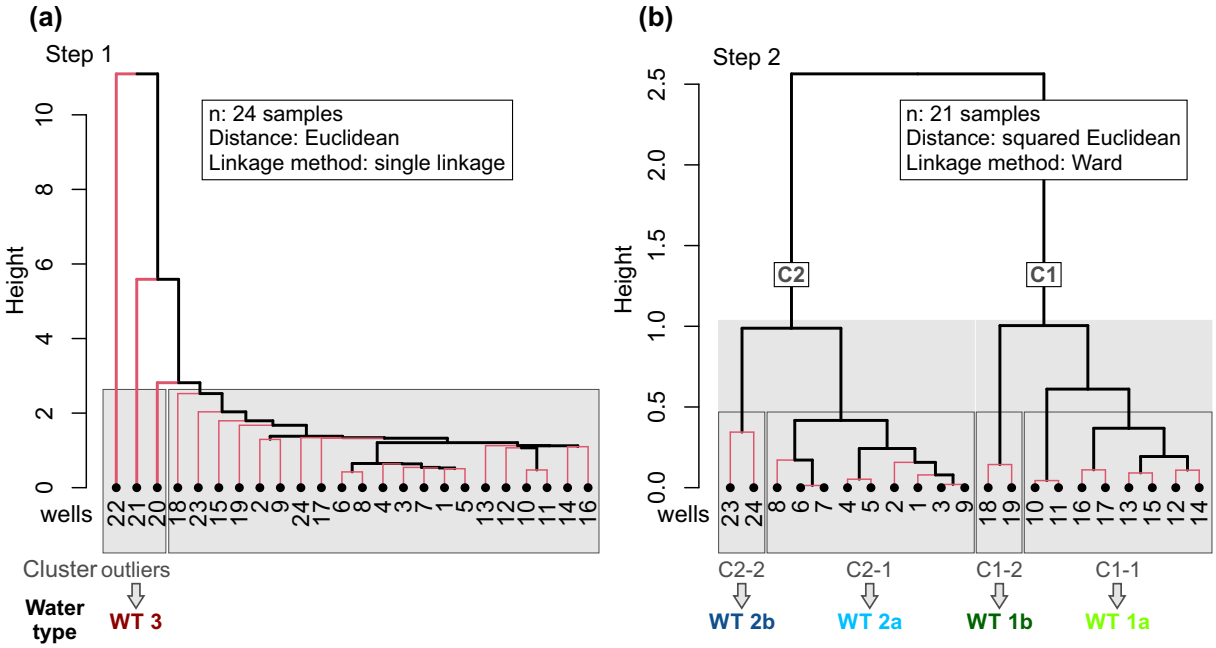

Figure 5.9: Dendrogram plots of hierarchical cluster analysis (HCA) (n = 24, m = 17) in two steps resulting in four clusters (C1-1 to C2-1) and outliers. (**a**) step 1 using single linkage method for outlier detection of observations with the greatest distance in the data set. (**b**) Step 2 using Ward's method to find clusters C1-1 to C2-1.

5.2.1.2 Identification of factors and hydrogeological processes affecting the hydrochemical water composition

Factor analysis was performed and resulting factor loadings (Tab. 5.5) were used for detecting dependencies between each parameter and to reveal underlying hydrogeological processes that influence the hydrochemical composition and, thus, the results of HCA of the thermal waters.

The interpretation of parallel analysis, empirical Kaiser criterion and Scree test resulted in a two-factor solution (Fig. 5.10). In contrast, a four-factor solution indicated by the Kaiser criterion (eigenvalues >1) resulted in (ultra-)Heywood-cases (communalities $h^2 \geq 1$, an impossible outcome (Costello and Osborne, 2005)), and was, therefore, declined. As a result, to increase the cumulative explained variance, a three-factor solution seems most reasonable.

The factoring method was multi-likelihood and an oblique (oblimin) rotation was performed as the variable factor loadings were not unique (Schumacker, 2016). The loadings of the rotated three-factor solution were 4.33 for FA1, 4.61 for FA2 and 2.91 for FA3 (Tab. 5.5). The explained variance of 70 % in the data set indicates that the three factors of the 17 used variables were not capable to cover all the hydrogeological processes affecting the hydrochemical composition of the thermal groundwater in this study.

EFA using multi-likelihood method and oblique (oblimin) rotation indicates that the system is driven by three statistical significant factors, which explain a variance of 70 % in the data set (Fig. 5.11). The factor loadings were 4.33 for FA1, 4.61 for FA2 and 2.91 for FA3 (Tab. 5.5). With the data set parameters used, the three factors are not capable of explaining the total variance of the entire data set and, therefore, may not cover all hydrogeological processes that influence the hydrochemical composition of thermal groundwater.

The explained variance, communalities h^2, for the parameters ranged between 0.26 ($^{87}Sr/^{86}Sr$) and 0.94 (HCO_3^-, SO_4^{2-}) (Tab. 5.5). The not explained variance (u^2) for the parameters $^{87}Sr/^{86}Sr$, F^-, Br^-, Sr^{2+} and B was therefore greater than the explained variance (h^2), which accords to the not explained variance of 30 % (Tab. 5.5). This implies that these parameters either describe or may be influenced by additional hydrogeological processes that are not characterised by the three factors, and that they may have only minor informative value for the processes described by the factors.

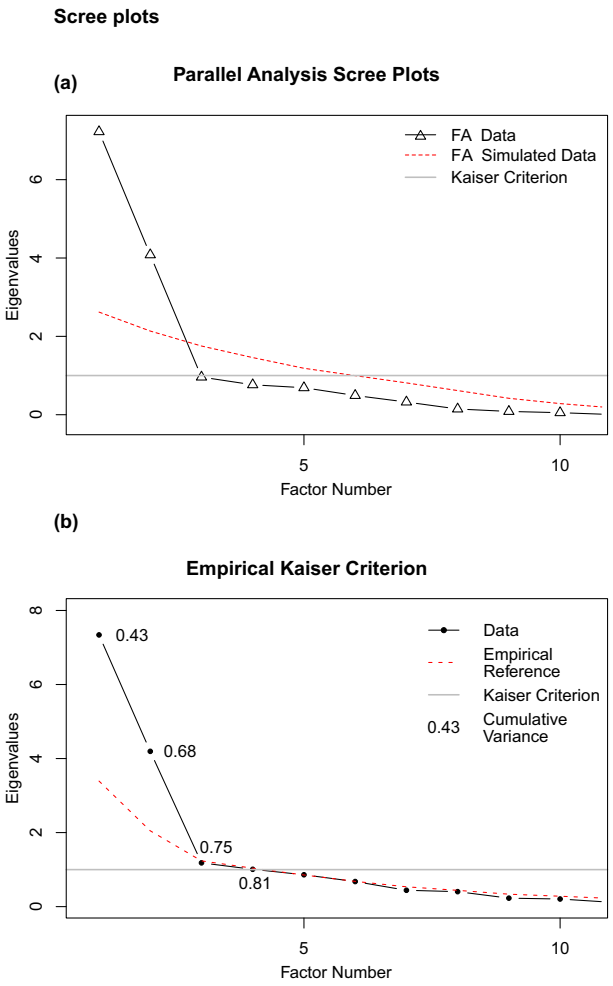

Figure 5.10: Scree plots of (**a**) parallel analysis and (**b**) empirical Kaiser criterion with cumulative variance of the eigenvalues.

The factor FA1 contains six parameters (Fig. 5.11) and may not only be related to one specific process. FA1 is represented by the earth-alkali metals Ca^{2+} and Mg^{2+} and, corresponding, HCO_3^-, which can be linked to the "hardness" or "alkalinity" of the water. The mineralisation, which is expressed by EC, is also mainly a proxy for FA1 and, therefore, may be more influenced by the earth-alkali elemental system rather than the salinity (FA3). Moreover, as Br^- is a proxy of FA1 and not of FA3 such as Na^+ and Cl^-, this may prefigure that the dominant processes on the salinity (NaCl) of the thermal water was not necessarily controlling the bromide content in groundwater. This could indicate different hydrogeological processes affecting the mineralisation and especially the salinity of the thermal waters.

Table 5.5: Factor loadings (>0.4) of the three-factor solution with the multi likelihood method and oblique (oblimin) rotation with communalities (h^2) and uniqueness (u^2) for each parameter, factor loadings and explained variance for each factor, as well as results of statistical tests: KMO-Test with MSA values; C-α from Cronbach's α test; and p-value of the Shapiro-Wilk test (SWT).

	FA1	FA2	FA3	h^2	u^2	MSA	C-α	p (SWT)
HCO_3^-	0.97			0.94	0.06	0.5	0.90	4.9×10^{-6}
Mg^{2+}	0.96			0.92	0.08	0.7	0.91	1.3×10^{-3}
Ca^{2+}	0.87			0.88	0.12	0.7	0.90	3.4×10^{-6}
EC	0.75			0.91	0.09	0.7	0.89	7.0×10^{-9}
Br^-	0.51			0.45	0.55	0.5	0.90	6.1×10^{-9}
$^{87}Sr/^{86}Sr$	0.47			0.26	0.74	0.6	0.91	1.1×10^{-1}
SO_4^{2-}		0.92		0.94	0.06	0.9	0.89	5.0×10^{-9}
Li^+		0.86		0.86	0.14	0.7	0.89	1.4×10^{-8}
F^-		0.71		0.36	0.64	0.7	0.90	1.7×10^{-1}
DOC		0.71		0.75	0.25	0.8	0.90	1.6×10^{-9}
SWI-dist		0.60		0.52	0.48	0.5	0.90	2.2×10^{-8}
B		0.42		0.36	0.64	0.9	0.90	3.0×10^{-8}
Sr^{2+}		0.70		0.47	0.53	0.7	0.90	1.9×10^{-7}
Na^+			0.93	0.92	0.08	0.7	0.89	2.5×10^{-9}
K^+			0.66	0.86	0.14	0.8	0.89	5.3×10^{-6}
Cl^-			0.64	0.80	0.20	0.7	0.89	2.7×10^{-9}
Rb^+	-0.52		0.52	0.65	0.35	0.9	0.91	1.1×10^{-3}
Loadings	4.33	4.61	2.91					
Proportion Variance	0.25	0.27	0.17					
Cumulative Variance	0.25	0.53	0.70					
Overall KMO and C-α						0.7	0.90	

The $^{87}Sr/^{86}Sr$ ratio as an indicator for specific water-rock interaction is also a proxy of FA1, but shows only a relatively low factor loading (0.47) compared to the other parameters of FA1. However, the $^{87}Sr/^{86}Sr$ ratios are not a proxy for the same factor than Sr^{2+}, which is often associated with Ca^{2+} in carbonate rocks (Faure and Powell, 1972). As a consequence, this may suggest that the $^{87}Sr/^{86}Sr$ ratios of the thermal water may be influenced by different processes or additional sources, as indicated by their high u^2 (Tab. 5.5), and that the $^{87}Sr/^{86}Sr$ signature may not necessarily linked to the strontium uptake from carbonate rocks.

FA2 links SO_4^{2-}, Li^+, F^-, DOC, Sr^{2+}, SWI-dist and B. Due to the correlation of B and DOC, B is likely controlled by the DOC mobility and, therefore, likely by the petroleum genesis (Whittemore, 1995). Therefore, DOC and B together with F^- and SO_4^{2-} may describe the influence of hydrocarbons from oilfield waters or methanogenesis induced by thermochemical sulphate-

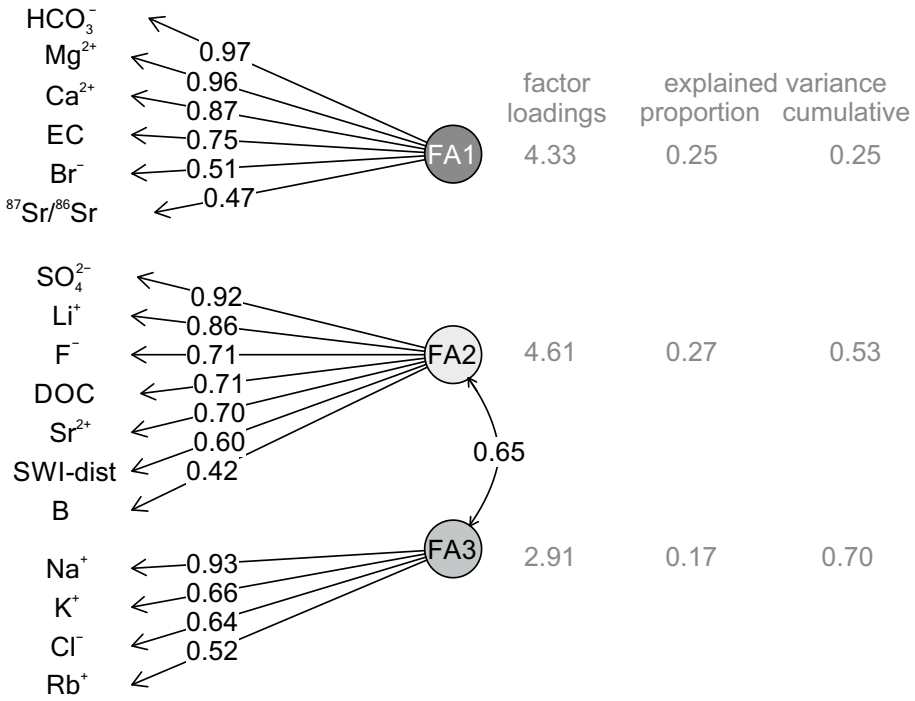

Figure 5.11: Factor loadings (>0.4) for the exploratory factor analysis (EFA) with the multi-likelihood method and oblique (oblimin) rotation and explained variance of each factor.

reduction (TSR) (Collins, 1975; Mayrhofer et al., 2014) as main process of FA2. These processes are probably linked to the information of the parameter SWI-dist, which corresponds to the meteoric origin on the one hand and the water-rock interaction of the thermal water on the other hand. Therefore, it can be concluded that a deviation of the stable water isotope signatures from the GMWL can mainly be caused by the influence of oilfield waters and corresponding organic (reduction) processes (Kharaka and Hanor, 2014).

FA3 is among others dominated by Na^+ and Cl^-, which control the "salinity" (NaCl) of the thermal water. The parameters Na^+, K^+ and Rb^+ are also proxies for interaction processes with silicate and likely clay minerals (Stober and Bucher, 2000), which may correspond to "ion-exchange processes" in the thermal water.

The factors FA2 and FA3 correlate with a R^2 of 0.65 indicating a common shared variance. This suggest that a portion of the salinity of the thermal water may also be related to the influence of oilfield waters and water-rock interaction.

Gypsum ($CaSO_4$) dissolution as a possible considerable process on the thermal water composition is not necessarily implied by the EFA. The significant factor loadings of Ca^{2+} and SO_4^{2-} are proxies of different factors, which is in accordance to the lithologic composition of the aquifer rocks (Mayrhofer et al., 2014) (Sec. 2.6).

Carbonate dissolution as a dominant reaction that affects the concentration of B may have no or only a little effect (Gemici and Tarcan, 2002) as both parameters DOC and B are proxies of FA2 and do not show a relation to the parameters Ca^{2+}, Mg^{2+} and HCO_3^-, which are proxies of FA1.

5.2.2 Chemical analyses of grouped water types

Tab. 5.6 summarises the hydrochemical parameters for the complete data set and each clustered water type with minimum, maximum and mean values. The hydrochemical facies after Furtak and Langguth (1967) of the water samples is displayed in the Piper plot with the EC as scale for the symbol size (Fig. 5.12).

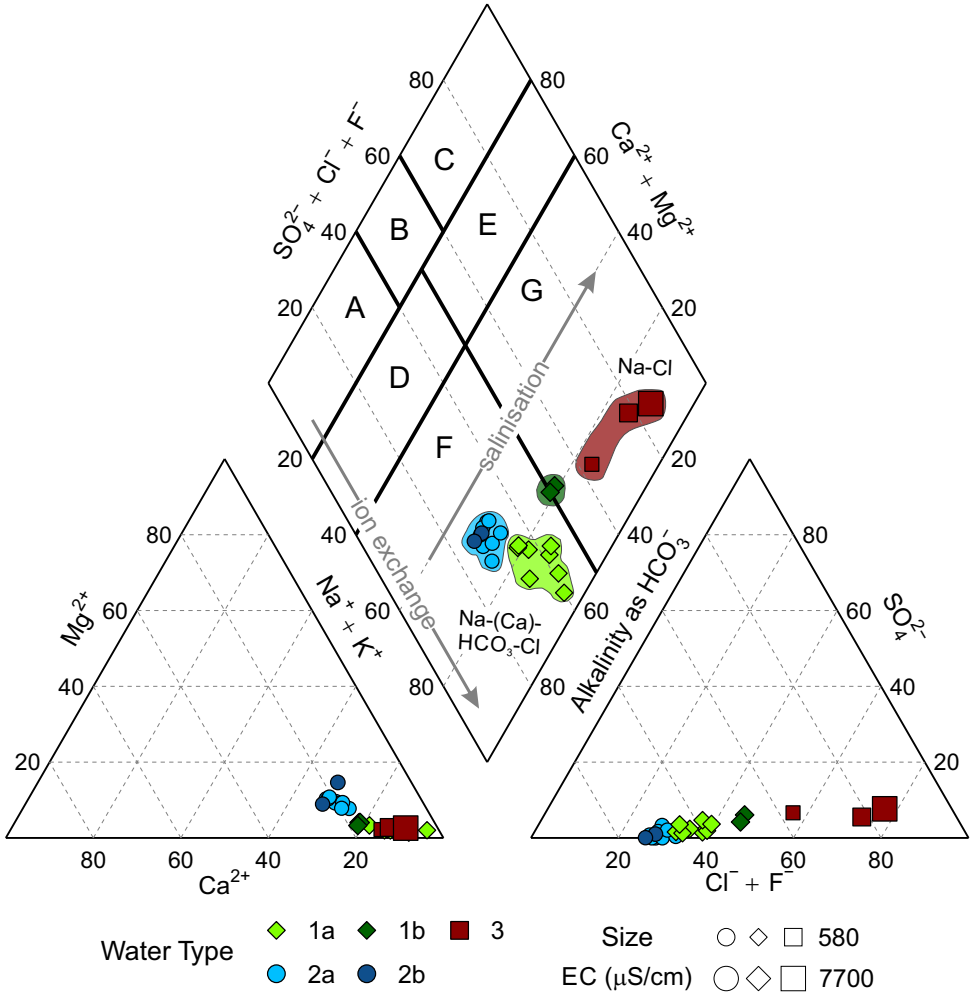

Figure 5.12: Piper plot and characterisation of the hydrochemical facies after Furtak and Langguth (1967) for thermal water samples classified as water types 1-3 based on HCA. The symbol size scale is in order to EC.

Table 5.6: Minimum (min), maximum (max) and mean values (mean) and standard deviation (SD) of the hydrochemical parameters for all water samples (summary) and for water type 1 to 3.

	Water type 1a			Water type 1b		
Parameter	min	max	mean ± SD	min	max	mean ± SD
pH value (-)	6.3	6.7	6.5 ± 0.2	6.4	6.4	6.4 ± 0.0
EC (µS/cm	587	746	671 ± 55	1029	1087	1058 ± 41
Ca^{2+} (mmol/l)	0.09	0.67	0.43 ± 0.20	0.90	0.95	0.92 ± 0.04
Mg^{2+} (mmol/l)	0.04	0.16	0.10 ± 0.04	0.17	0.21	0.19 ± 0.03
Ca^{2+}/Mg^{2+} (-)	1.4	6.2	4.56 ± 1.47	4.2	5.5	4.8 ± 0.9
Na^{+} (mmol/l)	5.15	6.24	5.60 ± 0.36	7.51	7.57	7.54 ± 0.04
K^{+} (mmol/l)	0.40	0.59	0.49 ± 0.07	0.80	0.82	0.81 ± 0.01
Li^{+} (mmol/l)	0.014	0.027	0.021 ± 0.004	0.034	0.038	0.036 ± 0.003
Sr^{2+} (mmol/l)	0.002	0.011	0.013 ± 0.006	0.012	0.016	0.014 ± 0.003
Rb^{+} (µmol/l)	0.50	0.78	0.67 ± 0.09	1.09	1.37	1.23 ± 0.20
HCO_3^{-} (mmol/l)	3.40	4.72	4.19 ± 0.50	5.10	5.10	5.10 ± 0.00
Cl^{-} (mmol/l)	1.95	2.70	2.23 ± 0.23	4.43	4.45	4.44 ± 0.01
SO_4^{2-} (mmol/l)	0.04	0.16	0.09 ± 0.05	0.21	0.32	0.27 ± 0.08
F^{-} (mmol/l)	0.11	0.42	0.22 ± 0.10	0.24	0.41	0.32 ± 0.12
Br^{-} (mmol/l)	0.002	0.007	0.005 ± 0.002	0.007	0.011	0.009 ± 0.003
Boron (mmol/l)	0.08	0.21	0.16 ± 0.06	0.27	0.31	0.29 ± 0.02
DOC (mg/l)	1.48	2.61	1.90 ± 0.40	3.80	4.20	4.00 ± 0.28
$\delta^{18}O$ (‰VSMOW)	-11.8	-11.0	-11.5 ± 0.2	-11.0	-10.8	-10.9 ± 0.1
δD (‰VSMOW)	-86.5	-84.8	-85.8 ± 0.6	-84.3	-82.8	-83.5 ± 1.0
SWI-dist (-)	0.20	0.82	0.43 ± 0.18	0.81	0.84	0.82 ± 0.02
$^{87}Sr/^{86}Sr$ (-)	0.70881	0.70925	0.70908 ± 0.00014	0.70862	0.70899	0.70881 ± 0.00026
^{4}He (ccSTP/g)	1.68×10^{-5}	2.53×10^{-5}	$2.27 \pm 0.34\times10^{-5}$	4.22×10^{-5}	1.58×10^{-4}	$1.00 \pm 0.82\times10^{-4}$
$^{3}He/^{4}He$ (-)	9.07×10^{-8}	1.13×10^{-7}	$1.03 \pm 0.09\times10^{-7}$	6.45×10^{-8}	7.31×10^{-8}	$6.88 \pm 0.61\times10^{-8}$
^{40}Ar (ccSTP/g)	4.95×10^{-4}	5.05×10^{-4}	$5.00 \pm 0.07\times10^{-6}$		3.02×10^{-3}	
$^{40}Ar/^{36}Ar$ (-)	296.2	301.2	298.7 ± 3.5		307.6	

Continuation of Tab. 5.6.

	Water type 2a			Water type 2b		
Parameter	min	max	mean ± SD	min	max	mean ± SD
pH value (-)	6.8	7.2	7.0 ± 0.1	7.0	7.5	7.2 ± 0.3
EC (µS/cm	697	756	723 ± 22	820	965	893 ± 103
Ca^{2+} (mmol/l)	0.68	0.96	0.81 ± 0.09	0.8	1.1	1.0 ± 0.2
Mg^{2+} (mmol/l)	0.30	0.44	0.38 ± 0.05	0.42	0.74	0.58 ± 0.22
Ca^{2+}/Mg^{2+} (-)	1.9	2.5	2.1 ± 0.2	1.15	2.58	1.87 ± 1.01
Na^{+} (mmol/l)	5.22	5.65	5.33 ± 0.13	5.98	6.52	6.25 ± 0.38
K^{+} (mmol/l)	0.19	0.39	0.35 ± 0.06	0.39	0.41	0.40 ± 0.01
Li^{+} (mmol/l)	0.014	0.028	0.018 ± 0.005	0.014	0.019	0.017 ± 0.003
Sr^{2+} (mmol/l)	0.006	0.008	0.007 ± 0.001	0.002	0.002	0.002 ± 0.000
Rb^{+} (µmol/l)	0.25	0.42	0.35 ± 0.07	0.46	0.48	0.47 ± 0.02
HCO_3^- (mmol/l)	4.95	5.80	5.37 ± 0.27	6.72	6.75	6.74 ± 0.02
Cl^- (mmol/l)	1.96	2.33	2.04 ± 0.12	2.25	2.64	2.45 ± 0.28
SO_4^{2-} (mmol/l)	0.01	0.14	0.06 ± 0.05	0.00	0.05	0.03 ± 0.03
F^- (mmol/l)	0.10	0.35	0.17 ± 0.09		0.14	
Br^- (mmol/l)	0.003	0.016	0.006 ± 0.004	0.005	0.007	0.006 ± 0.001
Boron (mmol/l)	0.05	0.23	0.13 ± 0.08	0.06	0.08	0.07 ± 0.02
DOC (mg/l)	0.54	1.67	0.95 ± 0.33	0.50	0.84	0.67 ± 0.24
$\delta^{18}O$ (‰VSMOW)	-12.0	-11.5	-11.7 ± 0.1	-11.7	-11.4	-11.6 ± 0.2
δD (‰VSMOW)	-86.8	-85.4	-86.2 ± 0.4	-85.7	-84.0	-84.9 ± 1.2
SWI-dist (-)	0.09	0.49	0.31 ± 0.11	0.26	0.35	0.30 ± 0.06
$^{87}Sr/^{86}Sr$ (-)	0.70907	0.70926	0.70921 ± 0.00006	0.70901	0.70926	0.70913 ± 0.00018
^{4}He (ccSTP/g)	1.80×10^{-5}	2.32×10^{-5}	$2.21 \pm 0.20\times10^{-5}$			
$^{3}He/^{4}He$ (-)	9.89×10^{-8}	1.36×10^{-7}	$1.12 \pm 0.14\times10^{-7}$			
^{40}Ar (ccSTP/g)		5.03×10^{-4}				
$^{40}Ar/^{36}Ar$ (-)		302.5				

Continuation of Tab. 5.6.

	Water type 3			Summary of all water samples	
Parameter	min	max	mean ± SD	min	max
pH value (-)	6.6	6.9	6.7 ± 0.2	6.3	7.5
EC (µS/cm	1596	7703	4366 ± 3092	587	7703
Ca^{2+} (mmol/l)	0.98	3.37	2.21 ± 1.20	0.09	3.37
Mg^{2+} (mmol/l)	0.16	1.19	0.64 ± 0.52	0.04	1.19
Ca^{2+}/Mg^{2+} (-)	2.9	6.0	4.3 ± 1.5	1.2	6.2
Na^{+} (mmol/l)	11.70	80.64	42.27 ± 35.13	5.15	80.64
K^{+} (mmol/l)	0.89	2.18	1.46 ± 0.66	0.19	2.18
Li^{+} (mmol/l)	0.055	0.275	0.154 ± 0.112	0.014	0.275
Sr^{2+} (mmol/l)	0.020	0.073	0.046 ± 0.027	0.002	0.073
Rb^{+} (µmol/l)	0.17	1.76	0.86 ± 0.81	0.17	1.76
HCO_3^- (mmol/l)	5.20	14.00	9.13 ± 4.47	3.40	14.00
Cl^- (mmol/l)	7.88	70.10	35.10 ± 31.83	1.95	70.10
SO_4^{2-} (mmol/l)	0.47	3.51	1.67 ± 1.61	0.00	3.51
F^- (mmol/l)	0.12	0.27	0.21 ± 0.08	0.10	0.42
Br^- (mmol/l)	0.008	0.124	0.057 ± 0.060	0.002	0.124
Boron (mmol/l)	0.81	3.24	1.84 ± 1.26	0.05	3.24
DOC (mg/l)	4.43	70.49	31.99 ± 34.36	0.50	70.49
$\delta^{18}O$ (‰VSMOW)	-10.5	-2.6	-6.9 ± 4.0	-12.0	-2.6
δD (‰VSMOW)	-82.3	-60.6	-72.5 ± 11.0	-86.8	-60.6
SWI-dist (-)	1.07	6.23	3.41 ± 2.61	0.09	6.23
$^{87}Sr/^{86}Sr$ (-)	0.70944	0.70970	0.70955 ± 0.00013	0.70862	0.70970
^{4}He (ccSTP/g)	5.44×10^{-5}	1.15×10^{-4}	$8.98 \pm 3.16\times10^{-5}$	1.68×10^{-5}	1.15×10^{-4}
$^{3}He/^{4}He$ (-)	6.26×10^{-8}	8.08×10^{-8}	$7.22 \pm 0.91\times10^{-8}$	6.26×10^{-8}	1.63×10^{-7}
^{40}Ar (ccSTP/g)	9.39×10^{-5}	1.98×10^{-4}	$1.46 \pm 0.74\times10^{-4}$	9.39×10^{-5}	3.02×10^{-3}
$^{40}Ar/^{36}Ar$ (-)	345.1	392.0	368.6 ± 33.2	296.2	392.0

Water type 1

The groundwater of water type 1 represent alkaline waters with a bicarbonate and chloride domination (field F and G in Fig. 5.12) and was classified as Na-HCO_3-Cl water (Furtak and Langguth, 1967). The water type 1 was separated due to the results of HCA into two subtypes, 1a and 1b (Sec. 5.2.1.1).

For water type 1a, the mean concentrations were 5.60 $\pm$ 0.36 mmol/l for Na^+ and 2.23 $\pm$ 0.23 mmol/l for Cl^- (Tab. 5.6). The concentrations of Ca^{2+} ranged from 0.09 to 0.67 mmol/l (mean value 0.43 $\pm$ 0.20 mmol/l), Mg^{2+} contents varied between 0.04 and 0.16 mmol/l (mean value 0.10 $\pm$ 0.04 mmol/l) while HCO_3^- showed concentrations between 3.4 and 4.7 mmol/l (mean value 4.2 $\pm$ 0.5 mmol/l).

Water type 1b samples were more mineralised with an EC of 1029 and 1087 µS/cm compared to the samples of water type 1a (mean value 671 $\pm$ 55 µS/cm). The difference in mineralisation between the subtypes 1a and 1b is mainly caused by the considerably elevated salinity as main process of FA2 (mean values: Na^+ 7.54 $\pm$ 0.03 mmol/l; Cl^- 4.44 $\pm$ 0.01 mmol/l) and elevated alkalinity as proxy of FA1 (mean values: Ca^{2+} 0.92 $\pm$ 0.04 mmol/l; HCO_3^- 5.1 $\pm$ 0.0 mmol/l) for type 1b. The mean Mg^{2+} concentration (0.19 $\pm$ 0.02 mmol/l) for type 1b was comparable but only slightly elevated to the values of water type 1a (Fig. 5.13a,b, Tab. 5.6). For samples of both subtypes 1a and 1b, the concentrations of K^+ (between 0.40 and 0.82 mmol/l), F^- (between 0.11 and 0.41 mmol/l) and SO_4^{2-} (between 0.04 and 0.32 mmol/l) were only subordinately represented.

Overall, both subtypes of water type 1 showed dominant influences of ion-exchange processes between Ca^{2+} and Na^+ (Figures 5.12 and 5.13a,c). Although Na^+ and HCO_3^- showed an excess compared to Cl^-, Ca^{2+} and Mg^{2+} (Fig. 5.13a,c), a positive trend of increasing HCO_3^- with Ca^{2+} and Mg^{2+} concentrations was observed (Fig. 5.13a). The concentrations of B and DOC, which may indicate influences of oilfield waters as a process of FA2 were relatively low between 0.08 and 0.31 mmol/l for B and 1.48 to 4.20 mg/L for DOC.

It can be concluded that the water chemical composition of water type 1b is comparable to water type 1a, but shows considerably higher levels of mineralisation, alkalinity and salinity, which may indicate hydrogeological processes influencing the hydrochemical evolution of these waters.

Water type 2

The Na-Ca-HCO_3-Cl groundwater of water type 2 is very homogeneously distributed in field F of the Piper plot (Fig. 5.12) and represent also alkaline waters with a bicarbonate and chloride domination after (Furtak and Langguth, 1967).

The EC for water type 2 ranged from 697 to 968 µS/cm with mean values for subtype 2a of 723 $\pm$ 22 µS/cm and slightly higher for subtype 2b with 893 $\pm$ 103 µS/cm. Ca^{2+} con-

tents ranged between 0.68 and 1.09 mmol/l (mean values: 0.81 ± 0.09 mmol/l (type 2a); 0.97 ± 0.17 mmol/l (type 2b)) and Mg^{2+} concentrations varied from 0.30 to 0.74 mmol/l (mean values: 0.38 ± 0.05 mmol/l (type 2a) and 0.58 ± 0.22 mmol/l (type 2b)). The HCO_3^- content of subtype 2b was also considerably elevated with a mean value of 6.7 ± 0.0 mmol/l compared to subtype 2a with 5.4 ± 0.3 mmol/l. The mean concentrations of Na^+ (5.33 ± 0.13 mmol/l (type 2a); 6.25 ± 0.38 mmol/l (type 2b)) and Cl^- (2.04 ± 0.12 mmol/l (type 2a); 2.45 ± 0.28 mmol/l (type 2b)) were slightly elevated for samples of subtype 2b compared to subtype 2a (Fig. 5.13c). However, both subtypes showed dominant influences of ion-exchange processes between Ca^{2+} and Na^+ due to the sodium and bicarbonate excess (Figures 5.12 and 5.13a,c).

For groundwater of both subtypes 2a and 2b, the concentrations of K^+ (between 0.19 and 0.41 mmol/l), F^- (between 0.10 and 0.14 mmol/l) and SO_4^{2-} (between 0.00 and 0.14 mmol/l) were only subordinately represented and generally lower than for type 1 waters. Oilfield water had probably no or only little effect on groundwater samples of type 2 which is documented by low concentrations of B between 0.05 and 0.23 mmol/l and DOC ranging from 0.50 to 0.23 mg/L

Overall, the water chemical composition of both subtypes of type 2 were quite similar to each other with slightly higher levels of salinity and alkalinity, especially HCO_3^-, for subtype 2b.

A considerable water chemical difference between the two water types 1 and 2 and their subtypes is expressed by their contents of calcium and magnesium, which were main proxies of the factor FA1 (Tab. 5.5), and, therefore, their Ca^{2+}/Mg^{2+} ratios (Fig. 5.13b). A molar Ca^{2+}/Mg^{2+} ratio of 1 is caused by the dissolution of pure dolomite whereas higher ratios above 2.2 indicate an increasing influence of calcite dissolution in the aquifer (Langmuir, 1971; Stichler et al., 1987; Mayo and Loucks, 1995; Mayrhofer et al., 2014). The molar Ca^{2+}/Mg^{2+} ratios (Tab. 5.6) above 2.2 for water type 1 (mean values: 4.6 ± 1.5 for subtype 1a; 4.8 ± 0.9 for subtype 1b) may indicate some influences of calcite dissolution from the rocks within the basin. In contrast, the molar Ca^{2+}/Mg^{2+} ratios around 2.2 for type 2 water samples (mean values: 2.1 ± 0.2 for subtype 2a; 1.9 ± 1.0 for subtype 1b) clearly indicate some influences of dolomite dissolution from the rocks within the basin.

Water type 3

Water type 3 showed a broad range of EC from 1596 to 7702 µS/cm with a mean value of 4366 ± 3092 µS/cm (Tab. 5.6). The major chemical parameters of the groundwater samples of type 3 plot heterogeneously distributed in field G of the Piper plot (Fig. 5.12), which represent alkaline waters with a chloride predomination (Na-Cl and Na-Cl-HCO_3 type). They plot clearly distinguishable from the other water types and also show great heterogeneity among themselves.

The Ca^{2+} concentrations varied from 0.98 to 3.37 mmol/l and Mg^{2+} concentrations ranged between 0.16 and 1.19 mmol/l. Contrary to water types 1 and 2, the samples of water type

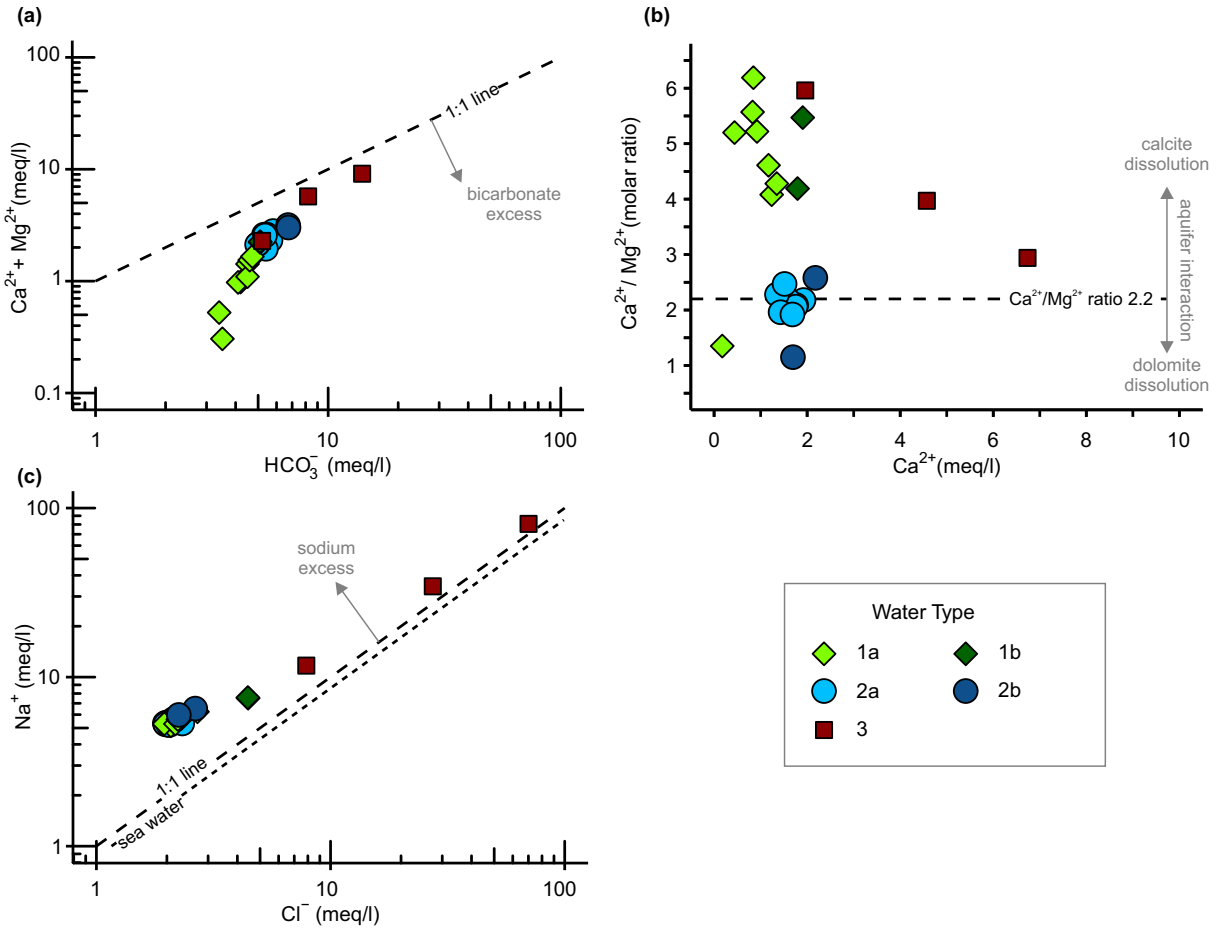

Figure 5.13: Distribution plots of water chemical parameters: (**a**) Ca^{2+}+ Mg^{2+} vs. HCO_3^-; (**b**) Ca^{2+}/ Mg^{2+} ratio vs. Ca^{2+}; (**c**) Na^+ vs. Cl^- with typical values for seawater (Clark, 2015).

3 were characterised by a predominant influence of the salinity (Na^+ and Cl^-), which was defined as one main influence of the factor FA3 (Sec. 5.2.1.2). The concentrations ranged from 11.70 to 80.64 mmol/l (mean value 42.27 ± 35.13 mmol/l) for Na^+ and varied between 7.88 and 70.10 mmol/l (mean value 35.10 ± 31.83 mmol/l) for Cl^-. With increasing concentrations of Na^+ and Cl^-, the groundwater samples of water type 3 converge to the 1:1 line in Fig. 5.13c, but showed as well predominant ion-exchange processes between the alkali ion Na^+ and the earth-alkali ions Ca^{2+} and Mg^{2+} (Fig. 5.13a,c). The molar Ca^{2+}/Mg^{2+} ratios ranged from 2.9 and 6.0 indicating distinct interaction between the fluid and calcite minerals. Interestingly, with increasing Ca^{2+} concentrations, the Ca^{2+}/Mg^{2+} ratio decreases indicating a higher influence of dissolved dolomites.

The clearly elevated concentrations of B (between 0.81 and 3.24 mmol/l) and DOC (4.43 to 70.49 mg/L) may indicate as proxies of FA2 additionally considerable influences from oilfield waters. The concentrations of major ions K^+, F^- and SO_4^{2-} were also consecutively elevated

and ranged between 0.89 and 2.18 mmol/l for K^+, between 0.12 and 0.27 mmol/l for F^- and between 0.47 an 1.84 mmol/l for SO_4^{2-}.

5.2.3 Assessing recharge conditions and water-rock interaction

5.2.3.1 Noble gas infiltration temperatures NGTs and stable water isotopes

Results of the CE modelling and discussion of possible limitations

The NGTs were calculated to obtain the temperature-driven recharge conditions of representative samples for each water type (Tab. 5.7). The NGTs range between 0.9 $\pm$ 0.5 °C and 1.4 $\pm$ 0.5 °C for water types 1a and 2a and is 3.1 to 3.2 $\pm$ 0.5 °C for sample 18 of water type 1b.

Table 5.7: Noble gas infiltration temperatures (NGTs) with PANGA (Jung and Aeschbach, 2018) using the CE-model (Aeschbach-Hertig et al., 2000) with Ne, Kr and Xe (Tab. A.3). Keys: fit - linear fitting model; MC - Monte Carlo simulations. Standard deviation as errors.

ID	Water type	A_{MC} (ccSTP/g)	F_{fit} (-)	T_{fit} (°C)	T_{MC} (°C)
9	2a	0.32 ± 0.03	0.94 ± 0.01	1.4 ± 0.4	1.4 ± 0.5
16	1a	0.26 ± 0.13	0.97 ± 0.17	0.9 ± 0.5	0.9 ± 0.4
17	1a	0.23 ± 0.15	0.98 ± 0.16	1.4 ± 0.4	1.4 ± 0.4
18	1b	0.36 ± 0.07	0.45 ± 0.01	3.2 ± 0.5	3.1 ± 0.5
21	3	-2.0 ± 3.85	-	-	- -
22	3	$-1.39 \times 10^{-7} \pm 1.87 \times 10^{7}$	-	-	- -

The calculated entrapped excess-air A ranged for the samples 9 (type 2a), 16, 17 (both type 1a) and 18 (type 1b) between 0.23 and 0.36 ccSTP/g. These values are above realistic values for natural groundwater (>0.2 ccSTP/g) (Aeschbach-Hertig et al., 2000). According to Jung et al. (2013), the unrealistically high values for A are usually not a limitation for the calculation of T with the CE model. Especially with the inclusion of Monte Carlo simulations, plausible NGTs may be fitted, but, however, they can slightly be overestimated. Nevertheless, an interpretation of these values is necessary to understand the underlying physical processes. The elevated levels of excess air A could possibly be explained by an equilibrium between groundwater and trapped air bubbles (Jung and Aeschbach, 2018) or rapid infiltration under high overburden pressure (Aeschbach-Hertig and Solomon, 2013), which will be discussed below.

Fractionation parameters F were fitted using the CE model (Aeschbach-Hertig et al., 2000) and ranged from 0.94 to 0.98 for samples 9, 16 and 17 and was 0.45 for sample 18. They lie within a reasonable range (F between 0 and 1) but also indicate most probably degassing of samples 9, 16 and 17 as F values were close to 1 (see Sec. 4.3). However, it was not possible

to calculate reasonable NGTs for the two samples of type 3 due to inappropriate noble gas mass balances and negative values for the excess air A with high errors (Tab. 5.7) (Jung and Aeschbach, 2018).

At this point it must also be mentioned that the sampled geothermal waters, in contrast to natural groundwater for which this interpretation model was mainly developed, were collected under special temperature and pressure conditions (see Sec. 4.1). Sampling effects may have an influence on the gas-physical composition of the water samples, e.g. degassing (Nakata et al., 2019), caused by the rapid expansion during sampling from the high-pressure thermal water system in the geothermal plant and by the cooling during sampling. Therefore, it must be examined whether the calculated temperatures have been influenced by these physical processes.

The stable water isotopes are capable of storing information regarding the climate conditions during infiltration or (geothermally driven) water-rock interaction in the subsurface (Clayton et al., 1966; Bottomley et al., 1994; Clark, 2015). They can also be used, among other things, to validate the plausibility of the calculated NGTs. In addition, the mixing range of stable water isotope signatures from literature data (Bertleff et al., 1993; Balderer, 1990) for Upper Jurassic and Tertiary Molasse Basin oilfield waters shown in Fig. 5.14 can be used to assess the nature of the water-rock interaction and possible mixing processes of different water bodies.

Water types 1 and 2

The stable water isotope signatures of both water types 1 and 2 are very homogeneously distributed with δD ranging from -86.8 to -82.8 ‰ and $\delta^{18}O$ values between -12.0 and -11.0 ‰ (Tab. 5.6). They scatter in Fig. 5.14 predominantly between the GMWL and LMWL indicating meteoric origin. Especially the stable water isotope signatures of water type 1a and both subtypes of 2 indicate a cold climatic origin that is typical for Pleistocene waters in that region (van Geldern et al., 2014). This is supported by the results of NGTs between 0.9 ± 0.5 °C and 1.4 ± 0.5 °C for water types 1a and 2a (Tab. 5.7). These results are in good accordance to a previously determined NGT (2.8 ± 0.5 °C) of groundwater from a Upper Jurassic geothermal well in this study area (Weise et al., 1991; Weise and Stichler, 1997). Results of noble gases stemming from other deep basins such as the Pannonian Basin also indicate comparable recharge conditions during the Pleistocene glacial period with NGTs below 4 °C (Varsányi et al., 2011). The distances to the GMWL, SWI-dist, ranged between 0.09 and 0.82 with mean values of 0.43 ± 0.18 for type 1a, 0.31 ± 0.11 for type 2a and 0.30 ± 0.06 for type 2b. These values do not imply considerable isotope exchange processes of hydrogen and oxygen during evaporation or with soil or bedrock after recharge.

In contrast, the stable water isotope signatures of two samples of water type 1b with δD values of -84.3 and -82.8 ‰ and $\delta^{18}O$ values of -11.0 and -10.8 ‰ plot slightly below the LMWL and were more isotopically enriched compared to the remaining samples of water types 1a, 2a and 2b. The observed enrichment of $\delta^{18}O$ values and, corresponding, the slightly elevated

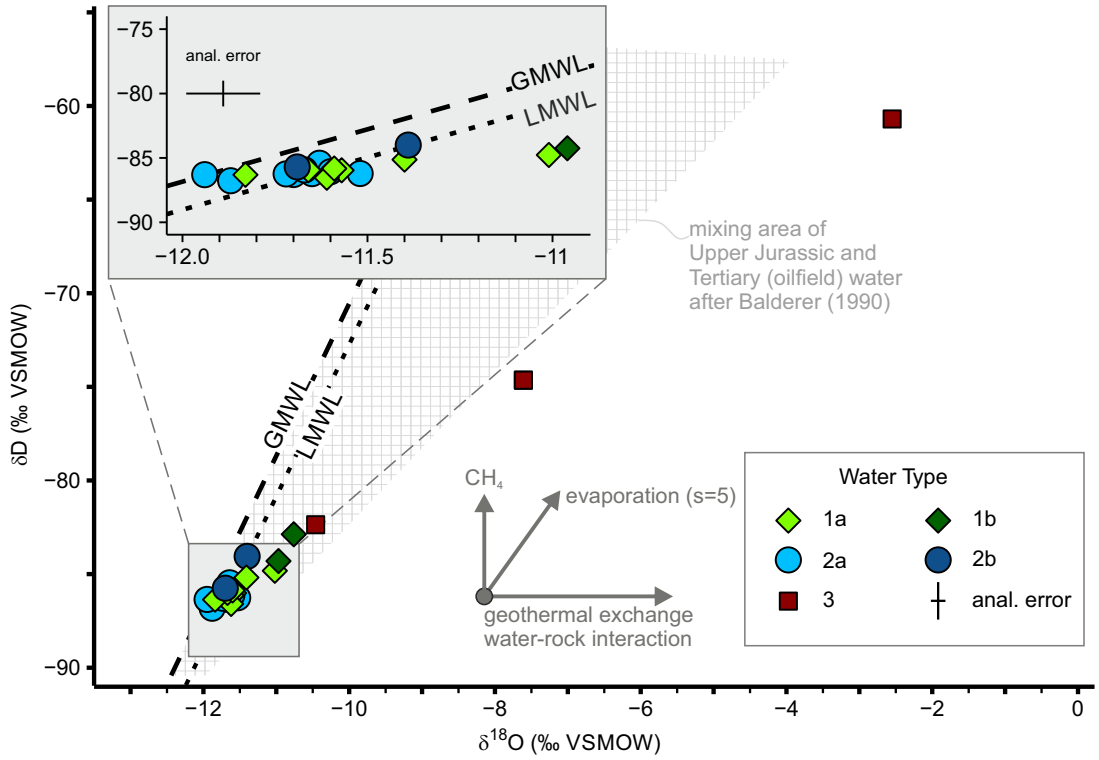

Figure 5.14: Plot of stable water isotope signatures for samples of water types 1 to 3 with global (GMWL) and local (LMWL) meteoric water lines (Craig, 1961; Stumpp et al., 2014) and main processes on the isotope chemistry (Clark, 2015).

mean value of SWI-dist (0.82 $\pm$ 0.02, Tab. 5.6) are typical for geothermally driven oxygen exchange due to water-rock interaction with carbonate rocks in sedimentary basins (Clayton et al., 1966; Kharaka and Hanor, 2014). The NGT of the water type 1b sample is elevated with 3.1 $\pm$ 0.5 °C compared to the other samples of type 1a and 2, but indicates together with the stable water isotope signatures meteoric Pleistocene cold climatic infiltration conditions (van Geldern et al., 2014). Thus, it can be concluded that water type 1b has probably been influenced by geothermal isotope exchange due to water-rock interaction after recharge during the Pleistocene. Mixing processes between Pleistocene water and fossil formation water that led to this additional isotopic shift in $\delta^{18}O$ could also be a reasonable explanation.

The information derived from the NGT and stable water isotope signatures that the water of both types 1 and 2a has been recharged under cold climatic conditions could also yield a plausible explanation for the high levels of excess air in the samples. The elevated values of the excess-air (A>0.2 ccSTP/g) for both water types 1 and 2a are above realistic levels for natural groundwater (Tab. 5.7 and Sec. 4.3). Vaikmäe et al. (2001) reported also unusual high values for excess air in northern Estonia and related them to subglacial recharge under high-pressure conditions. Glacial ice contains a lot of trapped air (Aeschbach-Hertig and Solomon, 2013). If

this ice melts at the bottom of the glacier and the trapped air cannot escape but is introduced into the subsurface together with infiltrating meltwater under the overburden pressure of the glacier masses, this could lead to the observed high values for excess air in groundwater. These considerations are supported by the dating results and apparent ^{81}Kr ages between 60,000 and 135,000 years for some type 1a and 2a water samples (Heidinger et al., 2019), which confirm a recharge during the Riss (300,000 to 130,000 years) and Wuerm (115,000 to 11,700 years) glaciations (Fig. 2.25 in Sec. 2.6.2.3). Although the values for A and F may be influenced by sampling effects, it seems that it was nevertheless possible to calculate realistic values for the NGT, as shown by the combined interpretation with the stable water isotopes. Finally, the influence of the altitude effect, which could also lead to an explanation for the stable isotope signatures of both water types 1 and 2a, is most likely excluded by this interpretation.

Water type 3

For water type 3, the δD values ranged between -82.3 and -60.6 ‰ and δ^{18}O values ranged from -10.5 to -2.6 ‰ (Tab. 5.6). The stable water isotope signatures plot heterogeneously distributed and clearly below both meteoric water lines (GMWL and LMWL) in Fig. 5.14. The initial recharge conditions of water type 3 can therefore not be delineated. The orthogonal distances to the GMWL (SWI-dist), ranging from 1.07 to 6.23, may indicate extensive water-rock interaction, as already suggested by the water chemical composition (Sec. 5.2.2). These stable water isotope signatures are typical for highly mineralised evaporated brines in deep sedimentary basins (Clayton et al., 1966; Kharaka and Hanor, 2014) and oil- and gasfield waters in the Molasse basin (Goldbrunner, 1987; Balderer, 1990; Stichler, 1997). They plot both inside and slightly outside of the mixing area of Upper Jurassic and Tertiary (oilfield) waters (Fig. 5.14), which illustrates the influence of water-rock interaction together with methanogenesis. The inappropriate noble gas mass balances indicate that the samples were most probably affected by the observed separate fluid phases and/or degassing processes during sampling (Jung and Aeschbach, 2018). Thus, this also implies considerable influences of oilfield waters to water type 3.

5.2.3.2 Tracing water-rock interaction with ^{87}Sr/^{86}Sr signatures

The ^{87}Sr/^{86}Sr ratio of groundwater is a very useful tracer to determine the dependency of water-rock interaction and mixing processes influencing the water chemical composition of the different water types (Capo et al., 1998; Probst et al., 2000; Shand et al., 2009). The ^{87}Sr/^{86}Sr signature of groundwater depends on the chemical evolution during recharge and infiltration through the unsaturated zone, the aquifer lithology, the rocks alteration level and intensity of water-rock interaction. Infiltrating water receives its ^{87}Sr/^{86}Sr signature in the soil zone, which

is then not fractionated and preserved unless mineral dissolution of the aquifer host rocks occur (Baublys et al., 2019).

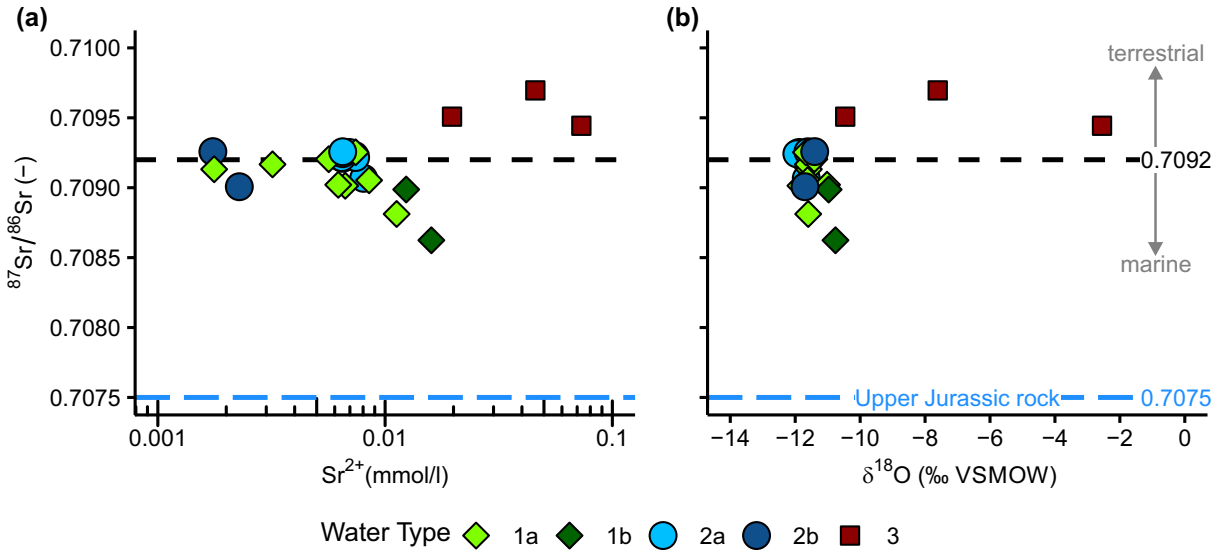

Figure 5.15: $^{87}Sr/^{86}Sr$ ratios of the thermal water in dependency of (**a**) the Sr^{2+} concentration and (**b**) the stable water isotope $\delta^{18}O$. $^{87}Sr/^{86}Sr$ value of 0.7075 represents the mean signature for Upper Jurassic carbonate rocks in the SGMB (Thuro et al., 2019) and 0.7092 the threshold between marine and terrestrial rocks (Veizer et al., 1999).

Water types 1 and 2

The mean $^{87}Sr/^{86}Sr$ ratios of water type 1, 0.70908 ± 0.00014 (type 1a) and 0.7088 ± 0.00026 (type 1b), and water type 2, 0.70921 ± 0.00006 (type 2a) and 0.70913 ± 0.00018 (type 2b), were clearly above the characteristic mean values of the Upper Jurassic carbonate rocks of the SGMB, which are around 0.7075 (Thuro et al., 2019). The radiogenic $^{87}Sr/^{86}Sr$ ratios are relatively constant and independent of the strontium content for type 1 and 2 waters with Sr^{2+} <0.008 mmol/l (Fig. 5.15a). This indicates that the strontium isotope chemistry of these waters was not predominantly influenced by the dissolution of Upper Jurassic carbonate rocks after recharge. With increasing Sr^{2+} concentrations >0.008 mmol/l, the type 1a waters show clearly decreasing $^{87}Sr/^{86}Sr$ ratios. Moreover, the water type 1b samples with higher Sr^{2+} concentrations ranging from 0.012 to 0.016 mmol/l showed also considerably lower $^{87}Sr/^{86}Sr$ ratios between 0.70862 and 0.70899. The higher Sr^{2+} concentrations corresponding with lower $^{87}Sr/^{86}Sr$ ratios of these type 1a and especially type 1b waters may therefore indicate dissolution of calcite carbonates most likely from Upper Jurassic rocks.

Fig. 5.15b shows an inverse relationship between decreasing $^{87}Sr/^{86}Sr$ ratios with enriching (less negative) $\delta^{18}O$ values for samples of both water types 1 and 2. This relationship supports the hypothesis that interaction of groundwater with the Upper Jurassic rocks due to the

geothermal exchange with the carbonate minerals (Clayton et al., 1966) or fossil formation waters may have been responsible for the observed isotopic shift in $\delta^{18}O$ (Fig. 5.14).

Water type 3

The relationship of $^{87}Sr/^{86}Sr$ signatures with Sr^{2+} concentrations and $\delta^{18}O$ values of type 3 water samples in Fig. 5.15a,b indicate a different influence on the hydrochemical composition and water-rock interaction compared to both water types 1 and 2. The $^{87}Sr/^{86}Sr$ ratios for type 3 waters are tending to more radiogenic signatures clearly above 0.7092 with values between 0.70941 and 0.70970. Subsequently, water type 3 was highly likely not dominated by the fluids in the rock matrix and rock geochemistry of the Upper Jurassic aquifer rock. The increased strontium concentrations between 0.020 and 0.073 mmol/l could therefore not be explained by the dissolution of marine carbonate rocks of the Upper Jurassic reservoir. As a result, the radiogenic $^{87}Sr/^{86}Sr$ ratios clearly indicate a strontium input from interaction with non-marine terrestrial rocks, fossil formation waters from terrestrial sediments, and also oilfield waters (Chaudhuri et al., 1987). It can be suggested that this radiogenic influence on the $^{87}Sr/^{86}Sr$ signatures of water type 3 is related to a hydraulic contact to overlying terrestrial Tertiary sediments and Tertiary fossil formation water.

5.2.3.3 Mixing processes and origin of salinity using $\delta^{18}O$ and Cl^-

Geochemically driven processes influencing the water chemistry and salinisation, such as mixing between fresh and highly saline fossil formation waters, can be differentiated by plotting the relationship of $\delta^{18}O$ with the conservative ion Cl^- (Stichler, 1997; Ettayfi et al., 2012). Based on the results so far, the mixing model was extended and adopted to the origin of salinity for water types 1b and 3 (Fig. 5.16). A hydrogeochemical evolution of type 1a and 2 waters that interact with the Upper Jurassic carbonate rocks of the SGMB is represented by a mixing zone where highest and lowest saline fluid inclusion data stemming from the Upper Jurassic rocks (Mraz et al., 2019) act as end members of the mixing model.

The samples of water type 1b plot along the mixing line of water types 1a and 2 that is characterised by the lower range of fluid inclusion values of Upper Jurassic rocks. This may indicate that the source of Cl^- in that water may be also related to the isotopic enrichment of $\delta^{18}O$ (Sec. 5.2.3.1), which was assumed to be caused by geothermal exchange processes of type 1a water with the Upper Jurassic reservoir rocks (Sec. 5.2.3.2). The associated enrichment of $\delta^{18}O$ with increasing Cl^- concentrations of type 1b waters may therefore indicate chloride uptake due to dissolution of the less saline Upper Jurassic carbonate minerals and also suggest an interaction with the fossil Upper Jurassic formation water that is stored in the rock matrix.

In contrast, the samples of water type 3 plot very heterogeneously distributed within the mixing zone of the mean values of type 1a and 2 waters with the upper and lower ranges of

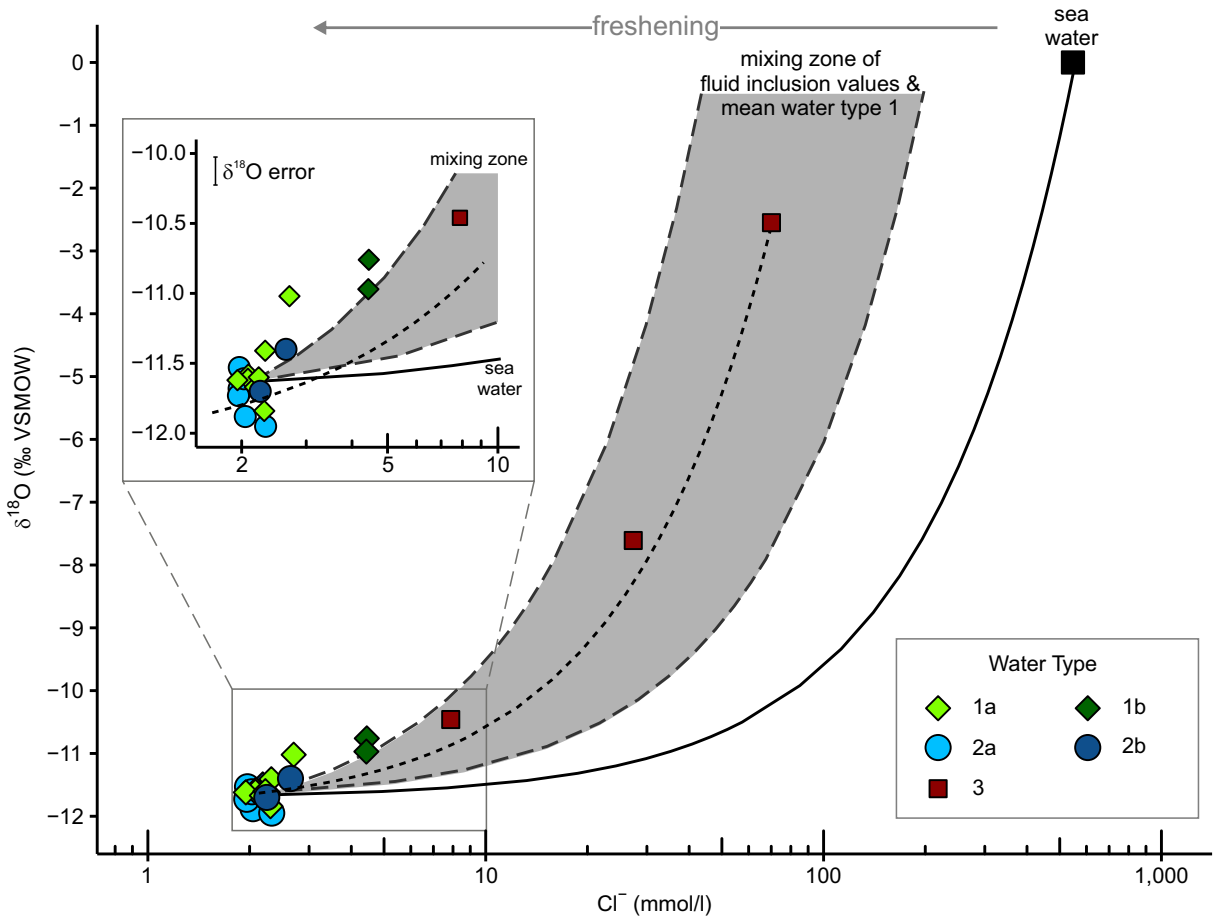

Figure 5.16: Cl^- concentrations and $\delta^{18}O$ values of the thermal waters. The dotted line is the mixing line between two end-members: the mean value of water types 1a and 2 with sample 22 of type 3. The mixing zone (grey with dashed lines) comprises the area starting from the mean value of water types 1a and 2 with the extreme values of fluid inclusion and rock data from Upper Jurassic rocks based on the data of Mraz et al. (2019).

the Upper Jurassic rock and fluid inclusion data in Fig. 5.16. The distinct isotopic enrichment of the $\delta^{18}O$ values of water type 3 is accompanied by much more significant chloride uptake compared to water type 1b. The maximum values of water type 3 form a positive and linear mixing correlation with type 1a and 2 waters, which can be clearly differentiated from the mixing processes with seawater. As the samples of water type 1b do not plot on that linear mixing line, it is assumed that the origin of salinity is likely different compared to water type 3. Together with the results of the strontium isotopes (Sec. 5.2.3.2), an influence of higher saline Tertiary formation water leading to an increased salinity (Sec. 5.2.2) and stable water isotope signatures that are typical for sedimentary brines (Sec. 5.2.3.1) is highly suggested

5.2.4 Calculation of apparent water ages by radiogenic noble gas isotopes

The noble gas isotope data were not considered in the multivariate statistical analyses as they were not obtained at every well in this study (see Sec. 4.5), but they also provide useful information about influences of hydrogeological processes as well as apparent mean residence time of the thermal groundwater. Increased apparent groundwater ages would be an indication of the influence of fossil formation waters and could allow conclusions about higher water-rock interaction due to reduced hydraulic permeability.

The noble gas isotope analyses of the thermal water samples from the deep Upper Jurassic reservoir in this study were partially affected by varying high amounts of the dissolved gases (e.g. CH_4, CO_2, N_2, H_2S), and probably partial degassing during uplift at sampling temperature (Heaton and Vogel, 1981; Wilson and McNeill, 1997; Peeters et al., 2003; Blaser et al., 2010; Lippmann et al., 2003, 2005; Nakata et al., 2019). Equilibration of noble gases dissolved in water with the non-atmospheric gas phases of CH_4 and H_2S could have induced undersaturation of the atmospheric signatures (Lippmann et al., 2003). However, it is assumed that the isotope ratios $^3He/^4He$ and $^{40}Ar/^{36}Ar$ of the samples were not be considerably affected by these processes.

The $^3He/^4He$ ratios in Fig. 5.17a indicate that all thermal groundwater samples were air saturated water that accumulated radiogenic $^4He_{ex}$ of crustal origin (R_c between 0.01 and 0.1 R_a (Ballentine and Burnard, 2002; Kulongoski and Hilton, 2012; Phillips and Castro, 2014)) with no or only little evidence of mantle-derived ^4He_m. The non-atmospheric portion of helium $^4He_{non\text{-}atm}$ for all samples is greater than 99 %. The $^3He/^4He$ ratios <0.1 R_a indicate considerable contributions from radiogenic $^4He_{ex}$ and thus probably high apparent mean residence times (Sano and Fischer, 2013).

The water samples of type 1a and 2a, which had overall no or only negligible separate gas phases, displayed relatively homogeneous ^4He concentrations of $2.27 \pm 0.34 \times 10^{-5}$ and $2.21 \pm 0.20 \times 10^{-5}$ ccSTP/g, respectively (Tab. 5.6). The mean $^3He/^4He$ ratios comprise a very narrow range for both subtype samples with $1.03 \pm 0.09 \times 10^{-7}$ for water type 1a and $1.12 \pm 0.14 \times 10^{-7}$ for water type 2a. The $^{40}Ar/^{36}Ar$ ratios of around 300.1 (between 299.8 and 302.5) for the three samples of type 1a and 2a were close to the ASW signature ($^{40}Ar/^{36}Ar$ 298.5 (Lee et al., 2006)) (Fig. 5.17b) with subsequently only minor contributions of radiogenic $^{40}Ar_{ex}$ between 2.17 and 6.65×10^{-6} ccSTP/g (Tab. A.2).

For water type 1b, the $^3He/^4He$ ratios were lower compared to type 1a and 2a samples and ranged between 6.45 and 7.31×10^{-8} while the ^4He concentrations were higher varying from 0.42 to 1.58×10^{-4} ccSTP/g (Tab. 5.6). The considerably elevated $^{40}Ar/^{36}Ar$ ratio of 307.6 resulted in a higher $^{40}Ar_{ex}$ concentration of 5.76×10^{-5} ccSTP/g (Tab. 5.8) compared to water type 1a and 2a. This indicates that the apparent groundwater age of water of type 1b may be higher than for water type 1a and 2a.

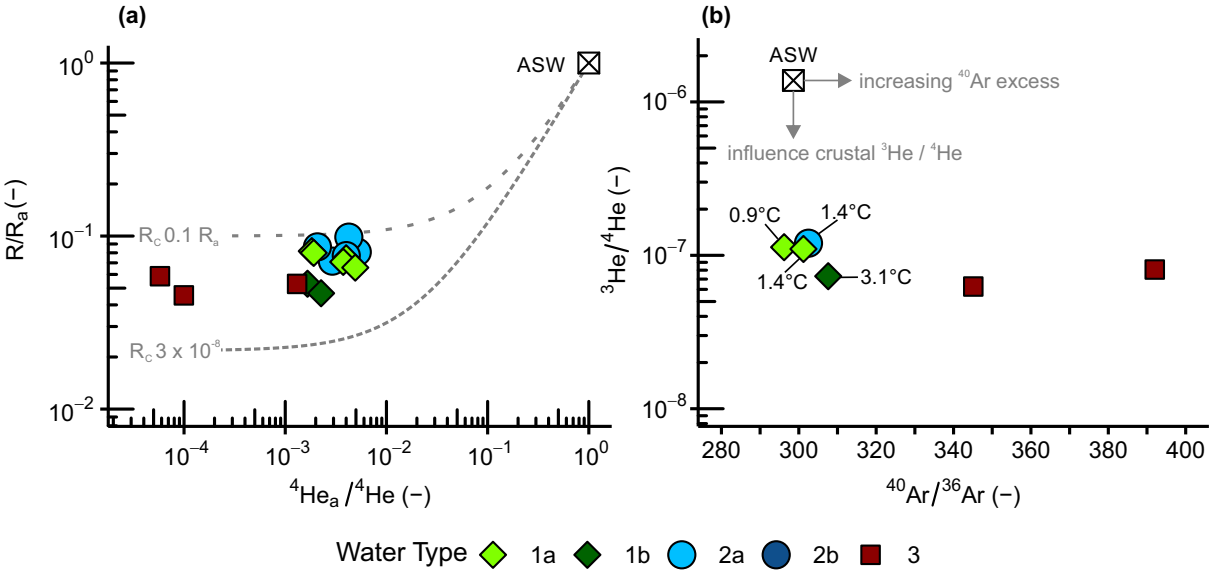

Figure 5.17: Results of noble gas isotope measurements. (**a**) Ratios of atmospheric and measured helium-4 ($^4He_a/^4He$) and $^3He/^4He$ ratios (R/R_a). The two curves represent binary mixing between the atmospheric end-member and a crustal end-member. (**b**) Noble gas isotope ratios of argon ($^{40}Ar/^{36}Ar$) and helium ($^3He/^4He$) and calculated noble gas infiltration temperatures (NGTs). Air saturated water (ASW): helium R_{ASW} 1.36 x 10^{-6} and ^4He_a 4.90 x 10^{-8} (at 0 °C) (Weiss, 1971; Clarke et al., 1976); argon R_a 298.5 (Lee et al., 2006).

However, the determination of apparent residence times based on the radiogenic accumulation of ^{4}He and ^{40}Ar is very complex due to the unknown advective vertical crustal fluxes $J_{^4He}$ and $J_{^{40}Ar}$ of the underlying crustal rocks in the SGMB. For two samples of this data set of water type 1a (sample 16) and water type 2a (sample 9), the apparent ^{81}Kr ages are quite similar with 110,000 and 135,000 years, respectively (Heidinger et al., 2019). Due to the almost identical radiogenic $^4He_{ex}$ values and comparable $^{40}Ar_{ex}$ values of these two samples, the crustal fluxes $J_{^4He}$ and $J_{^{40}Ar}$ were calculated under the assumption of a closed Upper Jurassic aquifer system using Equation 4.11. The resulting fluxes, $J_{^4He}$ 7.87 $\times$ 10^{-7} ccSTP/cm^2/yr and $J_{^{40}Ar}$ 1.38 $\times$ 10^{-7} ccSTP/cm^2/yr (Tab. 5.8), are within a comparable range of crustal fluxes from other studies for $J_{^4He}$ between 2.1 and 4 $\times$ 10^{-7} ccSTP/cm^2/yr (Stute et al., 1992; Osenbrück et al., 1998) and for $J_{^{40}Ar}$ between 0.3 and 1.1 $\times$ 10^{-6} ccSTP/cm^2/y (Wasserburg et al., 1963; Torgersen et al., 1989). Since the fluxes were determined on only two samples of water type 1a and 2a, it had to be tested whether comparable apparent water ages could also be calculated by the assumed accumulation at the other wells with these water types where helium and argon were also determined. For this purpose, the mean values of the $^{40}Ar_{ex}$ and $^4He_{ex}$ of water types 1a and 2a were calculated and the apparent ages were determined for their minimum, maximum and mean values. Accordingly, with the mean values for all samples of water types 1a and 2a of $^4He_{ex}$ 2.23 $\times$ 10^{-5} ccSTP/g and $^{40}Ar_{ex}$ 4.41 $\times$ 10^{-6} ccSTP/g, apparent mean res-

idence times between 112,000 ($t_{^4He}$) and 128,000 years ($t_{^{40}Ar}$) could have been calculated. The calculated minimum ages ranged from 63,000 to 84,000 years and the maximum ages ranged from 126,000 to 193,000 years. Interesting, these values, especially the mean values, are in good accordance with the ^{81}Kr ages between 60,000 and 135,000 years (Heidinger et al., 2019), which implies that the calculated crustal fluxes $J_{^4He}$ and $J_{^{40}Ar}$ of the two samples 9 and 16 lead to realistic apparent groundwater ages for all samples of water types 1a and 2a.

Table 5.8: Determination of crustal fluxes $J_{^4He}$ and $J_{^{40}Ar}$ with apparent ^{81}Kr groundwater ages ($t_{^{81}Kr}$) for two samples (Heidinger et al., 2019) to calibrate the helium ($t_{^4He}$) and argon ($t_{^{40}Ar}$) age calculation for type 1b waters.

ID	$^4He_{ex}$	$^{40}Ar_{ex}$	$t_{^{81}Kr}$	$J_{^4He}$	$J_{^{40}Ar}$	$t_{^4He}$	$t_{^{40}Ar}$
	(ccSTP/g)		(ka)	(ccSTP/cm^2/yr		(ka)	
9 (Type 2a)	2.30×10^{-5}	6.65×10^{-6}	135	3.35×10^{-7}	9.85×10^{-8}	-	-
16 (Type 1a)	2.52×10^{-5}	2.17×10^{-6}	110	4.52×10^{-7}	3.94×10^{-8}	-	-
Types 1a and $2a_{mean}$	2.23×10^{-5}	4.41×10^{-6}		7.87×10^{-7}	1.38×10^{-7}	112	128
Types 1a and $2a_{min}$	1.67×10^{-5}	2.17×10^{-6}				84	63
Types 1a and $2a_{max}$	2.52×10^{-5}	6.65×10^{-6}				126	193
Type $1b_{mean}$	6.70×10^{-5}	5.76×10^{-5}				335	1,668

It can, therefore, be assumed that these crustal fluxes are relatively uniform in the central Molasse Basin and can be used to calculate the groundwater residence times of the water type 1b. With the calculated crustal fluxes for water types 1a and 2a, differences of apparent mean residence times between both water types 1a and 2a and the water type 1b were determined. Accordingly, for water type 1b, considerably higher apparent mean residence times of $t_{^4He}$ 335,000 years and $t_{^{40}Ar}$ 1.67 million years were derived with mean values for $^4He_{ex}$ 6.70 $\times$ 10^{-5} ccSTP/g and $^{40}Ar_{ex}$ 5.76 $\times$ 10^{-5} ccSTP/g (Tab. 5.8). The estimated apparent mean residence times with the two applied noble gas isotopes differ clearly. However, the apparent mean residence times of water type 1b are clearly higher compared to both water types 1a and 2a, and are in accordance with the higher $^{40}Ar/^{36}Ar$ ratio of the water type 1b sample.

The contradiction of the derived mean residence times for water type 1b between 335,000 ($t_{^4He}$) and 1.67 million years ($t_{^{40}Ar}$) may be explained by the fundamentally different behaviour of the radiogenic $^4He_{is}$ and $^{40}Ar_{is}$ as well as different diffusive fluxes into overlying sediments (Castro et al., 1998b,a). Moreover, the crustal argon flux $J_{^{40}Ar}$ can also vary basin-wide (Torgersen et al., 1989) and an additional external ^{40}Ar source cannot be excluded. In-situ produced helium releases easily and almost completely from the rocks into groundwater in time scales of >100,000 years (Tolstikhin et al., 1996; Kulongoski and Hilton, 2012). Radiogenically produced $^{40}Ar_{is}$ is retained in minerals much better than $^4He_{is}$ and is liberated mainly by diagenetic processes (Tolstikhin et al., 1996; Kipfer et al., 2002). In low permeable rocks with less open (frac-

ture) surfaces, which are required for water-rock interaction, $^{40}Ar_{is}$ can accumulate and may be diffusively released over long time-scales (Tolstikhin et al., 1996). As the diffusive flux of helium is much stronger than of argon, helium may diffuse in a non-advective dominated system to a higher level than argon (Castro et al., 1998b,a). Therefore, based on this contradiction between apparent $t_{^{40}Ar}$ and $t_{^{4}He}$ ages for water type 1b, this may suggest that this groundwater could occur in lower permeability aquifer rocks compared to type 1a and 2a waters.

The very radiogenic $^{3}He/^{4}He$ signatures between 6.26 and 8.08 $\times$ 10^{-8} and increased ^{4}He concentration ranging from 0.54 to 1.00 $\times$ 10^{-4} ccSTP/g of water type 3 samples are typical for Tertiary groundwater in this region (Stichler, 1997) and may indicate either higher apparent mean residence times or an origin of more radiogenic source rocks (Tab. 5.6, Fig. 5.17). This clearly suggests a hydraulic interaction with overlying Tertiary sediments and influences of infiltrating Tertiary groundwater. The $^{40}Ar/^{36}Ar$ ratios between 345.1 and 392.0 are considerably elevated to ASW and apparently higher $^{40}Ar_{ex}$ concentrations, which could not be calculated for type 3 samples due to the degassing, also suggest higher mean residence times for this groundwater, or appreciable mixing with very old fossil water components.

5.2.5 Regional linking of water type classification and hydrogeochemical genesis of the Upper Jurassic reservoir

Based on water chemistry and environmental isotope data, which have been evaluated in combination with an HCA, different water types within the Upper Jurassic aquifer have been identified. Fig. 5.18 displays the geographical occurrence of the water types, which leads to a conclusive areal distribution with three major hydrochemical zones of the Upper Jurassic thermal reservoir: the Southeastern (water type 1), the Northeastern (water type 2) and the Western (water type 3) Central Molasse Basin. In addition, Stiff diagrams, which are useful to compare the water quality of the three water types, are shown in Fig. 5.18.

The EFA resulted in three factors that described main hydrogeological processes influencing the hydrochemical evolution of the thermal water, which were used for distinguishing the water types. Overall, the hydrochemical composition of water types 1 and 2 was relatively homogeneous compared to water type 3. Both water types 1 and 2 were lowly mineralised, which is not typical for deep sedimentary formation waters (Kharaka and Hanor, 2014), and showed a comparable water chemical composition with dominant ion-exchange processes of Na^{+} and Ca^{2+}. They have been likely recharged during Pleistocene, as indicated by stable water isotope signatures, NGTs and ^{81}Kr ages from literature (Heidinger et al., 2019). The radiogenic $^{87}Sr/^{86}Sr$ ratios of both water types were considerably elevated to typical values for Upper Jurassic rocks, which indicated only low water-rock interaction of these waters within this aquifer. In contrast, the levels of alkalinity and earth-alkali elements Ca^{2+} and Mg^{2+} of

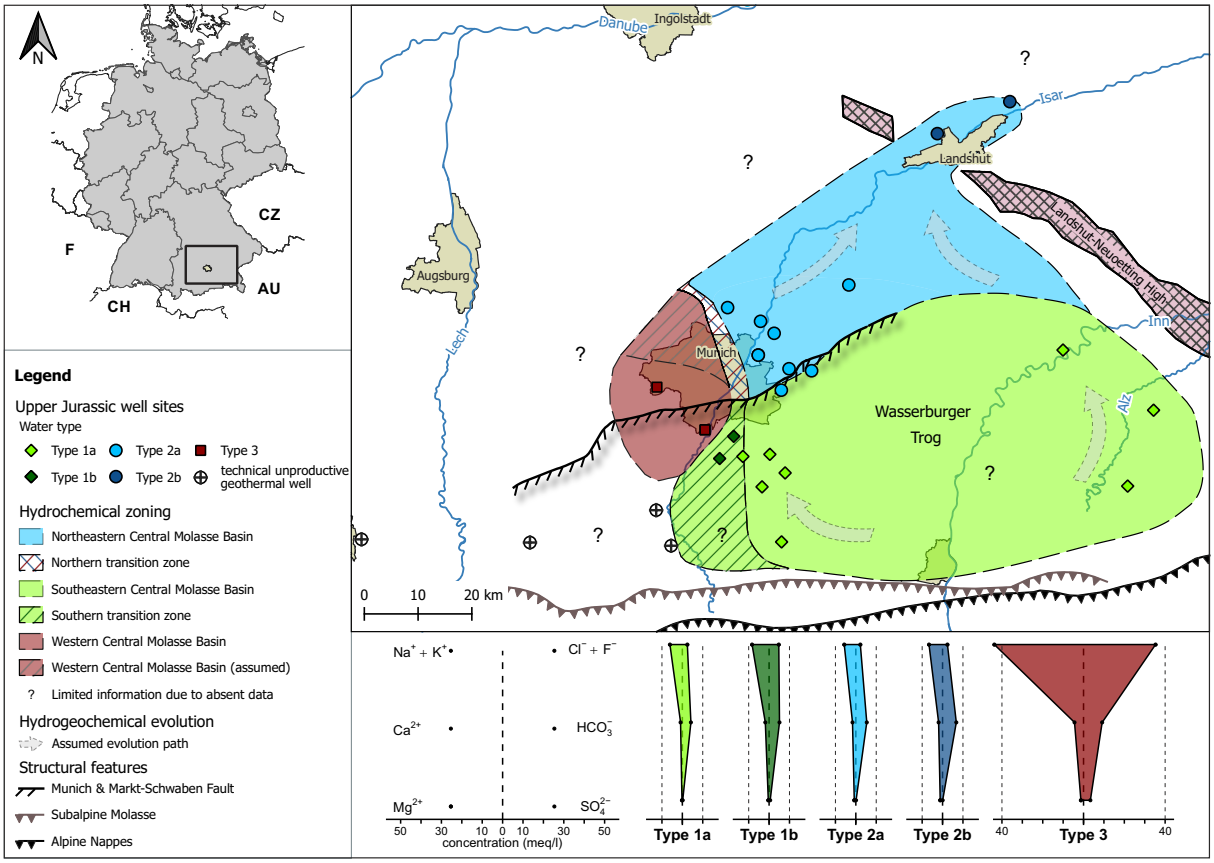

Figure 5.18: Areal distribution of the water types and hydrochemical zoning of the Upper Jurassic aquifer with Stiff diagrams.

water types 1 and 2 differed remarkably while the Ca^{2+}/Mg^{2+} ratios indicated influences of a predominated dissolution of calcite carbonates for water type 1 and a dissolution of dolomite-rich carbonates for water type 2. However, in addition to the main characteristics of water types 1 and 2, their subtypes also showed different influences on their hydrochemical composition.

The wells with water type 1a are located in a large area between the east of Munich south of the MSF and the Landshut-Neuoetting High in the east of the Wasserburger Trog. The hydrochemical zone of the Southeastern Central Molasse Basin was therefore interpolated between these occurrences. Water type 1b was characterised by increased levels of salinity and slight influences of water-rock interaction with the Upper Jurassic reservoir. With increasing Sr^{2+} concentration related to calcite dissolution (Ca^{2+}/Mg^{2+} >4.2), the $^{87}Sr/^{86}Sr$ ratios of water type 1b approximated to lower values closer to the Upper Jurassic host rocks. Together with the increased salinity and a higher apparent mean residence time of water type 1b compared to water types 1a and even 2a, the water type 1b could also be influenced by fossil formation water of the Upper Jurassic aquifer. This influence is likely associated with distinct water-rock

interaction within the Upper Jurassic reservoir. Therefore, it seems plausible that the hydrochemically matured water 1b was evolved from water type 1a due to water-rock interaction. This could be caused by a lower permeability of the aquifer rocks in south of the city of Munich, which is in accordance to the tendency of decreasing permeability from north to south of the city of Munich (Konrad et al., 2021) and appearing technical unproductive wells in that area (Fig. 5.18). The occurrence of the geochemically matured water type 1b can therefore be regarded as representative of the probably low permeable Southern transition zone between the Southeastern and Western Central Molasse Basin and the technically unproductive geothermal wells in the south-west.

The hydrochemically homogeneous water type 2 occurs at wells north of the major fault system MSF and forms the hydrochemical zone of the Northeastern Central Molasse Basin (Fig. 5.18). The hydrochemical zone was interpolated between the wells of subtype 2a around the city of Munich and subtype 2b close to the city of Landshut. The groundwater of the two subtypes 2a and 2b differ slightly in higher mineralisation and especially Na^+ and HCO_3^- concentrations of subtype 2b, but a considerably higher salinity or water-rock interaction with the Upper Jurassic aquifer rock was not evident. No considerable and distinct hydrogeological process based on EFA could be detected that would explain the minor differences in the chemical composition of the water type 2b compared to water type 2a. Therefore, due to similar $^{87}Sr/^{86}Sr$ ratios between water types 2a and 2b, it is assumed that the samples of subtype 2b could have been evolved from waters of type 2a without any significant hydrogeological process influencing the hydrochemical composition described by the processes of EFA. However, the hydrochemical evolution of type 2b waters from type 2a waters would indicate a flow northwards, which is also in accordance to Weise (Weise et al., 1991), Prestel (Prestel, 1988) and partly Frisch and Huber (Frisch and Huber, 2000), who postulated an exfiltration of water from the central SGMB into the river Danube at the north-eastern boundary of the SGMB.

Overall, due to the water chemical composition and environmental isotope characteristics of water types 1 and 2, it can be concluded that meteoric waters have flushed away most of the primary fossil formation water in the highly porous and permeable rocks of the Upper Jurassic carbonate aquifer in the Southeastern and Northeastern Central Molasse Basin. These waters seem to form a very active hydraulic flow system in the eastern central SGMB as this freshening process of the aquifer may have occurred repeatedly during the last glaciations as documented by ^{81}Kr dating (Heidinger et al., 2019). This hypothesis is also supported by an observed freshening process of Upper Jurassic vein calcites and fluid inclusions (Mraz et al., 2019) as well as by an assumed freshening process in Tertiary oil and gas fields in the central SGMB (Stichler, 1997). The data patterns together with the occurrence of water type 1 and 2 within the Northeastern and Southeastern Central Molasse Basin indicate that the existing concept of recharge at the outcropping Swabian Alb located in the west of the SGMB (Lemcke,

1976; Frisch and Huber, 2000; Birner et al., 2011) may fall short. Hence, based on the results of this study, a recharge area with subglacial infiltration and cross-formational flow through the Tertiary sediments in the south of the SGMB in proximity of the Alps, as also postulated by (Heidinger et al., 2019), is the most conclusive explanation for the hydrogeochemical evolution of the groundwater of water type 1 and 2.

The occurrence of water type 3 defines the hydrochemical zone of the Western Central Molasse Basin, which is roughly in accordance to the highly saline hydrochemical province described in previous studies (Birner et al., 2011; Mayrhofer et al., 2014). The zone is separated from the major hydrochemical zones of the North- and Southeastern Central Molasse Basin by the Northern and Southern transition zones. Water type 3 was highly mineralised and showed clearly water-rock interaction with terrestrial, non-marine sediments, which could be found in overlying Tertiary sediments. The $^{40}Ar/^{36}Ar$ ratios indicated considerably higher mean residence times for these waters compared to both water types 1 and 2 and the radiogenic $^{3}He/^{4}He$ ratios and ^{4}He concentrations suggested dominant influences of radiogenic crustal material. It seems plausible due to the increased levels of salinity, B and DOC that the hydrochemical composition of type 3 waters was affected by higher saline fossil formation waters and oil- and gas-field waters, as they showed also high gas loadings (Köhl et al., 2020b; Mayrhofer et al., 2014), separate gas and oil phases in the water, and heavy degassing during sampling. Oilfield waters with comparable hydrochemical characteristics are typical for Tertiary hydrocarbon reservoirs in the SGMB (Stichler, 1997; Andrews et al., 1987; Goldbrunner, 1999; Hahn-Weihnheimer et al., 1979). However, caused by the missing covering layers of the Purbeck and Cretaceous in the west of Munich, the geographic distribution of these highly saline waters of type 3 is most likely linked to the direct contact between the Upper Jurassic aquifer with overlying Tertiary sediments and their fluids (Fig. 2.12). Especially the interaction with Tertiary fossil formation waters might also be responsible for the more radiogenic noble gas isotope signatures of type 3 water samples. Subsequently, the occurrence of type 3 waters in the western central SGMB leads to the conclusion that the original formation water of Upper Jurassic and Tertiary origin in that hydrochemical zone was most probably not completely washed out of the aquifer due to a limited connection to the hydraulic active flow system of water type 1.

5.2.6 Subglacial groundwater recharge - a plausibility assessment

It remains to be discussed to what extent the theory of a subglacial infiltration of the Upper Jurassic groundwater is plausible on the basis of the collected data and geological conditions in the central SGMB.

5.2.6.1 Specific signatures of stable water isotopes

It has already been described in detail in Sec. 5.2.3.1 that the high contents of excess air in selected samples of water type 1 an 2a fit to a subglacial infiltration of glacial meltwater. The stable water isotope signatures of the Upper Jurassic groundwater do imply cold climatic recharge conditions most probably during Pleistocene. This is also affirmed by the calculated NGTs indicating low recharge temperatures below 1.5 °C. However, if the deep Upper Jurassic groundwater has been recharged as glacial meltwater, its $\delta^{18}O$ values should have been within the typical range for glacial meltwater between -40 and -20 ‰(Person et al., 2007; Masson-Delmotte, 2007; McIntosh et al., 2012), which is considerably more depleted than in the Upper Jurassic groundwater in the central SGMB (>-12 ‰). Nevertheless, subglacially recharged groundwater is a mixture of drainage above (supraglacial), within (englacial) and below (subglacial) glacier bodies, all of whose waters may contain different stable water isotope signatures (Fig. A.3 in Appendix A.4) (Grundl et al., 2013). Moreover, it was found that subglacial water at the bottom of warm based glaciers may primarily derived from supraglacial melting of surface waters (Grundl et al., 2013). Consequently, subglacial water infiltrating into the bedrock may be derived from a mixture of basal melt and drainage of surface melt through the englacial system and, therefore, does not show quite as much depleted isotope signatures as glacial meltwater.

In addition, a second reasonable explanation for the derived stable water isotope values in the Upper Jurassic groundwater of type 1 and 2 within the hydraulically active system in the eastern central SGMB is the time scale of recharge and infiltration. It seems plausible that the process of subglacial recharge may have occurred repeatedly during the last glaciations (LGM and MEG). This implicates that the groundwater volume within the Molasse Basin, which may has also undergone interstadial groundwater recharge, must firstly have been squeezed out by the subglacially infiltrated groundwater before the relatively youngest glacial meltwater, with the most depleted stable water isotope signatures, have entered the Upper Jurassic aquifer. In this consequence, the infiltrating groundwater in the Upper Jurassic aquifer would also be a mixture of different recharge events, resulting in a mixed isotope signature, which is likely also less than the initial glacial meltwater. It can therefore be concluded that the stable water isotope signatures at the Upper Jurassic groundwater of water type 1 and 2 very likely conform to the subglacial infiltration theory.

5.2.6.2 Subglacial recharge systematic and recharge area

The concept and mechanism of subglacial infiltration and their implications on Pleistocene groundwater recharge is well studied for other deep sedimentary basins (Siegel, 1991; Vaikmäe et al., 2001; Person et al., 2007; Grundl et al., 2013). It is known, that the distribution of permafrost has also a great impact on groundwater recharge (Lemieux et al., 2008). Grasby and

Chen (2005) have shown that rocks underlying glaciers can effectively drain glacial meltwater, even with high thicknesses of permafrost of more than 50 m and low hydraulic conductivities of the bedrock. However, the thickness and influence of permafrost below the glaciers is assumed to be negligible (Lemieux et al., 2008; Grundl et al., 2013).

A possible area for subglacial recharge in the central SGMB may be located in the south of Lake Chiemsee east of the city of Rosenheim (Fig. 4.1). In this area, the strata of the lowermost Tertiary sediments of UMM are tilted and reach the surface, as the alpine cover layers are missing in the so-called Bernau syncline (Ortner et al., 2015) (Fig. A.4 in Appendix A.4). Additionally, the overburden of the last glaciations were also very high with thicknesses up to 500 m above surface (Seguinot et al., 2018). This would correspond to an infiltration below the so-called Inn glacier with a very large thickness and extension in this region during the last ice age. Furthermore, a subglacial infiltration of larger amounts of cold groundwater could also be consistent with the negative temperature anomaly within the Wasserburger Trog in the eastern central SGMB between the city of Munich and the LNH (Fig. 2.17).

It might be possible that large amounts of water have been subglacially infiltrated and were forced both, first vertically and then horizontally due to the pressure induced by the glacier masses. One way of transporting these infiltrated large water quantities could then have been via so-called seal bypass or channel systems (Cartwright et al., 2007) that were found in the Tertiary layers around the city of Munich (Rioseco et al., 2019, 2018). It is also possible that the groundwater have firstly infiltrated into the Cretaceous sediments and was then further transported via suitable layers, such as the Gault Green Sandstone (see Sec. 2.6.1) before entering the Upper Jurassic aquifer. This is supported, among other things, by a comparable water chemical composition of the groundwater in these layers (Hänel et al., 1984), who have already assumed a hydraulic contact between these two aquifers at an early stage. Consequently, the groundwater could have been transported over greater distances and infiltrated into the Upper Jurassic aquifer away from the intended recharge area of the Bernau syncline somewhere in a suitable area with hydraulic contact between the Upper Jurassic aquifer and the overlying sediments.

Due to the favourable geological conditions, the great influence of the mighty Inn glacier as well as the thermal anomaly in the Wasserburger Trog, the region south of Lake Chiemsee seems to be very suitable for subglacial infiltration of large amounts of cold water. The transport into the Upper Jurassic aquifer may therefore have occurred either via seal bypass or channel systems in the Tertiary strata, which would additionally explain the ion-exchange character of water type 1 and 2, and the hydraulic contact to Cretaceous sediments via fault structures. In summary, these considerations may provide a conclusive hypothesis for the subglacial infiltration theory in the southern central SGMB.

5.2.7 Short conclusion

This study demonstrates the potential for coupling large-scale hydrochemical data with multivariate statistical methods and provides water chemical and environmental isotope analyses of the deep Upper Jurassic thermal groundwater. Three water types with different hydrochemical compositions and hydrogeochemical evolution were classified in the central SGMB, resulting in hydrochemical zoning of the Upper Jurassic geothermal reservoir and a new groundwater recharge area south of the SGMB.

These results represent important insights for understanding the local and regional flow regime and provide key information for sustainable resource management of the investigated Upper Jurassic geothermal system.

Chapter 6

Synoptic discussion and conclusions

Everything we hear is an opinion, not a fact.
Everything we see is a perspective, not the truth.

Marcus Aurelius

The deep Upper Jurassic carbonate aquifer in the SGMB represents an important geothermally used groundwater reservoir whose comprehensive understanding is crucial for sustainable resource management. In this thesis, the research questions were addressed in two parts (i) to enhance the possibility of determining apparent groundwater ages in deep sedimentary basins and (ii) to reveal a comprehensive hydrogeological picture of the deep Upper Jurassic reservoir based on consistent hydrochemical zoning of the Upper Jurassic groundwater in the central SGMB.

In the first part of this work, the applicability of radiocarbon dating in dissolved organic carbon ($^{14}C_{DOC}$) has been considerably improved, which is crucial for future research of old groundwater in deep sedimentary basins, especially within carbonate aquifers. In the second part, the combination of water chemical data and numerous environmental isotopes with multivariate statistical analyses has proven very useful in the evaluation for obtaining a conclusive hydrogeological picture of the Upper Jurassic groundwater over large geographic distances.

In conclusion, these evidence-based hydrochemical results lead to an enhanced understanding of the groundwater recharge areas, interaction with overlying formations and, thus, infiltration history of the deep Upper Jurassic groundwater. Furthermore, they underline the great importance of hydrochemical analyses of groundwater for the interpretation of flow systematics in large deep sedimentary basins. The results represent an essential contribution to the understanding of the groundwater flow system in the highly potential hydrothermal Upper Jurassic reservoir, which is crucial for improved and sustainable groundwater resource management and for future geothermal development.

6.1 Implications of groundwater dating with $^{14}C_{DOC}$

It is shown in this work that the easy applicable, simple and robust DOC extraction method using SPE-PPL, which was systematically applied for the first time on Upper Jurassic groundwater, provides valid and replicable apparent $^{14}C_{DOC}$ groundwater ages based on the simplified piston-flow model. This method is very well suited for radiocarbon dating of groundwater

with very low DOC contents in carbonate aquifers. The results represent a clear benefit for the delineation of groundwater flow systematics based on dating of old groundwater with mean residence times of several thousand years.

Based on the $^{14}C_{DOC}$ dating results at a few deep groundwater wells in the western and northern SGMB, which are also in good accordance to ^{81}Kr dating results of Heidinger et al. (2019), only assumptions can be made about the overall groundwater flow systematic and circulation dynamic in the Upper Jurassic aquifer. However, the calculated apparent $^{14}C_{DOC}$ groundwater ages are consistent with the concept of groundwater recharge within the intermediate flow system by Bertleff et al. (1993) and Bertleff and Watzel (2002). Within this intermediate flow system, the groundwater recharge most likely occurred in the southwestern margins of the SGMB at Lake Constance during the Pleistocene with drainage towards the river Danube in the north. An admixture of younger, locally and recently recharged groundwater during the Holocene takes most likely place in the northern marginal areas of the SGMB. In contrast, the deep groundwater of the two Upper Jurassic wells investigated in the greater area of the city of Ingolstadt at the northern central SGMB indicate no influence of the groundwater that was recharged at Lake Constance during the Pleistocene. Therefore, a westward flow parallel to the river Danube of this Pleistocene groundwater is considered to be very unlikely.

In order to further support these findings and to derive a better overview of the local and, above all, intermediate groundwater flow system, a systematically conducted large-scale dating campaign at numerous Upper Jurassic wells would be necessary. Additionally to the very proven dating method with $^{14}C_{DOC}$, young water tracers, such as ^{3}H, ^{85}Kr, ^{39}Ar or even trace gases, could be applied to determine possible young water fractions and their mean residence times in shallow Upper Jurassic wells using lumped-parameter models (LPM).

6.2 Deduction of the groundwater circulation system in the central SGMB

The results of the second part of this thesis lead to a consistent hydrochemical zoning of the Upper Jurassic reservoir in the central SGMB. Based on a multi-parameter approach using water chemical data and environmental isotopes, a fundamentally different pattern is deduced from the concepts for groundwater flow systems that have existed in the literature so far (see Sec. 2.6.2).

6.2.1 Groundwater recharge and flow system

The geographical distribution of the three characterised water types and hydrochemical zoning point to a hydraulically active flow system in the hydrochemical zone of the Eastern Central

Molasse Basin, where a relatively young, lowly mineralised groundwater of water type 1 and 2 occurs. This groundwater has been meteorically recharged under cold climatic conditions and shows only minor water-rock interaction with the Upper Jurassic aquifer, but notable ion exchange processes of sodium for calcium. This is an indication of percolation through low permeability clayey layers in the subsurface as the ion-exchange very probably did not take place in the carbonate Upper Jurassic aquifer. Furthermore, the interpretation of stable water and noble gas isotope analyses indicates groundwater recharge under large overburden pressure conditions.

The results of the hydrochemical zoning, together with the pattern of ^{81}Kr groundwater ages from Heidinger et al. (2019), lead to the conclusion that groundwater of type 1 and 2 has most likely been recharged subglacially at the southern margin of the SGMB. The infiltrating groundwater may have migrated cross-formationally through the overlying Tertiary and Cretaceous sediments where ion-exchange processes may have occurred. Overall, there is no evidence in the hydrochemical composition and hydrogeochemical evolution of water type 1 and 2 that lowly mineralised Upper Jurassic groundwater has flown eastwards from the northwestern recharge areas into the central SGMB. A considerable influence of seeping highly saline Tertiary fossil formation waters, as suggested by the latest groundwater flow models (Birner et al., 2011; Wagner et al., 2009; Frisch and Huber, 2000), cannot be delineated by the obtained results in this work. Moreover, the occurrence of considerably highly mineralised and saline type 3 waters, which show intensive hydraulic interaction with overlying terrestrial Tertiary sediments, also stand in contrast to the previous groundwater flow models. According to the salinity distribution within the Upper Jurassic aquifer (Fig. 2.26), the hydrochemical zone of the Western Central Molasse Basin with type 3 waters could be extrapolated to the west of the SGMB at the Lake Constance area. A groundwater flow direction from west to east from possible recharge areas in the Swabian Alb or at Lake Constance, as suggested by Frisch and Huber (2000), can therefore not be explained hydrochemically. The hydrogeochemical evolution from type 3 to type 1 or 2 is so far not possible by the gained results of this study. However, a northern bypass around the hydrochemical zone of the Western Central Molasse Basin, which may be comparable to the southward bending flow direction around the hydrochemical province V by Birner et al. (2011) (see Figs. 2.18 & 2.24) is neither hydrochemically and hydraulically plausible nor proven due to the absence of (sampled) Upper Jurassic groundwater wells in this region. Consequently, it must be questioned whether there is then an integrated supra-regional groundwater flow system within the Upper Jurassic reservoir at all, which has been the basic premise for almost all interpretations of hydraulic studies in the past (see Sec. 2.6.2).

The delineated groundwater flow direction of groundwater in the central SGMB is most likely to the north, which is recognisable from the characteristics of the type 2b water indicating hydrogeochemical evolution from type 1 and 2a water (see Sec. 5.2.5). This interpretation is

also supported by the ^{81}Kr groundwater dating results by Heidinger et al. (2019) as well as the observed exfiltration of groundwater with comparable hydrochemical composition into the river Danube at the described discharge areas in the northeastern SGMB (see Sec. 2.6.2). This would imply that the subglacial infiltration and cross-formational flow systematics that have been established in the western SGMB may also similarly be applied to the recharge systematic of the deep Upper Jurassic groundwater in the central SGMB.

6.2.2 Increased water-rock interaction - an indicator for low matrix permeabilities

The type 1b water occurs in the southern transition zone south of the city of Munich (Fig. 5.18) and is characterised by an increased degree of water-rock interaction with the Upper Jurassic reservoir rocks as well as higher apparent groundwater ages by noble gas isotopes compared to water type 1a and 2a (see Sec. 5.2.5). This may indicate that the hydraulic permeability and the effective pore space or pore size of the aquifer rock matrix is reduced in this area compared to the hydraulic active areas where water type 1a and 2 occurs. This observation may also be supported by the proximity to the non-water-bearing Upper Jurassic boreholes nearby, to the south and west of the southern transition zone. This is in accordance to Konrad et al. (2021) who have shown a trend of decreasing matrix permeability in a southward direction in this area (Fig. 2.16). This raises the question of why these low permeabilities occur in the southern transition zone but (apparently) not in the hydraulically active hydrochemical zone of the Southeastern Central Molasse Basin and what consequences this has for the flow and infiltration systems of type 1 and 2 groundwater. Bohnsack et al. (2021) have shown the dependence of the composition of aquifer carbonates (dolomite, calcite) and the degree of dolomitisation with the reactions in the change of hydraulic permeability to overpressure. Furthermore, Mraz (2019) found that the fractures at one non-water-bearing well south-west of the southern transition zone have healed with calcite cement. This leads to the hypothesis that (secondary) fluids may have circulated in this area of low permeability, which then most likely precipitated under changed pressure or/and temperature conditions. In contrast, the favourable geological conditions in the hydraulically active areas and the intended subglacial recharge further east have probably prevented this reduction in effective porosity and hydraulic permeability.

In conclusion, the hydrochemical composition of water type 1b is, therefore, most probably caused by the lower matrix permeability of the aquifer rocks in this area. Conversely, this also means that the hydraulic matrix permeability in the hydrochemical zones of the Southeastern Central Molasse Basin is likely considerably higher, which also points to a hydraulically active flow system.

6.2.3 Outlook and future research

This work represents a solid basis for further studies of the deep Upper Jurassic aquifer in the SGMB. On the one hand, it is yet only hypothesised under which infiltration conditions and by which preferential flow paths the deep thermal water have reached the Upper Jurassic aquifer. It should be noted that according to the theory of subglacial infiltration at the southern margin of the SGMB and subsequent cross-formational flow, the infiltrating groundwater may have passed more than 5,000 m of Tertiary Molasse and Cretaceous sediments. An open question that also emerges in this context is, however, via which flow systematic the water has got trough some Tertiary sediments against the large pore overpressure in the south of the SGMB (Drews et al., 2020, 2018). In this work, it is assumed that the groundwater has subglacially infiltrated via so-called Bernau syncline in the area south of Lake Chiemsee (Fig. A.4) in several cycles below the massive glacier masses. Groundwater transport could then have occurred via seal bypass or channel systems in the SGMB before infiltrating into the Upper Jurassic aquifer, which would need to be further proven. Confirmation of this hypothesis, however, can only be made on the basis of systematically and consistently obtained water analyses at numerous deep groundwater boreholes in several horizons in this area.

Although the hydrochemical composition of the groundwater in the eastern central SGMB does not show strong interaction with the Tertiary horizons, except for a few ion-exchange processes, the $^{87}Sr/^{86}Sr$ signatures reveal strontium uptake from terrestrial sediments. Therefore, a large-scale measurement series of $^{87}Sr/^{86}Sr$ ratios of overlying Tertiary and Cretaceous aquifer rocks could be achieved to find the specific formation that is responsible for the $^{87}Sr/^{86}Sr$ signatures found in the Upper Jurassic groundwater. Furthermore, the proof of a possible younger groundwater component in the deep Upper Jurassic groundwater that may have been transported via the seal bypass or channel structures, could provide further evidence of a Late Pleistocene component in the groundwater. This would also confirm the probably repeatedly occurred subglacial recharge systematic during the latest ice age. For this purpose, groundwater dating at the southern located deep geothermal wells using the novel approach with $^{14}C_{DOC}$ is highly recommended. Finally, the delineated groundwater flow direction to the north of the deep groundwater of the central SGMB could also be investigated by further groundwater dating at several wells with ^{81}Kr and $^{14}C_{DOC}$ along the flow path. The very appropriate water chemical, environmental isotope and multivariate statistical methods used in this work could also be extended to the deep Upper Jurassic groundwater of the entire SGMB as well as to the groundwater from overlying Tertiary and Cretaceous aquifers, to refine the hydrogeological picture obtained in this work.

Bibliography

Aeschbach-Hertig, W., El-Gamal, H., Wieser, M., Palcsu, L., 2008. Modeling excess air and degassing in groundwater by equilibrium partitioning with a gas phase. Water Resour. Res. 44, 1–12. DOI: 10.1029/2007WR006454, arXiv:2014WR016527.

Aeschbach-Hertig, W., Peeters, F., Beyerle, U., Kipfer, R., 2000. Palaeotemperature reconstruction from noble gases in ground water taking into account equilibration with entrapped air. Nature 405, 1040–1044. DOI: 10.1038/35016542.

Aeschbach-Hertig, W., Solomon, D.K., 2013. Noble Gas Thermometry in Groundwater Hydrology, in: Noble Gases as Geochemical Tracers. January, pp. 81–122. DOI: 10.1007/978-3-642-28836-4_5.

Agemar, T., Alten, J.A., Ganz, B., Kuder, J., Kühne, K., Schumacher, S., Schulz, R., 2014a. The Geothermal Information System for Germany – GeotIS. Z. Dt. Ges. Geowiss. (German J. Geosci.) 165, 129–144. DOI: 10.1127/1860-1804/2014/0060.

Agemar, T., Weber, J., Schulz, R., 2014b. Deep Geothermal Energy Production in Germany. Energies 7, 4397–4416. DOI: 10.3390/en7074397.

Aiken, G.R., McKnight, D.M., Wershaw, R.L., MacCarthy, P., 1985. An Introduction to Humic Substances in Soil, Sediment, and Water. p. 692. John Wiley & Sons, Inc.

Aldinger, H., Engelhardt, W., Elberskirch, W., Fahrion, H., Füchtbauer, H., Hoenes, D., Lemcke, K., Palme, W., Straub, E., Weber, E., Zöbelein, H., 1955. Die Erdölaufschlußbohrung Scherstetten 1 südwestlich Augsburg. Geol. Bavarica 24, 1–175.

Amajor, L.C., Gbadebo, A.M., 1992. Oilfield brines of meteoric and connate origin in the Eastern Niger Delta. J. Pet. Geol. 15, 481–488. DOI: 10.1306/BF9AB715-0EB6-11D7-8643000102C1865D.

Amro, M., Arab, A., Baisch, S., Bems, C., Blaschek, P., Blöcher, G., Häfner, F., Hild, S., Joswig, M., Kaulisky, A., Klapperich, H., Kreuter, H., Merkel, B., Moeck, I., Schrage, C., Steiger, T., Uhlig, S., 2013. Forschungsprojekt Geothermie Allgäu 2.0. bbr - Fachmagazin für Brunnen- und Leitungsbau, Sonderh. Geotherm. 2014 , 74–79.

Andres, G., Claus, G., 1964. Das Karstwasser in der Südlichen und Mittleren Frankenalb. Geol. Bavarica 53, 194–208.

Andres, G., Frisch, H., 1981. Hydrogeologie und Hydraulik im Malmkarst des Molassebeckens und der angrenzenden Fränkisch-Schwäbischen Alb, in: Andres, G., Wirth, H. (Eds.), Die Therm. und Schwefelwasservorkommen von Bad Gögging. Schriftenreihe Bayerisches Landesamt für Wasserwirtschaft, München. Volume 15. Chapter 11, pp. 108–117.

Andres, G., Wirth, H., 1981. Die Thermal- und Schwefelwasservorkommen von Bad Gögging. Schriftenr. Bayer. Landesamt für Wasserwirtschaft 15, 1–144.

Andrews, J., Goldbrunner, J., Darling, W., Hooker, P., Wilson, G., Youngman, M., Eichinger, L., Rauert, W., Stichler, W., 1985. A radiochemical, hydrochemical and dissolved gas study of groundwaters in the Molasse basin of Upper Austria. Earth Planet. Sci. Lett. 73, 317–332. DOI: 10.1016/0012-821X(85)90080-9.

Andrews, J.N., Lee, D.J., 1979. Inert gases in groundwater from the Bunter Sandstone of England as indicators of age and palaeoclimatic trends. J. Hydrol. 41, 233–252. DOI: 10.1016/0022-1694(79)90064-7.

Andrews, J.N., Youngman, M.J., Goldbrunner, J.E., Darling, W.G., 1987. The geochemistry of formation waters in the molasse basin of upper Austria. Environ. Geol. Water Sci. 10, 43–57. DOI: 10.1007/BF02588004.

Apel, R., 1971. Hydrogeologische Untersuchungen im Malmkarst der Südlichen und Mittleren Frankenalb. Geol. Bavarica 64, 268–355.

Appelo, C., Postma, D., 2004. Geochemistry, Groundwater and Pollution. p. 649. 2 ed., CRC Press, Leiden/London/New York/Philadelphia/Singapore. DOI: 10.1201/9781439833544.

Aravena, R., Wassenaar, L., 1993. Dissolved organic carbon and methane in a regional confined aquifer, southern Ontario, Canada: Carbon isotope evidence for associated subsurface sources. Appl. Geochemistry 8, 483–493. DOI: 10.1016/0883-2927(93)90077-T.

Aravena, R., Wassenaar, L.I., Plummer, L.N., 1995. Estimating 14 C Groundwater Ages in a Methanogenic Aquifer. Water Resour. Res. 31, 2307–2317. DOI: 10.1029/95WR01271.

Artinger, R., Buckau, G., Geyer, S., Fritz, P., Wolf, M., Kim, J., 2000. Characterization of groundwater humic substances: influence of sedimentary organic carbon. Appl. Geochemistry 15, 97–116. DOI: 10.1016/S0883-2927(99)00021-9.

Artinger, R., Buckau, G., Kim, J., Geyer, S., Wolf, M., 1996. Influence of sedimentary organic matter on dissolved fulvic acids in groundwater, in: Int. At. Energy Agency. International Atomic Energy Agency, Vienna, Austria. Volume SM-336/26, pp. 57–72.

Bachmann, G., Müller, M., Weggen, K., 1987. Evolution of the Molasse Basin (Germany, Switzerland). Tectonophysics 137, 77–92. DOI: 10.1016/0040-1951(87)90315-5.

Back, W., 1960. Origin of Hydrochemical Facies of Ground Water in the Atlantic Coastal Plain, in: 21st Int. Geol. Congr. Copenhagen, Rep. Part 1, pp. 87–95.

Back, W., 1966. Hydrochemical Facies and Ground-Water Flow Patterns in Northern Part of Atlantic Coastal Plain. Technical Report. p. 50. U.S. Geological Survey. Washington.

Backhaus, K., Erichson, B., Plinke, W., Weiber, R., 2016. Multivariate Analysemethoden. Volume 14 of *Springer-Lehrbuch*. p. 854. Springer Berlin Heidelberg, Berlin, Heidelberg. DOI: 10.1007/978-3-662-46076-4.

Balderer, W., 1990. Hydrogeologische Charakterisierung der Grundwasservorkommen innerhalb der Molasse der Nordostschweiz aufgrund von hydrochemischen und Isotopenuntersuchungen. [Hydrogeological Characterization of the Groundwater Reservoirs in the Molasse of the North-East of Switzerland on the Basis of Hydrochemical Investigations and Isotope Methods]. Steir. Beitr. z. Hydrogeologie 41, 35–104.

Ballentine, C.J., Burnard, P.G., 2002. Production, Release and Transport of Noble Gases in the Continental Crust. Rev. Mineral. Geochemistry 47, 481–538. DOI: 10.2138/rmg.2002.47.12.

Barker, J.F., Fritz, P., Brown, R.M., 1979. Carbon-14 measurements in aquifers with methane, in: Int. At. Energy Agency. International Atomic Energy Agency, Vienna, Austria. Volume SM-228/33, pp. 661–678.

Batlle-Aguilar, J., Banks, E.W., Batelaan, O., Kipfer, R., Brennwald, M.S., Cook, P.G., 2017. Groundwater residence time and aquifer recharge in multilayered, semi-confined and faulted aquifer systems using environmental tracers. J. Hydrol. 546, 150–165. DOI: 10.1016/j.jhydrol.2016.12.036.

Baublys, K.A., Hamilton, S.K., Hofmann, H., Golding, S.D., 2019. A strontium (87Sr/86Sr) isotopic study on the chemical evolution and migration of groundwaters in a low-rank coal seam gas reservoir (Surat Basin, Australia). Appl. Geochemistry 101, 1–18. DOI: 10.1016/j.apgeochem.2018.12.020.

Bauer, J.E., Williams, P.M., Druffel, E.R.M., 1992. 14C activity of dissolved organic carbon fractions in the north-central Pacific and Sargasso Sea. Nature 357, 667–670. DOI: 10.1038/357667a0.

Bauer, M., Freeden, W., Jacobi, H., Neu, T., 2014. Handbuch Tiefe Geothermie. p. 854. Springer Berlin Heidelberg, Berlin, Heidelberg. DOI: 10.1007/978-3-642-54511-5.

Beaupré, S.R., Druffel, E.R.M., Griffin, S., 2007. A low-blank photochemical extraction system for concentration and isotopic analyses of marine dissolved organic carbon. Limnol. Oceanogr. Methods 5, 174–184. DOI: 10.4319/lom.2007.5.174.

Belkhiri, L., Boudoukha, A., Mouni, L., Baouz, T., 2010. Application of multivariate statistical methods and inverse geochemical modeling for characterization of groundwater — A case study: Ain Azel plain (Algeria). Geoderma 159, 390–398. DOI: 10.1016/j.geoderma.2010.08.016.

Benner, R., Pakulski, J.D., McCarthy, M., Hedges, J.I., Hatcher, P.G., 1992. Bulk Chemical Characteristics of Dissolved Organic Matter in the Ocean. Science (80-.). 255, 1561–1564. DOI: 10.1126/science.255.5051.1561.

Bertani, R., 2016. Geothermal power generation in the world 2010–2014 update report. Geothermics 60, 31–43. DOI: 10.1016/j.geothermics.2015.11.003.

Bertleff, B., 1986. Das Strömungssystem der Grundwässer im Malm-Karst des West-Teils des süddeutschen Molassebeckens. Ph.D. thesis. p. 271. Abh. geol. Landesamt Baden-Württemberg. Freiburg i. Br.

Bertleff, B., Ellwanger, D., Szenkler, C., Eichinger, L., Trimborn, P., Wolfendale, N., 1993. Interpretation of hydrochemical and hydroisotopical measurements on palaeogroundwaters in Oberschwaben, south German alpine foreland, with focus on quaternary geology, in: Int. At. Energy Agency. International Atomic Energy Agency, Vienna, Austria. Volume SM-329/63, pp. 337–357.

Bertleff, B., Goldbrunner, J.E., Stichler, W., Andrews, J.N., Darling, G., 1987a. Characterization of Deep Groundwater in South Germany and Upper Austria by Means of Isotopic and Hydrochemical Investigations, in: Int. At. Energy Agency. International Atomic Energy Agency, Vienna, Austria. Volume SM-299/8P, pp. 705–706.

Bertleff, B., Hammer, W., Joachim, H., Koziorowski, G., Stober, I., Strayle, G., Villinger, E., Werner, J., 1987b. Hydrogeothermiebohrungen in Baden-Württemberg. Eine Übersicht. Z. dt. geol. Ges. 138, 411–423.

Bertleff, B., Watzel, R., 2002. Tiefe Aquifersysteme im südwestdeutschen Molassebecken. Eine umfassende hydrogeologische Analyse als Grundlage eines zukünftigen Quantitäts- und Qualitätsmanagements. Abh. geol. Landesamt Baden-württemb. 15, 75–90.

Bethke, C.M., Johnson, T.M., 2002. Paradox of groundwater age. Geology 30, 107–110. DOI: 10.1130/0091-7613(2002)030<0107:POGA>2.0.CO;2.

Bethke, C.M., Johnson, T.M., 2008. Groundwater Age and Groundwater Age Dating. Annu. Rev. Earth Planet. Sci. 36, 121–152. DOI: 10.1146/annurev.earth.36.031207.124210.

Birner, J., 2013. Hydrogeologisches Modell des Malmaquifers im Süddeutschen Molassebecken. [Hydrogeological model of the Malm aquifer in the South German Molasse Basin]. Dissertation. p. 86. Freie Universität Berlin.

Birner, J., Fritzer, T., Jodocy, M., Savvatis, A., Schneider, M., Stober, I., 2012. Hydraulische Eigenschaften des Malmaquifers im Süddeutschen Molassebecken und ihre Bedeutung für die geothermische Erschließung. [Hydraulic characterisation of the Malm aquifer in the South German Molasse basin and its impact on geothermal exploitations]. Z. geol. Wiss. 40, 133–156.

Birner, J., Mayr, C., Thomas, L., Schneider, M., Baumann, T., Winkler, A., 2011. Hydrochemie und Genese der tiefen Grundwässer des Malmaquifers im bayerischen Teil des süddeutschen Molassebeckens. [Hydrochemistry and evolution of deep groundwaters in the Malm aquifer in the bavarian part of the South German Molasse Basin]. Z. geol. Wiss. 39, 291–308.

Blaser, P., Coetsiers, M., Aeschbach-Hertig, W., Kipfer, R., Van Camp, M., Loosli, H., Walraevens, K., 2010. A new groundwater radiocarbon correction approach accounting for palaeoclimate conditions during recharge and hydrochemical evolution: The Ledo-Paniselian Aquifer, Belgium. Appl. Geochemistry 25, 437–455. DOI: 10.1016/j.apgeochem.2009.12.011.

Böhm, F., Savvatis, A., Steiner, U., Schneider, M., Koch, R., 2013. Lithofazielle Reservoircharakterisierung zur geothermischen Nutzung des Malm im Großraum München. [Lithofacies and characterization of the geothermal Malm reservoir in the greater area of Munich]. Grundwasser 18, 3–13. DOI: 10.1007/s00767-012-0202-4.

Bohnsack, D., Potten, M., Freitag, S., Einsiedl, F., Kai, Z., 2021. Stress sensitivity of porosity and permeability under varying hydrostatic stress conditions for diferent carbonate rock types of the geothermal Malm reservoir in Southern Germany. Geotherm. Energy , 1–59DOI: 10.1186/s40517-021-00197-w.

Bohnsack, D., Potten, M., Pfrang, D., Wolpert, P., Zosseder, K., 2020. Porosity–permeability relationship derived from Upper Jurassic carbonate rock cores to assess the regional hydraulic matrix properties of the Malm reservoir in the South German Molasse Basin. Geotherm. Energy 8, 47. DOI: 10.1186/s40517-020-00166-9.

Bottomley, D.J., Conrad Gregoire, D., Raven, K.G., 1994. Saline ground waters and brines in the Canadian Shield: Geochemical and isotopic evidence for a residual evaporite brine component. Geochim. Cosmochim. Acta 58, 1483–1498. DOI: 10.1016/0016-7037(94)90551-7.

Bouchaou, L., Michelot, J.L., Vengosh, A., Hsissou, Y., Qurtobi, M., Gaye, C.B., Bullen, T.D., Zuppi, G.M., 2008. Application of multiple isotopic and geochemical tracers for investigation of recharge, salinization, and residence time of water in the Souss-Massa aquifer, southwest of Morocco. J. Hydrol. 352, 267–287. DOI: 10.1016/j.jhydrol.2008.01.022.

Bouchaou, L., Warner, N.R., Tagma, T., Hssaisoune, M., Vengosh, A., 2017. The origin of geothermal waters in Morocco: Multiple isotope tracers for delineating sources of water-rock interactions. Appl. Geochemistry 84, 244–253. DOI: 10.1016/j.apgeochem.2017.07.004.

Boving, T.B., Grathwohl, P., 2001. Tracer diffusion coefficients in sedimentary rocks: correlation to porosity and hydraulic conductivity. J. Contam. Hydrol. 53, 85–100. DOI: 10.1016/S0169-7722(01)00138-3.

Bozau, E., Sattler, C.D., van Berk, W., 2015. Hydrogeochemical classification of deep formation waters. Appl. Geochemistry 52, 23–30. DOI: 10.1016/j.apgeochem.2014.10.018.

Braeken, J., van Assen, M.A.L.M., 2017. An empirical Kaiser criterion. Psychol. Methods 22, 450–466. DOI: 10.1037/met0000074.

BRD, 2019. Eckpunkte für das Klimaschutzprogramm 2030. Technical Report. p. 23. Bundesregierung der Bundesrepublik Deutschland.

Broek, T.A., Walker, B.D., Guilderson, T.P., McCarthy, M.D., 2017. Coupled ultrafiltration and solid phase extraction approach for the targeted study of semi-labile high molecular weight and refractory low molecular weight dissolved organic matter. Mar. Chem. 194, 146–157. DOI: 10.1016/j.marchem.2017.06.007.

Buchner, E., Seyfried, H., van den Bogaard, P., 2003. 40Ar/39Ar laser probe age determination confirms the Ries impact crater as the source of glass particles in Graupensand sediments (Grimmelfingen Formation, North Alpine Foreland Basin). Int. J. Earth Sci. 92, 1–6. DOI: 10.1007/s00531-002-0299-2.

Buckau, G., Artinger, R., Geyer, S., Wolf, M., Fritz, P., Kim, J.I., 2000. Groundwater in-situ generation of aquatic humic and fulvic acids and the mineralization of sedimentary organic carbon. Appl. Geochemistry 15, 819–832. DOI: 10.1016/S0883-2927(99)00078-5.

Burke, W.H., Denison, R.E., Hetherington, E.A., Koepnick, R.B., Nelson, H.F., Otto, J.B., 1982. Variation of seawater 87Sr/86Sr throughout Phanerozoic time. Geology 10, 516. DOI: 10.1130/0091-7613(1982)10<516:VOSSTP>2.0.CO;2.

Burr, G.S., Thomas, J.M., Reines, D., Jeffrey, D., Courtney, C., Jull, A.J.T., Lange, T., 2001. Sample Preparation of Dissolved Organic Carbon in Groundwater for AMS 14C Analysis. Radiocarbon 43, 183–190. DOI: 10.1017/S0033822200037991.

Capo, R.C., Stewart, B.W., Chadwick, O.A., 1998. Strontium isotopes as tracers of ecosystem processes: theory and methods. Geoderma 82, 197–225. DOI: 10.1016/S0016-7061(97)00102-X.

Carpenter, A.B., 1978. Origin And Chemical Evolution Of Brines In Sedimentary Basins. SPE Annu. Fall Tech. Conf. Exhib. SPE-7504-M, 1–8. DOI: 10.2118/7504-MS.

Carreira, P.M., Marques, J.M., Graça, R.C., Aires-Barros, L., 2008. Radiocarbon application in dating "complex" hot and cold CO2-rich mineral water systems: A review of case studies ascribed to the northern Portugal. Appl. Geochemistry 23, 2817–2828. DOI: 10.1016/j.apgeochem.2008.04.004.

Cartwright, I., Cendón, D., Currell, M., Meredith, K., 2017. A review of radioactive isotopes and other residence time tracers in understanding groundwater recharge: Possibilities, challenges, and limitations. J. Hydrol. 555, 797–811. DOI: 10.1016/j.jhydrol.2017.10.053.

Cartwright, I., Currell, M.J., Cendón, D.I., Meredith, K.T., 2020. A review of the use of radiocarbon to estimate groundwater residence times in semi-arid and arid areas. J. Hydrol. 580, 1–12. DOI: 10.1016/j.jhydrol.2019.124247.

Cartwright, J., Huuse, M., Aplin, A., 2007. Seal bypass systems. Am. Assoc. Pet. Geol. Bull. 91, 1141–1166. DOI: 10.1306/04090705181.

Case, L., 1955. Origin and Current Usage of the Term Connate Water. Am. Assoc. Pet. Geol. Bull. 39, 1879–1882. DOI: 10.1306/5CEAE29B-16BB-11D7-8645000102C1865D.

Castro, M.C., Goblet, P., Ledoux, E., Violette, S., de Marsily, G., 1998a. Noble gases as natural tracers of water circulation in the Paris Basin: 2. Calibration of a groundwater flow model using noble gas isotope data. Water Resour. Res. 34, 2467–2483. DOI: 10.1029/98WR01957.

Castro, M.C., Jambon, A., de Marsily, G., Schlosser, P., 1998b. Noble gases as natural tracers of water circulation in the Paris Basin: 1. Measurements and discussion of their origin and mechanisms of vertical transport in the basin. Water Resour. Res. 34, 2443–2466. DOI: 10.1029/98WR01956.

Cattell, R.B., 1966. The Scree Test For The Number Of Factors. Multivariate Behav. Res. 1, 245–276. DOI: 10.1207/s15327906mbr0102_10.

Charrad, M., Ghazzali, N., Boiteau, V., Niknafs, A., 2014. NbClust : An R Package for Determining the Relevant Number of Clusters in a Data Set. J. Stat. Softw. 61. DOI: 10.18637/jss.v061.i06.

Chaudhuri, S., 1978. Strontium isotopic composition of several oilfield brines from Kansas and Colorado. Geochim. Cosmochim. Acta 42, 329–331. DOI: 10.1016/0016-7037(78)90186-2.

Chaudhuri, S., Broedel, V., Clauer, N., 1987. Strontium isotopic evolution of oil-field waters from carbonate reservoir rocks in Bindley field, central Kansas, U.S.A. Geochim. Cosmochim. Acta 51, 45–53. DOI: 10.1016/0016-7037(87)90005-6.

Chebotarev, I., 1955a. Metamorphism of natural waters in the crust of weathering—1. Geochim. Cosmochim. Acta 8, 22–48. DOI: 10.1016/0016-7037(55)90015-6.

Chebotarev, I., 1955b. Metamorphism of natural waters in the crust of weathering—2. Geochim. Cosmochim. Acta 8, 137–170. DOI: 10.1016/0016-7037(55)90010-7.

Clark, I., 2015. Groundwater Geochemistry and Isotopes. p. 421. CRC Press Taylor & Francis Group, Boca Raton, London, New York.

Clark, I.D., Fritz, P., 1997. Environmental Isotopes in Hydrogeology. p. 328. 1 ed., CRC Press. DOI: 10.1201/9781482242911.

Clark, I.D., Phipps, G., Bajjali, W., 1996. Constraining 14C Ages in Sulphate Reducing Groundwaters. Two case studies from arid regions, in: Int. At. Energy Agency. International Atomic Energy Agency, Vienna, Austria. Volume SM-336/10, pp. 43–56.

Clarke, W., Jenkins, W., Top, Z., 1976. Determination of tritium by mass spectrometric measurement of 3He. Int. J. Appl. Radiat. Isot. 27, 515–522. DOI: 10.1016/0020-708X(76)90082-X.

Clayton, R.N., Friedman, I., Graf, D.L., Mayeda, T.K., Meents, W.F., Shimp, N.F., 1966. The Origin of Saline Formation Waters. J. Geophys. Res. 71, 3869–3882. DOI: 10.1029/JZ071i016p03869.

Cloutier, V., Lefebvre, R., Therrien, R., Savard, M.M., 2008. Multivariate statistical analysis of geochemical data as indicative of the hydrogeochemical evolution of groundwater in a sedimentary rock aquifer system. J. Hydrol. 353, 294–313. DOI: 10.1016/j.jhydrol.2008.02.015.

Cohen, K.M., Finney, S.C., Gibbard, P.L., Fan, J.X., 2013. International Chronostratigraphic Chart (updated). ICS Int. Chronostratigr. Chart 36, 199–204.

Collins, A.G., 1975. Geochemistry of Oilfield Waters. p. 496. 1 ed., Elsevier, Amsterdam, Oxford, New York.

Cook, P.G., Herczeg, A.L., 2000. Environmental Tracers in Subsurface Hydrology. p. 529. Springer US, Boston, MA. DOI: 10.1007/978-1-4615-4557-6.

Coppola, A.I., Walker, B.D., Druffel, E.R., 2015. Solid phase extraction method for the study of black carbon cycling in dissolved organic carbon using radiocarbon. Mar. Chem. 177, 697–705. DOI: 10.1016/j.marchem.2015.10.010.

Costello, A.B., Osborne, J.W., 2005. Best Practices in Exploratory Factor Analysis: Four Recommendations for Getting the Most From Your Analysis. Pract. Assessment, Res. Eval. 10, 9. DOI: 10.7275/jyj1-4868.

Craig, H., 1961. Isotopic Variations in Meteoric Waters. Science (80-.). 133, 1702–1703. DOI: 10.1126/science.133.3465.1702.

Cramer, H., 1953. Thermalwasser aus tiefliegenden Karsthöhlen des Bayerischen Innviertels. Geol. Bavarica 17, 164–177.

Dalzell, B., Minor, E., Mopper, K., 2009. Photodegradation of estuarine dissolved organic matter: a multi-method assessment of DOM transformation. Org. Geochem. 40, 243–257. DOI: 10.1016/j.orggeochem.2008.10.003.

Dansgaard, W., 1964. Stable isotopes in precipitation. Tellus 16, 436–468. DOI: 10.3402/tellusa.v16i4.8993.

Dasch, E., 1969. Strontium isotopes in weathering profiles, deep-sea sediments, and sedimentary rocks. Geochim. Cosmochim. Acta 33, 1521–1552. DOI: 10.1016/0016-7037(69)90153-7.

Davis, S.N., 1964. Discussion on: The Chemistry of Saline Waters by R. A. Krieger (1963). Ground Water 2, 51–51. DOI: 10.1111/j.1745-6584.1964.tb01747.x.

Davis, S.N., Bentley, H.W., 1982. Dating Groundwater, in: Currie, L.A. (Ed.), Nucl. Chem. Dating Tech.. ACS Symposium Series Vol. 176. Chapter 11, pp. 187–222. DOI: 10.1021/bk-1982-0176.ch011.

Davis, S.N., Whittemore, D.O., Fabryka-Martin, J., 1998. Uses of Chloride/Bromide Ratios in Studies of Potable Water. Ground Water 36, 338–350. DOI: 10.1111/j.1745-6584.1998.tb01099.x.

Dehnert, J., Nestler, W., Freyer, K., Treutler, H., Neitzel, P., Walther, W., 1996. Bestimmung der notwendigen Abpumpzeiten von Grundwasserbeobachtungsrohren mit Hilfe der natürlichen Radonaktivitätskonzentration, in: Merkel, B., Dietrich, P., Struckmeier, W., Löhnert, E. (Eds.), Grundwasser und Rohstoffgewinnung. GeoCongress 2, Verlag Sven von Loga. pp. 40–45.

DiStefano, C., Zhu, M., Mîndrilă, D., 2009. Understanding and Using Factor Scores: Considerations for the Applied Researcher. Pract. Assessment, Res. Eval. 14, 1–11. DOI: 10.7275/da8t-4g52.

Dittmar, T., Koch, B., Hertkorn, N., Kattner, G., 2008. A simple and efficient method for the solid-phase extraction of dissolved organic matter (SPE-DOM) from seawater. Limnol. Oceanogr. Methods 6, 230–235. DOI: 10.4319/lom.2008.6.230.

Dokken, T., Andersson, C., Risebrobakken, B., 2015. Relative abundance of planktic foraminifera and calculated SSTs and SST anomaly (0-25.5 ka BP) in sediment core MD99-2284. DOI: 10.1594/PANGAEA.846924.

Donahue, D.J., Linick, T.W., Jull, A.J.T., 1990. Isotope-Ratio and Background Corrections for Accelerator Mass Spectrometry Radiocarbon Measurements. Radiocarbon 32, 135–142. DOI: 10.1017/S0033822200040121.

Dotsika, E., Poutoukis, D., Michelot, J.L., Kloppmann, W., 2006. Stable Isotope and Chloride, Boron Study for Tracing Sources of Boron Contamination in Groundwater: Boron Contents in Fresh and Thermal Water in Different Areas in Greece. Water. Air. Soil Pollut. 174, 19–32. DOI: 10.1007/s11270-005-9015-8.

Drews, M.C., Bauer, W., Caracciolo, L., Stollhofen, H., 2018. Disequilibrium compaction overpressure in shales of the Bavarian Foreland Molasse Basin: Results and geographical distribution from velocity-based analyses. Mar. Pet. Geol. 92, 37–50. DOI: 10.1016/j.marpetgeo.2018.02.017.

Drews, M.C., Hofstetter, P., Zosseder, K., Shipilin, V., Stollhofen, H., 2020. Predictability and controlling factors of overpressure in the North Alpine Foreland Basin, SE Germany: an interdisciplinary post-drill analysis of the Geretsried GEN-1 deep geothermal well. Geotherm. Energy 8, 20. DOI: 10.1186/s40517-020-00175-8.

Drews, M.C., Seithel, R., Savvatis, A., Kohl, T., Stollhofen, H., 2019. A normal-faulting stress regime in the Bavarian Foreland Molasse Basin? New evidence from detailed analysis of leak-off and formation integrity tests in the greater Munich area, SE-Germany. Tectonophysics 755, 1–9. DOI: 10.1016/j.tecto.2019.02.011.

Druffel, E.R.M., Griffin, S., Coppola, A.I., Walker, B.D., 2016. Radiocarbon in dissolved organic carbon of the Atlantic Ocean. Geophys. Res. Lett. 43, 5279–5286. DOI: 10.1002/2016GL068746.

Dussel, M., Lüschen, E., Thomas, R., Agemar, T., Fritzer, T., Sieblitz, S., Huber, B., Birner, J., Schulz, R., 2016. Forecast for thermal water use from Upper Jurassic carbonates in the

Munich region (South German Molasse Basin). Geothermics 60, 13–30. DOI: 10.1016/j.geothermics.2015.10.010.

Eichinger, L., 1983. A Contribution to the Interpretation of 14 C Groundwater Ages Considering the Example of a Partially Confined Sandstone Aquifer. Radiocarbon 25, 347–356. DOI: 10.1017/S0033822200005634.

Einsele, G., Josopait, V., Seiler, K.P., Werner, J., 1983. Beiträge zu tiefen Grundwässern und zum Grundwasser-Wärmehaushalt. - I. Tiefe Grundwässer - Bedeutung, Begriffe, Eigenschaften, Erkundungsmethoden. DVWK Schriften 61, 107.

Einsiedl, F., Hertkorn, N., Wolf, M., Frommberger, M., Schmitt-Kopplin, P., Koch, B.P., 2007. Rapid biotic molecular transformation of fulvic acids in a karst aquifer. Geochim. Cosmochim. Acta 71, 5474–5482. DOI: 10.1016/j.gca.2007.09.024.

Elderfield, H., 1986. Strontium isotope stratigraphy. Palaeogeogr. Palaeoclimatol. Palaeoecol. 57, 71–90. DOI: 10.1016/0031-0182(86)90007-6.

Ettayfi, N., Bouchaou, L., Michelot, J., Tagma, T., Warner, N., Boutaleb, S., Massault, M., Lgourna, Z., Vengosh, A., 2012. Geochemical and isotopic (oxygen, hydrogen, carbon, strontium) constraints for the origin, salinity, and residence time of groundwater from a carbonate aquifer in the Western Anti-Atlas Mountains, Morocco. J. Hydrol. 438-439, 97–111. DOI: 10.1016/j.jhydrol.2012.03.003.

Evans, G., Otlet, R., Downing, R., Monkhouse, R., Rae, G., 1979. Some problems in the interpretation of isotope measurements in United Kingdom aquifers, in: Int. At. Energy Agency. International Atomic Energy Agency, Vienna, Austria. Volume SM-228/34, pp. 679–706.

Eyerer, S., Schifflechner, C., Hofbauer, S., Bauer, W., Wieland, C., Spliethoff, H., 2020. Combined heat and power from hydrothermal geothermal resources in Germany: An assessment of the potential. Renew. Sustain. Energy Rev. 120, 1–15. DOI: 10.1016/j.rser.2019.109661.

Faure, G., Powell, J.L., 1972. Strontium Isotope Geology, in: von Engelhardt, W., Hahn, T., Roy, R., Wyllie, P. (Eds.), Miner. Rocks Inorg. Mater.. Springer Berlin Heidelberg, Berlin, Heidelberg, New-York. Chapter 5, p. 188. DOI: 10.1007/978-3-642-65367-4.

Ferguson, G., Cuthbert, M.O., Befus, K., Gleeson, T., McIntosh, J.C., 2020. Rethinking groundwater age. Nat. Geosci. 13, 592–594. DOI: 10.1038/s41561-020-0629-7.

Fetter, C.W., 2001. Applied Hydrogeology. Volume 4. p. 599. 4 ed., Prentice-Hall.

Fischer, M., Wolf, M., Fritz, P., Geyer, S., Weise, S., Forster, M., Rauert, W., Ramm, K., 1992. Possible evidence for 14C isotope exchange between groundwater and carbonate rocks in

the eastern Donau Ried, Bavaria, Germany, in: Int. At. Energy Agency. International Atomic Energy Agency, Vienna, Austria, pp. 153–166.

Fontes, J.C., Garnier, J.M., 1979. Determination of the initial 14C activity of the total dissolved carbon: A review of the existing models and a new approach. Water Resour. Res. 15, 399–413. DOI: 10.1029/WR015i002p00399.

Freudenberger, W., Schwerd, K., 1996. Erläuterungen zur Geologischen Karte von Bayern 1:500000. p. 329. 4 ed., Bayerisches Geologisches Landesamt, Munich.

Frisch, H., Huber, B., 2000. Ein hydrogeologisches Modell und der Versuch einer Bilanzierung des Thermalwasservorkommens im Malmkarst des süddeutschen Molassebeckens. [A Hydrogeological Model and the Attempt of a Balance of the Thermal Water for the Malmkarst in the Southgerman and the Neighbouring Upper Austrian Molasse Basin]. Hydrogeol. und Umwelt 20, 25–43.

Frisch, H., Werner, J., 1991a. Hydrogeothermische Energiebilanz und Grundwasserhaushalt des Malmkarstes im Süddeutschen Molassebecken - Schlussbericht 1. Technical Report. p. 335. Bayerisches Landesamt für Wasserwirtschaft; Geologisches Landesamt Baden-Württemberg. München, Freiburg i.Br.

Frisch, H., Werner, J., 1991b. Hydrogeothermische Energiebilanz und Grundwasserhaushalt des Malmkarstes im Süddeutschen Molassebecken - Schlussbericht 2. Technical Report. p. 272. Bayerisches Landesamt für Wasserwirtschaft; Geologisches Landesamt Baden-Württemberg. München, Freiburg i.Br.

Fritzer, T., Settles, E., Dorsch, K., 2019. Bayerischer Geothermieatlas. Hydrothermale Energiegewinnung. Technical Report. p. 96. Bayerisches Staatsministerium für Wirtschaft, Landesentwicklung und Energie. München.

Frye, G.C., Thomas, M.M., 1993. Adsorption of organic compounds on carbonate minerals. Chem. Geol. 109, 215–226. DOI: 10.1016/0009-2541(93)90071-P.

Furtak, H., Langguth, H., 1967. Zur hydrochemischen Kennzeichnung von Grundwässern und Grundwassertypen mittels Kennzahlen. Mem. IAH-Congress VII, 86–96.

GAB, 2020. Tiefengeothermie in Bayern. Forschungsprojekt Geothermie-Allianz Bayern. Technical Report. p. 16. Bayerisches Staatsministerium für Wissenschaft und Kunst; Technische Universität München. München.

Gallagher, D., McGee, E.J., Kalin, R.M., Mitchell, P.I., 2000. Performance of Models for Radiocarbon Dating of Groundwater: An Appraisal using Selected Irish Aquifers. Radiocarbon 42, 235–248. DOI: 10.1017/S003382220005904X.

van Geldern, R., Baier, A., Subert, H.L., Kowol, S., Balk, L., Barth, J.A., 2014. Pleistocene paleogroundwater as a pristine fresh water resource in southern Germany – evidence from stable and radiogenic isotopes. Sci. Total Environ. 496, 107–115. DOI: 10.1016/j.scitotenv.2014.07.011.

Gemici, Ü., Tarcan, G., 2002. Distribution of boron in thermal waters of western Anatolia, Turkey, and examples of their environmental impacts. Environ. Geol. 43, 87–98. DOI: 10.1007/s00254-002-0608-x.

Gerber, C., Vaikmäe, R., Aeschbach, W., Babre, A., Jiang, W., Leuenberger, M., Lu, Z.T., Mokrik, R., Müller, P., Raidla, V., Saks, T., Waber, H.N., Weissbach, T., Zappala, J.C., Purtschert, R., 2017. Using 81Kr and noble gases to characterize and date groundwater and brines in the Baltic Artesian Basin on the one-million-year timescale. Geochim. Cosmochim. Acta 205, 187–210. DOI: 10.1016/j.gca.2017.01.033.

Geyer, O., Gwinner, M., 2011. Geologie von Baden-Württemberg. p. 630. 5 ed., Schweizerbart, Stuttgart.

Geyer, S., 1994. Isotopengeochemische Untersuchungen an Fraktionen von gelöstem organischem Kohlenstoff (DOC) zur Bestimmung der Herkunft. Dissertation. p. 183. Ludwig-Maximilian-Universität München.

Geyer, S., Wolf, M., Wassenaar, L.I., Fritz, P., Buckau, G., Kim, J.I., 1993. Isotope investigations on fractions of dissolved organic carbon for 14C groundwater dating, in: Int. At. Energy Agency. International Atomic Energy Agency, Vienna, Austria, pp. 359–380.

Geyh, M.A., 2000. An Overview of 14C Analysis in the Study of Groundwater. Radiocarbon 42, 99–114. DOI: 10.1017/S0033822200053078.

Glynn, P.D., Plummer, L.N., 2005. Geochemistry and the understanding of ground-water systems. Hydrogeol. J. 13, 263–287. DOI: 10.1007/s10040-004-0429-y.

Goldbrunner, J., 1999. Hydrogeology of Deep Groundwaters in Austria. Mitteilungen der Österreichischen Geol. Gesellschaft 92, 281–294.

Goldbrunner, J.E., 1987. Zum Stand der geothermischen und balneologischen Tiefengrundwassernutzung im Oststeirischen Becken und im Oberösterreichischen Molassebecken. [The Status of Geothermic and Balneologic Utilization of Deep Groundwater in the East Styrian Basin and the Upper Austrian Molasse Basin]. Z. dt. geol. Ges. 138, 513–526.

Goldscheider, N., Mádl-Szőnyi, J., Erőss, A., Schill, E., 2010. Review: Thermal water resources in carbonate rock aquifers. Hydrogeol. J. 18, 1303–1318. DOI: 10.1007/s10040-010-0611-3.

Goode, D.J., 1996. Direct Simulation of Groundwater Age. Water Resour. Res. 32, 289–296. DOI: 10.1029/95WR03401.

Graham, D.W., 2002. Noble Gas Isotope Geochemistry of Mid-Ocean Ridge and Ocean Island Basalts: Characterization of Mantle Source Reservoirs. Rev. Mineral. Geochemistry 47, 247–317. DOI: 10.2138/rmg.2002.47.8.

Grasby, S.E., Chen, Z., 2005. Subglacial recharge into the Western Canada Sedimentary Basin—Impact of Pleistocene glaciation on basin hydrodynamics. Geol. Soc. Am. Bull. 117, 500. DOI: 10.1130/B25571.1.

Green, N.W., Perdue, E.M., Aiken, G.R., Butler, K.D., Chen, H., Dittmar, T., Niggemann, J., Stubbins, A., 2014. An intercomparison of three methods for the large-scale isolation of oceanic dissolved organic matter. Mar. Chem. 161, 14–19. DOI: 10.1016/j.marchem.2014.01.012.

Greene, S., Battye, N., Clark, I., Kotzer, T., Bottomley, D., 2008. Canadian Shield brine from the Con Mine, Yellowknife, NT, Canada: Noble gas evidence for an evaporated Palaeozoic seawater origin mixed with glacial meltwater and Holocene recharge. Geochim. Cosmochim. Acta 72, 4008–4019. DOI: 10.1016/j.gca.2008.05.058.

Griffin, S., Beaupré, S.R., Druffel, E.R.M., 2010. An Alternate Method of Diluting Dissolved Organic Carbon Seawater Samples for 14C Analysis. Radiocarbon 52, 1224–1229. DOI: 10.1017/S0033822200046300.

Grootes, P.M., Nadeau, M.J., Rieck, A., 2004. 14C-AMS at the Leibniz-Labor: Radiometric dating and isotope research. Nucl. Instruments Methods Phys. Res. Sect. B Beam Interact. with Mater. Atoms 223-224, 55–61. DOI: 10.1016/j.nimb.2004.04.015.

Grundl, T., Magnusson, N., Brennwald, M.S., Kipfer, R., 2013. Mechanisms of subglacial groundwater recharge as derived from noble gas, 14C, and stable isotopic data. Earth Planet. Sci. Lett. 369-370, 78–85. DOI: 10.1016/j.epsl.2013.03.012.

Guo, L., Santschi, P.H., 1996. A critical evaluation of the cross-flow ultrafiltration technique for sampling colloidal organic carbon in seawater. Mar. Chem. 55, 113–127. DOI: 10.1016/S0304-4203(96)00051-5.

Hahn-Weihnheimer, P., Hirner, A., Lemcke, K., 1979. Zur Herkunft süddeutscher Erdöle - Geochemische Ergebnisse und Versuch einer geologischen Interpretation. [On the origin of crude oils from Southern Germany - Geochemical results and a tentative geological interpretation]. Bull. Ver. schweiz. Pet. u. -Ing. 45, 35–46. DOI: 10.5169/seals-203883.

Han, L.F., Plummer, L.N., 2013. Revision of Fontes & Garnier's model for the initial 14C content of dissolved inorganic carbon used in groundwater dating. Chem. Geol. 351, 105–114. DOI: 10.1016/j.chemgeo.2013.05.011.

Han, L.F., Plummer, L.N., 2016. A review of single-sample-based models and other approaches for radiocarbon dating of dissolved inorganic carbon in groundwater. Earth-Science Rev. 152, 119–142. DOI: 10.1016/j.earscirev.2015.11.004.

Han, L.F., Plummer, L.N., Aggarwal, P., 2012. A graphical method to evaluate predominant geochemical processes occurring in groundwater systems for radiocarbon dating. Chem. Geol. 318-319, 88–112. DOI: 10.1016/j.chemgeo.2012.05.004.

Hänel, R., Kleefeldt, M., Koppe, I., 1984. Geothermisches Energiepotential. Pilotstudie: Abschätzung der geothermischen Energievorräte an ausgewählten Beispielen in der Bundesrepublik Deutschland. Technical Report. p. 141. Niedersächsisches Landesamt für Bodenforschung. Hannover.

Heaton, T., Vogel, J., 1981. "Excess air" in groundwater. J. Hydrol. 50, 201–216. DOI: 10.1016/0022-1694(81)90070-6.

Hebig, K.H., Ito, N., Scheytt, T., Marui, A., 2012. Review: Deep groundwater research with focus on Germany. Hydrogeol. J. 20, 227–243. DOI: 10.1007/s10040-011-0815-1.

Hedges, J.I., 1992. Global biogeochemical cycles: progress and problems. Mar. Chem. 39, 67–93. DOI: 10.1016/0304-4203(92)90096-S.

Heidinger, M., Eichinger, F., Purtschert, R., Mueller, P., Zappala, J., Wirsing, G., Geyer, T., Fritzer, T., Groß, D., 2019. Altersbestimmung an thermalen Tiefenwässern im Oberjura des Molassebeckens mittels Krypton-Isotopen. [81Kr/85Kr-Dating of thermal groundwaters in the Upper Jurassic (Molasse Basin)]. Grundwasser 24, 287–294. DOI: 10.1007/s00767-019-00431-0.

Heine, F., Einsiedl, F., 2021. Groundwater dating with dissolved organic radiocarbon: A promising approach in carbonate aquifers. Appl. Geochemistry 125, 1–13. DOI: 10.1016/j.apgeochem.2020.104827.

Heine, F., Peña, A., Zosseder, K., Einsiedl, F., 2018. Schlussbericht: IsoMol - Untersuchungen zum verbesserten Reservoirverständnis des Malmaquifers im bayerischen Molassebecken. Technical Report. p. 122. Technische Universität München; Bayerisches Landesamt für Umwelt. München.

Heine, F., Zosseder, K., Einsiedl, F., 2019. Lessons learned: Erfahrungen aus hydro- und isotopenchemischen Probenahmen sowie Analysen von Geothermalwässern im Bayerischen Molassebecken, in: Der Geotherm. DGK, 19.-21. Novemb. 2019, München. p. 28.

Heine, F., Zosseder, K., Einsiedl, F., 2021. Hydrochemical Zoning and Chemical Evolution of the Deep Upper Jurassic Thermal Groundwater Reservoir Using Water Chemical and Environmental Isotope Data. Water 13, 1–35. DOI: 10.3390/w13091162.

Hershey, R.L., Fereday, W., Thomas, J.M., 2016. Dissolved organic carbon 14C in southern Nevada groundwater and implications for groundwater travel times. Technical Report 45268. p. 39. Nevada Field Office National Nuclear Security Administration U.S. Department of Energy, Las Vegas, Nevada. Las Vegas.

Horn, J.L., 1965. A rationale and test for the number of factors in factor analysis. Psychometrika 30, 179–185. DOI: 10.1007/BF02289447.

Huber, B., 1999. Das Thermalwasservorkommen im niederbayerisch-oberösterreichischen Molassebecken. Technical Report. p. 21. Freistaat Bayern, vertreten durch das Bayer. Landesamt für Wasserwirtschaft. München.

Huber, B., Gödecke, H.J., Schuler, G., 1998. Detailmodell zur Bilanzierung der Thermalwasservorkommen im Niederbayerisch-Oberösterreichischen Molassebecken - Endbericht - Teil 1 : Hydrogeologisches Modell. Technical Report. p. 242. Geotechnisches Ing. Büro für Erd- und Grundbau, Ingenieur- und Hydrogeologie GbRmH. Augsburg.

Ivanovich, M., Wolf, M., Geyer, S., Fritz, P., 1996. Isotopic Characterization of Humic Colloids and Other Organic and Inorganic Dissolved Species in Selected Groundwaters from Sand Aquifers at Gorleben, Germany, in: Gaffney, J.S., Marley, N.A., Clark, S.B. (Eds.), ACS Symp. Ser.. American Chemical Society, Washington DC. Volume 651. Chapter 14, pp. 220–243. DOI: 10.1021/bk-1996-0651.ch014.

Jacobson, R.L., Usdowski, H.E., 1976. Partitioning of strontium between calcite, dolomite and liquids: An experimental study under higher temperature diagenetic conditions, and a model for the prediction of mineral pairs for geothermometry. Contrib. to Mineral. Petrol. 59, 171–185. DOI: 10.1007/BF00371306.

Jain, C., Vogt, C., Clauser, C., 2015. Maximum potential for geothermal power in Germany based on engineered geothermal systems. Geotherm. Energy 3, 15. DOI: 10.1186/s40517-015-0033-5.

Jasechko, S., 2019. Global Isotope Hydrogeology—Review. Rev. Geophys. 57, 835–965. DOI: 10.1029/2018RG000627.

Jasechko, S., Perrone, D., Befus, K.M., Bayani Cardenas, M., Ferguson, G., Gleeson, T., Luijendijk, E., McDonnell, J.J., Taylor, R.G., Wada, Y., Kirchner, J.W., 2017. Global aquifers dominated by fossil groundwaters but wells vulnerable to modern contamination. Nat. Geosci. 10, 425–429. DOI: 10.1038/ngeo2943.

Jorgensen, T.D., Pornprasertmanit, S., Schoemann, A.M., Rosseel, Y., 2020. semTools: Useful tools for structural equation modeling.

Jung, M., Aeschbach, W., 2018. A new software tool for the analysis of noble gas data sets from (ground)water. Environ. Model. Softw. 103, 120–130. DOI: 10.1016/j.envsoft.2018.02.004.

Jung, M., Wieser, M., von Oehsen, A., Aeschbach-Hertig, W., 2013. Properties of the closed-system equilibration model for dissolved noble gases in groundwater. Chem. Geol. 339, 291–300. DOI: 10.1016/j.chemgeo.2012.08.006.

Jurgens, B.C., Böhlke, J.K., Eberts, S.M., 2012. TracerLPM (Version 1): An Excel Workbook for Interpreting Groundwater Age Distributions from Environmental Tracer Data. Technical Report Version 1. p. 60. U.S. Geological Survey.

Kaiser, H.F., 1960. The Application of Electronic Computers to Factor Analysis. Educ. Psychol. Meas. 20, 141–151. DOI: 10.1177/001316446002000116.

Kassambara, A., 2017. Practical Guide To Cluster Analysis in R. p. 187. 1 ed., STHDA.

Kharaka, Y., Hanor, J., 2014. Deep Fluids in Sedimentary Basins, in: Holland, H.D., Turekian, K.K. (Eds.), Treatise on Geochemistry. Elsevier. Volume 7, pp. 471–515. DOI: 10.1016/B978-0-08-095975-7.00516-7.

Kharaka, Y.K., Thordsen, J.J., 1992. Stable Isotope Geochemistry and Origin of Waters in Sedimentary Basins, in: Clauer, N., Chaudhuri, S. (Eds.), Isot. Signatures Sediment. Rec.. 2 ed., pp. 411–466.

Kim, S., Simpson, A.J., Kujawinski, E.B., Freitas, M.A., Hatcher, P.G., 2003. High resolution electrospray ionization mass spectrometry and 2D solution NMR for the analysis of DOM extracted by C18 solid phase disk. Org. Geochem. 34, 1325–1335. DOI: 10.1016/S0146-6380(03)00101-3.

Kipfer, R., Aeschbach-Hertig, W., Peeters, F., Stute, M., 2002. Noble Gases in Lakes and Ground Waters, in: Porcelli, D.P., Ballentine, C.J., Wieler, R. (Eds.), Noble Gases. De Gruyter, Berlin, Boston. Volume 47. Chapter 14, pp. 615–700. DOI: 10.1515/9781501509056-016.

Klaus, T., Vollmer, C., Werner, K., Lehmann, H., Müschen, K., 2010. 2050: 100 % Erneuerbarer Strom. Technical Report. p. 194. Umweltbundesamt.

Koepnick, R.B., Denison, R.E., Burke, W.H., Hetherington, E.A., Dahl, D.A., 1990. Construction of the Triassic and Jurassic portion of the Phanerozoic curve of seawater 87Sr/86Sr. Chem. Geol. Isot. Geosci. Sect. 80, 327–349. DOI: 10.1016/0168-9622(90)90014-4.

Köhl, B., Elsner, M., Baumann, T., 2020a. Hydrochemical and operational parameters driving carbonate scale kinetics at geothermal facilities in the Bavarian Molasse Basin. Geotherm. Energy 8, 1–26. DOI: 10.1186/s40517-020-00180-x.

Köhl, B., Grundy, J., Baumann, T., 2020b. Rippled scales in a geothermal facility in the Bavarian Molasse Basin: a key to understand the calcite scaling process. Geotherm. Energy 8, 1–23. DOI: 10.1186/s40517-020-00177-6.

Konrad, F., Savvatis, A., Degen, D., Wellmann, F., Einsiedl, F., Zosseder, K., 2021. Productivity enhancement of geothermal wells through fault zones: Efficient numerical evaluation of a parameter space for the Upper Jurassic aquifer of the North Alpine Foreland Basin. Geothermics 95, 102119. DOI: 10.1016/j.geothermics.2021.102119.

Konrad, F., Savvatis, A., Wellmann, F., Zosseder, K., 2019. Hydraulic behavior of fault zones in pump tests of geothermal wells: a parametric analysis using numerical simulations for the Upper Jurassic aquifer of the North Alpine Foreland Basin. Geotherm. Energy 7, 1–25. DOI: 10.1186/s40517-019-0137-4.

Kruger, B.R., Dalzell, B.J., Minor, E.C., 2011. Effect of organic matter source and salinity on dissolved organic matter isolation via ultrafiltration and solid phase extraction. Aquat. Sci. 73, 405–417. DOI: 10.1007/s00027-011-0189-4.

Kuhlemann, J., Kempf, O., 2002. Post-Eocene evolution of the North Alpine Foreland Basin and its response to Alpine tectonics. Sediment. Geol. 152, 45–78. DOI: 10.1016/S0037-0738(01)00285-8.

Kulongoski, J., Hilton, D., 2012. Applications of Groundwater Helium, in: Baskaran, M. (Ed.), Handb. Environ. Isot. Geochemistry. Springer Berlin Heidelberg, Berlin, Heidelberg. Advances in Isotope Geochemistry. Chapter 15, pp. 285–304. DOI: 10.1007/978-3-642-10637-8.

Kulongoski, J.T., Hilton, D.R., Izbicki, J.A., 2003. Helium isotope studies in the Mojave Desert, California: implications for groundwater chronology and regional seismicity. Chem. Geol. 202, 95–113. DOI: 10.1016/j.chemgeo.2003.07.002.

Lane, A.C., 1908. Mine waters and their field assay. Geol. Soc. Am. Bull. 19, 501–512. DOI: 10.1130/GSAB-19-501.

Lang, S.Q., Bernasconi, S.M., Früh-Green, G.L., 2012. Stable isotope analysis of organic carbon in small (μg C) samples and dissolved organic matter using a GasBench preparation device. Rapid Commun. Mass Spectrom. 26, 9–16. DOI: 10.1002/rcm.5287.

Lang, S.Q., Früh-Green, G.L., Bernasconi, S.M., Wacker, L., 2013. Isotopic (δ13 C, Δ14 C) analysis of organic acids in marine samples using wet chemical oxidation. Limnol. Oceanogr. Methods 11, 161–175. DOI: 10.4319/lom.2013.11.161.

Lang, S.Q., McIntyre, C.P., Bernasconi, S.M., Früh-Green, G.L., Voss, B.M., Eglinton, T.I., Wacker, L., 2016. Rapid 14C Analysis of Dissolved Organic Carbon in Non-Saline Waters. Radiocarbon 58, 505–515. DOI: 10.1017/RDC.2016.17.

Langmuir, D., 1971. The geochemistry of some carbonate ground waters in central Pennsylvania. Geochim. Cosmochim. Acta 35, 1023–1045. DOI: 10.1016/0016-7037(71)90019-6.

Lara, R., Thomas, D., 1994. XAD-fractionation of "new" dissolved organic matter: is the hydrophobic fraction seriously underestimated? Mar. Chem. 47, 93–96. DOI: 10.1016/0304-4203(94)90016-7.

Leduc, G., Schneider, R.R., Kim, J.H., Lohmann, G., 2010. Alkenone-derived Holocene Sea Surface Temperature database. DOI: 10.1594/PANGAEA.737301.

Lee, J.Y., Marti, K., Severinghaus, J.P., Kawamura, K., Yoo, H.S., Lee, J.B., Kim, J.S., 2006. A redetermination of the isotopic abundances of atmospheric Ar. Geochim. Cosmochim. Acta 70, 4507–4512. DOI: 10.1016/j.gca.2006.06.1563.

Lemcke, K., 1976. Übertiefe Grundwässer im süddeutschen Alpenvorland. Bull. Ver. schweiz. Pet. u. -Ing. 42, 9–18.

Lemcke, K., 1981. Geologie und Stratigraphie der Thermal- und Schwefelwasserbohrung, in: Andres, G., Wirth, H. (Eds.), Die Therm. und Schwefelwasservorkommen von Bad Gögging. Schriftenreihe Bayerisches Landesamt für Wasserwirtschaft. Chapter 8, pp. 55–63.

Lemcke, K., 1987. Zur Frage der alten Verkarstung des Malm im Untergrund des deutschen Molassebeckens und an dessen Nordwestrand. Bull. der Vereinigung Schweiz. Pet. und -Ingenieure 53, 33–46.

Lemcke, K., 1988. Geologie von Bayern I. - Das bayerische Alpenvorland vor der Eiszeit - Erdgeschichte - Bau - Bodenschätze. p. 175. Schweizerbart, Stuttgart.

Lemcke, K., Tunn, W., 1956. Tiefenwasser in der süddeutschen Molasse und ihrer verkarsteten Malmunterlage. Bull. Ver. schweiz. Pet. u. -Ing. 23, 35–56.

Lemieux, J.M., Sudicky, E.A., Peltier, W.R., Tarasov, L., 2008. Dynamics of groundwater recharge and seepage over the Canadian landscape during the Wisconsinian glaciation. J. Geophys. Res. 113, 1–18. DOI: 10.1029/2007JF000838.

Li, Y., Harir, M., Lucio, M., Kanawati, B., Smirnov, K., Flerus, R., Koch, B.P., Schmitt-Kopplin, P., Hertkorn, N., 2016. Proposed Guidelines for Solid Phase Extraction of Suwannee River Dissolved Organic Matter. Anal. Chem. 88, 6680–6688. DOI: 10.1021/acs.analchem.5b04501.

Liedmann, W., Koch, R., 1990. Diagenesis and fluid inclusions of Upper Jurassic sponge-algal reefs in SW Germany. Facies 23, 241–267. DOI: 10.1007/BF02536715.

Lippmann, J., Erzinger, J., Zimmer, M., Schloemer, S., Eichinger, L., Faber, E., 2005. On the geochemistry of gases and noble gas isotopes (including 222Rn) in deep crustal fluids: the 4000 m KTB-pilot hole fluid production test 2002-03. Geofluids 5, 52–66. DOI: 10.1111/j.1468-8123.2004.00108.x.

Lippmann, J., Stute, M., Torgersen, T., Moser, D., Hall, J., Lin, L., Borcsik, M., Bellamy, R., Onstott, T., 2003. Dating ultra-deep mine waters with noble gases and 36Cl, Witwatersrand Basin, South Africa. Geochim. Cosmochim. Acta 67, 4597–4619. DOI: 10.1016/S0016-7037(03)00414-9.

Malcolm, R.L., 1990. The uniqueness of humic substances in each of soil, stream and marine environments. Anal. Chim. Acta 232, 19–30. DOI: 10.1016/S0003-2670(00)81222-2.

Małoszewski, P., 2000. Lumped-parameter models as a tool for determining the hydrological parameters of some groundwater systems based on isotope data, in: Tracers Model. Hydrogeol. (Proceedings TraM'2000 Conf. held Liège, Belgium, May 2000), pp. 271–276.

Małoszewski, P., Zuber, A., 1982. Determining the turnover time of groundwater systems with the aid of environmental tracers. J. Hydrol. 57, 207–231. DOI: 10.1016/0022-1694(82)90147-0.

Masson-Delmotte, V., 2007. EPICA Dome C - 800KYr Deuterium Data and Temperature Estimates: https://www.ncdc.noaa.gov/paleo/study/6080. DOI: 10.1594/PANGAEA.683655.

Matiatos, I., Alexopoulos, A., Godelitsas, A., 2014. Multivariate statistical analysis of the hydrogeochemical and isotopic composition of the groundwater resources in northeastern Peloponnesus (Greece). Sci. Total Environ. 476-477, 577–590. DOI: 10.1016/j.scitotenv.2014.01.042.

Matter, A., Peters, T., Ramseyer, K., 1987. 87Sr/86Sr-Verhältnisse und Sr-Gehalte von Tiefengrundwässern, Mineralien sowie Gesteinen aus dem Kristallin und der Trias der Nordschweiz. Eclogae Geol. Helv. 80, 579–592.

Mayer, A., Sültenfuß, J., Travi, Y., Rebeix, R., Purtschert, R., Claude, C., Le Gal La Salle, C., Miche, H., Conchetto, E., 2014. A multi-tracer study of groundwater origin and transit-time in the aquifers of the Venice region (Italy). Appl. Geochemistry 50, 177–198. DOI: 10.1016/j.apgeochem.2013.10.009.

Mayo, A.L., Loucks, M.D., 1995. Solute and isotopic geochemistry and ground water flow in the central Wasatch Range, Utah. J. Hydrol. 172, 31–59. DOI: 10.1016/0022-1694(95)02748-E.

Mayrhofer, C., Niessner, R., Baumann, T., 2014. Hydrochemistry and hydrogen sulfide generating processes in the Malm aquifer, Bavarian Molasse Basin, Germany. Hydrogeol. J. 22, 151–162. DOI: 10.1007/s10040-013-1064-2.

McArthur, J., Howarth, R., Shields, G., 2012. Strontium Isotope Stratigraphy, in: Gradstein, F.M., Ogg, J.G., Schmitz, M.D., Ogg, G.M. (Eds.), Geol. Time Scale. Elsevier. Volume 1-2, pp. 127–144. DOI: 10.1016/B978-0-444-59425-9.00007-X.

McGuire, K.J., McDonnell, J.J., 2006. A review and evaluation of catchment transit time modeling. J. Hydrol. 330, 543–563. DOI: 10.1016/j.jhydrol.2006.04.020.

McIntosh, J.C., Schlegel, M.E., Person, M., 2012. Glacial impacts on hydrologic processes in sedimentary basins: evidence from natural tracer studies. Geofluids 12, 7–21. DOI: 10.1111/j.1468-8123.2011.00344.x.

Menció, A., Folch, A., Mas-Pla, J., 2012. Identifying key parameters to differentiate groundwater flow systems using multifactorial analysis. J. Hydrol. 472-473, 301–313. DOI: 10.1016/j.jhydrol.2012.09.030.

Meyer, R.K.F., Schmidt-Kaler, H., 1989. Paläogeographischer Atlas des süddeutschen Oberjura (Malm). Geol. Jahrb. 115, 3–77.

Millot, R., Guerrot, C., Innocent, C., Négrel, P., Sanjuan, B., 2011. Chemical, multi-isotopic (Li–B–Sr–U–H–O) and thermal characterization of Triassic formation waters from the Paris Basin. Chem. Geol. 283, 226–241. DOI: 10.1016/j.chemgeo.2011.01.020.

Mills, G.L., Quinn, J.G., 1981. Isolation of dissolved organic matter and copper-organic complexes from estuarine waters using reverse-phase liquid chromatography. Mar. Chem. 10, 93–102. DOI: 10.1016/0304-4203(81)90025-6.

Minor, E.C., Swenson, M.M., Mattson, B.M., Oyler, A.R., 2014. Structural characterization of dissolved organic matter: a review of current techniques for isolation and analysis. Environ. Sci. Process. Impacts 16, 2064–2079. DOI: 10.1039/C4EM00062E.

Moeck, I.S., 2014. Catalog of geothermal play types based on geologic controls. Renew. Sustain. Energy Rev. 37, 867–882. DOI: 10.1016/j.rser.2014.05.032.

Moeck, I.S., Dussel, M., Weber, J., Schintgen, T., Wolfgramm, M., 2020. Geothermal play typing in Germany, case study Molasse Basin: a modern concept to categorise geothermal resources related to crustal permeability. Netherlands J. Geosci. 98, 1–10. DOI: 10.1017/njg.2019.12.

Mook, W., 1976. The dissolution-exchange model for dating groundwater with 14C, in: Int. At. Energy Agency. IAEA, Vienna, Austria, pp. 213–225.

Mook, W.G., 1972. On the reconstruction of the initial 14C content of groundwater from the chemical and isotopic composition, in: Proc. 8th Int. Conf. Radiocarb. Dating (Lower Hutt, New Zealand), Royal Society of New Zealand, Wellington. p. 11.

Mraz, E., 2019. Reservoir Characterization to Improve Exploration Concepts of the Upper Jurassic in the Southern Bavarian Molasse Basin. Dissertation. p. 126. Technical University of Munich.

Mraz, E., Bohnsack, D., Stockinger, G., Käsling, H., Zosseder, K., Thuro, K., 2018. The importance of analogue outcrops of the Upper Jurassic to interprete the lithology of the deep geothermal borehole Geretsried. Jahresberichte und Mitteilungen des Oberrheinischen Geol. Vereins 100, 517–548. DOI: 10.1127/jmogv/100/0016.

Mraz, E., Wolfgramm, M., Moeck, I., Thuro, K., 2019. Detailed Fluid Inclusion and Stable Isotope Analysis on Deep Carbonates from the North Alpine Foreland Basin to Constrain Paleofluid Evolution. Geofluids vol. 2019, Article ID 8980794, 1–23. DOI: 10.1155/2019/8980794.

Müller, T., 1999. Wörterbuch und Lexikon der Hydrogeologie. p. 367. Springer Berlin Heidelberg, Berlin, Heidelberg. DOI: 10.1007/978-3-642-58514-2.

Murphy, E.M., 1987. Carbon-14 measurements and characterization of dissolved organic carbon in ground water. Phd. p. 180. University of Arizona.

Murphy, E.M., Davis, S.N., Long, A., Donahue, D., Jull, A.J.T., 1989a. 14C in fractions of dissolved organic carbon in ground water. Nature 337, 153–155. DOI: 10.1038/337153a0.

Murphy, E.M., Davis, S.N., Long, A., Donahue, D., Jull, A.J.T., 1989b. Characterization and isotopic composition of organic and inorganic carbon in the Milk River Aquifer. Water Resour. Res. 25, 1893–1905. DOI: 10.1029/WR025i008p01893.

Nakata, K., Hasegawa, T., Solomon, D., Miyakawa, K., Tomioka, Y., Ohta, T., Matsumoto, T., Hama, K., Iwatsuki, T., Ono, M., Marui, A., 2019. Degassing behavior of noble gases from groundwater during groundwater sampling. Appl. Geochemistry 104, 60–70. DOI: 10.1016/j.apgeochem.2019.03.007.

Nathan, H., 1949. Geologische Ergebnisse der Erdölbohrungen im Bayerischen Innviertel. Geol. Bavarica 1, 1–68.

Nowak, M., Smajgl, D., Mandic, M., 2019. Carbon and oxygen isotope analyses by mid-infrared laser spectroscopy as a tool for stratigraphic classification of Upper Jurassic carbonate rocks. Thermoscientific Whitepapers 30540, 1–8.

O'brien, B., Stout, J., 1978. Movement and turnover of soil organic matter as indicated by carbon isotope measurements. Soil Biol. Biochem. 10, 309–317. DOI: 10.1016/0038-0717(78)90028-7.

Ortner, H., Aichholzer, S., Zerlauth, M., Pilser, R., Fügenschuh, B., 2015. Geometry, amount, and sequence of thrusting in the Subalpine Molasse of western Austria and southern Germany, European Alps. Tectonics 34, 1–30. DOI: 10.1002/2014TC003550.

Osenbrück, K., Lippmann, J., Sonntag, C., 1998. Dating very old pore waters in impermeable rocks by noble gas isotopes. Geochim. Cosmochim. Acta 62, 3041–3045. DOI: 10.1016/S0016-7037(98)00198-7.

Ozima, M., Podosek, F.A., 2002. Noble Gas Geochemistry. p. 286. Cambridge University Press, Cambridge.

Panda, U.C., Sundaray, S.K., Rath, P., Nayak, B.B., Bhatta, D., 2006. Application of factor and cluster analysis for characterization of river and estuarine water systems – A case study: Mahanadi River (India). J. Hydrol. 331, 434–445. DOI: 10.1016/j.jhydrol.2006.05.029.

Paschen, H., Oertel, D., Grünwald, R., 2003. Möglichkeiten Geothermischer Stromerzeugung in Deutschland - Sachstandsbericht. Technical Report. p. 124. Büro für Technikfolgen-Abschätzung beim Deutschen Bundestag.

Pearson, F.J., White, D.E., 1967. Carbon 14 ages and flow rates of water in Carrizo Sand, Atascosa County, Texas. Water Resour. Res. 3, 251–261. DOI: 10.1029/WR003i001p00251.

Peeters, F., Beyerle, U., Aeschbach-Hertig, W., Holocher, J., Brennwald, M.S., Kipfer, R., 2003. Improving noble gas based paleoclimate reconstruction and groundwater dating using 20Ne/22Ne ratios. Geochim. Cosmochim. Acta 67, 587–600. DOI: 10.1016/S0016-7037(02)00969-9.

Person, M., McIntosh, J., Bense, V., Remenda, V.H., 2007. Pleistocene hydrology of North America: The role of ice sheets in reorganizing groundwater flow systems. Rev. Geophys. 45, n/a–n/a. DOI: 10.1029/2006RG000206.

Petersen, J., Deschamps, P., Hamelin, B., Fourré, E., Gonçalvès, J., Zouari, K., Guendouz, A., Michelot, J.L., Massault, M., Dapoigny, A., Team, A., 2018. Groundwater flowpaths and residence times inferred by 14C, 36Cl and 4He isotopes in the Continental Intercalaire aquifer (North-Western Africa). J. Hydrol. 560, 11–23. DOI: 10.1016/j.jhydrol.2018.03.003.

Phillips, F., Castro, M., 2014. Groundwater Dating and Residence-Time Measurements, in: Treatise on Geochemistry. Elsevier. Volume 7, pp. 361–400. DOI: 10.1016/B978-0-08-095975-7.00513-1.

Piotrowska, N., 2013. Status report of AMS sample preparation laboratory at GADAM Centre, Gliwice, Poland. Nucl. Instruments Methods Phys. Res. Sect. B Beam Interact. with Mater. Atoms 294, 176–181. DOI: 10.1016/j.nimb.2012.05.017.

Prestel, R., 1988. Hydrochemische Untersuchungen im süddeutschen Molassebecken, in: Frisch, H., Werner, J. (Eds.), Schlussbericht Forschungsvorhaben 03 E 6240 A/B Hydrogeothermische Energiebilanz und Grundwasserhaushalt des Malmkarstes im süddeutschen Molassebecken, 1991. Bayerisches Landesamt für Wasserwirtschaft, Geologisches Landesamt Baden-Württemberg. Chapter 4, p. 64.

Probst, A., El Gh'mari, A., Aubert, D., Fritz, B., McNutt, R., 2000. Strontium as a tracer of weathering processes in a silicate catchment polluted by acid atmospheric inputs, Strengbach, France. Chem. Geol. 170, 203–219. DOI: 10.1016/S0009-2541(99)00248-X.

Pu, J., Yuan, D., Zhang, C., Zhao, H., 2012. Tracing the sources of strontium in karst groundwater in Chongqing, China: a combined hydrogeochemical approach and strontium isotope. Environ. Earth Sci. 67, 2371–2381. DOI: 10.1007/s12665-012-1683-2.

Purdy, C.B., Burr, G.S., Rubin, M., Helz, G.R., Mignerey, A.C., 1992. Dissolved Organic and Inorganic 14C Concentrations and Ages for Coastal Plain Aquifers in Southern Maryland. Radiocarbon 34, 654–663. DOI: 10.1017/S0033822200063943.

R Core Team, 2020. R: A Language and Environment for Statistical Computing.

Reichenbacher, B., Böttcher, R., Bracher, H., Doppler, G., Von Engelhardt, W., Gregor, H.J., Heissig, K., Heizmann, E., Hofmann F., Kälin, D., Lemcke, K., Luterbacher, H., Martini, E., Pfeil, F., Reiff, W., Schreiner, A., Steininger, F., 1998. Graupensandrinne - Ries-Impakt: Zur Stratigraphie der Grimmelfinger Schichten, Kirchberger Schichten und Oberen Süsswassermolasse (nördliche Vorlandmolasse, Süddeutschland). Zeitschrift der Dtsch. Geol. Gesellschaft 149, 127–161.

Revelle, W., 2019. psych: Procedures for Psychological, Psychometric, and Personality Research.

Rioseco, E.M., Ziesch, J., Hartmann, H.V., Buness, H., 2019. Geothermal reservoir modeling and simulation of the Upper Jurassic aquifer for district heating in the city of Munich (Germany), in: Eur. Geotherm. Congr. 2019 Den Haag, Netherlands, 11-14 June 2019, pp. 1–12.

Rioseco, E.M., Ziesch, J., Wawerzinek, B., Hartmann, H.V., Thomas, R., Buness, H., 2018. 3-D Geothermal Reservoir Modeling of the Upper Jurassic Carbonate Aquifer in the City of Munich (Germany) under the Thermal-Hydraulic Influence of Optimized Geothermal Multi-Well Patterns – Project GeoParaMoL, in: 43rd Work. Geotherm. Reserv. Eng. Stanford Univ. Stanford, California, Febr. 12-14, 2018, Stanford. pp. 1–12.

Rosner, M., 2010. Geochemical and instrumental fundamentals for accurate and precise strontium isotope data of food samples: Comment on "Determination of the strontium isotope ratio by ICP-MS ginseng as a tracer of regional origin" (Choi et al., 2008). Food Chem. 121, 918–921. DOI: 10.1016/j.foodchem.2010.01.019.

Sahib, L.Y., Marandi, A., Schüth, C., 2016. Strontium isotopes as an indicator for groundwater salinity sources in the Kirkuk region, Iraq. Sci. Total Environ. 562, 935–945. DOI: 10.1016/j.scitotenv.2016.03.185.

Sano, Y., Fischer, T.P., 2013. The Analysis and Interpretation of Noble Gases in Modern Hydrothermal Systems, in: Burnard, P. (Ed.), Noble Gases as Geochemical Tracers. Springer-Verlag Berlin Heidelberg, Berlin, Heidelberg, pp. 249–317. DOI: 10.1007/978-3-642-28836-4_10.

Santoni, S., Huneau, F., Garel, E., Aquilina, L., Vergnaud-Ayraud, V., Labasque, T., Celle-Jeanton, H., 2016. Strontium isotopes as tracers of water-rocks interactions, mixing processes and residence time indicator of groundwater within the granite-carbonate coastal aquifer of Bonifacio (Corsica, France). Sci. Total Environ. 573, 233–246. DOI: 10.1016/j.scitotenv.2016.08.087.

Savvatis, A., Steiner, U., Huber, B., Fritzer, T., Schneider, M., 2015. Limitierungen bei der Ermittlung der Grundwasserfließrichtung in tiefen Aquiferen am Beispiel des Malms im Süddeutschen Molassebecken. [Limitations in the identification of the groundwater flow direction in deep aquifers using the example of the Malm in the Southern German Molasse Basin]. Grundwasser 20, 271–280. DOI: 10.1007/s00767-015-0304-x.

Schellschmidt, R., Sanner, B., Pester, S., Schulz, R., 2010. Geothermal Energy Use in Germany, in: Proc. World Geotherm. Congr. 2010, Bali, Indones. 25-29 April 2010, pp. 1–19. DOI: 10.18635/2071-2219-2020-6-18-23.

Schneider, M., Schubert, A., Baumann, T., Böhm, F., Steiner, U., Mayr, C., 2009. Vorstellung eines aktuellen Forschungsvorhabens zur hydrogeologischen Charakterisierung des Malm als tiefer Grundwasserleiter, in: Der Geotherm. 2009, Bochum, Ger. 17-19 Novemb. 2009, pp. 1–5.

Schneider, M., Thomas, L., 2012. Wissenschaftliche und technische Grundlagen zur strukturgeologischen und hydrogeologischen Charakterisierung tiefer geothermisch genutzter Grundwasserleiter am Beispiel des süddeutschen Molassebeckens. Technical Report. p. 237. Bundesministerium für Umwelt, Naturschutz und Reaktorsicherheit. Berlin.

Schulz, R., Thomas, R., 2012. Geothermische Charakterisierung von karstig-klüftigen Aquiferen im Großraum München. Technical Report. p. 98. Leibniz Institut für Angewandthe Geophysik (LIAG). Hannover.

Schumacker, R.E., 2016. Using R with Multivariate Statistics. p. 408. SAGE Publications, Los Angeles, USA.

Seguinot, J., Ivy-Ochs, S., Jouvet, G., Huss, M., Funk, M., Preusser, F., 2018. Modelling last glacial cycle ice dynamics in the alps. The Cryosphere 12, 3265–3285. DOI: 10.5194/tc-12-3265-2018.

Shand, P., Darbyshire, D., Love, A., Edmunds, W., 2009. Sr isotopes in natural waters: Applications to source characterisation and water–rock interaction in contrasting landscapes. Appl. Geochemistry 24, 574–586. DOI: 10.1016/j.apgeochem.2008.12.011.

Siegel, D.I., 1991. Evidence for dilution of deep, confined ground water by vertical recharge of isotopically heavy Pleistocene water. Geology 19, 433. DOI: 10.1130/0091-7613(1991)019<0433:EFDODC>2.3.CO;2.

Simjouw, J.P., Minor, E.C., Mopper, K., 2005. Isolation and characterization of estuarine dissolved organic matter: Comparison of ultrafiltration and C18 solid-phase extraction techniques. Mar. Chem. 96, 219–235. DOI: 10.1016/j.marchem.2005.01.003.

Smalley, P.C., Higgins, A.C., Howarth, R.J., Nicholson, H., Jones, C.E., Swinburne, N., Bessa, J., 1994. Seawater Sr isotope variations through time: A procedure for constructing a reference curve to date and correlate marine sedimentary rocks. Geology 22, 431. DOI: 10.1130/0091-7613(1994)022<0431:SSIVTT>2.3.CO;2.

Stichler, W., 1997. Isotopengehalte in Tiefengrundwässern aus Erdöl- und Erdgasbohrungen im süddeutschen Molassebecken. [Isotope contents of deep groundwater from oil and gas wells located in the South German Molasse basin]. Beiträge zur Hydrogeol. 48, 81–88.

Stichler, W., Rauert, W., Weise, S., Wolf, M., Koschel, G., Stier, P., Prestel, R., Hedin, K., Bertleff, B., 1987. Isotopenhydrologische und hydrochemische Untersuchungen zur Erkundung des Fließsystems im Malmkarstaquifer des süddeutschen Alpenvorlandes. [Isotope-hydrological and Hydrochemical Investigations of the Flow System of the Malmkarst Aquifer in the Pre-Alpine Region of South Germany]. Z. dt. geol. Ges. 138, 387–398.

Stober, I., 2013. Die thermalen Karbonat-Aquifere Oberjura und Oberer Muschelkalk im Südwestdeutschen Alpenvorland. [The thermal carbonate aquifers Upper Jurassic and Upper Muschelkalk in the Southwest-German alpine foreland]. Grundwasser 18, 259–269. DOI: 10.1007/s00767-013-0236-2.

Stober, I., 2014. Hydrochemical properties of deep carbonate aquifers in the SW German Molasse basin. Geotherm. Energy 2, 13. DOI: 10.1186/s40517-014-0013-1.

Stober, I., Bucher, K., 2000. Herkunft der Salinität in Tiefenwässern des Grundgebirges – unter besonderer Berücksichtigung der Kristallinwässer des Schwarzwaldes. Grundwasser 3, 125–140. DOI: 10.1007/s767-000-8359-8.

Stober, I., Jodocy, M., 2011. Geothermische Nutzhorizonte im westlichen Teil des Süddeutschen Molassebeckens. [Geothermal target formations in the western part of the Molasse Basin in South Germany]. Zeitschrift für Geol. Wissenschaften 39, 161–172.

Stober, I., Wolfgramm, M., Birner, J., 2014. Hydrochemie der Tiefenwässer in Deutschland. [Hydrochemistry of deep waters in Germany]. Z. geol. Wiss. 41/42, 339–380.

Stuiver, M., Polach, H.A., 1977. Discussion Reporting of 14 C Data. Radiocarbon 19, 355–363. DOI: 10.1017/S0033822200003672.

Stumpp, C., Klaus, J., Stichler, W., 2014. Analysis of long-term stable isotopic composition in German precipitation. J. Hydrol. 517, 351–361. DOI: 10.1016/j.jhydrol.2014.05.034.

Stute, M., Schlosser, P., 1993. Principles and Applications of the Noble Gas Paleothermometer, in: Swart, P.K., Lohmann, K.C., Mckenzie, J., Savin, S. (Eds.), Clim. Chang. Cont. Isot. Rec.. AGU, Washington DC, pp. 89–100. DOI: 10.1029/GM078p0089.

Stute, M., Sonntag, C., Deák, J., Schlosser, P., 1992. Helium in deep circulating groundwater in the Great Hungarian Plain: Flow dynamics and crustal and mantle helium fluxes. Geochim. Cosmochim. Acta 56, 2051–2067. DOI: 10.1016/0016-7037(92)90329-H.

Sültenfuß, J., Roether, W., Rhein, M., 2009. The Bremen mass spectrometric facility for the measurement of helium isotopes, neon, and tritium in water. Isotopes Environ. Health Stud. 45, 83–95. DOI: 10.1080/10256010902871929.

Swenson, M.M., 2014. Rapid solid phase extraction of dissolved organic matter. Master. p. 75. University of Minnesota Duluth.

Swenson, M.M., Oyler, A.R., Minor, E.C., 2014. Rapid solid phase extraction of dissolved organic matter. Limnol. Oceanogr. Methods 12, 713–728. DOI: 10.4319/lom.2014.12.713.

Tabachnik, B.G., Fidell, L.S., 2013. Using Multivariate Statistics. p. 983. 6 ed., Pearson, New York, USA.

Tamers, M.A., 1975. Validity of radiocarbon dates on ground water. Geophys. Surv. 2, 217–239. DOI: 10.1007/BF01447909.

Taylor, R., Long, A., Kra, R.S., 1992. Radiocarbon After Four Decades. p. 596. Springer New York, New York, USA. DOI: 10.1007/978-1-4757-4249-7.

Thomas, J.M., Hershey, R.L., Fereday, W., Burr, G., 2021. Using Carbon-14 of dissolved organic carbon to determine groundwater ages and travel times in aquifers with low organic carbon. Appl. Geochemistry 124, 17. DOI: 10.1016/j.apgeochem.2020.104842.

Thurman, E.M., 1985. Organic Geochemistry of Natural Waters. p. 497. 9, Springer, Dordrecht, Netherlands. DOI: 10.1007/978-94-009-5095-5.

Thurman, E.M., Malcolm, R.L., 1981. Preparative isolation of aquatic humic substances. Environ. Sci. Technol. 15, 463–466. DOI: 10.1021/es00086a012.

Thuro, K., Zosseder, K., Bohnsack, D., Heine, F., Konrad, F., Mraz, E., Stockinger, G., 2019. Dolomitkluft: Erschließung, Test und Analyse des ersten kluftdominierten Dolomitaquifers im tiefen Malm des Molassebeckens zur Erhöhung der Erfolgsaussichten. Technical Report. p. 193. Technische Universität München. München.

Tolstikhin, I., Lehmann, B., Loosli, H., Gautschi, A., 1996. Helium and argon isotopes in rocks, minerals, and related ground waters: A case study in northern Switzerland. Geochim. Cosmochim. Acta 60, 1497–1514. DOI: 10.1016/0016-7037(96)00036-1.

Torgersen, T., 1980. Controls on pore-fluid concentration of 4He and 222Rn and the calculation of 4He/222Rn ages. J. Geochemical Explor. 13, 57–75. DOI: 10.1016/0375-6742(80)90021-7.

Torgersen, T., Clarke, W.B., 1985. Helium accumulation in groundwater, I: An evaluation of sources and the continental flux of crustal 4He in the Great Artesian Basin, Australia. Geochim. Cosmochim. Acta 49, 1211–1218. DOI: 10.1016/0016-7037(85)90011-0.

Torgersen, T., Kennedy, B., Hiyagon, H., Chiou, K., Reynolds, J., Clarke, W., 1989. Argon accumulation and the crustal degassing flux of40Ar in the Great Artesian Basin, Australia. Earth Planet. Sci. Lett. 92, 43–56. DOI: 10.1016/0012-821X(89)90019-8.

Torgersen, T., Stute, M., 2013. Helium (and other noble gases) as a tool for understanding long time-scale groundwater transport, in: Isotope Methods for Dating Old Groundwater. International Atomic Energy Agency (IAEA). Chapter 8, p. 52.

Tóth, J., 1999. Groundwater as a geologic agent: An overview of the causes, processes, and manifestations. Hydrogeol. J. 7, 1–14. DOI: 10.1007/s100400050176.

Traub, F., 1971. Zur Wasserversorgung der Stadt Ingolstadt. Geol. Bavarica 64, 356–364.

Tullborg, E.L., Gustafsson, E., 1999. 14C in bicarbonate and dissolved organics—a useful tracer? Appl. Geochemistry 14, 927–938. DOI: 10.1016/S0883-2927(99)00031-1.

TUM, 2020. Bewertung Masterplan Geothermie. Technical Report. p. 104. Technische Universität München, School of Engineering. München.

UBA, 2020. Erneuerbare Energien in Deutschland - Daten zur Entwicklung im Jahr 2019. Technical Report. p. 27. Umweltbundesamt. Dessau-Roßlau.

Udluft, P., 1975. Das tiefere Grundwasser zwischen Vindelicischem Rücken und Alpenrand. [The deeper groundwater between the Vindelician ridge and the margin of the Alps]. Geol. Jahrb. C11, 3–29.

Ueckert, M., Baumann, T., 2019. Hydrochemical aspects of high-temperature aquifer storage in carbonaceous aquifers: evaluation of a field study. Geotherm. Energy 7, 1–22. DOI: 10.1186/s40517-019-0120-0.

UNFCCC, 2015. Paris Agreement. Technical Report. p. 25. United Nations. Paris, France.

Vaikmäe, R., Vallner, L., Loosli, H.H., Blaser, P.C., Juillard-Tardent, M., 2001. Palaeogroundwater of glacial origin in the Cambrian-Vendian aquifer of northern Estonia. Geol. Soc. London, Spec. Publ. 189, 17–27. DOI: 10.1144/GSL.SP.2001.189.01.03.

Varsányi, I., Palcsu, L., Kovács, L.Ó., 2011. Groundwater flow system as an archive of palaeotemperature: Noble gas, radiocarbon, stable isotope and geochemical study in the Pannonian Basin, Hungary. Appl. Geochemistry 26, 91–104. DOI: 10.1016/j.apgeochem.2010.11.006.

Veizer, J., 1989. Strontium Isotopes in Seawater through Time. Annu. Rev. Earth Planet. Sci. 17, 141–167. DOI: 10.1146/annurev.ea.17.050189.001041.

Veizer, J., Ala, D., Azmy, K., Bruckschen, P., Buhl, D., Bruhn, F., a.F. Carden, G., Diener, A., Ebneth, S., Godderis, Y., Jasper, T., Korte, C., Pawellek, F., Podlaha, O.G., Strauss, H., 1999. 87Sr/86Sr, δ13C and δ18O evolution of Phanerozoic seawater. Chem. Geol. 161, 59–88. DOI: 10.1016/S0009-2541(99)00081-9.

Veizer, J., Compston, W., 1974. 87Sr/86Sr composition of seawater during the Phanerozoic. Geochim. Cosmochim. Acta 38, 1461–1484. DOI: 10.1016/0016-7037(74)90099-4.

Véron, J., 2005. The Alpine Molasse Basin: review of petroleum geology and remaining potential. Bull. angew. Geol. 10, 75–86. DOI: 10.5169/seals-225567.

Villinger, E., 1977. Über Potentialverteilung und Strömungssysteme im Karstwasser der Schwäbischen Alb (Oberer Jura, SW-Deutschland). [On Potential Distribution and Flow Systems of the Karstwater of the Swabian Alb (Upper Jurassic, South-West-Germany)]. Geol. Jahrb. C18, 3–93.

Villinger, E., 1986. Untersuchungen zur Flußgeschichte von Aare-Donau, Alpenrhein und zur Entwicklung des Malm-Karsts in Südwestdeutschland. Jahreshefte des Geol. Landesamts Baden-Württemberg 28, 297–362.

Villinger, E., 1988. Bemerkungen zur Verkarstung des Malms unter dem westlichen süddeutschen Molassebecken. [Comments on the karstification of the Malm under the western molasse basin in South Germany]. Bull. Ver. schweiz. Pet. u. -Ing. 54, 41–59. DOI: 10.5169/seals-211748.

Vogel, J., Ehhalt, D., 1963. The Use of the Carbon Isotopes in Groundwater Studies, in: Int. At. Energy Agency. IAEA, Vienna, Austria, pp. 383–395.

Waber, H.N., Heidinger, M., Lorenz, G., Traber, D., 2014. Arbeitsbericht NAB 13-63: Hydrochemie und Isotopenhydrogeologie von Tiefengrundwässern in der Nordschweiz und im angrenzenden Süddeutschland. Technical Report. p. 247. Nationale Genossenschaft für die Lagerung radioaktiver Abfälle. Wettingen, Suisse.

Wagner, B., Kus, G., Kainzmauer, B., Spörlein, T., Wilferth, T., Veit, W., Fritsch, P., Wrobel, M., Lindenthal, W., Neumann, J., Sprenger, W., 2009. Erläuterungen zur Hydrogeologischen Karte von Bayern. p. 88. Bayerisches Landesamt für Umwelt, Augsburg.

Wanner, C., Eichinger, F., Jahrfeld, T., Diamond, L.W., 2017. Causes of abundant calcite scaling in geothermal wells in the Bavarian Molasse Basin, Southern Germany. Geothermics 70, 324–338. DOI: 10.1016/j.geothermics.2017.05.001.

Ward, J.H., 1963. Hierarchical Grouping to Optimize an Objective Function. J. Am. Stat. Assoc. 58, 236–244. DOI: 10.1080/01621459.1963.10500845.

Wassenaar, L., Aravena, R., 1992. Radiocarbon Contents of Dissolved Organic and Inorganic Carbon in Shallow Groundwater Systems, in: Int. At. Energy Agency. International Atomic Energy Agency, Vienna, Austria. Volume SM-319/5, pp. 143–151.

Wassenaar, L., Aravena, R., Fritz, P., Barker, J., 1990. Isotopic composition (13C, 14C, 2H) and geochemistry of aquatic humic substances from groundwater. Org. Geochem. 15, 383–396. DOI: 10.1016/0146-6380(90)90165-V.

Wassenaar, L., Aravena, R., Hendry, J., Fritz, P., 1991. Radiocarbon in Dissolved Organic Carbon, A Possible Groundwater Dating Method: Case Studies From Western Canada. Water Resour. Res. 27, 1975–1986. DOI: 10.1029/91WR00504.

Wasserburg, G., Mazor, E., Zartman, R., 1963. Isotopic and chemical composition of some terrestrial natural gases, in: Geiss, J., Goldberg, E. (Eds.), Earth Sci. Meteorites. Amsterdam, Netherlands, pp. 219–240.

Weber, J., Born, H., Moeck, I., 2019. Geothermal Energy Use, Country Update for Germany 2016-2018, in: Eur. Geotherm. Congr. 2019, Den Haag, Ned. 11-14 June 2019, Den Haag, Netherlands. p. 16.

Weise, S., Moser, H., 1987. Groundwater dating with helium isotopes, in: Int. At. Energy Agency. International Atomic Energy Agency, Vienna, Austria. Volume SM-299/44, pp. 105–126.

Weise, S., Stichler, W., 1997. Edelgasisotopen-Methoden als Werkzeug zur Untersuchung tiefreichender Grundwasser-Fließsysteme am Beispiel des süddeutschen Molassebeckens. [Noble gas isotope methods as a tool for investigations of deep circulating groundwater flowsystems in the South German Molasse basin]. Beiträge zur Hydrogeologie 48, 69–80.

Weise, S., Wolf, M., Fritz, P., Rauert, W., Stichler, W., Prestel, R., Bertleff, B., Stute, M., 1991. Isotopenhydrologische Untersuchungen im Süddeutschen Molassebecken, in: Frisch, H., Werner, J. (Eds.), Schlussbericht Forschungsvorhaben 03 E 6240 A/B Hydrogeothermische Energiebilanz und Grundwasserhaushalt des Malmkarstes im süddeutschen Molassebecken, 1991. Bayerisches Landesamt für Wasserwirtschaft, Geologisches Landesamt Baden-Württemberg, München, Freiburg i.Br.. Chapter 5, p. 106.

Weiss, R.F., 1971. Solubility of Helium and Neon in Water and Seawater. J. Chem. Eng. Data 16, 235–241. DOI: 10.1021/je60049a019.

Werner, J., 1987. Das Forschungsvorhaben Hydrogeothermische Energienutzung und Grundwasserhaushalt des Malmkarsts im süddeutschen Molassebecken - Ziele und Zwischenergebnisse. Zeitschr. dt. geol. Ges. 138, 399–409.

Wersin, P., Mazurek, M., Waber, H.N., Mäder, U., Gimmi, T., Rufer, D., de Haller, A., 2013. Rock and porewater characterisation on drillcores from the Schlattingen borehole. Technical Report. p. 207. Institute of Geological Sciences, University of Bern. Bern, Suisse.

White, D.E., 1957. Magmatic, Connate, and Metamorphic Waters. Bull. Geol. Soc. Am. 68, 1659–1682. DOI: 10.1130/0016-7606(1957)68[1659:MCAMW]2.0.CO;2.

White, D.E., Hem, J.D., Waring, G., 1963. Chemical Composition of Subsurface Waters, in: Fleischer, M. (Ed.), Data Geochemistry. 6 ed.. Geological Survey Professional Paper 440-F, pp. 1–67.

Whittemore, D.O., 1995. Geochemical differentiation of oil and gas brine from other saltwalter sources contaminating water resources: Case studies from Kansas and Oklahoma. Environ. Geosci. 2, 15–31.

Wickham, H., 2008. Applied Spatial Data Analysis with R. pp. 21–54. Springer New York, New York, NY. DOI: 10.1007/978-0-387-78171-6.

Wigley, T.M.L., 1976. Effect of mineral precipitation on isotopic composition and 14C dating of groundwater. Nature 263, 219–221. DOI: 10.1038/263219a0.

Wilson, G., McNeill, G., 1997. Noble gas recharge temperatures and the excess air component. Appl. Geochemistry 12, 747–762. DOI: 10.1016/S0883-2927(97)00035-8.

Wolfgramm, M., Bartels, J., Hoffmann, F., Kittl, G., Lenz, G., Seibt, P., Schulz, R., Thomas, R., Unger, H.J., 2007. Unterhaching geothermal well doublet: structural and hydrodynamic reservoir characteristic; Bavaria (Germany), in: Proc. Eur. Geotherm. Congr. 2007, pp. 1–6.

Wrobel, J.P., Fritzer, T., Mikulla, C., Schuldes, D., Suckow, A., 2002. Forschungsbohrung Altdorf bei Landshut/Niederbayern - Erkundung einer geothermischen Anomalie im Bereich des Landshut-Neuöttinger-Hochs. Grundwasser , 14–24DOI: 10.1007/s007670200002.

Zhu, G., Li, Z., Su, Y., Ma, J., Zhang, Y., 2007. Hydrogeochemical and isotope evidence of groundwater evolution and recharge in Minqin Basin, Northwest China. J. Hydrol. 333, 239–251. DOI: 10.1016/j.jhydrol.2006.08.013.

Zwick, W.R., Velicer, W.F., 1982. Factors Influencing Four Rules For Determining The Number Of Components To Retain. Multivariate Behav. Res. 17, 253–269. DOI: 10.1207/s15327906mbr1702_5.

Appendices

Chapter A

List of Appendix

Appendix A.1: Results of data measurements for Sec. 5.2

Appendix A.2: Correlation matrix for Sec. 5.2

Appendix A.3: Results of Monte Carlo simulation for deriving NGT

A.1 Results of data measurements for Sec. 5.2

Table A.1: Physico-chemical composition of the groundwater samples. Key:$^+$ results from duplicate measurements.

ID	pH	EC	Ca^{2+}	Mg^{2+}	Na^+	K^+	Li^+	Sr^{2+}	Rb^+	HCO_3^-	Cl^-	SO_4^{2-}	F^-	Br^-	DOC	B
	(-)	(µS/cm)							(mg/l)							
1	7.1	715	31.8	9.4	121.9	15.2	0.12	0.57	0.022	329	70.0	1.6	2.4	0.38	0.7	2.3
2^+	6.9	756	38.5	10.7	129.8	14.5	0.20	0.71	0.034	354	75.6	13.4	5.1	0.22	0.8	0.7
3	6.8	723	35.3	10.2	120.0	12.8	0.11	0.61	0.035	333	72.6	6.4	2.8	1.27	1.0	0.6
4	7.0	722	31.9	8.9	123.8	7.3	0.14	0.65	0.023	345	70.4	2.9	1.8	0.43	1.2	2.5
5	7.1	740	35.1	10.4	122.0	13.8	0.10	0.56	0.033	323	69.8	<1.6	2.7	0.27	0.9	0.7
6	7.1	700	27.1	7.2	122.5	14.8	0.11	0.65	0.036	329	69.5	<1.6	1.9	0.39	0.8	0.8
7	6.9	697	28.6	8.8	120.9	14.3	0.10	0.57	0.033	305	69.9	<1.6	3.3	0.43	0.5	0.8
8	6.9	700	30.4	7.5	122.3	14.7	0.12	0.57	0.036	302	82.5	1.4	2.2	0.39	1.7	2.1
9^+	7.2	752	33.7	10.7	120.0	14.1	0.16	0.57	0.022	326	72.0	7.8	6.6	0.42	0.9	2.2
10	6.5	587	3.5	1.6	130.1	17.2	0.10	0.16	0.053	214	74.0	4.1	3.0	0.33	1.6	1.1
11	6.3	600	8.8	1.0	118.5	15.9	0.12	0.28	0.059	207	73.8	5.3	3.6	0.40	2.6	0.8
12	6.5	653	16.9	1.7	121.6	19.8	0.14	0.75	0.063	256	69.1	4.8	2.0	0.19	1.7	<0.3
13	6.7	699	23.4	3.1	131.0	21.2	0.16	0.59	0.059	275	81.7	8.2	4.2	<0.1	2.0	2.2
14	6.3	689	16.6	1.8	134.7	22.9	0.17	0.50	0.067	250	82.2	15.8	5.1	<0.1	1.5	2.1
15	6.4	746	18.5	2.1	143.5	20.6	0.19	0.55	0.066	275	95.8	13.9	7.9	0.55	2.3	<0.3
16^+	6.7	681	24.8	3.7	121.6	15.8	0.13	0.65	0.043	281	77.1	4.3	4.6	<0.1	1.6	2.2
17^+	6.5	713	27.0	3.8	129.1	18.9	0.15	0.99	0.053	288	79.0	12.5	2.7	0.33	1.9	2.2
18^+	6.4	1087	35.9	5.2	172.6	32.1	0.24	1.40	0.118	311	157.6	30.9	7.7	0.84	3.8	3.3
19	6.4	1029	38.2	4.2	174.0	31.3	0.27	1.09	0.094	311	157.1	20.6	4.5	0.55	4.2	3.0
20	6.9	1596	39.3	4.0	269.0	34.9	0.38	1.73	0.057	317	279.3	45.0	2.2	0.62	4.4	8.8
21^+	6.6	3800	91.6	13.9	792.1	51.8	0.92	4.02	0.015	500	968.9	100.6	5.1	3.19	21.1	15.8
22^+	6.6	7703	135.0	29.0	1854.0	85.2	1.91	6.40	0.150	854	2485.0	337.0	4.6	9.92	70.5	35.0
23	7.5	965	34.0	17.9	149.8	15.4	0.13	0.15	0.041	410	93.7	4.6		0.53	0.8	0.9
24	7.0	820	43.6	10.2	137.4	15.9	0.10	0.20	0.039	412	79.7	0.3	2.7	0.40	0.5	0.7

Table A.2: Isotope measurements and noble gas concentration results. Key:$^{+}$ results from duplicate measurements of stable water isotopes.

ID	$\delta^{18}O$	δD	$^{87}Sr/^{86}Sr$	^{4}He	$^{3}He/^{4}He$	$^{4}He_{rad}$	^{40}Ar	$^{40}Ar/^{36}Ar$	$^{40}Ar_{rad}$
	(‰ VSMOW)		(-)	(ccSTP/g)	(-)	(ccSTP/g)		(-)	(ccSTP/g)
1	-11.7	-86.3	0.70921						
2^{+}	-11.7	-86.2	0.70907	2.30×10^{-5}	9.89×10^{-8}	2.29×10^{-5}			
3	-11.9	-86.8	0.70925	2.22×10^{-5}	1.01×10^{-7}	2.21×10^{-5}			
4	-11.6	-85.4	0.70923						
5	-11.7	-85.9	0.70922	1.80×10^{-5}	1.12×10^{-7}	1.79×10^{-5}			
6	-11.7	-86.2	0.70922	2.30×10^{-5}	1.36×10^{-7}	2.29×10^{-5}			
7	-11.5	-86.2	0.70922	2.32×10^{-5}	1.06×10^{-7}	2.31×10^{-5}			
8	-12.0	-86.3	0.70924						
9^{+}	-11.6	-86.1	0.70926	2.31×10^{-5}	1.20×10^{-7}	2.30×10^{-5}	5.03×10^{-4}	302.5	6.65×10^{-6}
10	-11.6	-86.0	0.70913						
11	-11.6	-86.1	0.70917						
12	-11.6	-86.5	0.70905	2.29×10^{-5}	1.03×10^{-7}	2.28×10^{-5}			
13	-11.8	-86.3	0.70901	2.42×10^{-5}	9.79×10^{-8}	2.41×10^{-5}			
14	-11.4	-85.1	0.70920						
15	-11.0	-84.8	0.70902	1.68×10^{-5}	9.07×10^{-8}	1.67×10^{-5}			
16^{+}	-11.7	-86.0	0.70925	2.53×10^{-5}	1.13×10^{-7}	2.52×10^{-5}	5.04×10^{-4}	299.8	2.17×10^{-6}
17^{+}	-11.6	-85.8	0.70881	2.42×10^{-5}	1.10×10^{-7}	2.42×10^{-5}	4.95×10^{-4}	301.2	4.39×10^{-6}
18^{+}	-10.8	-82.8	0.70862	9.20×10^{-5}	7.31×10^{-8}	9.19×10^{-5}	1.65×10^{-3}	307.6	5.76×10^{-5}
19	-11.0	-84.3	0.70899	4.22×10^{-5}	6.45×10^{-8}	4.21×10^{-5}			
20	-10.5	-82.3	0.70951	5.44×10^{-5}	7.31×10^{-8}	5.43×10^{-5}			
21^{+}	-7.6	-74.6	0.70970	1.15×10^{-4}	6.26×10^{-8}	1.15×10^{-4}	1.98×10^{-4}	345.1	
22^{+}	-2.6	-60.6	0.70944	1.00×10^{-4}	8.08×10^{-8}	1.00×10^{-4}	9.39×10^{-5}	392	
23	-11.4	-84.0	0.70926						
24	-11.7	-85.7	0.70901						

Table A.3: Results of noble gas concentrations.

ID	He	ΔHe	Ne	ΔNe	Ar	ΔAr	Kr	ΔKr	Xe	ΔXe
					(ccSTP/g)					
1										
2			3.08×10^{-7}							
3			4.63×10^{-7}							
4										
5			4.26×10^{-7}							
6			4.49×10^{-7}							
7			4.27×10^{-7}							
8										
9	2.31×10^{-5}	9.78×10^{-8}	2.20×10^{-7}	2.64×10^{-9}	5.05×10^{-4}	1.96×10^{-6}	1.20×10^{-7}	1.58×10^{-9}	1.75×10^{-8}	2.64×10^{-10}
10										
11										
12			4.21×10^{-7}							
13			4.14×10^{-7}							
14										
15			3.80×10^{-7}							
16	2.53×10^{-5}	1.05×10^{-7}	2.12×10^{-7}	1.83×10^{-9}	5.07×10^{-4}	2.64×10^{-6}	1.20×10^{-7}	1.62×10^{-9}	1.73×10^{-8}	2.72×10^{-10}
17	2.31×10^{-5}	9.78×10^{-8}	2.20×10^{-7}	2.64×10^{-9}	5.05×10^{-4}	1.96×10^{-6}	1.20×10^{-7}	1.58×10^{-9}	1.75×10^{-8}	2.64×10^{-10}
18	2.87×10^{-4}	1.15×10^{-6}	8.24×10^{-7}	1.31×10^{-8}	3.03×10^{-3}	6.28×10^{-6}	5.27×10^{-7}	8.54×10^{-9}	7.53×10^{-8}	1.04×10^{-9}
19			4.37×10^{-7}							
20			3.04×10^{-7}							
21	1.15×10^{-4}	4.74×10^{-7}	5.10×10^{-8}	5.99×10^{-10}	1.99×10^{-4}	7.36×10^{-7}	4.48×10^{-8}	6.56×10^{-10}	7.70×10^{-9}	1.11×10^{-10}
22	1.00×10^{-4}	4.20×10^{-7}	2.52×10^{-8}	3.20×10^{-10}	9.42×10^{-5}	3.91×10^{-7}	2.08×10^{-8}	3.25×10^{-10}	4.14×10^{-9}	6.59×10^{-11}
23										
24										

A.2 Correlation matrix for Sec. 5.2

Table A.4: Ranked correlation matrix with Spearman's ρ coefficient.

	F^-	Rb^+	Na^+	Cl^-	SWI	Li^+	SO_4^{2-}	K^+	DOC	Sr^{2+}	B	$^{87}Sr/^{86}Sr$	Br^-	Mg^{2+}	HCO_3^-	EC	Ca^{2+}
F^-	1																
Rb^+	0.27	1															
Na^+	0.20	0.43	1														
Cl^-	0.40	0.48	0.83	1													
SWI	0.48	0.41	0.49	0.48	1												
Li^+	0.48	0.38	0.64	0.69	0.62	1											
SO_4^{2-}	0.59	0.51	0.62	0.75	0.68	0.90	1										
K^+	0.36	0.70	0.75	0.74	0.68	0.66	0.74	1									
DOC	0.33	0.60	0.50	0.67	0.59	0.69	0.78	0.76	1								
Sr^{2+}	0.14	0.15	0.35	0.32	0.39	0.68	0.57	0.43	0.55	1							
B	0.15	0.11	0.49	0.55	0.37	0.59	0.51	0.49	0.54	0.56	1						
$^{87}Sr/^{86}Sr$	-0.21	-0.43	-0.02	0.09	0.05	0.08	0.01	-0.17	0.02	0.11	0.29	1					
Br^-	0.11	0.03	0.41	0.49	0.46	0.35	0.41	0.23	0.37	0.32	0.32	0.33	1				
Mg^{2+}	-0.05	-0.53	0.18	0.11	-0.07	0.13	-0.01	-0.28	-0.29	0.18	0.15	0.51	0.44	1			
HCO_3^-	-0.14	-0.45	0.32	0.16	-0.06	0.18	0.05	-0.15	-0.23	0.29	0.21	0.45	0.52	0.93	1		
EC	0.20	0.00	0.67	0.62	0.37	0.61	0.53	0.32	0.27	0.46	0.41	0.24	0.71	0.69	0.75	1	
Ca^{2+}	0.06	-0.20	0.49	0.43	0.18	0.40	0.32	0.12	0.08	0.49	0.36	0.32	0.62	0.80	0.86	0.91	1

A.3 Results of Monte Carlo simulation for deriving NGT

Fitting of parameter A

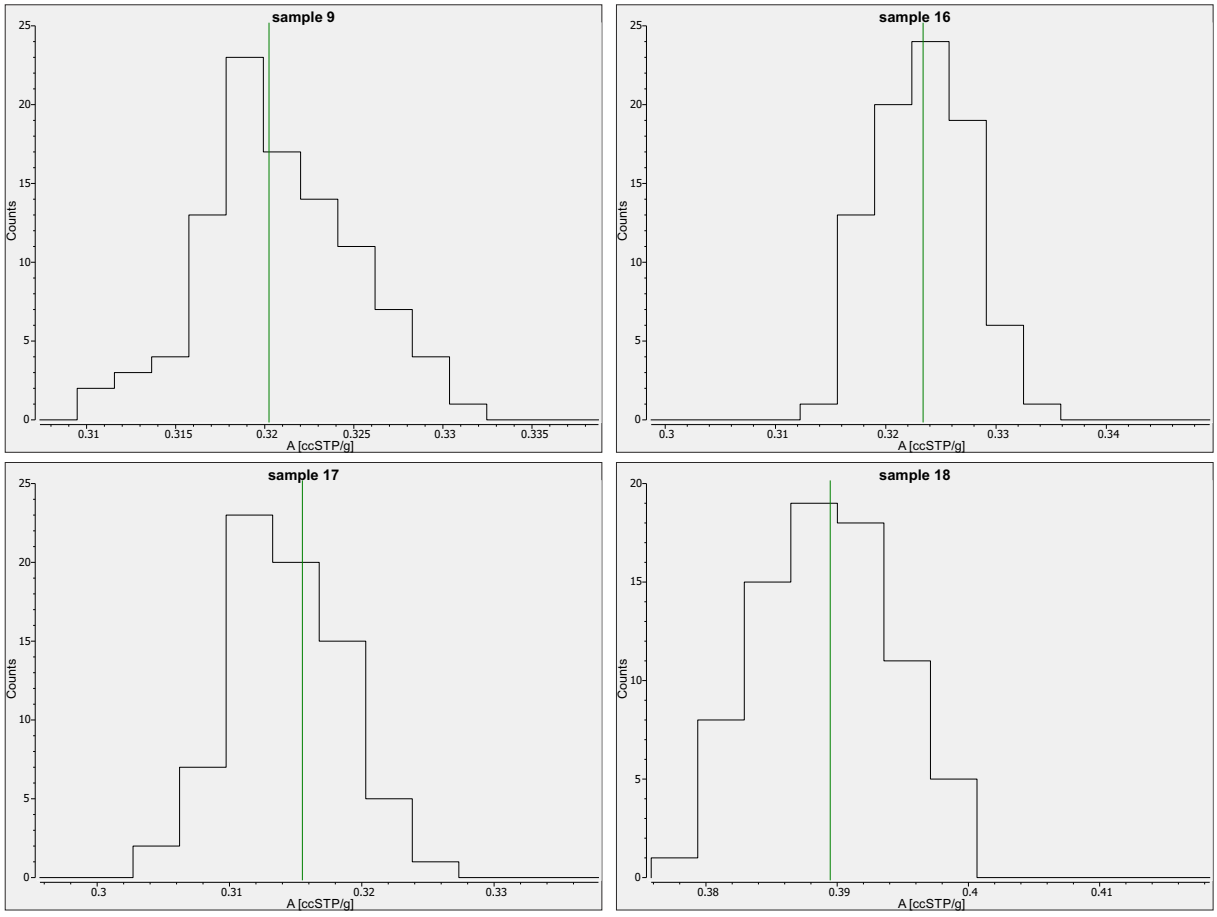

Figure A.1: Output of PANGA (Jung and Aeschbach, 2018) for Monte Carlo simulation results (5000 runs) for the fitting parameter A (excess air) using the CE-model (Aeschbach-Hertig et al., 2000).

Fitting of parameters F and T

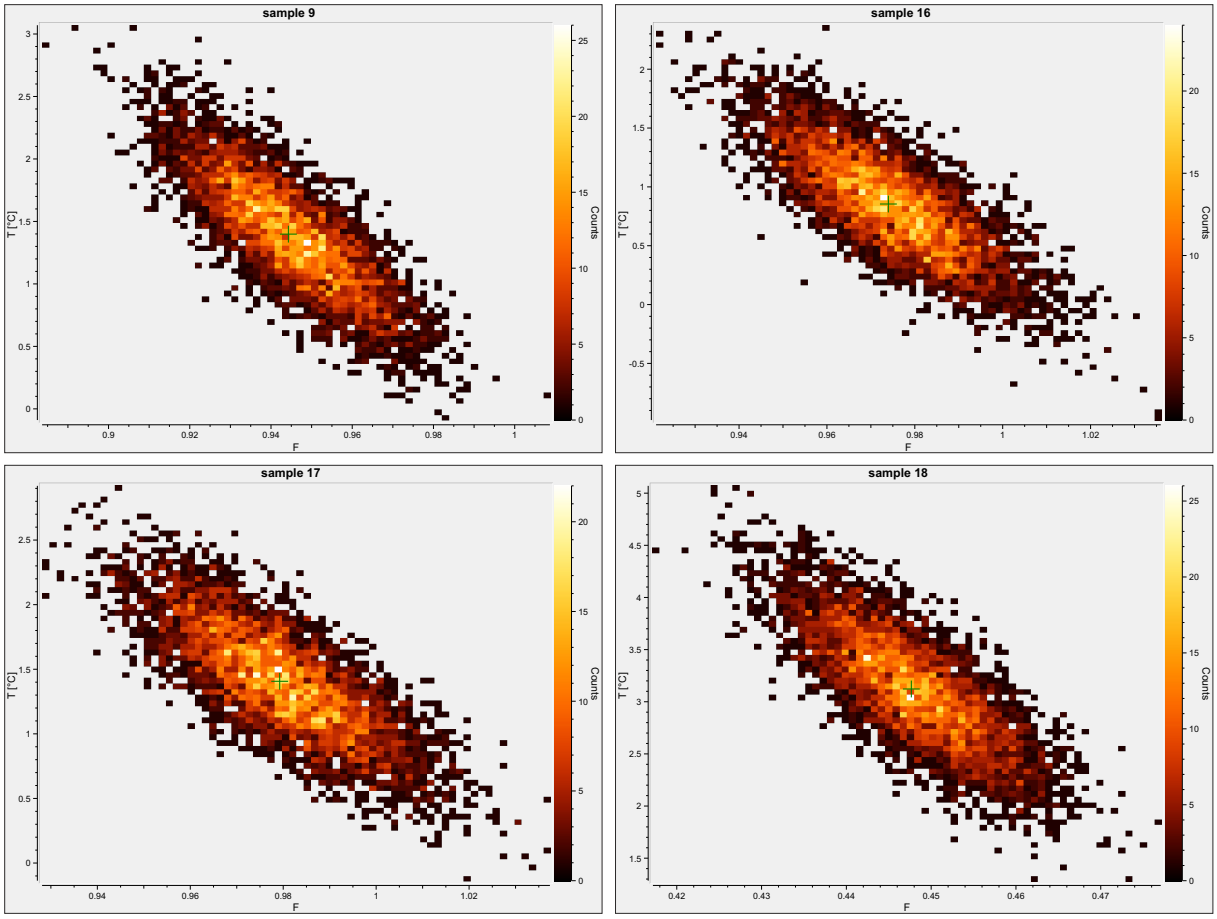

Figure A.2: Output of PANGA (Jung and Aeschbach, 2018) for Monte Carlo simulation results (5000 runs) for the fitting parameters F (fractionation factor) and T (noble gas equilibrium temperature) using the CE-model (Aeschbach-Hertig et al., 2000).

A.4 Supplementary figures

Structure of a glacier and glacier cycle

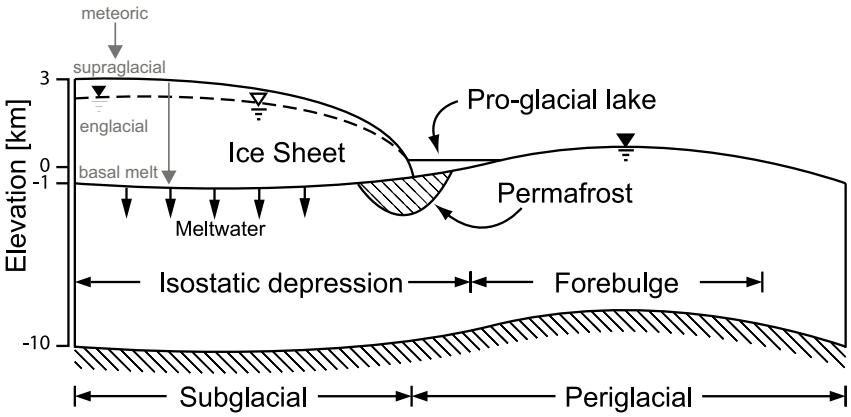

Figure A.3: Cross section along an ice flow line showing hydraulic conditions during a glacial cycle after Lemieux et al. (2008) and Grundl et al. (2013)

.

Bernau syncline

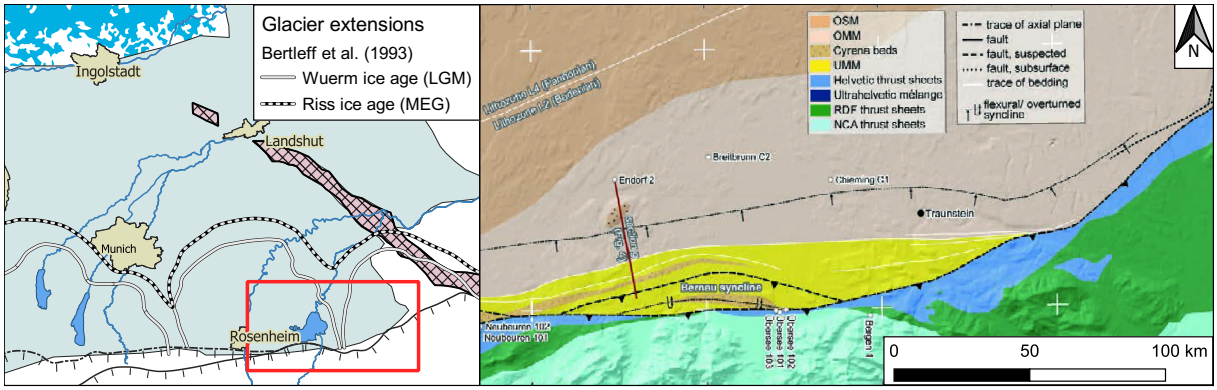

Figure A.4: Tectonic map of the Subalpine Molasse of Upper Bavaria between Rosenheim and Salzburg (after Ortner et al. (2015)) with extents of glaciers during the last ice ages (Bertleff et al., 1993).